



Fang, Yi (2024) *Concentrated solar thermal gasification of biomass for continuous electricity generation*. PhD thesis.

<https://theses.gla.ac.uk/84151/>

Copyright and moral rights for this work are retained by the author

A copy can be downloaded for personal non-commercial research or study, without prior permission or charge

This work cannot be reproduced or quoted extensively from without first obtaining permission from the author

The content must not be changed in any way or sold commercially in any format or medium without the formal permission of the author

When referring to this work, full bibliographic details including the author, title, awarding institution and date of the thesis must be given

Enlighten: Theses

<https://theses.gla.ac.uk/>
research-enlighten@glasgow.ac.uk



University
of Glasgow

**Concentrated solar thermal gasification of
biomass for continuous electricity generation**

Yi Fang

**Submitted in fulfilment of the requirements for the
Degree of Doctor of Philosophy**

**School of Engineering
College of Science and Engineering
University of Glasgow**

September 2023

©2023

Abstract

Bioenergy production is one of the key strategies for reducing CO₂ emissions and replacing fossil fuels. Along with other renewable energy sources and emission reduction methods, it provides a variety of solutions for addressing global energy challenges and climate change. Although gasification-based bioenergy generation has been extensively researched, there are still challenges in terms of energy efficiency, environmental sustainability, and economic viability in practical applications. Concentrated solar thermal gasification of biomass (CSTGB) system offers a promising solution. It utilizes concentrated solar thermal energy to enhance gasification efficiency, improve environmental sustainability, increase energy security, and possess potential economic viability.

Under optimal conditions geared towards maximizing energy conversion efficiency, the CSTGB system boasts impressive results, including a remarkable 30% improvement in biomass utilization and substantial 40% increase in total energy efficiency compared to conventional gasification methods. This represents a notable leap forward in the quest for sustainable and efficient bioenergy production. Gasification technologies have been widely investigated for converting biomass into syngas, which can be further utilized for heat or electricity generation. To optimize this process, a stochastic gasification kinetic model has been developed, employing a Monte Carlo (MC) approach coupled with the powerful random forest (RF) algorithm. This innovative approach aims to predict the ideal gasification process parameters, encompassing variables such as water content, particle size, porosity, thermal conductivity, emissivity, shape, and reaction temperature, all with the goal of achieving maximum producer gas yield and quality. The model's accuracy and reliability have been rigorously confirmed through comparison with existing literature data, underscoring its value as a valuable tool for the design and operation of gasification processes.

This system emerges as a highly promising solution to reduce greenhouse gas (GHG) emissions and address energy cost challenges. To evaluate the system comprehensively, a life cycle assessment (LCA) and techno-economic analysis (TEA) were conducted with a focus on global warming potential (GWP) and economic feasibility. Sensitivity analysis has effectively pinpointed cost and emissions hotspots within the system. While the net present worth (NPW) of the proposed system at 30th year stands at

approximately €–0.7 billion, two key strategies can be employed to enhance its economic viability. These strategies include a 19% reduction in operation and maintenance (O&M) costs to 43.9 €/MWh or a 20% increase in overall system efficiency. The proposed system has the potential to annually save 787.7 kgCO₂-eq/ton_{waste-wood} and generate approximately 0.8 million MWh of electricity, concurrently promoting energy security and contributing significantly to carbon emission reduction. This synthesis of sustainable technologies underscores its pivotal role in our transition towards a greener and more energy-efficient future.

The multi-objective optimization (MOO) of the proposed system on LCA and TEA is conducted. The analysis employed the long short-term memory recurrent neural network (LSTM-RNN) algorithm and MC approach expand scenarios due to limited specialized models and experimental. Influenced by considerations related to carbon taxes (CT), the results highlight a robust optimal configuration capable of reducing GWP by 415,960 tons of CO₂ and generating a NPW of €4,298 million over a 30-year life span. However, in the absence of CT revenue, the analysis reveals trade-offs, resulting in a reduction of 132,615 tons of CO₂ and a net present worth of €3,042 million.

List of publications

List of publications from this thesis:

P1. Fang, Y., Paul, M. C., Varjani, S., Li, X., Park, Y. K., & You, S. “Concentrated solar thermochemical gasification of biomass: Principles, applications, and development.” *Renewable and Sustainable Energy Reviews*, 150(2021): 111484, <https://doi.org/10.1016/j.rser.2021.111484>

P2. Fang, Y., Li, W., & You, S. “Techno-economic analysis of biomass thermochemical conversion to biofuels.” *Value-Chain of Biofuels*, (2022): 379-394, <https://doi.org/10.1016/B978-0-12-824388-6.00023-3>

P3. Fang, Y., Ma, L., Yao, Z., Li, W., & You, S. “Process optimization of biomass gasification with a Monte Carlo approach and random forest algorithm.” *Energy Conversion and Management* 264(2022): 115734, <https://doi.org/10.1016/j.enconman.2022.115734>

P4. Fang, Y., Li, X., Ascher, S., Li, Y., Dai, L., Ruan, R., & You, S. “Life cycle assessment and cost benefit analysis of concentrated solar thermal gasification of biomass for continuous electricity generation.” *Energy* 284(2023): 128709, <https://doi.org/10.1016/j.energy.2023.128709>

P5. Fang, Y., Li, Y., Ahmed, A., & You, S. “Development, economics, and global warming potential of lignocellulose biorefinery.” *Biomass, Biofuels, Biochemicals* (2021):1-13, <https://doi.org/10.1016/B978-0-12-820294-4.00012-0>

List of publications under review and under preparation:

R1. Machine learning-based multi-objective optimization of concentrated solar thermal gasification of biomass incorporating life cycle assessment and cost benefit analysis (under review on *Energy Conversion and Management*).

R2. Sustainable energy from sunlight, biomass, and solid waste for a clean future (under preparation).

List of conference poster and oral presentation from this thesis:

1. Fang, Y., Taylor, E. P., & You, S. (2020). Forecast of renewable wind power generation in Scottish farms for optimal renewable energy management.

To my family

Acknowledgements

I wish to extend my deepest gratitude to my esteemed supervisor, **Dr Siming You**, whose unwavering dedication, intensive guidance, and continuous encouragement have been instrumental in shaping the development of this work. His expert insights and valuable support have undoubtedly elevated the quality of my research.

In addition, I am profoundly thankful to **Dr Xian Li**, whose invaluable advice and mentorship have significantly influenced the direction and refinement of my study. **Dr Li's** willingness to invest his precious time and expertise in my research has been both humbling and inspiring.

Furthermore, I must express my sincere appreciation to **Dr Zhiyi Yao** for his exceptional guidance and support in the intricate domain of gasification kinetic modelling. His expertise and patient mentorship have been pivotal in unraveling complex aspects of my work.

I am also indebted to the University of Minnesota, particularly **Prof Roger Ruan** and **Dr Leilei Dai**, for their gracious support in obtaining valuable experimental results. Their collaboration has enriched the validity and credibility of my findings.

Beyond academia, I owe a debt of gratitude to my beloved parents, **Mr Qiang Fang** and **Mrs Hong Yao**, whose unwavering belief in my abilities and unwavering support throughout the past four years have been a source of strength and motivation. Lastly, I am deeply thankful to my wife, **Mrs Wenjuan Ding**, whose unwavering support and encouragement have been a constant source of inspiration during this journey. Her belief in me and her understanding of the challenges I faced have been my anchor, enabling me to navigate through the highs and lows of academic pursuit. I express my gratitude towards our unborn child, **Nianke Fang**, who shall emerge as the newfound beacon of hope in my existence. I eagerly anticipate the sharing of life's quintessential moments with him, witnessing his development, fostering his innate potential, and providing unwavering support and guidance, thereby inspiring him to pursue his aspirations.

Declaration

I declare that, except where explicit reference is made to the contribution of others, that this dissertation is the result of my own work and has not been submitted for any other degree at the University of Glasgow or any other institution.

Signature:

Printed name: Yi Fang

Table of contents

Abstract	II
List of publications	IV
Acknowledgements	VII
Declaration	VIII
Table of contents	IX
List of Figures	XIII
List of Tables	XV
Glossary	XVII
Chapter 1 Introduction	1
1.1 Background	1
1.2 Aim and objectives	5
1.3 Layout of the thesis	6
Chapter 2 Literature Review	6
2.1 Biomass	7
2.2 Conversion processes	8
<i>2.2.1 Pyrolysis</i>	10
<i>2.2.2 Gasification</i>	12
2.3 Types of gasifiers	13
<i>2.3.1 Fixed bed gasifier</i>	13
<i>2.3.2 Fluidized bed gasifier</i>	17
<i>2.3.3 Entrained flow gasifier</i>	19
2.4 Parameters affecting gasification process	19
<i>2.4.1 Particle size</i>	19
<i>2.4.2 Reaction temperature</i>	21

	X
2.4.3 Catalysts	22
2.4.4 Gasifying agent	24
2.5 Gasification modelling	26
2.5.1 Thermodynamic equilibrium models	26
2.5.2 Kinetic models	27
2.5.3 CFD models	29
2.5.4 Stochastic based kinetic models	32
2.5.5 Machine learning models	33
2.6 Solar collector methods	36
2.6.1 Solar collector type	36
2.6.2 Influential factors	38
2.6.3 CST technical challenges	39
2.7 CSTGB system development	41
2.8 CSTGB system evaluation	44
2.8.1 Life cycle assessment of CSTGB system	44
2.8.2 Economics analysis of the CSTBG system	45
2.8.3 Multi objectives optimization	45
2.9 CSTGB system limitations and commercialization barriers	46
2.9.1 Technological challenges	46
2.9.2 Economic barriers	47
2.9.3 Market and policy challenges	48
2.9.4 Research and development gaps	49
2.10 Summary	50
Chapter 3 Development and process optimization of biomass gasification with a Monte Carlo approach and random forest algorithm	53
3.1 Methodology	54
3.1.1 Kinetic model development	54

3.1.2 Monte Carlo simulation 62

3.1.3 Random Forest model evaluation 65

3.2 Results and discussion 67

3.2.1 Kinetic model validation 67

3.2.2 Random forest model 69

3.3 Summary 74

Chapter 4 Life cycle assessment and techno-economic analysis of concentrated solar thermal gasification of biomass for continuous electricity generation 77

4.1 Methodology 78

4.1.1 Thermodynamic analysis of the CSTGB system 79

4.1.2 Life cycle assessment 82

4.1.3 Techno-economic analysis 85

4.2 Results and discussion 88

4.2.1 Thermodynamic analysis 88

4.2.2 Environmental impacts 84

4.2.3 Economic analysis 86

4.3 Summary 88

Chapter 5 Machine learning-based multi-objective optimization of concentrated solar thermal gasification of biomass incorporating life cycle assessment and techno-economic analysis 89

5.1 Methodology 90

5.1.1 Overview of the CSTGB system 92

5.1.2 Dataset and features description 94

5.1.3 LSTM-RNN model 96

5.1.4 Monte Carlo simulation 97

5.1.5 Life cycle assessment 98

5.1.6 Techno-economic analysis 107

5.1.7 Multi-objective optimization 109

5.2 Results and discussion	110
5.2.1 <i>Forecasting of electricity generation and carbon saving by CSTGB system</i>	110
5.2.2 <i>Performance evaluation of LSTM-RNN model</i>	114
5.2.3 <i>Evaluation of MOO results</i>	115
5.3 Summary	118
Chapter 6. Conclusions and recommendations for future work	119
6.1 General conclusions	119
6.2 Recommendations for future work	120
Reference	123

List of Figures

Figure 1.1 An illustration of the CSTGB system.....	3
Figure 1.2 Layout of this thesis. CSTGB: concentrated solar thermal gasification of biomass; CST: concentrated solar tower; TES: thermal energy storage; HTM: heat transfer material; ML: machine learning; LHV: low heating value; LCA: life cycle assessment, TEA: techno-economic analysis.	7
Figure 2.1 Schematic diagram of a typical CSTGB system.	9
Figure 2.2 ML classifications.....	34
Figure 3.1 Overview of the methodology.	54
Figure 3.2 A schematic diagram of the kinetic model coupling the shrinkage core model and fixed bed gasification.	62
Figure 3.3 The schematic diagram of the topological structure of the RF algorithm.	66
Figure 3.4 Comparisons between the kinetic model predictions and experimental results.	68
Figure 3.5 Test results for determining the optimal tree numbers in RF algorithm for H ₂ , CO, and CH ₄ ((a) uniform and (b) normal distributions).	70
Figure 3.6 Measured relative importance of each input parameter for producer gas yield ((a) uniform and (b) normal distributions).....	71
Figure 3.7 Validation results of RF algorithm for producer gas yields ((a) uniform and (b) normal distributions).	73
Figure 4.1 The schematic illustration of the methodology. CSTGB: concentrated solar thermal gasification of biomass; CST: concentrated solar tower; TES: thermal energy storage; CCGT: combined cycle gas turbine; CCS: carbon captured system; ML: machine learning; LHV: low heating value.	79
Figure 4.2 The schematic diagram of the proposed CSTGB system.	80
Figure 4.3 (A) Effects of air to feedstock ratio on producer gas flow rate, producer gas LHV, and system CGE; (B) Effects of air to feedstock ratio on producer gas composition.....	81
Figure 4.4 LCA boundary of the CSTGB system.	83
Figure 4.5 The optimal heliostat field layout of the CST subsystem.....	84
Figure 4.6. Hourly net power and efficiency of the system in the representative days, (A) the day of March 19 th , (B) June 22 nd , (C) September 22 nd , and (D) December 21 st .	

.....	84
Figure 4.7. Monthly and cumulative data: (A) electricity production, (B) CO ₂ captured and stored, and (C) onsite CO ₂ released to environment.	84
Figure 4.8. Comparison of the GWP of case 1 (CSTGB system with CST and TES subsystems) and case 2 (without CST and TES subsystems), ‘+’ represents positive impact on GWP value while ‘-’ indicates carbon reduction.....	85
Figure 4.9. Sensitivity analysis results (influences of major factors on the GWP of CSTGB).	86
Figure 4.10. PW and NPW results of the CSTGB system in the economic analysis. .	87
Figure 4.11. Sensitivity analysis results (influences of major factors on the NPW of CSTGB).	88
Figure 5.1 Schematic illustration of the proposed methodology. CSTGB: concentrated solar thermal gasification of biomass; CST: concentrated solar tower; TES: thermal energy storage; CCGT: combined cycle gas turbine; CCS: carbon captured system; SOO: single-objective optimization; MOO: multi-objective optimization: TOPSIS: technique for order of preference by similarity to ideal solution; LSTM-RNN: long short-term memory recurrent neural network; MSE: mean squared error.	92
Figure 5.2 The schematic diagram of the proposed CSTGB system.....	93
Figure 5.3. Hourly DNI data profiles for locations A, B, C, D, and E.....	95
Figure 5.4 Main steps of the proposed LSTM-RNN model	96
Figure 5.5 LCA boundary of the CSTGB system.	99
Figure 5.6 125 scenarios set descriptive statistics.	113
Figure 5.7 (A). the proposed LSTM-RNN model evaluation, (B). comparison of predict and actual annual electricity generation, (C). comparison of predict and actual annual carbon captured.....	114
Figure 5.8 The decision making of the optimal scenario: A). the CSTGB system with considered CT as revenue, B). the CSTGB system without considered CT as revenue.	117

List of Tables

Table 1.1 Comparison between the CSTGB system and the conventional gasifier.....	4
Table 1.2 Comparative cost analysis of various energy system over a 25-years lifecycle (2019 exchange rate: 1 USD = 0.89 EUR).	5
Table 2.1 Fixed bed gasifier studied.	15
Table 2.2 Fluidized bed gasifier used for CSTGB system.	18
Table 2.3 Impacts of particle size on CSTGB system.	21
Table 2.4 Equilibrium & CFD models of gasification.	31
Table 2.5 Characteristics of CST technologies.	38
Table 2.6 Comparative economic analysis of electricity production from CSTGB system and conventional gasifier.	49
Table 3.1 Gasification reactions (where ‘j’ denotes heterogeneous reactions and ‘i’ represents homogeneous reactions).	59
Table 3.2 List of model inputs and parameters (153, 166, 298).	61
Table 3.3 Summary of process parameters for constructing the probability distributions.	63
Table 3.4 Means and standard deviations for the distributions of the process parameters.	64
Table 3.5 Composition of feedstocks and gasifier process parameters from three existing experimental studies.	68
Table 3.6 Quality indicators of RF algorithm based on the training data (uniform and normal distributions).	69
Table 3.7 Quality indicators of the RF algorithm based on the testing data (uniform and normal distributions).	72
Table 3.8 Comparison of producer gas yields and optimal process parameters from the RF algorithm to the experimental data.	76
Table 4.1 Design parameters of the proposed CSTGB system.	85
Table 4.2 Life cycle inventory (LCI) for the construction stage of the CSTGB system. The data are normalised based on the functional unit (i.e., 1 ton _{waste-wood}).	88
Table 5.1 Feedstock compositions (dry ash free basis) and locations.	95
Table 5.2 The lower and upper bounds of selected decision variables for the CSTGB system.	98

Table 5.3 Design parameters of the CSTGB system in each location.	101
Table 5.4 LCI for the construction stage of the CSTGB system is normalized based on the functional unit (i.e., 1 ton _{biomass-waste}) in each location.	105
Table 5.5 CAPEX, O&M, and transportation costs for the CSTGB system at each location.....	109

Glossary

Nomenclature

A	Cross sectional area of the bed (m^2)
A_V	Specific surface area (m^2)
cp	Specific heat capacity ($\text{J kg}^{-1} \text{K}^{-1}$)
D	Diffusivity (m^2s^{-1})
d	Diameter (m)
F	Mass flow rate (kg s^{-1})
h	Heat transfer coefficient ($\text{W m}^{-2} \text{K}^{-1}$)
k	Mass transfer coefficient (m s^{-1})
M	Molecular weight (kg mol^{-1})
m	Mass (kg)
Nu	Nusselt number (-)
q	Heat flux (W m^{-2})
R	Gas constant ($8.314 \text{ J mol}^{-1} \text{K}^{-1}$)
Re	Reynolds number (-)
r	Radius (m)
Sc	Schmidt number (-)
Sh	Sherwood number (-)
T	Temperature (K)
t	Time (s)
u	Velocity (m s^{-1})
L_{bed}	Bed height (m)
V	Volume (m^3)
V_{ad}	Volume fraction of ash (m^3)
X_B	Dry-ash-free biomass conversion rate
Y	Mass fraction (-)
ε	Porosity (-)
ρ	Density (kg m^{-3})

ν	Stoichiometric number (-)
μ	Effective viscosity ($\text{kg m}^{-1} \text{s}^{-1}$)
η	Dynamic viscosity (Pa s^{-1})
ϵ	Particle emissivity (-)
σ	Stefan-Boltzmann constant ($5.67 \times 10^{-8} \text{ W m}^{-2} \text{K}^{-4}$)
κ	Thermal conductivity ($\text{W m}^{-1} \text{K}^{-1}$)

Subscripts

gs	Heat/mass transfer in gas-solid phase
g,p	Gas phase in porous biomass particle
s,p	Solid phase in porous biomass particle
i	Species/component in gas phase with index i
j	Species/component in solid phase with index j
k	Reaction number with index k
p	Particle phase
sat	Saturation
surf	Surface
t	Transient variables
vap	Vaporization
vol	Volume
w	Water
P	Particle
mfv	Minimum fluidization velocity

Abbreviations

AI	Artificial intelligence
ANN	Artificial neural network
AW	Annual worth
CAEPX	Capital expenditure
CART	Classification and Regression Tree
CBA	Cost benefit analysis

CC	Concentrated collector
CCGT	Combined cycle gas turbine
CEPCI	Chemical Engineering Plant Cost Index
CFD	Computational Fluid Dynamics
CCS	Carbon captured storage
CSP	Concentrated solar power
CT	Carbon tax
DACR	Direct absorption receiver
DNI	Direct nominal irradiation
EFG	Entrained flow gasifier
EEA	European Environment Agency
E-E	Eulerian-Eulerian
E-L	Eulerian-Lagrangian
ER	Equivalent ratio
ES	Electricity selling
FBG	Fluidized bed gasifier
GI	Gini index
GHG	Greenhouse gas
GHI	Global horizontal irradiance
GWP	Global warming potential
HRSG	Heat recovery steam generator
HTM	Heat transfer material
IB	In Bag
IEA	International Energy Agency
IncNodePurity	Total decrease in node impurity
IncMSE	Percentage increase in mean square error
IRENA	International Renewable Energy Agency
IRR	Internal rate of return
LCA	Life cycle assessment
LCI	Life cycle inventory
LCIA	Life cycle impact assessment
LHV	Lower heating value
MAE	Mean absolute error
MC	Monte Carlo

ML	Machine learning
MSE	Mean squared error
MOO	Multi-objective optimization
MTCR	Multi-tube receiver
MTER	Multi-tube external receiver
NCC	Non-concentrated collector
NPW	Net present worth
NS	Non-stoichiometric
NTER	Non-thermal equilibrium reactor
OOB	Out Of Bag
O&M	Operation and maintenance
PCM	Phase change material
PDC	Parabolic dish collector
PVGIS	Photovoltaic Geographical Information System
RF	Random forest
RMSE	Root mean square error
S/B	Steam to biomass
SDFBG	Solar-driven dual fluidized bed gasifier
SNG	Synthetic natural gas
SOO	Single-objective optimization
SR	Sensitive ratio
STM	Screw transfer machine
TEA	Techno-economic analysis
TES	Thermal energy storage
TE	Thermodynamic equilibrium
TMY	Typical meteorological year
TOPSIS	Technique for order of preference by similarity to ideal solution
UUFBG	Upgraded updraft fixed bed gasifier
VCR	Volumetric receiver
WGS	Water-gas shift

Chapter 1 Introduction

1.1 Background

Renewable energy stands out as a crucial solution to address the escalating global energy demand and combat the pressing issue of climate change. Within the realm of renewable energy development, biomass holds a pivotal position in international renewable energy strategies. This prominence is attributed to its carbon-neutral characteristics and widespread availability (1). As the most abundant source of renewable carbon, biomass has experienced a growing utilization for the generation of bio-product (2). The massive consumption of fossil fuels has caused various environmental problems, such as global warming and air quality degradation with high levels of GHG and inhalable particulate matter (IPM) (*i.e.*, PM₁₀ and PM_{2.5}) emissions. The reduction of GHG emissions and IPM are two of the most significant challenges in this century and calls for urgent actions. Meanwhile, the depletion of fossil fuel reserves is in clear contrast with the growing energy demand worldwide. Renewable energy plays a critical role for meeting the growing energy demand and serves as an essential means to mitigate climate change.

Biomass is one of the primary renewable energy sources (3). It accounted for 977–1,051 TWh (29.90–32.53%) electricity generation in the European Union between 2017 and 2018 (4) 15–20% of the world's fuel consumption in 2018 (5). Thermochemical technologies (*i.e.*, pyrolysis, gasification, combustion, liquefaction, *etc.*) can convert biomass into high value bioproducts in various forms (*i.e.*, solid, liquid, and gas) (6). Gasification is one of the main technologies for energy recovery from biomass. It refers to the incomplete combustion of biomass materials in an oxygen-limited environment to convert the biomass into synthesis gas (or syngas, mainly a mixture of hydrogen, carbon monoxide and methane) and a solid residue by-product consisting of ash and biochar. The heat required for conventional gasification is supplied by the combustion of feedstock (*i.e.*, biomass) (7). High energy efficiency is critical for the economics and widespread implementation of the technology (8).

To enhance the efficiency of biomass gasification, innovative methods such as the CSTGB system have been developed, as shown in Figure 1.1. This advanced system marks a significant breakthrough in biomass conversion technology. Unlike the conventional methods, the CSTGB system integrates solar thermal energy into the

conventional gasification process, utilizing solar power to drive the gasification (7). This not only improves the thermal efficiency of the process but also fosters a more sustainable and environmentally friendly approach to biomass energy conversion. This innovative strategy either replaces or supplements traditional biomass combustion, achieving the higher temperatures essential for efficient gasification. This enhancement leads to a more thorough conversion of biomass into producer gas, a versatile and valuable energy carrier. It also reduces the reliance on combusting biomass as a fuel source, thereby optimizing biomass usage and substantially lowering the carbon footprint of the process. One of the key goals of the CSTGB system is to produce higher-quality producer gas with lower levels of contaminants (*i.e.*, tar), enhancing the overall efficiency of biomass-to-energy conversion and streamlining downstream processing.

Figure 1.1 presents an illustration of the CSTGB system, it is one of the attempts to enhance the efficiency of gasification. In this process, solar energy is utilized to drive biomass gasification, aiming to increase biomass utilization rate and the quality of product gas, and reduce pollutant emissions (*i.e.*, NO_x, PM₁₀, and VOCs) as compared to the conventional gasification process (9). The system features concentrated solar collector (*i.e.*, heliostat fields and solar dish), which absorb solar radiation and converts it to thermal energy and then transferred to the gasifier. The solar concentration ratio that defines the enhancement in the incident energy flux ranges from 250 to 3000 (10). It is carried by a thermal fluid (*e.g.*, molten salt, quartz sand, etc.) with a temperature range of 250–2000 serving as the heat source of the gasification process where biomass is converted into producer gas as a chemical energy carrier (11).

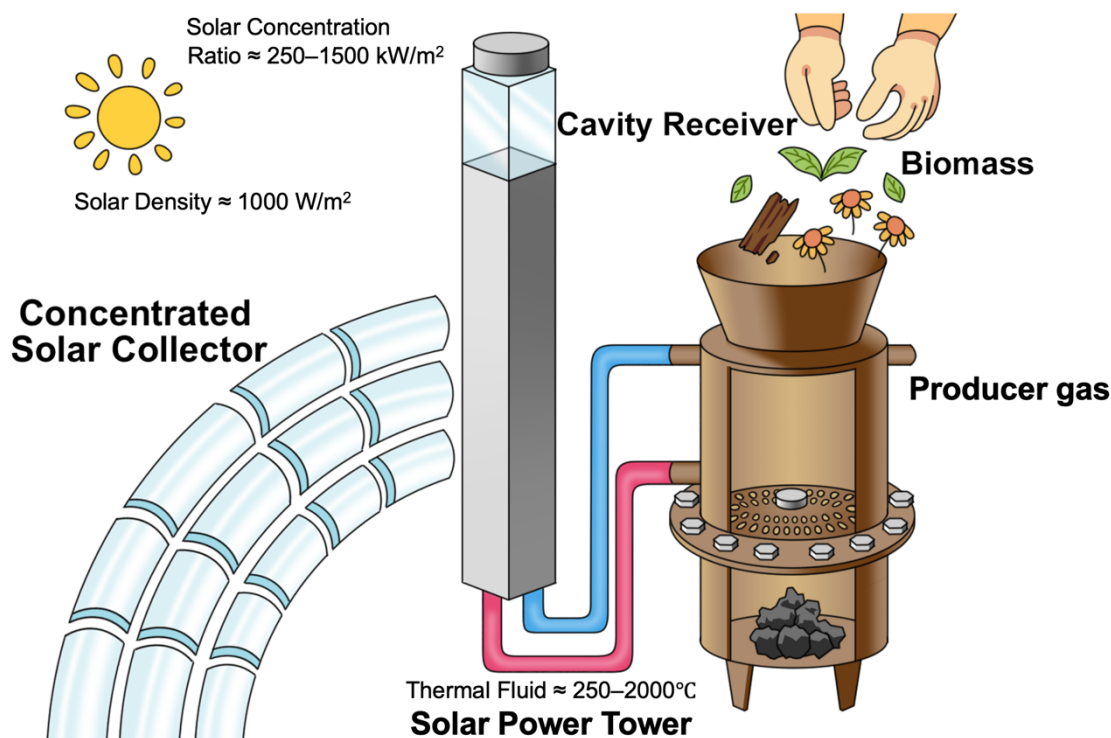


Figure 1.1 An illustration of the CSTGB system

Table 1.1 illustrates that the CSTGB system consistently outperforms the conventional gasification process in terms of efficiency. Compared to the conventional biomass gasifier, the CSTGB system relies on solar energy as its primary heat source. This reduces dependence on fossil fuels and lowers related emissions, showcasing its environmental advantages. Utilizing solar energy as the power supply significantly enhances the overall efficiency of the system (typically by 25–50%). This heightened efficiency implies that the CSTGB system requires less feedstock to produce the same amount of energy as compared to the conventional one. In the realm of comprehensively understanding the full advantages of the CSTGB system, several significant research outcomes have been achieved. For example, Loutzenhiser *et al.* (12) summarized the CSTGB system, including thermodynamic and kinetic analyses as well as modelling, fabrication, and testing of thermochemical reactors. Pramanik *et al.* (13) demonstrated that the use of CSTGB system to produce syngas is a promising renewable pathway that effectively reduces CO₂ emission (<100 kg/MWh). Puig-Arnavat *et al.* (14) have described that the CSTGB system as an alternative to the conventional gasification process, especially emphasizing its capability to generate high-quality and high-yield producer gas. Their research further highlights the advantages of the CSTGB system as a solar thermal chemical storage method, allowing the storage of solar energy in an

easily transportable fuel form. These studies not only affirm the technical superiority of the CSTGB system but also provide important theoretical and practical bases for future energy transformation and sustainable development.

Table 1.1 Comparison between the CSTGB system and the conventional gasifier.

Feedstock	CSTGB system		Conventional gasifier		Ref
	Efficiency ^a	Syngas yield (mmol/g _{biomass})	Efficiency ^a	Syngas yield (mmol/g _{biomass})	
Beech wood	58.7–73.0%	H ₂ : 31.9–41.9 CO: 26.8–31.1 CO ₂ : 2.4–3.2	50.0–65.0%	H ₂ : 2.7–12.4 CO: 6.6–14.3	(15, 16)
Straw	79.0%	H ₂ : 18.0 CO: 52.0 CH ₄ : 9.0 CO ₂ : 4.8–7.2	42.0–60%	H ₂ : 2.7–12.4 CO: 6.6–14.3 CH ₄ : 0–12.7	(17, 18)
Sugarcane bagasse	61.5–99.9%	H ₂ : 30.0–54.5 CO: 30.7–34.3 CH ₄ : 0.8–13.4 CO ₂ : 2.5–3.8	50.0–70%	H ₂ : 25.0–31.0 Other producer gas: 57.0–60.0	(19, 20)
Wood	73.1–81.1%	H ₂ : 36.1–48.1 CO: 42.3–43.6 CH ₄ : 0.6–16.7 CO ₂ : 3.6–3.7	52.7–70.9%	H ₂ : 10.4–15.6 CO: 18.7–35.8 CH ₄ : 1.0–11.7 CO ₂ : 12.0–25.8	(15, 21-23)
Torrefied wood	70.0–93.5%	H ₂ : 53.9–57.8 CO: 30.6–37.0 CH ₄ : 2.2–3.8 CO ₂ : 2.2–3.8	55.2–70.1%	H ₂ : 12.6–18.6 CO: 22.3–41.8 CH ₄ : 2.0–9.2 CO ₂ : 12.0–17.2	(21, 24, 25)
Dried wood	83.0–87.7%	H ₂ : 28.3–43.3 CO: 45.3–47.4 CH ₄ : 0.8–2.1 CO ₂ : 8.3–20.5	55.0–68.0%	H ₂ : 12.0–18.6 CO: 21.0–40.8 CH ₄ : 0.6–9.0 CO ₂ : 12.0–22.0	(21, 23, 26, 27)
Wheat	70–90%	H ₂ : 28.3–42.5 CO: 45.3–28.1 CH ₄ : 0.8–5.5 CO ₂ : 2.7–9.2	45.2–65.5%	H ₂ : 4.4–11.6 CO: 8.7–16.8 CH ₄ : 1.0–8.7 CO ₂ : 10.0–18.8	(28-30)

^a The efficiency is defined as a ratio of the calorific value of producer gas to the heating value of feedstock.

The CSTGB system effectively resolves key issues faced by conventional gasifiers, such as low efficiency and high CO₂ emissions. This technological innovation not only significantly enhances the efficiency of processing various feedstock, like beech wood, straw, and sugarcane bagasse (as shown in Table 1.1), but also greatly reduces the overall CO₂ emissions. This advancement marks a revolutionary step in the bioenergy field, showcasing the tremendous potential of integrating renewable energy with modern gasification technology.

Furthermore, the CSTGB system also displays notable advantages from an economic standpoint. Table 1.2 provides a comparative cost analysis over 25-year lifecycle for various energy systems (31-33). Despite the CSTGB system has higher capital cost (3,560–5,340 €/kW_{th} of installed capacity) compared to conventional gasifier (2,225–4,005 €/kW_{th}) and other renewable sources like solar PV (1,068–2,670 €/kW_{th}) and wind energy (1,157–2,225 €/kW_{th}), the CSTGB system offers lower H₂ production costs (1.8–4.0 €/kg) than solar and wind alternatives. In terms of operational and maintenance (O&M) costs, the CSTGB system (53.4–89.0 €/kWh) is comparable to coal power (35.6–66.8 €/kWh) and more economical than nuclear energy (80.1–115.7 €/kWh). The cost analysis demonstrated the CSTGB system is a clear path towards long-term sustainability in energy production, and it is a cost-effective and environmentally sustainable solution. By balancing higher initial investments against lower long-term operational costs and reduced environmental impact, the CSTGB system emerges as a compelling choice in the shift towards greener energy technologies.

Table 1.2 Comparative cost analysis of various energy system over a 25-years lifecycle (2019 exchange rate: 1 USD = 0.89 EUR).

Energy system	Capital cost (per kW of capacity, €)	Operational & maintenance cost (per kW per year, €)	Cost of H ₂ production/electricity (per kg/kW, €)	Ref(s)
CSTGB system	3,560–5,340	53.4–89.0	1.8–4.0	(31-33)
Conventional gasifier	2,225–4,005	35.6–71.2	1.3–3.1	(34-36)
Solar PV	1,068–2,670	13.4–31.2	2.7–5.3	(37-39)
Wind energy	1,157–2,225	17.8–35.6	2.2–4.5	(40-42)
Nuclear energy	5,340–8,010	80.1–115.7	Electricity cost: 0.04–0.09	(43, 44)
Coal power	3,115–4,450	35.6–66.8	Electricity cost: 0.03–0.05	(45-47)

1.2 Aim and objectives

The aim of this PhD thesis was to develop a simulation of the CSTGB system to produce electricity from biomass/waste residues. To achieve the aim several objectives were set:

- Develop a stochastic kinetic model for gasifier to find the optimal reaction parameters.
- Determine the effect of water content, particle size, particle porosity, particle shape, thermal conductivity, emissivity, and reaction temperature on the properties of producer gas production in gasification process.

- Determine the effect of operating conditions in a proposed CSTGB system to produce electricity.
- Investigate the environmental impacts and economic feasibility of the CSTGB system to generate electricity.
- Multi-objective optimization of the CSTGB system on environmental impact and economic viability.

1.3 Layout of the thesis

Chapter 1 primarily introduces the CSTGB system, it is an advancement in the field of sustainable energy. This chapter provides a comprehensive overview of various aspects the CSTGB system, with a special emphasis on its importance in energy production. It particularly presents the system's advantages in improving efficiency, increasing product yield, and reducing emissions compared to conventional methods. The objectives and purposes of this research, which are to promote the development of sustainable energy production and minimize adverse environmental impacts. This work represents a significant step towards these aims, focusing on innovative methodologies and practical applications. Additionally, this chapter briefly introduces the layout of the thesis and outlines the author's role as the principal researcher and main contributor in each published paper. Additionally, this chapter briefly outlines the layout of the thesis. Figure 1.2 provides a schematic representation of the key components and concepts explored throughout the thesis. It also encompasses the following elements: CSTGB system, CST, TES, HTM, ML algorithm, LHV, LCA, and TEA. This figure serves as a visual guide, offering a clear and concise overview of the thesis structure and the interconnection of various concepts and components within the CSTGB system.

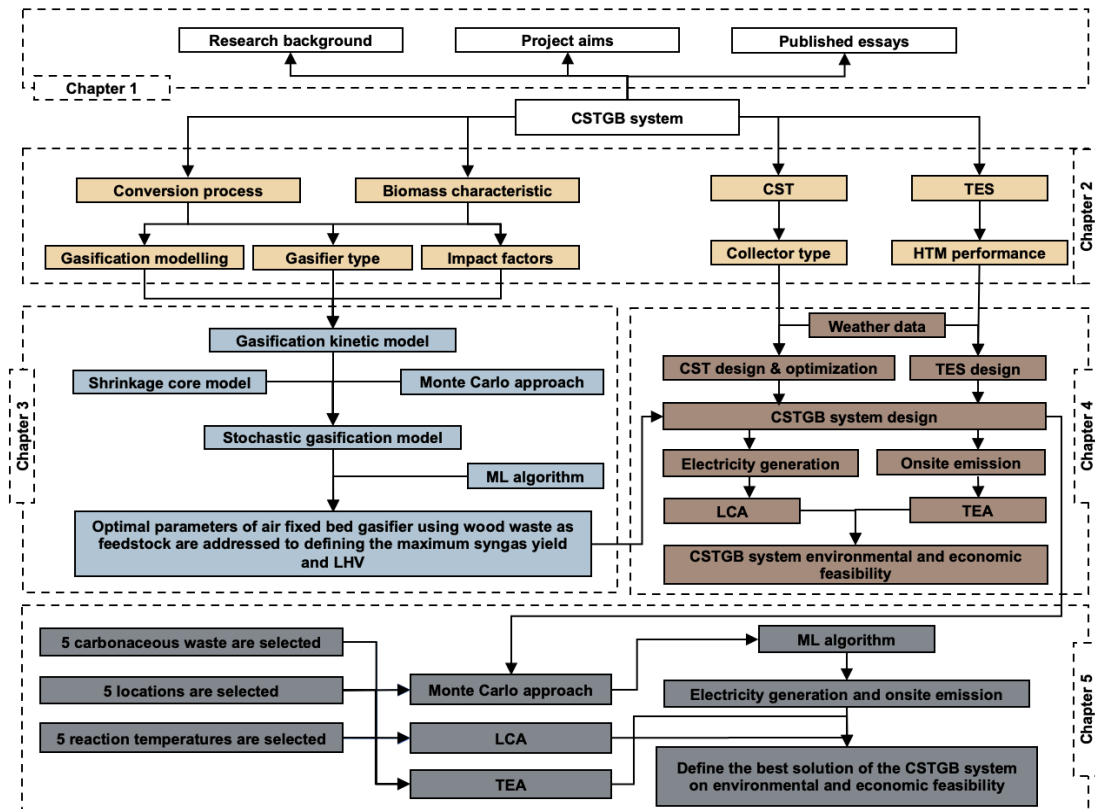


Figure 1.2 Layout of this thesis. CSTGB: concentrated solar thermal gasification of biomass; CST: concentrated solar tower; TES: thermal energy storage; HTM: heat transfer material; ML: machine learning; LHV: low heating value; LCA: life cycle assessment, TEA: techno-economic analysis.

Chapter 2 provides a comprehensive examination of the CSTGB system, integrating insights from the author’s previously published journal referenced as [P1] and [P2] in the **List of Publications**. This chapter provides a detailed exposition on the thermochemical gasification process for converting biomass into high-value producer gas. The chapter illustrates that concentrated solar thermal techniques can enhance the gasification efficiency while reducing environmental impacts and costs. The research in this chapter not only reveals the innovation of the CSTGB system at both theoretical and practical levels but also demonstrates significant advancements in the environmental, economic, and multi-objective optimization. These achievements are rooted in the comprehensive methodological research described in [P1] and [P2]. Through these studies, there has been a significant enhancement in the technical depth and application breadth within the field of CSTGB systems.

Chapter 3 focuses on the research detailed in the article [P3] from the **List of**

Publications, addressing the optimization of biomass gasification using a Monte Carlo (MC) approach and a random forest (RF) algorithm. This chapter provides detailed conclusion on various aspects of biomass gasification. In this chapter, a robust stochastic gasification kinetic model based on MC simulation has been developed to meet the specific requirements of the study. This model is adept at capturing a board range of process parameters and their impact on the yield of producer gas, thereby offering an extensive overview of the gasification process. The accuracy and practical relevance of the model have been substantiated through comparisons with experimental data. Moreover, this chapter discusses innovative adjustments made to the input data of the stochastic kinetic model. These adjustments (includes the incorporation of both normal and uniform distributions) result in the generation of two distinct sets of output data. These datasets have been employed to train the RF model, which in turn facilitates the prediction of outcomes for a wider range of conditions. This approach is instrumental in determining the maximum yield of producer gas and identifying the optimal process conditions. Extensive validation of these predictions has been conducted to ensure the model's reliability and accuracy in real-world applications. This chapter not only showcases significant contributions and innovative methods in the field of biomass gasification but also emphasizes the practical applicability and precision of the research methodologies employed.

Chapter 4 examines the research presented in the article referenced as [P4] in the **List of Publications**. It offers a detailed analysis of the CSTGB system, demonstrating a deep understanding of the system alongside of the application of advanced research methods. The study involves a detailed assessment of the system's construction, manufacturing stages, resource consumption, and its entire life cycle, thereby revealing both environmental and economic impacts of the system. The LCA technique highlights environmental considerations, it combined with data analysis and model development of the CSTGB system was used in this chapter. The TEA segment convers the entire life cycle costs, operational efficiency, and long-term economic benefits of the system, providing essential insights into its overall sustainability and assesses its economic benefits and potential market viability. Moreover, the research findings have been validated with experimental data from various related literatures. This process not only confirms the accuracy and reliability of the results but also strengthens the scientific foundation of the research and find their potential role in advancing sustainable energy technologies were detailed.

Chapter 5 is based on the research from the article identified as [R1] in the **List of publications under review and under preparation in List of Publications**. This chapter examines the CSTGB system as a promising solution for reducing GHG emissions. The study in [R1] utilizes a MOO approach, integrating results from both LCA and TEA as objectives. To address the dynamic nature of the CSTGB system, the LSTM-RNN model has been integrated into the study. Due to limited specialized models and experimental data, the MC approach has been used to expand the range of potential scenarios for the system. The Technique for Order Preference by Similarity to Ideal Solution (TOPSIS) approach, which is instrumental in identifying the most suitable scenario and configuration for the CSTGB system. This approach effectively evaluates the environmental and economic potential of the system. This work involved determining optimal parameters for the CSTGB system. This work contributes to enhance the CSTGB system in terms of environmental and economic feasibility, demonstrating a comprehensive and accurate approach to research in sustainable energy systems.

Chapter 6 provides a comprehensive summary of the findings and suggests directions for future research.

Chapter 2 Literature Review

In the pre-chapter, the concentrated solar thermal gasification of biomass (CSTGB) system has already been demonstrated as highly efficient, yielding high productivity, and exhibiting low carbon emissions. The objectives of this chapter are to delve deeper into which design parameters significantly influence the efficiency of the CSTGB system, which existing models can more accurately simulate the system, and to explore how the system performs under existing life cycle, economic, and multi-objective optimization evaluations. This research has been published in the form of two journal articles⁽⁴⁸⁾⁽⁴⁸⁾ (as mentioned in the Layout of the thesis). This chapter comprehensively analyzes the CSTGB system, including optimal models, parameter settings, environmental feasibility, and economic viability. It summarizes the principles, applications, recent developments, and challenges of the CSTGB system. Specifically, it will review a) the fundamental principles and development status of the technology, b) efficiency research and the obstacles faced by the technology, c) the latest developments and applications of gasifiers and related equipment in the system, and d) assessing the environmental impact through the life cycle assessment (LCA), evaluating the economic viability through the techno-economic analysis (TEA), and exploring multi-objectives optimization (MOO) evaluations to understand the system performance concerning different objectives simultaneously. In this chapter, crucial process parameters closely associated with producer gas production (*i.e.*, water content, particle size, and reaction temperature) have been identified from the literature. The most suitable model for the gasifier in the CSTGB system is a kinetic model. Regarding LCA, it emphasizes the need to clearly state data applicability and methodological limitations in further modelling studies to enhance result transparency and usability. In terms of TEA, the CSTGB system offers notable environmental benefits in reducing GHG emissions and increasing electricity generation. However, the CSTGB system faces economic challenges due to construction and operational and maintenance (O&M) costs, which can be offset by factors like plant size and technology selection (the integration of energy storage and carbon capture can potentially improve its viability). Finally, a holistic approach that combines environmental and economic considerations through MOO techniques can facilitate informed decision-making for a greener future.

2.1 Biomass

Biomass serves as a valuable fuel source or raw material, distinct from traditional fossil fuels that require millions of years to form. Biomass sources encompass a diverse range of natural and processed materials, including woody and herbaceous plants, agricultural and industrial byproducts, discarded paper products, municipal solid waste, and animal and aquatic residues (49). While biomass may not constitute a primary source of industrial fuel, it does contribute significantly, accounting for approximately 15–20% of the world's total fuel consumption (50). Its predominant application is in non-industrialized economies, primarily for household heating and cooking purposes. In industrialized nations, biomass utilization as a fuel source is primarily limited to the utilization of by-products stemming from forestry, paper, and sugar industries. Nevertheless, there is a growing impetus in industrialized countries to promote biomass utilization as part of a broader strategy aimed at reducing CO₂ emissions (51).

The selection of a conversion process and the subsequent challenges in processing are contingent upon the inherent characteristics of the biomass source. During the subsequent stages of energy production, it is essential to take in to account critical material characteristics, including moisture content, calorific value, ratios of fixed carbon and volatiles, ash content, and the presence of alkali metals (52). In the context of dry biomass conversion methods, the foremost consideration pertains to the first five properties mentioned, while in the case of wet biomass conversion, the central emphasis revolves around moisture content and the ratio of cellulose to lignin (53).

Considering the importance of biomass in the CSTGB system, it is essential to thoroughly investigate its unique characteristic and properties, analogous to the attention given in conventional gasification process (54, 55). Such research contributes to optimizing the performance and efficiency of CSTGB system, ensuring effective utilization of biomass resource and facilitating the transition towards sustainable energy production (56-59). The composition of feedstocks (*i.e.*, wood, crop residues, municipal solid waste (MSW), algae, sludge, *etc.*) is an important factor affecting the gasification product. The MSW is a mixture of different waste biomass whose compositions vary widely across different cities and even countries (60), the thermochemical simulations for it are typically challenging. Meanwhile, the biomass feedstock (*i.e.*, waste wood) is of relatively consistent compositions and is well suitable for gasification to achieve high producer gas yields with H₂: 30.0–54.5 mmol/g_{wood} and CO: 26.8–34.2 mmol/g_{wood}

(31). It is a type of primary biomass and accounts for 53–70wt.% of waste in countries like Egypt, China, Canada, Mexico, Philippines, Greece, Spain, and United Kingdom (31). Accordingly, it has been extensively researched in gasification studies with a pool of data for model validation. Hence, biomass as feedstock is focused by the CSTGB system as the starting point. It is worth mentioning that the model can always be adapted to suit other types of biomasses when relevant data is available for model validation. Moreover, understanding the characteristics of biomass (particularly the composition of the biomass) is essential in selecting the appropriate conversion process (61).

2.2 Conversion processes

In the CSTGB system, concentrated solar thermal energy primarily serves to replace the traditional biomass combustion heating phase in the gasification process. Specifically, concentrated solar thermal substitutes the biomass combustion phase in the gasifier, and it also provides heat for the subsequent pyrolysis and gasification stages. This design effectively utilizes solar thermal energy to drive the entire gasification process, thereby optimizing the energy conversion efficiency of biomass. Figure 2.1 described a schematic illustration of the CSTGB system, including the integration of essential components such as the heliostat field, CST receiver, and the TES subsystem. The size of each energy supply component (*i.e.*, the heliostat field, the dimensions of the CST receiver, and the capacity of the TES subsystem) in the CSTGB system were determined based on the regional direct normal irradiance (DNI) and the specific thermal energy demands of the gasifier (as mentioned in Table 5.3). Effective gasification requires stringent control of thermal conditions, ensuring temperatures and heat flux are sufficient to catalyze the conversion of feedstock into producer gas within the gasifier.

Within the CSTGB system, a screw transfer machine (STM) is employed for conveying thermally charged heat transfer material (HTM) (*i.e.*, salt and sand) and feedstock particles are kept separate, and a specific gas leakage (approximately 5–10% as defined from literatures (62, 63)) between the gasifier and the STM equipment is considered. Thermochemical processes (*i.e.*, pyrolysis and gasification) are the most suitable and prevalent methods within the CSTGB system for achieving highly efficient conversion of biomass feedstock into producer gas. These thermochemical processes offer conversion rates exceeding 90% (64). The specific type of thermochemical process and the corresponding conversion rates depend on various process conditions,

including temperature, heating rate, the utilization of oxygen, particle size, catalysts, and gasifying agents (as mentioned in Section 2.4). The high-quality producer gas, characterized by a notably elevated low heating value (LHV) due to the solar thermal heating, is the principal output of the CSTGB system, marking a significant advancement in the field of biomass conversion technologies.

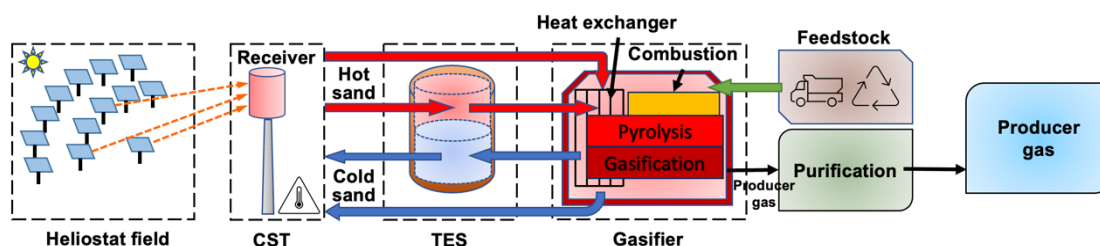


Figure 2.1 Schematic diagram of a typical CSTGB system.

The gasification process in the CSTGB system includes several stages, with the emphasis primarily on pyrolysis and gasification. The pyrolysis stage involves the decomposition of feedstock in the absence of oxygen, producing char and volatile compounds (12). Subsequently, the gasification stage transforms these products into a high-quality producer gas with an elevated LHV (65), greatly enhanced by solar thermal heating. Notably, the combustion stage, typically essential for providing the necessary heat for the gasification process, it can be significantly reduced or bypassed in the CSTGB system when fully driven by solar thermal energy (66). However, some CSTGB systems are designed to partially rely on combustion of feedstock to supplement the required heat in scenarios of insufficient solar energy (during nighttime or overcast conditions) (31). This hybrid approach ensures continuous operation and maintains high efficiency in conversion, even in the absence of optimal solar conditions (67). This adaptability highlights the CSTGB system's innovation in integrating renewable solar energy with conventional biomass conversion techniques.

2.2.1 Pyrolysis

Pyrolysis is a critical component of the gasifier, it decomposes biomass feedstocks into solid biochar, bio-oil, and producer gas under oxygen free conditions. The efficiency of this process is significantly enhanced by the consistent and high temperatures achieved through concentrated solar thermal energy. This leads to an improved yield and quality of the produced products (*i.e.*, char, fuel, and producer gas), aligning with the goal of efficient biomass conversion (68).

The pyrolysis process is categorized into slow, fast, and flash pyrolysis, each distinguished by the heating rate and residence time (69). Flash pyrolysis operates at higher heating rates and shorter residence times (<2s) and requires specific feedstock particle sizes (105–250 μm) (70). Fast pyrolysis heats feedstocks rapidly to 450–600°C in the absence of air, efficiently producing producer gas and biochar (71). This method can convert up to 60–75wt.% of feedstock into biofuel with yields from 35.4% (*i.e.*, corn stover) (72) to 60.3% (*i.e.*, tulip poplar) (73). Moreover, it increase the energy density by about 6.5 times and reduces the land area required for fuel storage and processing by 50% (74).

In the CSTGB system, the pyrolysis process represents a critical component of the gasifier. Integrating solar thermal energy into pyrolysis technologies employ diverse methods to process various types of feedstocks aiming to produce different products under specific heat flux densities and reactor configurations. Antal *et al.* (75) represented a solar driven pyrolysis method use small particle biomass as the feedstock. They utilized a solar simulator equipped with high-power tungsten halogen lamps and elliptical mirrors. In this setup, biomass was placed at the focal point of the elliptical mirror converting the biomass into biofuel more effectively through control of focused thermal energy. Small particles (*i.e.*, sawdust and agricultural residues) were rapidly heated under high heat flux density, leading to swift pyrolysis reactions. Consequently, the more complete decomposition of biomass converted in biofuel with high conversion rate up to 70%.

Chan *et al.* (76) developed a solar driven pyrolysis method using large particle feedstock. This method involved the use of a single-particle glass reactor to process wood pellets of 5–15 mm thickness and applied a heat flux of 80–130 kW/m^2 by using a 1,000-watt xenon arc lamp for unidirectional heating (in the horizontal direction). They indicated that both particle thickness and heat flux have a combined effect on the distribution of pyrolysis products. High temperatures and extended residence times

inside the particle enhanced secondary tar reactions, resulting in the lowest tar yield and highest gas yield when the thickest particles were subjected to the highest heat fluxes. Gronli *et al.* (77) utilized wood pellets (*i.e.*, Norwegain birch, pine, and spruce) in a uniform cylindrical shape were one-dimensionally heated on one side in a single-particle bell-shaped Pyrex reactor using a xenon arc lamp. The experiments utilized two different heat fluxes (low heat flux as 80 kW/m^2 and high heat flux as 130 kW/m^2). They extend the heating time from 5 to 10 minutes resulted in a significant increase of approximately 77% in the conversion fraction. Concomitantly, there was an observed elevation in the ultimate yields, with char increasing from 25.7wt.% to 29.8wt.% and producer gas yields rising from 34.5wt.% to 45.8wt.%.

Antal *et al.* (78) developed and operated a solar driven biomass flash pyrolysis reactor specifically for the production of biocrude. This reactor achieves a maximum heat flux density of 1.3 MW/m^2 in the focal zone, equivalent to a total maximum power of 400 kW. In the process, biomass particles (*i.e.*, corn cob and hard wood) ranging in diameter from 425–710 μm were fed into the top of vertical reactor using screw feeder. The biomass particles then fell into a region of intense solar radiation surrounded by a water-cooled reflective cylindrical cavity. Subsequently, N_2 at a flow rate of 200–1,000 ml/min was employed to purge the screw feeder and remove the gaseous phase pyrolysis products (*i.e.*, vapors) were trapped at the top of the reactor. Due to insufficient residence time in the high temperature coal zone, a maximum of only 50% of the biomass particles underwent pyrolysis. stream flowed upwards to create a countercurrent flow of biomass particles and gases, reducing the descending velocity of the biomass particles. Contrary to expectations, the process yielded lower quantities of biocrude and a significant volume of hydrocarbon-rich gases. A considerable fraction of the biocrude condensed on the incoming biomass was reintroduced into the reactor, promoting secondary reactions. These reactions notably increased gas yield, with CO concentrations increasing from 46.7 to 54.6mol%, H_2 from 13.4 to 21.8mol%, and CH_4 from 8.5 to 13.0mol%.

Beattie *et al.* (79) employed high-temperature pyrolysis using coal as feedstock to yield producer gas in a vertical solar furnace (operating within a heat flux range of $1\text{--}9 \text{ MW/m}^2$). This technique achieves a maximum devolatilization rate of 51% and an optimal producer gas yield of 31 mmol/g_{coal} at solar flux level of 1 MW/m^2 . These solar driven pyrolysis methods showcase the adaptability of solar energy in processing various materials, each producing distinct products under different conditions. The

most abundant gases produced were H₂ as 23.7 mmol/g_{coal} and the yield of CO₂ was 0.71 mmol/g_{coal} increasing with the heat flux. These solar-driven pyrolysis methods demonstrate the adaptability of solar energy in processing various materials, each producing different products under varying conditions. This adaptability has been further enhanced by recent advancements in pyrolysis technology (*i.e.*, catalytic fast pyrolysis) significantly aiding in the production of high-quality biofuels and chemicals, and enhancing the heating value of biofuels and the overall efficiency of the biomass conversion process (80).

In the field of solar-driven pyrolysis, numerous methods are utilized to process biomass into products (*i.e.*, biochar, biofuel, and producer gas), showcasing the capacity of solar energy to enhance pyrolysis efficiency and product quality, especially through precise heat flux density control and reactor design. Beyond driving the pyrolysis process, solar energy also plays a crucial role in the gasification process. Gasification extends the process of pyrolysis by directly converting biomass into valuable producer gas.

2.2.2 Gasification

Gasification is another thermochemical conversion process different than the pyrolysis, in which producer gas as the main product (mainly consisting of H₂, CO, and CH₄) is produced in the presence of the gasifying agent (*e.g.*, air, oxygen, and steam) supplying limited oxygen (81). The gasification process consists of four stages (*i.e.*, drying, pyrolysis, combustion, and reduction) (82). The moisture content of biomass feedstocks is usually reduced to 5–10% in the drying stage (49, 83). In the pyrolysis stage, biomass is decomposed into volatile matter and char in the absence of oxygen (84). In the reduction stage, the char is reduced to generate H₂, CO, and CH₄. In the combustion zone, the most amount of heat is from the volatile gas reacting with gasifying agent (*i.e.*, steam, air, or oxygen) at high temperatures, this heat supply is crucial in driving the gasification process effectively. Moreover, it is important to note that different gasifying agents have a significant impact on the efficiency and the products (81).

The equipment required for air gasification is simpler than others (*i.e.*, steam and oxygen gasification), it is easy to operate and maintain with low cost (85-87). However, air gasification has lower reaction efficiency and the calorific value of the producer gas because additional heat is lost in the form of N₂. A higher amount of air is

needed to increase the temperature of gasification process, which will degrade the quality of producer gas (88, 89).

Incorporating the CSTGB system within the overall framework, the air gasification plays a central role in generating producer gas, which can subsequently be converted into electricity using a steam/gas turbine, thus contributing to the production of clean and sustainable energy.

2.3 Types of gasifiers

The CSTGB system incorporates an upgraded/modified gasifier, which is an improved version of the conventional gasification reactor. Gasifiers can be classified into different types based on the bed configuration, including fixed bed ones (*e.g.*, downdraft and updraft gasifiers), fluidized bed ones (*e.g.*, bubbling and circulating bed gasifiers), and entrained flow ones (90).

2.3.1 Fixed bed gasifier

Among the various fixed bed gasifiers, the downdraft fixed bed gasifier exhibits relatively lower heat transfer rates compared to others (*i.e.*, updraft, fluidized bed, and entrained flow gasifier). This limitation hampers the efficiency of thermal energy utilization in thermochemical reactions and potentially reduces the calorific value of producer gas. In a downdraft reactor, the gasifying agent (*i.e.*, air) and feedstocks are introduced from the upper part and products leave from the bottom. Besides, a large amount of heat is expelled from the bottom with the producer gas, and it ultimately reduces the overall efficiency of the system.

An updraft fixed bed gasifier introduces gasifying agents and feedstocks from the bottom, with producer gas is generated near the gate at the bottom through thermochemical reaction and leaves from the top part (52). Updraft gasifiers are considered appropriate for feedstocks characterized by an ash content (up to 15wt.%) due to the presence of a filtering effect in the bed reduces the likelihood of interaction between the deposited ash and the producer gas (64). However, the formation of tar poses a major technical challenge in updraft gasification. Gerone *et al.* (91) found that the type of gasifying agent, residence time, and average reaction temperature influenced the main product yield. In their study, the tar as the main product its yield was 137 g/kg_{feedstock} in air gasification and 163 g/kg_{feedstock} in steam gasification. The product type was inversely proportional to the residence time and proportionate to the average

temperature of the reactor.

In the CSTGB system, upgraded updraft fixed bed gasifiers (UUFBGs) are designed to flexibly harness solar thermal energy, either directly or indirectly. For direct utilization, UUFBGs are integrated with the CST system, which focuses and reflects solar radiation directly onto the gasification bed, effectively using the concentrated solar energy for the gasification process. On the other hand, the indirect utilization involves an upgraded design of gasifiers that leverage a thermal energy storage (TES) system. Solar thermal energy is captured and stored within the TES, enabling the gasifier to operate continuously and efficiently during the period of solar intermittency or unavailability. This ensures a stable thermal energy supply to the gasifier, essential for its consistent performance. In both approaches within the CSTGB system, the integration of sophisticated heat storage and a control system is important for efficient energy management, allowing for the precise control and effective storage of thermal energy, thereby optimizing the operation and performance of the UUFBGs.

Table 2.1 demonstrates that the solar driven UUFBGs are suitable for small biomass particles and have various advantages such as stable thermochemical reaction process, high producer gas yield rates and quality, high conversion rates, and high feedstock utilization rates (21, 92-94). Boujjat *et al.* (95) found that variability in solar energy (caused by cloud passages and shut off at night) created inherent obstacles to the utilization of solar assisted thermochemical processes. They built a dynamic model for a large-scale concentrated solar thermal UUFBG to determine the temperature and gas production evolution during day and night, considering both solar-only and hybrid solar/autothermal modes. They found that storing intermittent solar energy into a heat storage system could stabilize process operation and ensure continuous production of producer gas during the night and during cloudy periods. Jin *et al.* (94) developed a thermodynamic model for solar-driven supercritical water UUFBGs that includes solar energy storage equipment (*i.e.*, TES) to overcome the disadvantage of solar discontinuity. They found that the model fraction of H₂ in the model reached 65.6% at 750°C. At 600–700°C, the highest energy and exergy efficiencies were 74.84% and 34.87%, respectively, and the producer gas yield efficiency was 18.15%.

Table 2.1 Fixed bed gasifier studied.

	Type of gasifier studied	Feedstock used	Parameter(s) studied	Findings	Ref(s)
Downdraft gasifier	Imbert downdraft gasifier	Woody biomass	Temperature, ash and moisture content, producer gas yield	<ul style="list-style-type: none"> An inherent constraint associated with woody biomass utilization pertains to the requirement of uniform size and shape for effective utilization purposes. The producer gas derived from woody biomass exhibits a lower tar-oil content (below 1%), elevated temperature (approximately 700 °C), and a comparatively higher concentration of particulate matter. 	(96)
	Throated downdraft gasifier	Cotton stalk and wheat straw	Fuel density, ash content, cold gas efficiency, and particle size	<ul style="list-style-type: none"> Introducing a rotating grate and double conical hopper improved downdraft gasifier efficiency and reduced bridging and slag agglomeration. 	(97)
	Downdraft gasifier	Rice husk and pellet	Temperature, feedstock feeding rate, gas heating value, and cold gas efficiency	<ul style="list-style-type: none"> The rigorous evaluation, it was established that the cold gas efficiency for rice husk gasification surpasses 60%, while the utilization of rice husk pellets further enhances this efficiency, achieving an impressive rate exceeding 70%. For the gasification process, it was determined that the ideal excess air ratio stands at approximately 0.6 when utilizing rice husks, while a more efficient ratio of 0.3 is recommended when working with rice husk pellet. The gasification process involved a temperature range spanning from 600 to 850 °C, accompanied by an excess air ratio of 0.45–0.60 for rice husk gasification and a narrower range of 0.20–0.32 for rice husk pellet gasification. 	(98)
Updraft gasifier	Steam and non-steam gasifier	Almond shell	Producer gas composition, agent, molar fraction, temperature	<ul style="list-style-type: none"> Steam addition affected the chemical species and thermal profile. Steam had a notable impact on the gasification process, resulting in enhanced hydrogen production. As a result, the cold gas efficiency improved, and there was a significant increase in the H₂ to CO ratio rising from 0.46 to 0.77. In a continuous-mode pilot plant operation, an examination of the producer gas composition was conducted at various heights within the biomass bed. 	(91)
	Air gasifier	Solid waste	Exergy efficiency, low heating value, temperature, equivalence ratio, and volatile content	<ul style="list-style-type: none"> Updraft fixed bed gasifiers have higher exergy efficiency, while downdraft fixed bed gasifiers produce gas with higher heating value. Air gasification exhibits higher exergy efficiency compared to steam and pure oxygen gasification. 	(99)

				<ul style="list-style-type: none"> The peak exergy efficiency is attained when the gasification temperature reaches approximately 1000 °C and maintains an equivalence ratio (ER) within 0.33 to 0.36. Gasification efficiency is higher when the raw materials have a higher volatile content. 	
UUFBG	Solar gasification reactor of vertical-axis parabolic concentrator	MSW	Biomass feeding rate, producer gas yield, temperature	<ul style="list-style-type: none"> Overheating reactors and excessive temperature changes will lead to more heat loss. The H₂:CO ratio in producer gas composition reduced during night. 	(92)
	Solar jet spouted bed reactor for biomass gasification	Beechwood	Temperature, biomass feeding rate, particles velocity	<ul style="list-style-type: none"> Direct heating the reactor can increase the H₂ yield. Smaller particles could increase both the solid and gas residence times. 	(93)
	Tubular solar reactor for biomass gasification	Woody biomass	Temperature, mass balance, energy conversion efficiencies,	<ul style="list-style-type: none"> Maximum H₂ and minimum CH₄ yields at 1,400°C. 93.5% of carbon conversion rates is generated during solar runs. 	(21)
	Solar driven supercritical water biomass gasification	Biomass	Temperature, molar fraction	<ul style="list-style-type: none"> The maximum hydrogen production is generated when the temperature reaches 750°C. Solar energy provides 75% energy and 35% exergy efficiency. 	(94)

2.3.2 Fluidized bed gasifier

Fluidized-bed gasifier (FBGs) exhibit superior suitability for CSTGB systems due to their enhanced heat and mass transfer facilitated by the fluidization of bed material through the gasification flow (100). FBGs promote the interaction between gas and solid phases, resulting in higher concentrations of hydrogen in the producer gas in Table 2.2 (100-102). They offer higher flexibility in terms of the selection of feedstocks (103). FBGs are further classified into bubbling and circulating ones. Bubbling beds gasifiers have lower gas velocities than circulating bed ones that are enhanced by pneumatic flow (104). In an upgraded FBG, feedstock particles are suspended, providing a larger surface area for thermochemical reactions and improving the utilization of solar thermal energy. Suarez-Almeida *et al.* (105) proposed a method for a steam gasification of biomass using solar energy in a solar-driven dual fluidized bed gasifier (SDFBG) and reported an increase of the efficiency by 115% under optimal gasification temperature conditions (900–1,000°C) as compared to the conventional (non-solar) one. They also claimed that the SDFBG technology has a 78% char conversion rate and shorter reaction time (20–30 mins) as compared to the conventional one (average char conversion rate of less than 50%).

Table 2.2 Fluidized bed gasifier used for CSTGB system.

Type of gasifier studied	Feedstock	Parameter studied	Findings	Ref (s)
Solar gasification of biomass in a dual fluidized bed	Biomass	Internal solid circulation ratio, biomass space-time, the char residence time in the gasifier, char conversion ratio, producer gas yield, and solar share.	<ul style="list-style-type: none"> • Solar gasifier system has high char conversion rate (80%) at summer. During winter, the char conversion rate is 18–60%. • The solar thermal storage system makes the solar gasifier more stable, and char conversions in gasifier can take place throughout the whole year. 	(105)
Solar-driven steam gasification with indirectly irradiated fluidized-bed reactor	Sewage sludge	Molar flow rate, particle density, diameter, shape, gasifying agent, superficial/minimum fluidization velocity, and solar flux.	<ul style="list-style-type: none"> • The fluidized bed reactor provides fast heat and mass transfer. 	(100)
Bubbling fluidized bed gasification	Coconut husk	Gas yield, temperature, and air humidity.	<ul style="list-style-type: none"> • Fluidized bed gasification provides higher H₂ concentration in the fuel gas than fixed bed gasification. 	(102)
Solar-driven steam gasification with indirectly irradiated fluidized-bed reactor	Sewage sludge	Total molar flow rate, temperature, solar power, gas concentration, location at bed height, lower heating value (LHV), H ₂ yield, H ₂ O content, and gas composition.	<ul style="list-style-type: none"> • The yield of H₂ obtained by solar gasifier is 61.2–67.6 g/kg. • Increasing the content of H₂O in gasifying agent, the lower heating value of cold gas can be improved (from 1.54 to 9.73 MJ/m³) • Increasing the H₂O content reduces the solar upgrade ratio and solar to fuel efficiency. 	(100)

2.3.3 Entrained flow gasifier

Entrained flow gasifiers (EFGs) are fed with small particles, in which oxidants (air/oxygen) and water are introduced at the same time. The oxidant and steam surroundings cause solid particles to be entrained as they pass through the reactor (106). They have high feedstock conversion rates (98.0–99.5%) due to high operating temperature (927–1,127°C), fine pulverization, and an extremely turbulent flow (107). Biomass can be introduced either in a dry form (using a lock hopper system) or as biomass slurry (using high-pressure water pumps). Although the biomass slurry mode is more natural to operate, it introduces an additional portion of water into the gasifier, which requires extra heat for evaporation. This method increases the H₂/CO ratio of producer gas and decrease the thermal efficiency of the process (108). Van Eyk *et al.* (109) investigated the effect of high-flux solar irradiation on biomass gasification in an entrained-flow reactor. They showed that the carbon in the gasification stage can be converted more quickly with sufficient solar energy (4 MW/m²). The combined concentrated solar thermal with gasification technology increased the H₂/CO ratio from 0.77 to 1.40, while the CO₂/CO ratio decreased from 0.29 to 0.05 as the solar flux increased from 0 to 100% of the maximum requirement. Besides, the instantaneous solar share increased from 0 to 37% and the upgrade factor $((LHV_{\text{producer gas}} \cdot m_{\text{producer gas}})/(LHV_{\text{feed}} \cdot m_{\text{feed}}))$ increased from 78% to 140%, when the solar flux rose from 0 to 100%.

2.4 Parameters affecting gasification process

The CSTGB system is influenced by various process conditions such as biomass particle size, temperature, and the existence of catalyst, *etc.*

2.4.1 Particle size

The size of biomass particles can impact thermochemical reaction processes, especially the heat transfer rate (101). Chuaboon *et al.* (110) conducted experimental studies on different biomass feedstocks using a 1.5 kW_{th} solar energy driven steam gasification device. They found that the yield of producer gas (especially H₂) was 83.2 mmol/g_{biomass} in the range of 0.3–0.4 mm in particle size. Krishnamoorthy *et al.* (111) indicated that the heat transfer on the surface and inside of particles becomes lowered with the increase of particle size, affecting the yield and composition of producer gas

(high heating rates corresponding to more small-molecule gases, and less char and tar). Besides, Safine *et al.* (112) presented that the heating rate of small particles is higher because of larger specific surface areas, improving the heat and mass transfer between the particles during the thermochemical reaction process and thus the efficiency of gasification. Hernandez *et al.* (113) indicated that the pyrolysis reactions were enhanced as the particle size was reduced. They found experimentally that the release of volatiles and particle carbonization in the pyrolysis phase gradually increased as the feedstock particle size decreased from 8.0 to 0.5 mm. For the particle size below 1.0 mm, the char gasification reaction would be more intensive. Kodama *et al.* (114) investigated the effect of particle size (*i.e.*, 200 μm and 300 μm) on the behavior of gasification. The fluidization porosity increased when the particle size decreased from 300 to 200 μm , resulting in a 33% increase in the bed height, which led to an increase in the diffusivity of incident thermal radiation through the bed. When the particle size was reduced, the total heat transfer area for a given volume increased more favorably for a fast and homogenous reaction. They also emphasized that over-small particle size led to increased heat loss through the reactor wall. When the particle size was reduced from 300 to 200 μm , the reactor wall temperature increased by 15%.

As summarized in Table 2.3, the impacts of different biomass particle size on the CSTGB system are significant and varied. This encompasses a range of biomass types (*i.e.*, beech wood, pine, oak, corn stover, wheat straw, coconut shell, rice husk, sugar cane, and almond shell). The studies indicate that the optimal particle size range is 0.28–2.5 mm, which achieves higher yields and purity of producer gas while reducing the content of CO_2 , char, and tar. This range promotes rapid and uniform reactions and enables efficient and rational utilization of thermal energy. Within this particle size spectrum (*e.g.*, reduces the CO_2 and tar/char content of the product; makes efficient and rational use of thermal energy and promotes fast and homogeneous reactions), the advantages of solar thermal chemical processes are maximized, leveraging the potential of solar energy in the biomass conversion process.

Table 2.3 Impacts of particle size on CSTGB system.

Feedstock	System scale	Particle size (mm)	Temperature (°C)	Char product yield (wt.%)	Oil product yield (wt.%)	Gas product yields (wt.%)	Ref (s)
Beech wood	N. A	0.2–0.5	300–900	17.0–39.0	44.0–53.0	18.0–27.0	(115)
		0.9–1.7		17.0–49.0	36.0–55.0	15.5–25.0	
		2.1–3.2		20.0–55.0	32.0–56.0	13.0–22.0	
Beech wood	1.5 kW _{th}	0.3	1,200	25.0–30.0	17.0–35.0	40.0–53.0	(116)
Beech wood	1.5 kW _{th}	0.5	1,100–1,300	7.0	N. A	22.0	(117)
		2.0		33.0	N. A	37.0	
		4.0		30.0	N. A	22.0	
		8.0		36.0	N. A	19.0	
Pine	10 MW _{th}	1.0	400–800	20.0–40.0	35.0–50.0	25.0–35.0	(118)
		2.5		25.0–45.0	30.0–45.0	25.0–40.0	
Oak	1 MW _{th}	1.0	400–800	15.35	47.5	35.0	(119)
		3.0		29.0	42.5	30.5	
Corn stover	N.A	1.0–2.5	300–700	10.0–32.0	20.0–45.0	23.0–50.0	(120)
Wheat straw	0.5 MW _{th}	1.0–2.5	300–700	8.0–23.0	15.0–33.0	18.0–35.0	(121)
Coconut shell	0.5 MW _{th}	0.5	500–900	22.0–36.0	28.0–42.0	30.0–45.0	(121)
Rice husk	15 MW _{th}	1.5	500–900	18.0–38.0	20.0–35.0	25.0–40.0	(122)
Sugar cane	100 kW _{th}	2.0	400–700	12.0–28.0	22.0–37.0	20.0–35.0	(19)
Almond shell	1 MW _{th}	2.5	400–800	20.0–35.0	25.0–40.0	20.0–30.0	(119)

2.4.2 Reaction temperature

Concentrated solar thermal energy plays a crucial role in the CSTGB system, particularly in providing the necessary heat for the pyrolysis and gasification stages. Concentrated solar energy focuses solar radiation to generate high-temperature thermal energy, which is conducive to increasing the yield of H₂. Chuayboon *et al.* (110) conducted an experimental study based on three biomass feedstocks (beech, pine, and spruce wood) using a 1.5 kW_{th} solar steam gasifier and presented that the feeding rate must be increased at the same time as the supply temperature, it improves the yield of producer gas and keeps the carbon conversion rate above 90%. Thus, the optimal temperature provided by the solar thermal collector is one of the critical design parameters. Ravenni *et al.* (123) presented a series of tar cracking and adsorption tests under different temperature conditions (250–800°C). The aromatic compounds in the char bed were decomposed to produce H₂ when the temperature of the char bed rose to 600°C. As the temperature rose to 800°C, the yield of H₂ increased significantly. At higher temperatures, the secondary tar cracking reactions at pyrolysis are accelerated, which would increase the H₂, CO, and hydrocarbon generation and enhance the decomposition of tars.

However, a major limitation of solar energy is its intermittency. Since solar

energy is unavailable at night, the CSTGB system is used to combust a portion of the feedstock at night to supplement the required heat in the same way as conventional gasifiers. While this method can maintain system operation in the absence of solar energy, it may reduce overall energy conversion efficiency and the quality of the producer gas. A more effective strategy involves the use of TES system. The TES system stores thermal energy when solar radiation is intense and then releases this energy during the night or periods of insufficient solar radiation. This approach not only ensures the CSTGB system's efficient operation at night but also helps to smooth out fluctuations in solar energy supply, enhancing the system's overall reliability and stability. For example, Salem *et al.* (124) established the modelling of tar formation, conversion, and destruction along a downdraft gasifier to reduce and eliminate the tar formation. Their model included sensitivity analyses of four major tar species (benzene, naphthalene, toluene, and phenol) at 0.20–0.35 equivalent ratios (ERs) and three different temperatures (800, 900, and 1,100°C). They found that the tar yield was lower (0.01–6.00 g/Nm³) when the ER value was 0.24–0.36, and the water content was less than 10wt.%. They also showed that effective control of tar yield and improved gasification efficiency can be achieved by appropriately adjusting operational parameters (equivalence ratios and temperature), even in the face of intermittent solar energy supply.

Overall, concentrated solar thermal energy is pivotal in the CSTGB system, not only providing essential high-temperature thermal energy during the day but also ensuring continuous and efficient operation through nighttime partial feedstock combustion or thermal energy storage system.

2.4.3 Catalysts

In CSTGB systems, research on catalyst usage is relatively limited. It is anticipated that the accumulated knowledge of catalyst use in conventional gasification processes could be applicable to CSTGB systems. However, more research is needed to adapt these principles to optimize CSTGB systems, considering its specific characteristics. The use of catalysts is primarily focused during the gasification process and in the post-gasification exhaust gas treatment stage to enhance biomass pyrolysis and gasification reactions. This improves gasification efficiency and the quality of produced gas. Catalysts play a crucial role in degrading tar during gasification, a major challenge for CSTGB systems. The presence of tar not only reduces the quality of

producer gas but also poses a significant barrier to CSTGB commercialization due to contamination of downstream equipment. Ren *et al.* (125) argued that the physical purification has non-negligible disadvantages, wet purification results in liquid mist in the producer gas, equipment is difficult to be cleaned, the purified liquid is difficult to recycle and cannot withstand high gasification temperature. The drying purification technology has a wide range of tar adaptability and high removal rates. However, it makes the equipment costly and inconvenient to operate. They concluded that the use of catalyst reduction methods (*i.e.*, heterogeneous catalysts, nickel-based catalysts, noble metal catalysts, natural catalysts, and wood charcoal catalysts) could effectively reduce tar production and increase hydrogen production to achieve efficient use of combustible gases at low temperatures. They presented those catalysts can reduce the activation energy required for pyrolysis reaction, reduce the input of gasification media and achieve more useful products through directional catalytic cracking of tars in biomass gasifier. Lind *et al.* (126) used the FeTiO_3 as a catalyst to reduce the tar content of gasification production (original tar content is 30 g/Nm^3) from Chalmers' gasifier by 35%. They observed that the FeTiO_3 catalyst remained active throughout the reaction, and the carbon deposits on FeTiO_3 were continuously removed by oxidation to carbon dioxide. The results demonstrated that the use of FeTiO_3 as a catalyst resulted in an increase in the H_2/CO ratio from 0.7 to 3.0. Moreover, typical catalysts used in conventional gasification processes include dolomite catalysts (CaO and MgO), alkali metal catalysts (*e.g.*, Li, Na, K, Rb, Cs, and Fr) and noble metal catalysts (*i.e.*, Pt, Pd, and Au) (127) could potentially be applicable to CSTGB systems.

The effective utilization of catalysts CSTGB systems is a crucial method for addressing the significant problem of tar formation, it is a byproduct of the gasification process that poses substantial commercial barriers. Tar can condense and accumulate within the gasification system, leading to equipment clogging and corrosion. This necessitates frequent maintenance and cleaning, thereby increasing operational downtime and costs, and reducing equipment lifespan. Additionally, tar complicates gas cleaning and upgrading processes, requiring more complex and expensive technologies to ensure the purity of the producer gas for further applications. To mitigate these issues, physical purification methods (*e.g.*, wet and dry purification) and chemical purification (thermochemical and catalytic reduction) are commonly employed for tar removal (127-129). Catalysts can be directly added into biomass through wet impregnation, it significantly reduces tar content and methane in producer gas. They can effectively

increase the gasification conversion rate by up to 30% as found by Qin *et al.* (130).

Dolomite catalysts have garnered significant attention in gasification research due to their promising properties. The dolomite catalyst acts as an effective catalyst in gasification process, particularly for tar reduction and enhancement of gas quality. Simell *et al.* (129) presented that the dolomite catalyst demonstrated 100% conversion of tar produced in an updraft gasification and 99% conversion of tar produced in a fluidized bed gasifier in a laboratory-scale reactor. They could increase the producer gas yields at the expense of liquid products and achieve a theoretical 0% tar formation. Alkali catalysts can be directly added into biomass by wet impregnation, which significantly reduces tar content and reduces the methane content of producer gas. They can act as secondary catalysts because of their high resistance to carbon deposition, but they are difficult to recover and relatively costly (130-133). In contrast, noble metal catalysts have higher and more stable activity in partial oxidation compared to alkali metal catalysts (134). It has high reducibility because of special electronic, optical and catalytic properties, and excellent chemical stability. Halder *et al.* (135) found the reducibility of a Cu-Ag-Au based noble catalyst was as high as 98.6%. The activity of noble metal catalysts in the gasification of biomass to producer gas was found to decrease in the order of Rh>Pd>Pt>Ru at 527 °C (136). Sikarwar *et al.* (137) summarized that noble metal catalysts had excellent properties for the gasification reaction in the range of 527–647 °C and about 98–99% of the carbon in biomass feedstocks was converted to gas at 600 °C. The carbon conversion rates for the conventional nickel-based and dolomite catalysts were 73% and 43% under the same condition. It also effectively reduced the sulfur and carbon contents in the producer gas.

In summary, the effective use of heterogeneous, nickel-based, noble metal-based, and natural catalysts in CSTGB systems is vital for de-tarring and enhancing gas quality. The future of CSTGB systems depends on the ability to effectively utilize catalysts during and after the gasification process to improve the yield and quality of producer gas, thereby addressing the commercial barrier posed by tar formation.

2.4.4 Gasifying agent

Gasifying agents such as air, oxygen, air-steam, and steam serve as oxygen sources of the gasification process. The equipment required for air gasification is simple, easy to operate and maintain, and with a low operating cost (85-87). However,

air gasification loses additional heat in the form of nitrogen; nitrogen is not conducive to gasification reactions and reduces the calorific value of producer gas.

Oxygen gasification can achieve a higher reaction temperature and higher efficiency as well as a higher calorific value of product gas than air gasification. Siwal *et al.* (138) found that increasing the amount of oxygen supply for gasification increased the LHV of producer gas produced by nearly 30–40%.

For steam gasification, the supply of steam drives the reversible water-gas shift (WGS) reaction in the forward direction ($\text{CO} + \text{H}_2\text{O} \leftrightarrow \text{CO}_2 + \text{H}_2$, $\Delta H^\circ = \pm 41 \text{ kJ/mol}$) and promotes the production of H_2 and the calorific value of the producer gas (139). Additionally, the use of steam would decrease the gasification temperature. The WGS reaction is exothermic and thus is thermodynamically unfavorable at a high temperature. This is illustrated by the continuous decreases in Gibbs free energy as a function of temperature and the corresponding decrease in equilibrium constants with increasing temperature. Hence, the lowered temperature due to the use of steam would also promote the WGS reaction in the forward direction. Meanwhile, Caitlin *et al.* (140) presented that the WGS reaction is temperature-sensitive, possessing a faster reaction rate with increasing temperature. They demonstrated a 20–40 times increases in the WGS reaction rate at temperatures from 327 to 1,727°C. Tang *et al.* (141) also presented that the H_2 concentration increased from 1.2% to 17.1% within the temperature increased from 250 to 550°C.

The steam to biomass (S/B) ratio has a significant impact on the composition of the producer gas. The solid carbon and methane are formed at a low S/B ratio. As more steam is supplied, the solid carbon and methane are converted to CO and H_2 . As the steam supply exceeds the biomass content, the formation of solid carbon and methane would decrease, and the yield of CO and H_2 would increase. Overall, the increasing in steam greatly facilitates the formation of H_2 in gasification. However, excess steam reduces the reaction temperature to the extent that large amounts of tar are produced, which is associated with the fact that the provision of excess steam lowers the reaction temperature resulting in a rapid reduction in the WGS reaction rate. Therefore, an optimized S/B ratio is desirable. Sepe *et al.* (142) stated that the S/B ratio directly affects the yield of H_2 , and the relatively high S/B ratio also increases the yield of CO_2 due to the saturation of the WGS reaction and the consequent consumption of CO. They used the CSTGB system and set the S/B ratio from 0.5 to 3.0 (the feedstock moisture

is 10wt.%), and the obtained producer gas had H₂ content increasing from 52.0% to 55.6% and CO content decreasing from 13% to 8%.

2.5 Gasification modelling

A comprehensive approach is crucial to effectively model the entire CSTGB system, encompassing the gasifier, TES, and heliostat field. Emphasis needs to be placed on the gasification model as it serves as the cornerstone of the system. The gasification model plays a pivotal role in ensuring the efficient conversion of feedstock through equilibrium or kinetic based approaches. Theoretical biomass gasification modelling can be divided into thermodynamic equilibrium and kinetic model. The thermodynamic equilibrium approach applies the method of Gibbs free energy minimization to reveal the thermodynamic boundaries under specific conditions (143-145). By incorporating materials balance, energy balance, and thermochemical balance considerations, equilibrium models enable an understanding of the gasification process from a thermodynamic standpoint. Kinetic models are based on the kinetic characteristics of the gasification process. While the TES and concentrated solar tower (CST) subsystem's primary purpose is to provide thermal energy to drive the gasification process in the gasifier. In this study, the TES and CST modelling focuses primarily on assessing the heating value required to meet the specific demands of the gasifier. Thus, it is imperative to integrate these auxiliary models with the gasification model, ensuring a cohesive and comprehensive understanding of the performance of the CSTGB system.

2.5.1 Thermodynamic equilibrium models

Thermodynamic equilibrium (TE) model is based on the axiomatic concept of thermodynamics to consider the internal state of a single thermodynamic system. There is no macroscopic change in an equilibrium system (*i.e.*, thermal, mechanical, chemical, and radiation equilibrium). For a TE state dictated by pressure and temperature, the Gibbs free energy is less than any other states at the same pressure and temperature. Introducing the standard Gibbs free energy in a thermodynamic model has a potential to calculate the maximum of reversible work at constant temperature and pressure, and to recognize if a reaction is spontaneous ($\Delta G < 0$) or non-spontaneous ($\Delta G > 0$) (146). Li *et al.* (147) showed that adding a non-stoichiometric (NS) equilibrium model improved the prediction performance for gasification through the equilibrium model and the NS

model evaluates the steam demand based on the water balance of feedstock and producer gas.

The TE model is the most suitable for preliminary studies about the effects of fuel types and process parameters and could also be used to predict the temperature of various parts of the gasifier and solar energy system. Wang *et al.* (148) used a TE model to analyze a CSTGB process and estimated the producer gas composition (17.7vol.% CO, 19.6vol.% CO₂, 3.0vol.% CH₄, 59.2vol.% H₂, and 0.4vol.% N₂) and supplementary energy (310 kW_{th} biomass energy and 60kW_{th} solar energy) based on the initial conditions of reaction temperature (900°C) and feedstock compositions (45.2wt.% C, 5.8wt.% H, 35.7wt.% O, 0.8wt.% N, and 0.1wt.% S), into the TE model to calculate the producer gas specie moles. The results showed that the CST technology could replace biomass combustion for heat generation and improve the utilization rate of biomass by 9.2%. Gomaa *et al.* (149) used a TE model to analyze the concentrated solar thermal fluidized bed gasifier. Lignite (77.3wt.% C, 5.3wt.% H, 14.2wt.% O, and 19.3wt.% N) and olive pomace (48.4wt.% C, 5.9wt.% H, 34.1wt.% O, and 0.9wt.% N) were blended into the fluidized bed with steam as the agent and temperature set at 827–977°C. They found that increasing the proportion of lignite in the mixture could increase the yield of H₂. The model confirmed that the concentration of H₂ and CO in the producer gas increased when the temperature increased from 727–927 °C. At the appropriate temperature (1,050–1,127°C), more O₂ lowered the content of H₂ and but increased the content of CO in the resulting producer gas. An increase in the H₂O level led to a greater H₂ production because the H₂O to C ratio had a strong negative correlation with temperature.

2.5.2 Kinetic models

In comparison to the equilibrium model, the kinetic approach offers a more comprehensive and precise depiction of the gasification process. This approach takes into account both the kinetic data and the thermodynamic characteristics of gasification reactions, resulting in a more detailed and accurate understanding of the process (150, 151). Kinetic models are often used to design and optimize the gasifier in a CSTGB system. Kinetic models are based on the estimation of main reactions' kinetics and the transfer phenomena for each phase in a gasification process, and they can be used to estimate the production of gas compositions under different operating temperatures

(152). Some researchers developed kinetic models for biomass gasification based on the shrinkage core models considering heterogeneous non-catalytic reactions. In these models, biomass particles act as porous media allowing water vapor and volatiles to escape into the reactor environment during the stage of pyrolysis. These models allow a detailed demonstration of transport phenomena and reaction kinetics within a biomass particle, including changes in temperature and reactant concentration gradients within the particle, as well as changes in the thermophysical properties (*i.e.*, conservation of mass, energy, and momentum) of reactants (153). Considering that biomass particles have different sizes and shapes, the effect of particle volume shrinkage during pyrolysis is generally not negligible. The shrinkage core models are based on the following assumptions: the biomass particle remains spherical, the thermal energy of the first order chemical reaction during pyrolysis is constant, the gas and solid phases within the biomass particle remain in the thermal equilibrium, the thickness of the reaction zone is constant, and the diffusion and mass transfer coefficients cannot change during the process (154).

Some kinetic models can clearly demonstrate the reaction process in different zones of the gasifiers and the suitable parameters for this zone could be defined easily. For example, Salem *et al.* (155) modeled four zones of a downdraft gasifier and found that the yield of producer gas was higher when the moisture content was less than 10wt.%, and the equivalent ratio was 0.30–0.35. Dejtkulwong *et al.* (156) used a kinetic model to simulate the drying zone for the downdraft gasification of biomass with a wide range of composition ($38.0 < C < 52.0$ wt.%, $5.5 < H < 7.0$ wt.%, and $36.0 < O < 45.0$ wt.%). It is shown that the water began to evaporate as the temperature reached 95°C and the pyrolysis process started at 200°C (157).

Sharma *et al.* (158) developed a kinetic model of a downdraft biomass gasifier to present that the oxidation zone provides the heat needed for drying and pyrolysis. Biomass combustion requires air to be completed, the process of gasification and reduction processes are performed to produce producer gas if the air is less than the required stoichiometry. They summarized that the oxidation order depends on the reaction rate of pyrolysis products and chemical reactions of the oxidation process: (1) hydrogen-containing substances are first oxidized, (2) CO oxidation occurs, (3) the CH₄ produced by pyrolysis is oxidized if the oxygen remains, (4) if more oxygen is available, the oxidation of the tar and char is re-oxidized. Hameed *et al.* (159) conducted

the kinetic model analysis of five biomass feedstocks (*i.e.*, wood sawdust, douglas fir bark, bagasse, rice husk, and peanut hull) under isothermal conditions. They found that the rate of producer gas formation increases from 0.05 to 0.15 within a temperature range of 727–927°C.

The kinetic model is based on the kinetic rate for the reaction, which is appropriately used to study the CSTGB system. Li *et al.* (100) established a kinetic model for the sludge gasification process and found that increasing H₂O content in the gasifier agent could increase the lower calorific value from 1.54 to 9.73 MJ/m³ at 1,000 W/m². The H₂ yield range around 61.2–67.6 g/kg was achieved by solar steam gasification of sewage sludge which was affected by H₂O content and solar radiation. The efficiency decreased by 18.5–32.9% when the H₂O content in sewage sludge from 0wt.% to 100wt.%.

2.5.3 CFD models

Computational fluid dynamics (CFD) modelling is a method to analyze, design, and optimize the performance of gasifiers that is appropriate for the development of multidimensional gasification models (160). CFD models have been used to predict the distribution of temperature, concentration, and gas yield in a reactor (161). CFD models are based on the set of equations for the solution of mass, momentum, energy conservation, and species in a gasifier. CFD simulations are classified into two types of methods, the Eulerian-Lagrangian (E-L) approach and the Eulerian-Eulerian (E-E) approach. In the E-L approach, the gas phase is described by the Navier-Stokes equations and the solid phase is treated as discrete. Newton's law calculates the trajectory of each particle and the collisions between particles are defined by the soft-sphere model or the hard-sphere model. In contrast, the E-E approach treats the solid phases as a continuum and requires less computation, the method uses the kinetic theory of granular flow to estimate the transport characteristics of a solid phase (162).

Boujjat *et al.* (163) established two CFD models. The first method used the E-L approach to simulate the flow of fluid into the fixed bed. For the governing transport equation, they considered the mixture of fluid and solid particles to determine the temperature and tracking discrete particles in the fixed bed. In order to simulate the directly irradiated sputtered bed particle, the second model used the E-E approach, which analyzes momentum, energy, and radiation intensity transfer. The E-E approach consumes fewer computing resources, and both gas and particle phases are considered

as an interpenetrating continuum. CFD modelling studies of CSTGB systems are summarized in Table 6. The CFD models can combine the continuity, motion, and energy equations with the kinetics of homogeneous and heterogeneous reactions to calculate the mass and energy transfer in CSTGB systems. The simulation results are generally in good agreement with experimental data (160, 164, 165).

Table 2.4 summarizes some of the studies that have simulated biomass gasification using thermodynamic equilibrium, kinetic, and CFD models. The thermodynamic equilibrium approach applied Gibbs free energy minimization to reveal the thermodynamic boundary for a given condition (143, 144). A kinetic model provides a more detailed and accurate description of the gasification process than an equilibrium model. It considers the kinetic information and hydrodynamic properties of gasification reactions. Some studies have obtained accurate results by means of the finite element method (150, 151) and finite volume method (153, 166). Meanwhile, it is also demonstrated that CFD modelling could achieve more detailed and accurate results as it incorporates the factors of reactor design, fluid mechanics, mass, heat transfer, *etc.* (167, 168). Highly accurate simulations become necessary and useful for predicting product composition and optimal process condition (169-171), as well as providing the basis for downstream techniques such as LCA (172, 173) and TEA (174, 175).

Table 2.4 Equilibrium & CFD models of gasification.

	Feedstock	Temperature	Model studies	Parameter studies	Findings	Ref(s)
Downdraft	Rice husk, wood pellet	600–1,200°C	Thermodynamic equilibrium model & Gibbs free energy, kinetic model	Air flow rate, temperature, bed height	<ul style="list-style-type: none"> Apply chemical equilibrium results taken from the combustion zone that can increase the accuracy in kinetic modelling. 	(176)
Downdraft	Corn cobs, corn stover	800°C	Thermodynamic equilibrium model & Gibbs free energy	Oxygen content in air, ER, calorific value	<ul style="list-style-type: none"> Root mean square error (RMSE) added into thermodynamic equilibrium model improved the prediction of the calorific value. 	(177)
Downdraft	Brewers spend grain pellets	700°C	Thermodynamic heterogeneous equilibrium, stoichiometric equilibrium	H ₂ /CO & CH ₄ /H ₂ molar ratio of ER,	<ul style="list-style-type: none"> Carbon boundary point concept applied to the stoichiometric could increase the accuracy 	(178)
Downdraft	Biomass	127–727°C	CFD model	Producer gas composition, ER, volatile matter decomposition	<ul style="list-style-type: none"> CFD model hardly presents the producer gas compositions. CFD model is suitable for displaying the temperature in each reaction zone. 	(160)
Fixed bed	Leaf pellets	600–650°C	CFD model	Temperature, producer gas compositions	<ul style="list-style-type: none"> CFD model quickly presents physical and thermochemical conversion process 	(164)
Fluidized bed	Coal	427–627°C	CFD model	Gas compositions, angle, temperature, S/B ratio, efficiency, heating value, used agent	<ul style="list-style-type: none"> CFD model is more suitable for S/B ratio analysis and simulation. 	(179)
Fluidized bed	Wood	1,200–1,300°C	CFD model	Temperature, heating value, carbon conversion efficiency, cold gas efficiency, solar-to-fuel efficiency	<ul style="list-style-type: none"> Al₂O₃ bed material has the best resistance to thermal shocks and chemical inertness. The influence of bed material on the composition of producer gas remains very low (less than 7% for H₂) 	(163)

2.5.4 Stochastic based kinetic models

Various models have been proposed to analyze and comprehend the gasification process, which include the volume model, unreacted shrinking core model, and random pore model (180). The random pore model is widely acknowledged for its incorporation of pore growth and coalescence effects during the reaction, allowing for a description of the maximum reaction rate and producer gas yield at low conversion levels (181). In order to address the uncertainties associated with predicting producer gas composition, stochastic based kinetic gasification models have been introduced (182, 183). Unlike the CFD model that solve transport equations in all spatial dimensions, stochastic based kinetic model describes variables and mixing processes using probability distribution functions, thereby offering enhanced computational efficiency and accuracy (184, 185).

The stochastic-based kinetic model integrates stochastic variables (*i.e.*, particles size, emissivity, porosity, *etc.*), which collectively represent ensembles of discrete elements within porous solid biomass particles and the surrounding gases (185). This model adeptly replicates the turbulent exchange of both heat and mass within a real-world system (180). Within this framework, each stochastic particle encapsulates intricate interactions among the solid phase, pore gas, and bulk gas. Additionally, the reactor model is seamlessly linked to a kinetic model that encompasses both surface reactions and gas-phase reactions (183). The numerical solution is derived through a Monte Carlo (MC) approach, employing operator splitting techniques to facilitate efficient computation (183). Weber *et al.* (183) presented the stochastic based kinetic model is able to accurately predict all major species in the producer gas composition with significantly less computational time required compared to the CFD model. Mazaheri *et al.* (186) described the gasification process using a stochastic kinetic model based on the MC approach. They applied the model to study the influences of process parameters on the efficiency of the conversion process. Ahmed *et al.* (187) involved the pyrolysis and gasification of lignite at reactor temperatures ranging from 800–950°C with intervals of 50 °C. They employed the Gillespie algorithm for stochastic simulations of lignite pyrolysis and explored two reaction mechanisms: a single-step mechanism and the FLASHCHAIN mechanism. Their stochastic simulation results demonstrated a strong fit with the experimental yield of CH₄, suggesting that a first-order reaction mechanism is well-suited to produce CH₄. However, Xing *et al.* (184) argued that the stochastic kinetic model considered a limited number of process parameters and might not be sufficient to demonstrate the complex non-linear

relationships in the kinetic parameters (*i.e.*, reaction temperature) and biomass properties (*i.e.*, water content, porosity, and density). They suggested that machine learning (ML) algorithms could be used to account for the non-linear relationships for improving the accuracy of gasification modelling.

2.5.5 Machine learning models

The ML is a widely employed artificial intelligence (AI) technology, finds application in various domains (signal processing, function approximation, simulation, and pattern recognition) (188). ML capitalizes on learning and extracting system features to effectively predict system outputs using limited experimental data (189, 190). Figure 2.2 illustrates that ML algorithms can be categorized into two main types: supervised and unsupervised (191).

In supervised learning, models are trained using known input data (referred to as decision variables) along with corresponding output data (targets). The model learns to establish a mapping between the input data and their respective targets (192). This trained model can make predictions for given inputs, which are iteratively improved by comparing these predictions with actual data and minimizing the discrepancies between predicted and observed output. The choice of an appropriate supervised learning method is influenced by the size and specific attributes of the available dataset (192). Within supervised learning, further distinction is made between regression and classification algorithms. Both types deal with labeled datasets and are frequently employed in ML predictions; however, they differ in their approach to solving ML problems (191). Classification methods aim to identify discernible behavioral patterns within datasets, while regression methods establish correlations between dependent and independent variables (193). In unsupervised learning, the model relies solely on input data to discern similarities and differences within the dataset for appropriate classification. It is crucial to underscore that unsupervised ML predominantly deals with unlabeled data and is adept at revealing concealed patterns (194).

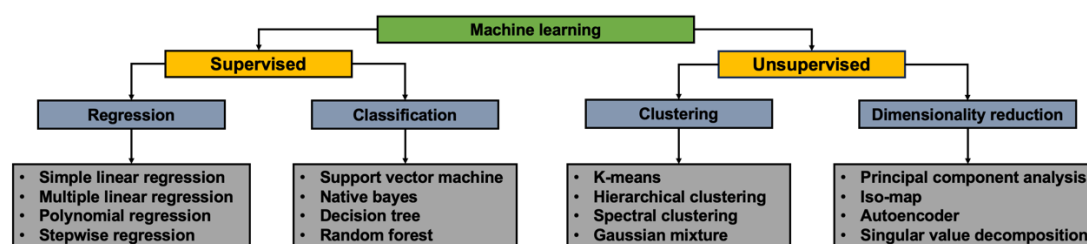


Figure 2.2 ML classifications.

The application of ML algorithms in CSTGB system is diverse, encompassing producer gas yield prediction, extensive parametric studies, process modelling, the quantification of char and tar formation as influenced by process parameters, and the advancement of catalysts for enhanced performance. Support vector machines (SVMs) are highly efficient in pattern recognition and classification tasks. They are particularly suitable for scenarios with smaller datasets or when precise classification is needed. They are effective in handling data in high-dimensional spaces and are generally more stable and accurate in solving classification problems than other algorithms (*i.e.*, Neural networks (NNs) and random forest (RF)).

NNs are widely used to simulate biomass gasification processes due to their capability in handling complex non-linear relationship (90). NN algorithms are highly suitable for simulating biomass gasification due to their remarkable flexibility in capturing and understanding the complex nonlinear relationships between input and output variables during the gasification process. Experimental data are often training the NN algorithm, while some of the metrics (*i.e.*, coefficient of determination (R^2), mean squared error (MSE), RMSE, *etc.*) are used to verify the model's accuracy (195). Shahbaz *et al.* (196) used the NNs to predict the composition of producer gas with high accuracy compared to experimental results. They found a maximum H_2 yield of 79.0vol.% at 692°C and CH_4 yield of 14.9vol.% at 650°C. Gopirajan *et al.* (190) utilized an RF algorithm for optimizing multi-parametric processes in biomass gasification (*i.e.*, biomass characteristics, temperature, pressure, steam/biomass ratio, and reaction time), achieving a model accuracy of 94%, thereby indicating the suitability of RF for optimizing complex gasification processes (*e.g.*, methanation, water-gas shift, steam reforming, pyrolysis, and hydrolysis) driven by multiple parameters. Xing *et al.* (184) employed empirical correlations (EC), NN and RF algorithms to study the impact of gasification parameters (*i.e.*, cellulose fraction, hemicellulose fraction, lignin fraction, and heating rate) on H_2 yield in fixed bed

gasification. They compared model predictions with experimental data and found that the NN and RF models presented high accurate predictions (determination coefficients < 0.8). They suggested that the EC model could not characterize complex non-linear relationships accurately. Instead, the NN and RF algorithms were better suited to represent these complex correlations, with the RF algorithm having the highest accuracy. RF algorithms excel in handling high-dimensional data and multi-parametric optimization. A notable advantage of RF is its lower requirement for training data and better resistance to overfitting. This makes RF a powerful tool, especially for analyzing and optimizing complex gasification processes that involve multiple influencing factors.

In the realm of CSTGB systems, characterized by the data-rich environments and complex inter-variable dynamics. The application of NNs, particularly long short-term (LSTM) – recurrent neural network (RNN) model emerges as profoundly effective. These models demonstrate exceptional proficiency in dissecting and interpreting the intricate, non-linear data patterns intrinsic to these systems (197). The LSTM-RNN architecture, distinguished by its sophisticated temporal analysis capabilities, is adept at navigating the complexities of both long-term and short-term data dependencies. This attribute is crucial for the precise forecasting of system behaviors and outcomes (198). The RF algorithm effectively addressing the gasification process in the CSTGB system. The RF algorithm is renowned for its robustness in multi-parametric data analysis and optimization, a critical aspect in understanding and improving gasifier performance. This robustness paired with a relatively lower demand for training data and enhanced resistance to overfitting (199). However, it is imperative to acknowledge that NNs (inclusive of LSTM-RNN models) typically necessitate extensive training data and substantial computational resources. This requirement can pose a significant constraint in situations where data availability or computational capability is limited (200). In this research, this challenge is navigated by developing foundational models upon which the RF and LSTM-RNN frameworks are trained, thereby maximizing the efficacy of the available data and computational resources.

The application of RF and LSTM-RNN algorithms in the CSTGB system not only enhances model accuracy and process parameter optimization but also amplifies overall system efficiency. The RF algorithm is specifically employed for simulating the gasification process, effectively managing the process's multi-parametric and high-dimensional data characteristics. In contrast, the LSTM-RNN model is utilized for

simulating the CSTGB system. its advanced capabilities in time-series analysis make it exceptionally adept at predicting both long-term and short-term system behaviors. This differentiated application offers a powerful tool for an understanding of complex CST system, aiding in future design and operational strategies. Future research should continue to explore the unique advantages of these algorithms to further optimize gasification performance within the CSTGB system.

2.6 Solar collector methods

At the Earth's surface, the energy density of solar radiation is approximately 1000 W/m^2 on a clear day, and the world's solar energy is 301 times of all existing coal power plants (201). The International Energy Agency (IEA) World Energy Balance report claimed that the solar energy accounted for 19% of renewable electricity generation in 2018 (5). The solar installations are experiencing significant growth with European Union-28 encouraging significant solar thermal development (202). Extensive studies have been performed to utilize concentrated solar energy as an economically viable and environmentally friendly heat source. Li *et al.* (203) proposed a new coupled optical, thermal and electricity model (model accuracy is 94.5%). They applied it to predict the performance of the concentrated photovoltaic thermal system under various operating conditions (*i.e.*, location, irradiation, environmental temperature, and wind speed) from April 8th to July 5th. They found that the system generated 6 hours of peak instant electricity per day (50 W/m^2) and produced 0.22 kWh/m^2 of electricity between May and July.

2.6.1 Solar collector type

A solar collector is an energy exchanger that converts solar to thermal energy. There are two categories of solar thermal collectors (*i.e.*, non-concentrated collectors (NCCs) and concentrated collectors (CCs)). The efficiency of the CSTGB system depends on the temperature and concentration ratio of solar energy ($1,000\text{--}3,000 \text{ kW/m}^2$) (204, 205). Table 2.5 summarizes the characteristics of concentrated solar tower (CST) technologies. NCCs allows heat transport, but the solar thermal concentration ratio is less than 1, and thus they are conventionally used in applications of domestic hot water and space heating (206-208). CC technology is more suitable for CSTGB system because it has very high concentration ratio (approximately $800\text{--}2,000 \text{ kW/m}^2$) (209, 210). Sun *et al.* (210) summarized and elaborated on two types of

concentrated collectors (line-focus and point-focus). Line-focus collectors (*i.e.*, parabolic trough collector and linear Fresnel reflector) are unsuitable for CSTGB system because they have a relatively low operating temperature (approximately 150–550°C), generally a low efficiency (14–22%) and low concentrating ratio (30–80 kW/m²). They presented that point-focus collectors (*i.e.*, central receiver system and parabolic dish) are suitable for CSTGB system because of their high operating temperatures (600–1,500°C) and concentrating ratio (200–3,000 kW/m²).

Solar tower as a central receiver collector is a type of CCs that consist of a heliostat field, a receiver mounted on a tower, thermal energy storage, and a gasifier. The mirror array reflects incident sun lights to an ordinary tower, where the central receiver absorbs and converts the solar radiation to thermal energy that can be directly transferred to heat transfer material (*i.e.*, salts and sand) (208). There are four typical receiver configurations for solar towers, such as multi-tube receiver (MTCR), multi-tube external receiver (MTER), volumetric receiver (VCR), and direct-absorption receiver (DACR) (211, 212).

The MTCR technology has a thermal efficiency around 27.7–29.5% and an exergy efficiency around 29.6–31.6% (213). Qiu *et al.* (212) found that the maximum solar concentrated ratio for a MTCR system was 5.14×10^5 W/m² based on a real-time optical performance analysis. Due to the uneven distribution of sunlight on the tubes, multi-point aiming and tracking technology was used to reduce the uneven sunlight distribution. They reported that the absorbed energy of the MTCR technology was increased to 65.9% efficiency. Lubkoll *et al.* (214) found that the MTER is a relatively inexpensive and straightforward technology as compared to the MTCR. The absorber of MTER consists of vertical tubes mounted on an external receiving tower. For the MTER technology, convection and radiation cause a large amount of heat loss. The maximum temperature of MTER receiver was reported to be 600°C.

Avila-Marin *et al.* (215) summarized the development of VCR technologies including structure (*i.e.*, configuration, geometry, dimensions, materials, *etc.*), efficiency, temperature, and overall system performance. They suggested that most of the VCR technologies can reach over 800°C, and some ceramic-made receivers have the capability of reaching 970–1,500°C.

The black liquid solar collector first proposed by Minaridi and Chuange (216) directly absorbed solar heat by a high-absorbable ‘black’ fluid (water and ink).

Subsequently, carbon nanofluids with improved thermophysical properties (endothermic and heat transfer) were also applied. Simonetti *et al.* (217) found that the DACR technology could utilize transparent shell made of plastic materials to reduce costs and provide more complex geometric pattern designs for solar concentrating collectors. Fang *et al.* (31) confirmed that the solar concentration ratio of SPTs is around 250–1,500 W/m² (operating temperature is about 250–2,000°C).

Parabolic dish collectors (PDCs) use the parabolic dish mirrors to concentrated solar radiation onto the receiver located at the focal point of the dish mirrors, where the heat transfer fluid is heated to required operating temperature and pressure (204, 218, 219). Although PDCs are the most expensive point-focus technology, they can provide a relatively higher solar concentration ratio and thermal efficiency. The operating temperature range of PDCs is from 400 to 1,500°C with a concentration ratio between 1,000 and 3,000 W/m², an average thermal efficiency of 18–25%, and a peak thermal efficiency is 28–32% (204, 210, 220). Sinha *et al.* (221) found that the radiant heat loss increases with the increase of cavity wall temperature, aspect ratio and emissivity. Some factors (*i.e.*, temperature, aspect ratio, and emissivity) can increase the total loss of the entire cavity by 14%.

Table 2.5 Characteristics of CST technologies.

	Land occupancy	Thermos efficiency	Operating temperature (°C)	Solar concentration ratio (W/m ²)	Ref(s)
SPT	Medium	High	300–565	250–1,500	(222)
SPT	Medium	Medium	250–650	300–1,000	(204, 205)
SPT	Small	High	600–2,000	1,000	(223)
PDC	Small	High	800	1,000–3,000	(204, 205)
PDC	Small	Medium	–	1,300–1,600	(220)

2.6.2 Influential factors

The solar radiation is much stronger at higher altitude where it is distributed over a smaller geographic area. The intensity of solar radiation is mainly determined by direct solar radiation under a clear sky; it is depended on scattered radiation when the sky is overcast; the intensity of direct radiation decreases and the intensity of scattered radiation increases when the sky is partly cloudy (224). Overall, 20% of the solar radiation is absorbed or scattered by aerosols in the atmosphere. As the elevation increases, there is less solar radiation absorbed by the atmosphere (156).

The distribution of concentrated solar flux in a concentrated solar power (CSP)

system is non-uniform, resulting in high local temperature and large temperature gradient in a solar receiver. The non-uniform solar flux has a great impact on both line-focus collectors (*i.e.*, parabolic trough collector) and point-focus collectors (*i.e.*, solar power tower). The non-uniform solar flux caused a large amount of heat concentrated at the bottom of the receiver tube (209). Due to the limited thermal conductivity and heat convection ability of the receiver, the non-uniform flux distribution inevitably leads to a non-uniform temperature field on the receiver's wall (225, 226). The high local temperature poses great challenges for the safety and efficient operation of the system. Yu *et al.* (227) found that there would be a safety risk to the receiving system of CSP when the solar flux value exceeds 580 W/m^2 . They confirmed that the performance (*i.e.*, maximum operating temperature) of the heat transfer material (HTM) would be limited when the local solar flux is too high and the coating tends to degrade. Additionally, the high local temperature may lead to the decomposition of HTMs (228, 229).

Most CSP systems use basic HTMs (*e.g.*, liquid sodium: $1.2\text{--}1.5 \text{ W/m}^2$, molten nitrate salt: 0.7 W/m^2 , liquid water: 0.7 W/m^2 , and air: 0.2 W/m^2), and their peak heat transfer values are around $0.2\text{--}1.5 \text{ W/m}^2$, which cannot cope with excessive local temperature caused by non-uniform solar flux. Enhanced heat transfer is important for overall efficiency improvement. Nanofluids refer to colloidal suspensions of nano-ions in basic HTMs, it has been proved to be effective for enhancing thermal performance. Adding suspending nano-particles (*i.e.*, diphenyl oxide, biphenyl, and Ag) to HTM boosted the thermal conductivity (increased by 6%) and intermediate efficiency (increased by 3%) (230).

2.6.3 CST technical challenges

2.6.3.1 Heat transfer material

One of the critical technical challenges facing CSTGB development stems from the property of the HTM (insulation and internal materials). The HTM is heated by radiation and converted through solar collector walls. Karim *et al.* (231) studied the molten salt nanofluid with the composition of graphite as nanoparticles in $\text{LiCO}_3\text{--K}_2\text{CO}_3$ based molten salt by using the computational fluid dynamics (CFD) model. They found that the solar receiver efficiency (60–75%) and total efficiency (40–48%) decreases at higher operating temperature, while the Carnot efficiency (61.5–68.0%) increases slightly with the increase of the receiver length. In most CSTGB systems, the

CST subsystem is connected to biomass gasification via a heat transfer tube. Through the study of 1 m heat transfer tube in a CSTGB system, they found that the HTM temperature drops sharply at the output point as the increases of tube length and HTM input speed. They summarized that the $\text{LiCO}_3\text{--K}_2\text{CO}_3$ based molten salt has no apparent effect on the overall efficiency, and it is more suitable for heat storage and heat transfer at higher operating temperature (over 800°C). Saha *et al.* (232) presented a numerical investigation to simulate the water based Al_2O_3 and TiO_2 nanofluids flowing through a horizontal circular pipe under uniform heat flux boundary conditions with some setting values (*i.e.*, Reynolds number (Re) of 10×10^3 , Prandtl number (Pr) of 7.04–20.29, nanoparticle volume concentration (χ) of 4–6%, and nanoparticle size diameter (d_p) of 10, 20, 30, and 40 nm). They found that the heat transfer rate increases with increasing particle volume concentration and the Re when the particle diameter decreased. Thus, they believed that water based Al_2O_3 nanofluids has a higher average shear stress ratio, higher thermal conductivity, and higher thermal performance factor than TiO_2 nanofluids.

2.6.3.2 Solar collector materials

The insulation and internal materials of the solar collector must be able to withstand a high temperature ($1,227^\circ\text{C}$), large thermal gradients, and high heating rates (233, 234). Lab-scale systems have used energy-intensive materials (*i.e.*, alloy, ceramics, and metal) to resist the thermal stress caused by concentrated solar radiation (235); however these materials cannot protect the interior of the reactor due to the severe thermal shock that often occurs in concentrated solar radiation applications. Thermal shock is a type of fast transient mechanical load caused by a rapid change in temperature at a certain point. It can cause differential expansion of different parts in a CSTGB system. When this stress exceeds the tensile strength of the material, cracks will be formed, leading to system breakdown. Evangelisti *et al.* (236) showed that external thermal shock testing is essential, which can provide information about the collector's ability to withstand severe thermal shock (accidental thunderstorms on sunny days). They believed that thermal insulation materials in solar collectors have not been thoroughly studied. Thus, a more comprehensive investigation may help to understand the strengths and weakness of material in this sector.

2.6.3.3 Others

Even though the CSTGB system is positioned and has many advantages to produce high-quality producer gas, its development is still at an early stage. In contrast to the conventional gasification, the CSTGB system has not yet been demonstrated on a pilot scale (237, 238). The CSTGB system remains economically challenging, requiring incentive-based environmental policies. Neither technology player nor research and government support for the widespread exploitation of the CSTGB system appear to be capable of successfully commercializing and disseminating the technology. Significant challenges remain in proving the efficiency of the process, which relate to the cost of solar concentrator, receiver, HTM, and gasifier. Finally, Piatkowski *et al.* (62) claimed that the CSTGB system may be difficult to develop in arid regions with large solar resources (direct nominal irradiation (DNI) >600 W/m² per year) due to the scarcity of water resources in some area (*i.e.*, Spain).

2.7 CSTGB system development

The CSTGB system concept was developed by Modell *et al.* (239) in 1978. Subsequently, research institutions in the USA, Japan, Germany, and China have conducted extensive research on various scientific and technical issues (*i.e.*, costs, performance, and onsite emissions) of CSTGB systems. The first CSTGB system, namely Plataforma Solar de Almeria, was successfully established in 2002 and generated 230 kWh of electricity (240). A CSTGB system with a capacity of 30 kg/h was built at Enschede in 2004, and it achieved a producer gas yield over 2 L/g_{wood sawdust} (241). Another CSTGB system with a capacity of 1 ton/day of waste wood and a system efficiency of 70% was built at Hiroshima University, Japan (242). Kuste *et al.* (243) built a pilot-scale CSTGB system in Germany ('VERENA') with a design capacity of 100 kg/h of biomass and 77vol.% of producer gas (main H₂) in 2007. Yakaboylu *et al.* (244) introduced a fluidized bed reactor into the CSTGB system at the Delft University of Technology in the Netherlands in 2018, which reached a maximum feeding rate of 50 kg/h with the highest carbon conversion efficiency of 73.9%. A larger commercial CSTGB system with a designed capacity of 200 kg/h of biomass slurry was built to generate electricity by the General Atomics Company in the USA (245).

Piatkowski *et al.* (246) developed a CSTGB system. This system transfers the indirect heat of concentrated solar radiation to the packed bed through a quartz window, while steam and feedstock are injected from the bottom of the gasifier during the solar

day. The solar packed bed gasifier provides reliable operation and robust performance for a wide range of feedstocks (*e.g.*, biomass, sewage sludge, *etc.*). The CSTGB system has a heat-transfer limitation because of the indirect solar thermal transfer through an emitter plate and lack of heat storage, causing the system only operatable on a solar day (247). It has the disadvantage of high thermal inertia, corresponding to a long preheating period of 2–4 h. It is possible to use a heat storage system to avoid the preheating time for each solar day or replace the fixed bed reactor with a fluidized bed reactor to increase the heat and mass transfer rates. Pantoleontos *et al.* (248) conducted a dynamic simulation of a heat storage subsystem in the CSTGB system, where a cobalt oxide redox pair system was considered for the reforming of reduction zone reactions. They found that the thermal energy storage (TES) subsystem could provide 24% of the required reaction energy during the night, and the rest had to be provided by an external heat supply.

Gokon *et al.* (249) proposed a CSTGB system consisting of an internally circulating fluidized bed reactor combined with concentrated solar radiation. In the proposed system, line-focus and point-focus solar collectors were employed to provide concentrated solar thermal energy (1,027–1,527°C). This system applied a beam-down configuration: a set of secondary mirrors mounted on the tower top redirected the solar radiation to the bottom. They found that the peak photochemical energy conversion rate (or chemical storage efficiency) is approximately 12% for an internally circulating fluidized bed reactor after 5 mins of light-irradiated reaction. The internal circulation fluidized bed is changed into a pouting bed to improve the heat transfer rate of the bed and the heat recirculation. Nathan *et al.* (250) proposed a method to improve the efficiency of the CSTGB system by increasing the heat flux on the bed surface, building large-scale heat recirculation, and utilization of the free-board material to absorb the irradiation. Bellouard *et al.* (21) claimed that the total thermochemical efficiency of a high-temperature CSTGB system can be increased to 28% at 1,127°C.

To address the limitations of the CSTGB system, such as low entire energy efficiency, low solar-to-chemical efficiency, high exergy loss, *etc.* Bai *et al.* (251) proposed a CSTGB power generation system with an integrated combined cycle gas turbine (CCGT) subsystem. A point-focus collector is used to reflect the concentrated solar beam to provide thermal energy of the gasification reaction at 877°C. Impurities (*e.g.*, ash and H₂S) are removed from the producer gas by condensation and purification.

The qualified producer gas is fed as gaseous fuel directly into the CCGT subsystem, which consists of dual pressure heat recovery steam generator. The total energy efficiency of this system is 26.72% and the net solar power efficiency is 15.93%. The exergy loss from the solar collection and gasification process is reduced by 19.30% as compared to the scenario without CCGT, and the daily average net solar-to-electricity efficiency is 19.04%.

Instability in solar thermal energy generation is one of the major barriers against the application of CSTBG systems. The variation and intermittent of solar radiation and sunshine duration, leading to the temperature variation of gasification. Heat storage is a promising approach to address the instability problem to sustain the operation of the process for continuous producer gas production under a stable temperature condition. With a TES subsystem, the CSTGB system can proceed throughout the day and avoid preheating time, leading to a 2.77 times increase in the producer gas yield as compared to a CSTGB system without the TES (252).

The TES subsystem stores the solar thermal energy into a tank, where the HTM transfers the thermal energy to the heat exchanger in the gasifier (253, 254). The TES system can be roughly divided into three categories: sensible heat storage, thermochemical heat storage, and latent heat storage. The sensible heat storage stores thermal energy by raising the temperature of substances stored in solids, liquids, and gases (255). The thermochemical heat storage is based on reversible chemical reactions, in which charging and discharging are carried out through endothermic and exothermic reactions, respectively (161). Carrillo *et al.* (161) found that the optimal operation requirement of the system to meet a series of an ideal storage medium and the characteristics of conceptual design includes high thermal energy storage material with density of 144 kWh/m³, high stability of material (30,000 h test or expected >30 years), high operation temperature of 565°C) high heat transfer rate (λ) of 0.5 W/m/K, and low toxicity, cheap and abundant materials of \$20–33/kWh. The latent heat storage stores heat in the form of phase change material (PCM) fusion latent heat. Gokon *et al.* (256) studied the application of iron-germanium alloy (Fe–Ge alloy) as a PCM at 800°C. They evaluated the cyclic performance, short- and long-term thermal stability of the alloy through thermal reliability tests. Compared to solar salt, the Fe–Ge alloy shows excellent potential as the next generation for solar thermal application due to a variety of strengths, such as rapid heat response and thermodynamic stability of the structure.

2.8 CSTGB system evaluation

2.8.1 Life cycle assessment of CSTGB system

The LCA is a standardized approach for assessing the environmental impacts of a given process, technology, system, or service throughout its whole life cycle. The LCA is defined by the ISO 14000 series of international standards, which consists of principles and framework (ISO 14040), goal and scope definition and inventory analysis (ISO 14041), life cycle impact assessment (ISO 14042), life cycle interpretation (ISO 14043), and requirements and guidelines (ISO 14044) (257).

CSTGB systems have proven to be highly efficient, their environmental benefit and economic viability should be clarified before commercialization and large-scale implementation (258-261). The LCA is a structured, standardized method for quantifying the environmental impact of a technology, system, or service throughout its whole life cycle (262). It can be used to evaluate the carbon footprint of production from CSTGB systems and to compare the influences of feedstocks, solar radiation, the parameters of gasifier, and the capacity of CCGT for hot spotting. It can also be used to support decision-making for policy makers and support practitioners to optimize CSTGB development (263).

Chen *et al.* (245) conducted a LCA study of the CSTGB system with a capacity of 1 ton/hr biomass, and it is shown that the system operation contributed approximately 58% to the total environmental impact. The global warming potential (GWP) of the operation phase is 4.4 kgCO₂-eq/kg of H₂; the other 42% of the GWP come from the manufacturing phase (*i.e.*, raw material manufacturing, biomass collection, and material transport) and end of life phase (*i.e.*, dismantling the plant and demolishing the buildings). Banaclouche *et al.* (264) studied the LCA of a CSTGB system with a TES system and CCS system in Tunisia, and the reported GWP is -77 kgCO₂-eq/MWh of electricity. Various approaches to the LCA studies currently exist (265, 266), while the importance of method selection, emission types, and the contribution of individual life cycle stages has not been critically assessed in the context of CSTGB system power generation. A systematic overview of the consequences of technology selection and performance is needed to provide a transparent and balanced basis for future LCA modelling of CSTGB system power generation technologies.

The CSTGB system integrated with TES and CCS subsystems allowing for stable 24/7 operation and lower onsite CO₂ emissions (31). However, previous study (267) has shown a 30% higher capital cost of construction, and a higher O&M cost as

7.8 €/MWh for the integrated system as compared to CSTGB systems without TES and CCS subsystems. Fang *et al.* (268) introduced a TES system and adopted a strategy of combusting a portion of the feedstock during nighttime or periods of low solar radiation to address the intermittency of solar energy. This approach enables the CSTGB system to utilize the solar thermal energy collected during the day for gasification reaction even at night. This modification results in a noteworthy reduction in carbon emissions. The CSTGB system with a CCS demonstrates the ability to reduce CO₂ emission by 787.7 kgCO₂-eq/ton_{waste-wood}, while also generating a total of ~ 0.8 million MWh of electricity annually. The TEA is one of the methods of economic analysis which is needed to evaluate, compare, and determine the selection of the project. It is used to determine the benefits of the project, compares the required investment and costs, and identifies the actions needed to maximize the return (269).

2.8.2 Economics analysis of the CSTBG system

The CSTGB system offers remarkable benefits in terms of mitigating GWP and augmenting electricity generation, they are counterbalanced by increased construction and O&M costs, leading to diminished project revenue (268). Economics analysis has been widely used to assess the economic viability of biomass, waste, and energy-related projects or schemes (270). By systematically analyzing and comparing benefits and costs, it answers questions such as whether a proposed project or scheme is worthwhile. The economic analysis (*i.e.*, TEA has mentioned in Section 2.8) serves as an effective tool for making decisions about the use and allocation of society's resources (169). However, existing TEA studies regarding CSTGB systems have demonstrated that the electricity generated by CSTGB was hardly affordable for end users (271, 272), which is challenging for the long-term viability of these systems. There are no comprehensive studies to assess the environmental sustainability and economic analysis of CSTGB systems, which are crucial for the decision-making process of policy makers and investors. The CSTGB system consists of multiple subsystems, and selecting the technology for each subsystem is crucial for ensuring the overall viability of the system (273). Among these subsystems, the selection of the thermochemical process reactor is based on the desired products (31). Two widely used methods, such as techno-economic analysis (TEA) and TEA are employed to evaluate the economic viability of the system, investments, and policies (274).

The TEA specifically evaluates the economic feasibility of the CSTGB system by analyzing its technological aspects. This method involves detailed research into the costs and performance of various technological options to identify the most efficient and cost-effective technology (275). The TEA considers factors such as capital expenditure (CAPEX), O&M costs, as well as the revenue generated by the system (276). And the TEA is a simulation-based economic analysis method that serves as a more comprehensive tool for evaluating the entire system than the TEA (277), includes the efficiency of the CSTGB system or policy by comparing its costs and benefits in monetary terms. The TEA considers various cost factors such as CAPEX, O&M costs, and replacement costs, while also considering the economic (*i.e.*, internal rate of return (IRR)), environmental (*i.e.*, GWP), and social benefits (*i.e.*, human health) (237).

Halliday *et al.* (278) conducted a study on a 50 MW_{th} CSTGB system, they used wheat straw as feedstock and employed an oxygen gasifier in conjunction with a synthetic natural gas (SNG) reactor to generate electricity with the estimated cost of electricity generated as 144–146 €/MWh. They conducted a comparative analysis by examining a modified system that used a fixed-bed gasifier and a Rankine cycle with switchgrass as the feedstock for electricity generation. In this scenario, the estimated cost of electricity was significantly lower as 133 €/MWh. Boujjat *et al.* (95) stated that the CSTGB system is suitable for both small-scale and large-scale plants. Large-scale implementation of the CSTGB system improves system efficiency and reduces product costs. Wei *et al.* (279) investigated a 660 MW_{th} CSTGB system that used wood pellets as feedstock and employed a supercritical CO₂ cycle for electricity generation, resulting in an estimated product cost of 132 €/MWh. Adnan *et al.* (280) upgraded the CSTGB system by integrating a supercritical water gasifier and an CCGT subsystem for electricity generation at the plant size of 180–270 MW_{th}. And the estimated cost of electricity as 104–134 €/MWh, which included the levelized cost of energy, CAPEX, O&M costs, as well as the total annualized revenue from electricity sales.

The integration of the TES subsystem into the CSTGB system has been proven effective in reducing product costs. Sahoo *et al.* (281) have explored a 15 MW_{th} system utilizing a gasifier and a SNG reactor with an estimated cost of electricity of 90.3 €/MWh. Pantaleo *et al.* (282) investigated a 5 MW_{th} system that utilized an air gasifier and TES for combined heat and power generation, resulting in an estimated cost of electricity of 149 €/MWh. Oyekale *et al.* (283) presented a 630 kW_{th} system that employed a fixed bed gasifier and TES for electricity generation with an estimated cost

of 116 €/MWh. Integrating the CCS subsystem can effectively reduce carbon emissions (as mentioned in Section 2.7). However, it decreases the system efficiency and increase the cost of electricity production. Mohamed *et al.* (284) investigated an 650 MW_{th} supercritical water based CSTGB system that was integrated with the CCS. They conducted a comparison between the system with and without CCS. The results indicated that the estimated cost of electricity production from the CSTGB system with CCS was 141 €/MWh, whereas the cost without CCS was 113 €/MWh. Through systemic analysis and comparison of benefits and costs, Fang *et al.* (268) indicated significant challenges in terms of the economic viability of the CSTGB system. The computed NPW for the system after 30 years is approximately €-0.7 billion. This deficiency is closely linked to the constraints imposed by existing environmental emission regulations (*i.e.*, carbon tax (CT)) and electricity prices.

Table 2.6 summarized a comparative economic analysis of electricity production from CSTGB systems and conventional gasifiers. These systems are categorized based on type of feedstock, plant size, reactor type, and the method employed or power generation. Conventional gasifier typically demonstrates lower electricity production costs in comparison to CSTGB systems. The cost-effectiveness of conventional gasification is attributed to its higher technological maturity, simpler system design, and lower initial and operational costs. The system employed fixed-bed gasifier in conjunction with steam Rankine cycle yield electricity at costs ranging from 70–90 €/MWh. This cost disparity primarily stems from the established maturity and scalability of conventional gasification technology, as opposed to CSTGB systems, which are marked by greater technical complexity and higher initial investment needs.

For CSTGB systems, diverse configurations (*i.e.*, supercritical water gasifier, CCGT, and CCS applications) exhibit a range of product costs (104–558 €/MWh). Specifically, CSTGB configurations using supercritical water gasifiers combined with CCGT can generate electricity at costs ranging between 104–151 €/MWh, but the integration of CCS technology elevates these costs. Simultaneously, CSTGB systems offer significant environmental sustainability benefits (*i.e.*, reducing GHG emissions and improving resource efficiency), which are vital for addressing climate change and achieving sustainable development goals.

The economic analysis furnishes comprehensive insights for decision-makers and stakeholders, delineating the economic feasibility of deploying CSTGB systems relative to conventional gasification techniques. While certain CSTGB configurations

exhibit higher production costs, their inherent environmental advantages, amplified by escalating fossil fuel prices, carbon tax incentives, and supportive policy framework, potentially bolster their long-term economic viability. This supports CSTGB systems' contribution towards the realization of a fully renewable energy future.

Table 2.6 Comparative economic analysis of electricity production from CSTGB system and conventional gasifier.

	Feedstock	Plant size	Reactor	Power generation method	Product cost	Ref
CSTGB based	Coal	180–270 MW _{th}	Supercritical water gasifier	CCGT	104–151 €/MWh	(280)
	Pine sawdust	650 MW _{th}	Supercritical water gasifier	CCGT+CCS/non-CCS	With CCS: 141 €/MWh Without CCS: 113 €/MWh	(284)
	Wood pellets	660 MW _{th}	Gasifier	Supercritical CO ₂ Cycle	132 €/MWh	(279)
	Biomass	275 MW _{th}	Gasifier	CCGT	558 €/MWh	(285)
	Wheat straw	50 MW _{th}	Oxygen gasifier	Steam Rankine Cycle	144–147 €/MWh	(278)
	Switch grass	50 MW _{th}	Fix bed gasifier	Rankine Cycle	44 €/MWh	(278)
	Olive waste residues	110 MW _{th}	Gasifier	Organic Rankine Cycle	245 €/MWh	(286)
	Biomass	15 MW _{th}	Gasifier	Steam Rankine Cycle	90 €/MWh	(281)
	Biomass	2.5 kW _{th}	Steam gasifier+TES	Combined heat and power	181–197 €/MWh	(287)
	Biomass	5 MW _{th}	Air gasifier+TES	Combined heat and power	149 €/MWh	(282)
	Biomass	630 kW _{th}	Gasifier+TES	Combined heat and power	116 €/MWh	(283)
	Conventional	Coal	200 MW _{th}	Gasifier	CCGT	100–120 €/MWh
Wood pellets		500 MW _{th}	Gasifier	Steam Rankine Cycle	130–150 €/MWh	(289)
Biomass		100 MW _{th}	Fixed bed gasifier	Organic Rankine Cycle	200–220 €/MWh	(290)
Switch grass		60 MW _{th}	Fluidized bed gasifier	Steam Rankine Cycle	70–90 €/MWh	(291)
Rice husk		80 MW _{th}	Fluidized bed gasifier	Steam Rankine Cycle	120–140 €/MWh	(292)
MSW		150 MW _{th}	Downdraft gasifier	Steam Rankine Cycle	150–170 €/MWh	(293)
Corn stover		70 MW _{th}	Entrained flow gasifier	Combined heat and power	130–150 €/MWh	(294)
Hardwood chips		120 MW _{th}	Gasifier	CCGT	110–130 €/MWh	(295)

2.8.3 Multi objectives optimization

A holistic approach encompassing both economic and environmental considerations become imperative within the context of CSTGB system's process design and operation. Balancing the pursuit of economic gains with the reduction of adverse environmental consequence frequently involve conflicting requirements (280). The evolution and refinement of MOO techniques have proven instrumental in addressing these intricacies associated with multiple conflicting objectives.

Within MOO and decision-making frameworks, the inclusion of both Pareto optimal solutions and the technique for order of preference by similarity to ideal solution (TOPSIS) methods is pivotal. These components play a crucial role in facilitating effective decision-making processes by offering comprehensive insights and evaluation criteria for complex, multi-dimensional problems (296). The pareto optimal solution involves finding solutions that cannot be improved in one criterion without worsening another. This concept plays a vital role in identifying the optimal compromise solutions within conflicting objective (48). Moreover, the TOPSIS method is used to rank alternatives based on their proximity to an ideal solution. These methods provide valuable insights into selecting the most suitable solutions that balance various criteria, considering the inherent trade-offs between objectives (297). Parhi *et al.* (298) employed the TOPSIS for selecting one pareto optimal solution for optimizing the energy system. Musharavati *et al.* (296) also applied a pareto optimal solution method to show cost and exergy efficiency objective functions and use the TOPSIS method to define the best scenario during the MOO process.

In the modelling of the CSTGB system, certain parameters (*i.e.*, feedstock compositions, reaction temperature, solar irradiation, and construction location) are typically assumed to be given as constant. However, the precise determination of these parameters in the real world poses challenges due to a lack of knowledge or uncertainties in coefficients (299). For instance, the feedstock composition and solar irradiation is not remained constant, and transportation costs could be uncertain depending on factors such as worker's skill and traffic congestion levels. In addition, employing a simulation model or devising pertinent mathematical equations poses a formidable challenge due to the numerous intricate chemical processes within the CSTGB system (298). The computationally intensive nature of simulating or solving model equations poses a significant obstacle. Thus, researchers have begun to utilize ML algorithms to construct models for objective functions and constraints based on historical data. This deliberate integration of ML opens up the opportunity to unveil complex associations between decision variables (input) and objective (outputs) (48).

However, the integration application of developed ML model for MOO within in the CSTGB systems remains a relatively uncharted territory (298). The application of the ML model as data-driven tools has demonstrated their potential, albeit limited to system modelling (48). The persistent challenge lies in the data-driven modeling domain, which is hampered by the absence of specialized models and experiments tailored for the CSTGB system. As a result, a MC simulation approach is employs to expand the dataset. This strategic expansion aims to reinforce the reliability of MOO results within the intricate CSTGB system. Inuiguchi *et al.* (299) had demonstrated the effective treatment of stochastic variables by employing data from literature to estimate their probability distributions. Integrating stochastic optimization methods with ML algorithms allows for improved transformations of MOO models with random coefficients into deterministic linear or nonlinear multi-objective faction problems. This integrated approach offers enhanced interactive algorithms that derive satisfactory solutions for decision makers in a more robust manner (300).

The application of MOO method on the LCA and TEA of the CSTGB system has gained significant attention in recent years (301). These analyses play a crucial role in evaluating the feasibility of CSTGB systems while considering various factors (*i.e.*, environmental impact and economic viability). The integrated approach empowers decision-makers to make informed choices when implementing and designing the CSTGB system by exploring trade-offs between environmental benefits and economic costs (302). Consequently, the utilization of MOO methods on the LCA and TEA represents a substantial advancement in sustainability assessments (303), providing valuable insights for sustainable energy planning and policymaking, and ultimately contributing to a greener and more sustainable future.

2.9 CSTGB system limitations and commercialization barriers

2.9.1 Technological challenges

The efficiency of CSTGB systems is critically influenced by the inherent variability in biomass feedstock, particularly in terms of moisture content and composition. Loutzenhiser *et al.* (12) demonstrated that fluctuations in biomass moisture content result in inconsistent producer gas quality and reduced gasification efficiency. To address this, the implementation of pre-treatment processes is recommended to standardize feedstock quality, thereby enhancing the consistency and efficiency of the gasification process. Complementarily, Boujjat *et al.* (95) advocated for the development of adaptive gasification systems capable of dynamically adjusting operational parameters in real-time to accommodate varying feedstock characteristics. This innovation is pivotal in bolstering the overall efficiency and reliability of CSTGB systems

against the backdrop of feedstock variability.

Transitioning to the system design, the complexity inherent in CSTGB systems stems from the necessity to efficiently amalgamate solar thermal components with biomass gasification technology. Optimal system designs are crucial, as underscored by Boujjat *et al.* (95), necessitating precise control systems and optimized solar concentrator configurations to maximize thermal energy capture while minimizing losses. The diverse and demanding operational challenges of CSTGB systems, highlighted by Hussain *et al.* (304), necessitate the incorporation of real-time monitoring and adaptive control mechanisms. These mechanisms are indispensable in countering the variability of solar irradiance and fluctuating biomass characteristics, thereby maintaining optimal operating conditions vital for the system's efficient and reliable functionality.

Furthermore, addressing the challenge of solar energy intermittency, the role of TES systems is paramount. The performance of TES systems, as evidenced by Fang *et al.* (31), varies significantly under diverse climatic conditions, impacting both efficiency and heat retention capabilities. This necessitates the customization of TES systems to align with specific geographic and climatic contexts, a critical factor in optimizing CSTGB system performance. However, as Wieckert *et al.* (305) presented, the integration of TES systems, while essential for mitigating energy intermittency effects, incurs substantial cost implications, potentially escalating initial investments by up to 20%. This figure varies with the system's scale and employs technology, representing a significant trade-off between enhancing system reliability through TES and maintaining the economic viability of CSTGB implementations.

2.9.2 Economic barriers

The initial cost of establishing CSTGB systems is significantly high due to the requirement for advanced technology, particularly high-efficiency solar concentrators and TES systems (306). The integration of TES systems effectively counters the intermittency of solar energy, but this approach also further decreases the economic feasibility (307).

The formation of tar in CSTGB systems presents a significant obstacle to the gas cleaning process, which is crucial for ensuring the quality and usability of the produced gas. Tar (formed during the thermal decomposition of biomass) is a complex mixture of hydrocarbons that can cause issues in subsequent stages of gas usage, especially in power generation or synthetic fuel production. Asadullah *et al.* (308) delved tar formation complicates the gas cleaning process. They presented that tar is sticky and viscous, and its presence can lead to the fouling of equipment, clogging of filters, and corrosion of pipelines. They addressed

that tar not only impacts the efficiency of gas cleaning equipment but also necessitates frequent maintenance and replacement of parts leading to increasing operational costs. Additionally, tar compounds in the gas stream can pose significant challenges in downstream applications. For instance, the presence of tar in power generation can lead to inefficient combustion and damage to turbines (309). Addressing these challenges requires the use of advanced tar cracking and reforming catalysts (as mentioned in Section 2.4.3), as well as the development and integration of more efficient and robust gas cleaning technologies. This includes advancements in filtration systems, scrubbers, and thermal cracking units capable of handling the complexity of tar compounds. The development and optimization of these technologies are crucial for reducing the impact of tar on the gas cleaning process, ultimately improving the economic and operational feasibility of CSTGB systems (31).

In summary, the challenges posed by tar formation to the gas cleaning process in CSTGB systems are multifaceted, affecting both operational efficiency and cost. Overcoming these challenges requires a comprehensive approach, including technological advancements in both tar mitigation and gas cleaning processes, to ensure the production of clean, high-quality gas suitable for various end-use applications.

2.9.3 Market and policy challenges

The market and policy challenges of CSTGB system are crucial to consider the introduction of carbon taxes and the supply-demand relationship in the electricity market. Carbon tax can increase the cost of fossil fuels, thereby enhancing the competitiveness of renewable energy technologies (*i.e.*, CSTGB system). Nicodemus *et al.* (310) demonstrated that the implementation of carbon taxes significantly enhances the economic attractiveness of CSTGB system, creating a more balanced competitive environment in the energy market. Additionally, Seo *et al.* (311) presented that as renewable energy sources increase their share in the electricity market, the impact of demand on prices becomes more pronounced, offering new opportunities for the development and market penetration of CSTGB systems.

Another major challenge in the commercialization of the CSTGB system is regulatory barriers. As highlighted in the study by Asadullah *et al.* (312), obtaining the necessary permits and complying with environmental regulations is both time-consuming and costly. These regulatory obstacles often lead to delays and additional expenses in deploying CSTGB systems, impeding their market acceptance. Thus, to facilitate the adoption and implementation of CSTGB system, there is a need for simplified regulatory processes and more supportive environmental policies.

Beyond market incentives and regulatory challenges, CSTGB systems also face commercial barriers in terms of capital investment, technological maturity, market promotion, and user acceptance. Sansaniwal *et al.* (313) addressed that the research and development, and deployment of CSTGB system require significant capital investment, and the lack of technological maturity raise concerns about reliability and performance among potential users. Moreover, CSTGB system needs to be compatible with existing power grids and energy systems, involving technical and strategic adjustments.

In summary, the commercialization of CSTGB systems requires a comprehensive approach that considers the impacts of carbon tax, electricity market supply and demand, capital investment, technological maturity, market promotion, user acceptance, and integration with existing energy infrastructures. Policymakers and industry stakeholders need to collaborate, employing technological innovation, policy support, and market strategy adjustments to overcome these commercial barriers and promote wider application of CSTGB systems. This integrated approach will facilitate the effective deployment and commercialization of CSTGB systems, paving the way for a broader application of renewable energy technologies.

2.9.4 Research and development gaps

In the realm of CSTGB system research, a significant development gap exists in the availability of comprehensive data and predictive model, essential for optimizing the operation of CSTGB systems. This deficiency hampers the potential for achieving maximum efficiency and cost-effectiveness in system design and operation. Saw *et al.* (314) presented the lack of detailed operational data and advanced modeling tools restricts the ability to fine-tune CSTGB systems to specific environmental conditions and operational requirements. Their research underscores the necessity for extensive data collection and the development of sophisticated simulation models that can accurately predict system performance under varying conditions.

Furthermore, the need for tailored solutions in CSTGB systems is another critical area requiring focused research and development. Due to the diverse nature of local conditions (i.e., variations in solar irradiance and biomass availability), CSTGB system cannot adopt a one-size-fits-all approach. As emphasized in research by Pinna-Hernandez *et al.* (119), designing CSTGB systems that are adaptable to local environmental and resource conditions is paramount. Their study suggests that customizing system components and operational parameters, based on regional characteristics, can significantly enhance system efficiency and output. This customization necessitates a deep understanding of local conditions and the

development of flexible system designs that can accommodate (*i.e.*, variability).

In summary, bridging the research and development gaps in CSTGB system requires the collection of comprehensive data and the development of predictive models for system optimization, and the reaction of tailored solution that consider local environmental and resource variations. Addressing these needs will not only enhance the efficiency and viability of the CSTGB system but also accelerate their adoption in diverse geographic regions, contributing to the broader implementation of this renewable energy technology.

2.10 Summary

This chapter reviewed the development of CSTGB based on consideration of two major units (*i.e.*, CST and biomass gasifier) of the technology. Several types of gasifiers (fixed bed, fluidized bed, and entrained flow) and influence factors (agents, catalysts, particle size, and reaction temperature) have been discussed, and the application of complementary high-temperature (250–2,000°C) solar energy has been highlighted. The concentrated solar tower and fixed bed reactor were preferred for a CSTGB system, it could provide approximately 600–2,000°C to drive the gasification process, increasing thermal efficiency by 27.65–29.50% and the energy efficiency by 29.58–31.56%. Salt and sand are suitable for HTM because they have high heat transfer value. For the CSTGB system, the ideal feedstock particle is in the range of 0.28–2.00 mm. The use of steam as the gasification agent (S/B ratio approximately equal to 3) would increase the H₂ content (55.5%) of producer gas. The use of catalysts has been effective in reducing tar production and increasing H₂ production for conventional gasification, while their impacts on the CSTGB need more research. The CSTGB system has been found to achieve an energy efficiency of 74.84% and an exergy efficiency of 51.23%.

The TE model has been beneficial in predicting the behavior of CSTGB systems, especially of concentrated solar tower. For fluidized bed gasifiers, the TE model accurately predicts the temperature profiles of gasification products in the oxidation zone. Some modified TE models incorporating empirical parameters and relevant experimental research achieved higher accuracy. Introducing S and NS models into the TE model, which can compute the predicted equilibrium product's composition based on using thermodynamic property data. The kinetic model is a powerful tool to analyze the gasifier in the CSTGB system; it utilizes mass and energy balance rules to calculate the product content (*i.e.*, gas, tar, and char) accurately and precisely under given operating conditions. The kinetic model can predict the progress and product composition along with the different locations of the reactor (*i.e.*, pyrolysis, combustion, and reduction zone). The CFD model has been used as an essential tool to study

the behavior of gasifiers. However, in order to conduct a comprehensive CFD model of the CSTGB system, detailed and accurate studies of the gasification process and solar thermal conversion, combined with specific numerical methods for multiphase flows, are required.

This chapter provides a foundation for making informed choices within the context of the CSTGB system, encompassing emission data, technological scopes, and methodological approaches. In the context of LCA results, it has been imperative to identify and thoroughly assess a spectrum of technological and methodological variations, aiming to gain a comprehensive understanding of their substantial influence on shaping the final outcomes. From a technical standpoint, the efficiency of key components such as the CST, gasifier, and CCS subsystems is critical in influencing system efficiency. For biomass-based systems, the type, quality, and origin of the feedstock composition also play a pivotal role. Looking at it from the perspective of the LCA methodology, the key factors influencing the consistency and transparency of results include how to define the functional unit (*i.e.*, assessing emissions for treating 1 ton of feedstock within the proposed system), the selected LCA methodology, allocation principles, and the expansion of system boundaries when applied. In the application of the CSTGB system for electricity generation, it is crucial to acknowledge that various assumptions, particularly those pertaining to upstream land-use-related factors, encompassing both direct and indirect aspects like biomass availability (including local biomass species) and transportation distances, exert a substantial and discernible impact on the resulting outcomes and findings. Highlighting the incorrect or ill-advised utilization of emission data and LCA results can potentially lead to misleading and erroneous conclusions, underscoring the significance of accurate data interpretation and context-aware analysis. Therefore, it is recommended that future LCA modelling studies involving electricity generation clearly state data applicability and methodological limitations. This step will substantially enhance the transparency and usability of the results obtained from the LCA.

In evaluating the economic feasibility of CSTGB system, TEA offers a comprehensive perspective encompassing economic, environmental, and social factors. CSTGB systems demonstrate significant environmental benefits in reducing GWP and increasing electricity generation. However, these benefits are offset by increased construction and operational costs, posing challenges to their long-term viability. Studies indicate that the costs of electricity generation in CSTGB systems vary based on factors (*i.e.*, feedstock composition, plant size, and technology selection). Large-scale implementation typically enhances efficiency and reduces costs. The integration of TES can decrease emissions but increase electricity production costs. Systematic analyses reveal economic challenges, with some studies

suggesting that the NPW may be adversely affected due to environmental regulations and electricity pricing constraints. Nonetheless, the potential of CSTGB systems to achieve 100% renewable energy is bolstered by rising fossil fuel prices, carbon tax credits, and government support.

In summarizing the challenges of CSTGB systems, it is evident that these are primarily concentrated in areas of market and policy environment, regulatory barriers, research and development gaps, and commercialization difficulties. In terms of market and policy, the lack of sufficient market incentives (i.e., carbon taxes and adjustments in the electricity market supply-demand relationship) limits the competitiveness of CSTGB systems against conventional energy sources. Regulatory challenges include the complexity and high cost of obtaining necessary permits and complying with environmental regulations, hindering the rapid deployment of CSTGB systems. In research and development, the absence of comprehensive data and advanced predictive models restricts the ability to optimize system design and operation, necessitating tailored solutions based on specific geographic and environmental conditions. Commercialization faces significant barriers including substantial capital investment requirements, insufficient technological maturity, difficulties in market promotion, user acceptance issues, and the need for integration with existing energy infrastructures.

Therefore, to advance the development and application of CSTGB system, collaborative efforts are required from policymakers, industry stakeholders, and research teams. These efforts focus on technological innovation and market strategy adjustments to overcome these challenges. MOO techniques, including Pareto optimal solutions and TOPSIS, along with ML algorithms, play a crucial role in addressing conflicting objectives and data limitations. Applying MOO to LCA and TEA enhances sustainability assessments, aiding in informed decision-making and contributing to a greener future.

Chapter 3 Development and process optimization of biomass gasification with a Monte Carlo approach and random forest algorithm

In the previous chapter, the prior literature review identified crucial process parameters closely associated with producer gas production, such as water content, particle size, and reaction temperature. Furthermore, the utilization of a kinetic model based on the single-particle shrinkage core model allowed for the analysis of certain micro-level parameters effects on producer gas production, such as porosity, thermal conductivity, emissivity, and particle shape. As mentioned in the Layout of the thesis, the content of this chapter has been published as a journal article ⁽⁴⁸⁾ in the journal Energy Conversion and Management. In this chapter, a stochastic biomass gasification kinetic model was developed by combining the Monte Carlo (MC) approach with the kinetic model (*i.e.*, single particle shrinkage core model). Two sets of different data were obtained by varying the distribution of input parameters, such as normal and uniform distributions. These two distinct datasets were then used to train the RF algorithm, resulting in a broader range of predictive outcomes to identify the maximum producer gas yield within specified parameters. The initial gasification kinetic model, provided by Dr ZhiYi Yao and based on the single particle shrinkage core model, it was extensively optimized to meet the specific requirements of this study. This optimization enhanced the model's ability to accurately represent a wide range of process parameters and their corresponding producer gas yields; it also significantly increased the model's reliability through validation against a substantial amount of experimental data. In the development of the model, Dr Li Ma's guidance played a decisive role, especially in transforming the model into a stochastic variant with higher precision and flexibility. The model underwent rigorous validation, utilizing existing experimental data to demonstrate its capability in predicting both maximum producer gas yield and composition. This comprehensive analysis significantly contributes to a deeper understanding of the biomass gasification process and its optimization potential. In this chapter, the reaction temperature has been defined as the most influential parameter affecting gas production in the gasifier through the application of stochastic kinetic model and machine learning (ML) algorithm. The moisture content and particle size of the feedstock also stand out as prominent factors that significantly influence gas production and compositions. Other factors, such as variables (particle shape, emissivity, thermal conductivity, and porosity) do not seem to exert a substantial impact on gas yield and gas composition. Specifically, optimizing the reaction temperature to $\sim 800^{\circ}\text{C}$, water content to $\sim 10\text{wt.}\%$, and particle size to $\sim 2\text{ mm}$ can

achieve the maximum yield and highest LHV of the producer gas.

3.1 Methodology

The research methodology adopted in this study is illustrated in Figure 3.1, which consists of 4 stages:

- The kinetic gasification model is developed and validate using experimental data.
- The MC simulation approach (two cases corresponding to uniform and normal distributions, respectively) is combined with the kinetic model to create statistical datasets (process conditions and producer gas yield) for random forest (RF) modelling.
- The RF model is trained and tested using 2,000 datasets from uniform and normal distributions, respectively: (water content, particle size, particle porosity, particle shape, thermal conductivity, emissivity, and reaction temperature) and producer gas (H₂, CO, CO₂, CH₄, and N₂) yields.
- Optimal process conditions are predicted and compared with experimental data from literature for model validation and the influences of process parameters on maximum producer gas yield are studied.

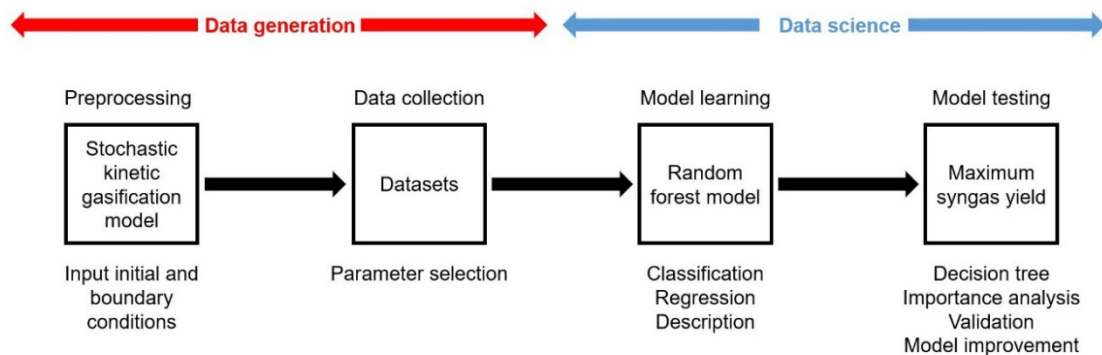


Figure 3.1 Overview of the methodology.

3.1.1 Kinetic model development

3.1.1.1 Kinetic model description and assumption

In this study, the kinetic model was coupled to a single particle shrinkage core model based on the one-dimensional fixed bed gasification with air being its gasifying agent schemes as shown in Figure 3.2. All species were assumed well mixed and moved from top to bottom in the gasifier. It is important to mention that the initial kinetic model was provided by Dr Zhiyi Yao. The process parameters (*i.e.*, $\rho_{g,p,0}=1.19\text{kg/m}^3$, $Y_{\text{O}_2,0}=0.21$, $Y_{\text{N}_2,0}=0.79$,

$T_{p,0}=25^{\circ}\text{C}$, and $r=r_0$) were used as the initial and boundary conditions. Biomass particles are porous media, and thus a shrinkage core model was used to achieve reasonable model accuracy. During the thermochemical reactions, the porosity inside a particle increases with time, leading to shrinkage until a certain critical value with the continuous release of producer gas or impurities (*i.e.*, particle matter (PM)). It was also considered that homogeneous reaction (*e.g.*, $\text{CO}+\text{H}_2\text{O}\rightarrow\text{CO}_2+\text{H}_2$) occurred in the gas phase and heterogeneous reactions (*e.g.*, $\text{C}+\text{H}_2\text{O}\rightarrow\text{CO}+\text{H}_2$) occurred at the gas and solid phases. The single particle model accounting for biomass particle properties was discretized in the radial direction.

Four solid or liquid species (water, volatiles, fixed carbon, and ash) and six producer gas (H_2 , CO , CO_2 , CH_4 , N_2 , and H_2O) were considered using a finite volume method and governing equations (mass and energy balance) were used to calculate the gas mixture composition (especially for the yields of H_2 , CO , and CH_4). The following assumptions were established and have been commonly adopted in existing kinetic modelling of fixed bed gasification (153, 166, 315-318).

- Biomass particle was represented in a one-dimensional time domain.
- Solid and gas phases had the same temperature and temperature gradient, the density of the solid phase was the same.
- Gaseous species were ideal gas.
- Gravity was negligible.
- The pressure at the surface of the particles was assumed to be the same as the inside of the reactor.
- The thickness of the reactive zone was constant.

3.1.1.2 Governing equation

In the kinetic model, the shape and aspect ratio of the shrinking particle do not change, even though the particle size continuously decreases. The considered species include biomass, char, liquid water, producer gas (include water vapor and inert gas), and tar. Biomass, char, and liquid water are considered by the equations of solid-phase species with their density being modelled, while producer gas and tar are considered by the equations of gas-phase species with their volume being quantified by the volume of the pores of the particle. In summary, the mass balance of a porous biomass particle is composed of instantaneous particle mass and cumulative mass, and it can be mathematically expressed as (319):

$$m_{B0} + m_{MC} = \int_{r_c}^{r_p} \rho_p (4\pi r^2) dr + 4\pi r_p^2 \varepsilon_p u \sum_i \rho_{g,p} \quad (3.1)$$

where m_{B0} is the initial mass of the unreacted particle, m_{MC} is the moisture content of the biomass particle, ρ_p is the density of the biomass particle, r_p is the initial radius of the biomass particle, r_c is the radius of biomass particle upon the finish of the gasification process shown in Figure 3.2, u is the velocity of biomass particle in the reactor, $\rho_{g,p}$ is the density of gas phase species.

The mass change of the biomass particle is equal to the cumulative mass of the gas released from the particle. The yield of gas species $Y_{i,g,p}$ is defined by (153):

$$Y_{i,g,p} = \left\{ \int_0^\infty \left[\int_{r_c}^{r_p} \rho_{g,p} (4\pi r^2) dr + \int_0^t \left(\frac{dm_{g,p}}{dt} \right) dt \right] \times E(t) dt \right\} / (m_{B0} + m_{MC}) \quad (3.2)$$

where $E(t)$ is defined as the distribution function of residence time for perfectly mixed gas phase species (320):

$$E(t) = \frac{1}{\tau_s} \times \exp\left(-\frac{t}{\tau_s}\right) \quad (3.3)$$

where the mean gas phase species residence time τ_s is obtained by dividing the particle mass with the mass flow rate of cumulative mass.

The instantaneous equilibrium equation of continuity (containing mass and energy) is solved by the finite control volume method. The continuity equation in the gas phase accounts for the convective mass transfer and the species produced in the heterogeneous reactions between the solid and gas phases. The mass balance of the overall gas species is expressed as (153):

$$\begin{aligned} \frac{d(\varepsilon_p \rho_{g,p})}{dt} = & -\frac{1}{r^2} \frac{d}{dr} (r^2 u_{g,p} \varepsilon_p \rho_{g,p}) + \frac{1}{r^2} \frac{d}{dr} \left[r^2 \varepsilon_p D_i \frac{d(\rho_{g,p} Y_{i,g,p})}{dr} \right] + \sum_k \varepsilon_p \dot{r}_{vol,k} v_{k,i} M_i \\ & + \sum_k (1 - \varepsilon_p) \dot{r}_{suf,k} v_{k,i} M_i A_v \end{aligned} \quad (3.4)$$

where ε_p is porosity of the particle, $\rho_{g,p}$ is density of gas species that can be calculated from the ideal gas law $\rho_{g,p} = \frac{pM}{RT_g}$, D_i is the diffusivity of gas species, $\dot{r}_{vol,k}$ is the volume reaction rate of the reaction numbered with k , $\dot{r}_{suf,k}$ is the surface reaction rate, $v_{k,i}$ is the stoichiometric number of gas species of the reaction numbered with k , and M_i is the molecular weight of gas species, A_v is the specific surface area, $u_{g,p}$ is the velocity of gas species, as given by:

$$u_{g,p} = \frac{1}{4\varepsilon_p \pi r^2} \int_{r_0}^{r_p} \frac{[\sum_i \varepsilon_p \dot{r}_{vol,k} v_{k,i} M_i + \sum_i (1 - \varepsilon_p) \dot{r}_{suf,k} v_{k,i} M_i A_v] dV}{\rho_{g,p}} dr \quad (3.5)$$

The composition and yields of the producer gases are determined using the source terms of convective mass transfer, diffusive mass transfer, and the species produced in homogeneous and heterogeneous reactions. Each species is assumed to be made of carbon, hydrogen, and oxygen. The mass balance of gas species is expressed as (153):

$$\begin{aligned} \frac{d(\varepsilon_p \rho_{g,p} Y_{i,g,p})}{dt} = & -\frac{1}{r^2} \frac{d}{dr} (r^2 u_{g,p} \varepsilon_p \rho_{g,p} Y_{i,g,p}) + \frac{1}{r^2} \frac{d}{dr} \left[r^2 \varepsilon_p D_i \frac{d(\rho_{g,p} Y_{i,g,p})}{dr} \right] + \sum_k \varepsilon_p \dot{r}_{vol,k} v_{k,i} M_i \\ & + \sum_k (1 - \varepsilon_p) \dot{r}_{suf,k} v_{k,i} M_i A_v \end{aligned} \quad (3.6)$$

The mass balance of the solid phase is expressed as (153):

$$\frac{d}{dt} \left[\frac{1}{3} \rho_{s,p} (r_p)^3 \right] = \sum_j \dot{r}_{suf,k} v_{k,j} M_j (r_p)^2 \quad (3.7)$$

Assuming the gas, liquid, and solid phase of the particle are the same local temperature, the energy equation is expressed as (153):

$$\frac{dT_s}{dt} = -\frac{1}{\rho_{s,p}cp_{s,p}} \frac{dq_{s,s}}{dz} + A_v \frac{q_{g,s}}{\rho_{s,p}cp_{s,p}} + \frac{\sum_k \varepsilon_p \dot{r}_{vol,k} \Delta H_k + \sum_k (1-\varepsilon_p) A_v \dot{r}_{suf,k} \Delta H_k}{\varepsilon_p \rho_{g,p} cp_{g,p} + (1-\varepsilon_p) \rho_{s,p} cp_{s,p}} \quad (3.8)$$

where $q_{s,s} = -\kappa_p \frac{dT_s}{dz}$ is the conductive heat transfer in the solid phase. $q_{g,s}$ is calculated from the temperature difference (convective and radiative heat transfer) between the solid and gas phases (153): $q_{g,s} = h_{g,s}(T_g - T_s) + \sigma \epsilon (T_g^4 - T_s^4)$.

The total energy balance conservation equation about the temperature of the particle combines the gas phase and solid phase, and it is expressed as (153):

$$\begin{aligned} \frac{d(\varepsilon_p \rho_p cp_p T_p)}{dt} = & -\frac{1}{r^2} \frac{d}{dr} (r^2 \varepsilon_p \rho_{g,p} cp_{g,p} u_{g,p} T_p) + \frac{1}{r^2} \frac{d}{dr} [r^2 (1-\varepsilon_p) \kappa_p \frac{dT_p}{dr}] \\ & + \sum_i \frac{1}{r^2} \frac{d}{dr} [r^2 \varepsilon_p cp_{g,p} D_i T_p \frac{d(\rho_{g,p} Y_{i,g,p})}{dr}] + \sum_k \varepsilon_p \dot{r}_{vol,k} \Delta H_k \\ & + \sum_k (1-\varepsilon_p) A_v \dot{r}_{suf,k} \Delta H_k \end{aligned} \quad (3.9)$$

All reaction rate constants are expressed in the first-order Arrhenius form, and the kinetic parameters and heat of reactions are summarized in Table 3.1. In addition, the kinetic rate expressions of 9 gasification reactions included in the model are listed in Table 3.1. The kinetic rate of methanation is much lower than that of the other heterogeneous reactions. CH₄ is produced rapidly at the high partial pressure of H₂ in reaction (8). The catalytic effects of metal components (*e.g.*, Ca, Na, and K) on gasification reactions are not considered in this model and are worth future exploration as many studies have shown that they have a significant influence on biomass gasification reactions for high ash content biomass (31).

Table 3.1 Gasification reactions (where ‘j’ denotes heterogeneous reactions and ‘i’ represents homogeneous reactions).

Heterogeneous reactions				
	Reactions	Kinetic reaction rate (m/s)	E_a (kJ/kmol)	Ref
Boudouard	$C + CO_2 \rightarrow 2CO$	$R_{j,1} = 0.6 \times 10^3 T_s \exp\left(-\frac{26800}{T_s}\right)$	222,829	(321)
C partial combustion	$2C + O_2 \rightarrow 2CO$	$R_{j,2} = 2.3 \times T_s \exp\left(-\frac{11100}{T_s}\right)$	79,000	(322)
C complete combustion	$C + O_2 \rightarrow CO_2$	$R_{j,2}/R_{j,3} = 2.5 \times 10^3 \exp\left(-\frac{6420}{T_g}\right)$	27,118	(323)
Methane	$C + 2H_2 \rightarrow CH_4$	$R_{j,4} = 3.4 \times 10^{-3} T_s \exp\left(-\frac{15600}{T_s}\right)$	129,706	(321)
Homogeneous reactions				
	Reactions	Kinetic reaction rate (kmol m ⁻³ s ⁻¹)	E_a (kJ/kmol)	Ref
CO partial combustion	$CO + \frac{1}{2}O_2 \rightarrow CO_2$	$R_{i,5} = 1.3 \times 10^{11} \varepsilon \exp\left(-\frac{15105}{T_g}\right) C_{H_2O}^{0.5} C_{O_2}^{0.5}$	125,600	(166)
Water-gas shift	$CO + H_2O \leftrightarrow CO_2 + H_2$	$R_{i,6} = 2.8 \varepsilon \exp\left(-\frac{1511}{T_g}\right) \left[C_{CO} C_{H_2O} - \frac{\exp\left(-\frac{7914}{T_g}\right) C_{CH_2} C_{H_2}}{0.0265} \right]$	12,560	(324)
Steam-methane reforming	$CH_4 + H_2O \leftrightarrow CO + 3H_2$	$R_{i,7} = 3.0 \times 10^8 \varepsilon \exp\left(-\frac{15083}{T_g}\right) C_{CH_4} C_{H_2O}$	30,000	(324)
H ₂ combustion	$H_2 + \frac{1}{2}O_2 \rightarrow H_2O$	$R_{i,8} = 3.5 \times 10^8 \varepsilon \exp\left(-\frac{3670}{T_g}\right) C_{H_2}^{1.1} C_{O_2}^{1.1}$	30,514	(325)

3.2.1.3 Numerical solution procedure

A schematic diagram of the kinetic model is shown in Figure 3.2. The governing equations are discretized using a finite volume scheme, and a representative particle was chosen and modelled as a shrinking sphere. The particle moves toward the z-direction to the bottom of the reactor with a velocity of u . input parameters include biomass properties (ΔH is the enthalpy of biomass, and k is the heat conductivity of biomass particle), gasifier bed properties (L is the length of gasifier reactor, L_a is the length of the region above gasifier reactor, A_c is the cross sectional area of gasifier reactor, and ε_b is the porosity of fixed bed), and species properties ($cp_{g,p}$ and $cp_{s,p}$ are specific heat capacity of gas-phase and solid-phase species, $k_{g,p}$ and $k_{s,p}$ are heat conductivity of gas-phase and solid-phase species, and η is dynamic viscosity). The values of model input and parameters are shown in Table 3.2.

Table 3.2 List of model inputs and parameters (153, 166, 298).

Characteristics of gasifier reactor	L (m)	0.50
	L_a (m)	0.25
	A_c (m ²)	0.07
	ε_b (-)	0.40
	Biomass resident time (sec)	360.00
Species properties	$cp_{g,p}$ (J kg ⁻¹ K ⁻¹)	$1053.92 - 0.40T_g + 9.55 \times 10^{-4}T_g^2 - 5.73 \times 10^{-7}T_g^3 + 6.99 \times 10^{-11}T_g^4$
	$cp_{s,p}$ (J kg ⁻¹ K ⁻¹)	1,350.00
	$k_{g,p}$ (W m ⁻¹ K ⁻¹)	$3.14 \times 10^{-4}T_g^{0.78} / (1 - \frac{0.71}{T_g} + \frac{2121.70}{T_g^2})$
	$k_{s,p}$ (W m ⁻¹ K ⁻¹)	0.08
	η (10 ⁻⁵ Pa s ⁻¹)	$-1.22 \times 10^{-3} + 0.01T_g - 7.45 \times 10^{-4}T_g^2 - 5.73 \times 10^{-7}T_g^3 + 6.99 \times 10^{-11}T_g^4$
Time step	Δt (sec)	10 ⁻³
Finite volume length	Δz (m)	0.01
Equivalent ratio	(-)	0.29
Feeding rate	(kg/h)	10

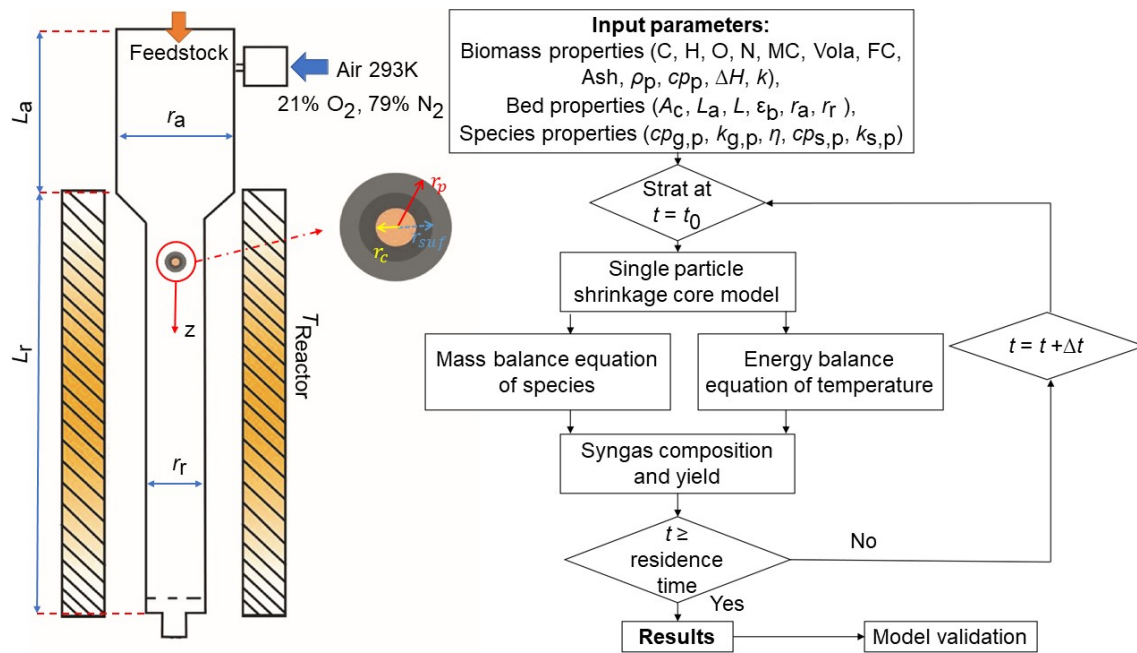


Figure 3.2 A schematic diagram of the kinetic model coupling the shrinkage core model and fixed bed gasification.

3.1.2 Monte Carlo simulation

The MC simulation is a stochastic approach based on a randomization process that involves probability distributions of data variables collected based on past data, and theoretical probability distribution (326). For an actual gasification process, numerous particles are involved and there are variations in the process parameters. To account for the variations and potential uncertainty of the parameters, a stochastic kinetic model was generated by combining the above kinetic model with the MC approach. It is unclear which probability distribution is most suitable for describing the process parameters for MC simulation. Hence, in this work, two types of probability distributions (*i.e.*, uniform and normal) were explored and defined based on experimental data to generate stochastic values for major process parameters (*i.e.*, water content, particle size, porosity, thermal conductivity, emissivity, shape, and reaction temperature) for the MC simulation. The MC approach for this model was to take random values for process parameters in uniform and normal distributions, and the data based on which the distributions were defined are from 10 experimental studies on fixed bed gasifier (wood as the feedstock) as summarized in Table 3.3. The water content ranges from 9.29wt.% to 11.29wt.%, the porosity data ranges from 0.20 to 0.35, the size data ranges from 1.00 to 2.00 mm, the thermal conductivity data ranges from 0.18 to 0.22 W/mK, the emissivity data ranges from 0.72 to 0.77, the particle shape data is spherical, cylinder, and flat, and the reaction temperature data ranges from 700 to 900°C.

Table 3.3 Summary of process parameters for constructing the probability distributions.

Feedstock	Water content (wt.%)	Porosity	Size (mm)	Thermal conductivity (W/mK)	Emissivity	Shape	Temperature (°C)	Ref
Wood	8.0	0.3	2.0	0.2	0.8	sphere	800.0	(166)
Wood	10.0	–	0.5–5.0	0.1–0.2	–	–	400.0–1,400.0	(327)
Wood	15.0	0.3–0.4	0.3–3.0	–	–	–	850.0–925.0	(23)
Wood	11.7	–	0.2–0.3	0.1	–	flat	700.0–900.0	(328)
Wood	12.0	–	2.0	–	0.8–0.9	flat	780.0–840.0	(329)
Wood	4.4–15.2	0.5	25.4	–	–	cylinder	800.0–900.0	(330)
Wood	9.0	–	0.3–1.0	–	–	sphere	800.0–1,000.0	(331)
Wood	7.0–16.1	–	6.0	–	–	cylinder	800.0–1,000.0	(332)
Wood	11.5	–	1.0–10.0	–	–	flat	900.0–1,050.0	(333)
Wood	9.5	0.5	2.0	–	0.9	cylinder	800.0–1,000.0	(334)

The mean (μ) and standard deviation (σ) of the distributions (uniform and normal) for each process parameter were calculated by Eq. (3.10) & (3.11) and were listed in Table 3.4.

$$\mu = \frac{\sum_{a=1}^N (x_a)}{N} \quad (3.10)$$

$$\sigma = \sqrt{\frac{1}{N} \sum_{a=1}^N (x_a - \mu)^2} \quad (3.11)$$

where N is the number of parameters, and x_i is the individual value of a parameter.

Table 3.4 Means and standard deviations for the distributions of the process parameters.

Input factors	Range	μ	σ
Feedstock			
Water content (wt.%)	9.29–11.29	10.28	0.36
Porosity	0.20–0.35	0.26	0.03
Size (mm)	1.00–2.00	1.50	0.19
Thermal conductivity (W/mK)	0.18–0.22	0.20	0.71×10^{-2}
Emissivity	0.72–0.77	0.75	0.89×10^{-2}
Shape	–	–	–
Reactor			
Temperature (°C)	700.00 – 900.00	802.99	34.95

3.1.3 Random Forest model evaluation

3.1.3.1 Evaluation metrics for decision tree

The RF algorithm is an ensemble learning method based on bagging (335). The standard binary decision tree used to solve this regression problem is defined with several branches, a root, several nodes, and leaves. Basically, a branch is a chain of nodes from the root to the leaves, with each node referring to an attribute (336). The splitting criteria for the regression tree is also known as Classification and Regression Trees (CART). During the growth of each regression tree, a Gini Index (GI) is the best principle to judge the classification quality in the CART (337). The dataset $D(o)$ is classified into subset $D(s)$ (containing the elements of all process parameters) and the GI for each subset was expressed as Eq. (3.12). The GI value reflects the purity of the subset. The lower GI value implies the higher quality of classification based on the optimal attribute k^* is selected as the results, and it expressed as Eq. (3.13).

$$\text{Gini_index}(D(o), k^*) = \sum \frac{|D(s)|}{|D(o)|} \text{Gini}(D(s)) \quad (3.12)$$

$$k^* = \arg \min \text{Gini_index}(D(o), k^*) \quad (3.13)$$

The schematic topological architecture of the RF algorithm is shown in Figure 3.3. The regression tree is trained by a bootstrap technique that randomly selects 2/3 of the training data as In Bag (IB) data, and the unselected training data were called Out Of Bag (OOB) data. The OOB data not involved in the training of the regression tree can be used to determine the optimal number of trees by a trial-and-error method (338). The ultimate predictions of the trained RF algorithm are the average predictions of all trees. The number of trees is chosen to be sufficiently large so that a stabilized OOB error can be achieved. In this study, the number of trees tested is from 1 to 500, and the number of process parameters set at each split is 6. The modelling process ends when the OOB data error has stabilized (being constant). This improves the usage of computational resources). The model was run using PC with Intel Core i9 10900K 5.3 GHz processor and 64 GB of RAM, running Windows 10. The splitting criterion for each decision tree depends on the importance of the process parameters which is determined by the value of the percentage increase in mean squared error (%IncMSE) and the total decrease in node impurity (IncNodePurity). The value of %IncMSE is normalization of average of the difference across all trees by the standard deviation: $\Delta\text{MSE}/\text{MSE}_0 \times 100\%$ (339). The value of

IncNodePurity is measured by using the Gini index, which averages the sum of overall number of trees when the variables are split at each node (340).

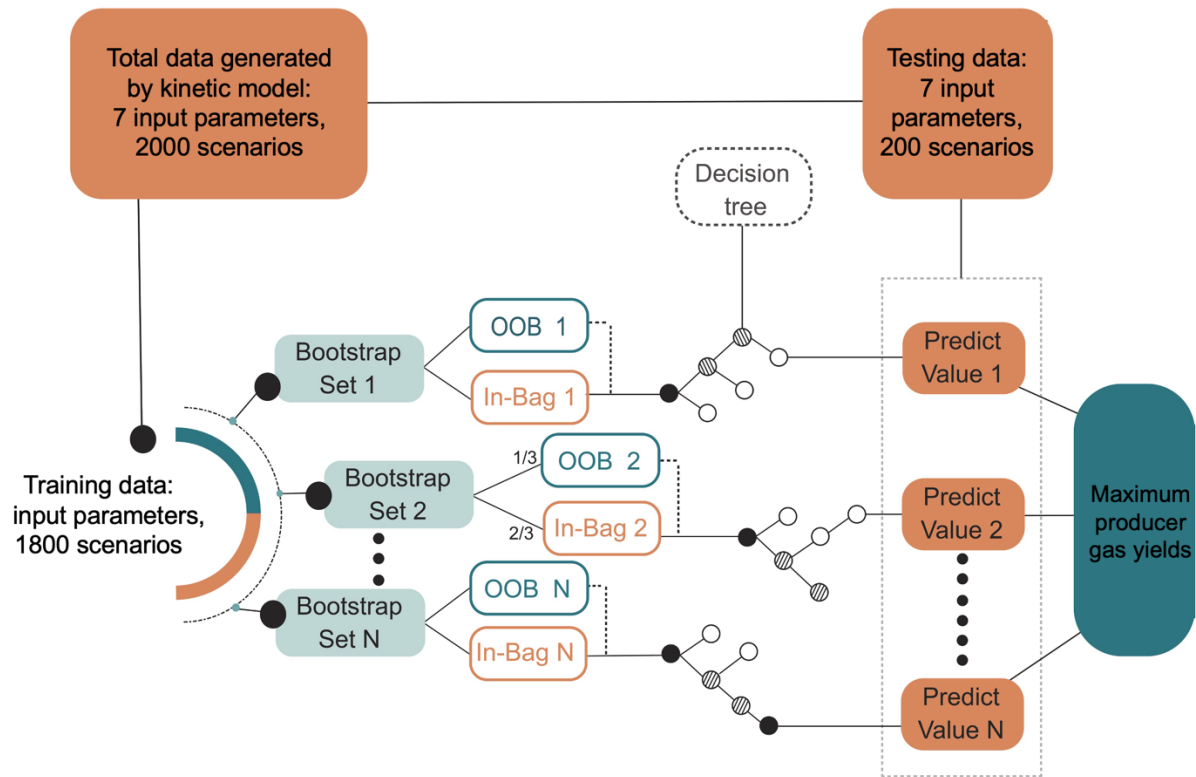


Figure 3.3 The schematic diagram of the topological structure of the RF algorithm.

3.1.3.2 Evaluation metrics for model performance

The RMSE, R^2 , and mean absolute error (MAE) are metrics to measure the accuracy of a RF algorithm in regression analysis by comparing the error between the predicted data and the test data (341). Lower values for the RMSE and MAE will imply the model is more accurate while higher values (close to 1) for R^2 will imply the model is more accurate. The RMSE measures the standard deviation of residuals and is expressed in Eq. (3.14). The R^2 represents the proportion of the variance in the dependent process parameter and is calculated by Eq. (3.15). And the MAE measures the average of the residuals in the dataset, which is expressed in Eq. (3.16).

$$\text{RMSE} = \sqrt{\frac{1}{N} \sum (y_{\text{predict}} - y_{\text{test}})^2} \quad (3.14)$$

$$R^2=1 - \frac{\sum (y_{\text{predict}} - y_{\text{test}})^2}{\sum (y_{\text{predict}} - \bar{y})^2} \quad (3.15)$$

$$\text{MAE} = \frac{1}{N} \sum |y_{\text{predict}} - y_{\text{test}}| \quad (3.16)$$

where N is the total number of total data, y_{predict} is the value of prediction, y_{test} is the value of a testing data, \bar{y} is the mean value of all the data. The validation of the RF algorithm was conducted by comparing its predictions with experimental data gathered from the literature.

3.2 Results and discussion

3.2.1 Kinetic model validation

The experimental process parameters (Table 3.5) of Garcia-Bacaicoa *et al.* (342), Jayah *et al.* (343), and Zainal *et al.* (344) were inputted into the kinetic model to predict the producer gas (*i.e.*, H₂, CO, CO₂, CH₄, and N₂) yields for validation. Figure 3.4 shows the comparison between the prediction of producer gas yields and the experimental results. The predicted yields of producer gas are within 6.6% of the experimental results of Garcia-Bacaicoa *et al.* (342). The difference between the experimental and modelling results could be attributed to the fact that only the composition of wood was applied as input parameters while 10–17% polyethylene was mixed with wood as the feedstock for the experiments. This is one of the limitations of the current model based on the consideration of biomass gasification, which warrants further improvement. The predicted yields of producer gas are within 12.8% of the experimental results of Jayah *et al.* (343). A comparison of H₂/CO ratio shows that the error is 2.25% against the experimental data of Garcia-Bacaicoa *et al.* (342), 5.75% of Jayah *et al.* (343), and 2.98% of Zainal *et al.* (344).

Table 3.5 Composition of feedstocks and gasifier process parameters from three existing experimental studies.

Feedstock	García-Bacaicoa <i>et al.</i> (342)	Jayah <i>et al.</i> (343)	Zainal <i>et al.</i> (344)
	Wood	Wood	Wood
C (wt.%)	35.12	50.60	46.40
H (wt.%)	7.57	6.50	5.70
O (wt.%)	56.96	42.00	47.70
N (wt.%)	-	0.20	0.20
Ash (wt.%)	0.32	0.70	1.10
Volatile matter (wt.%)	60.76	80.10	-
Fix carbon (wt.%)	9.92	19.20	-
Water content (wt.%)	29.00	14.50	-
Mean particle size (mm)	40.00	44.00	50.00
Mean air flowrate (kg/h)	36.70	34.60	-
Reaction temperature (°C)	1,092.00	1,000.00	1,000.00
Gasifier type	Fixed	Fixed	Fixed

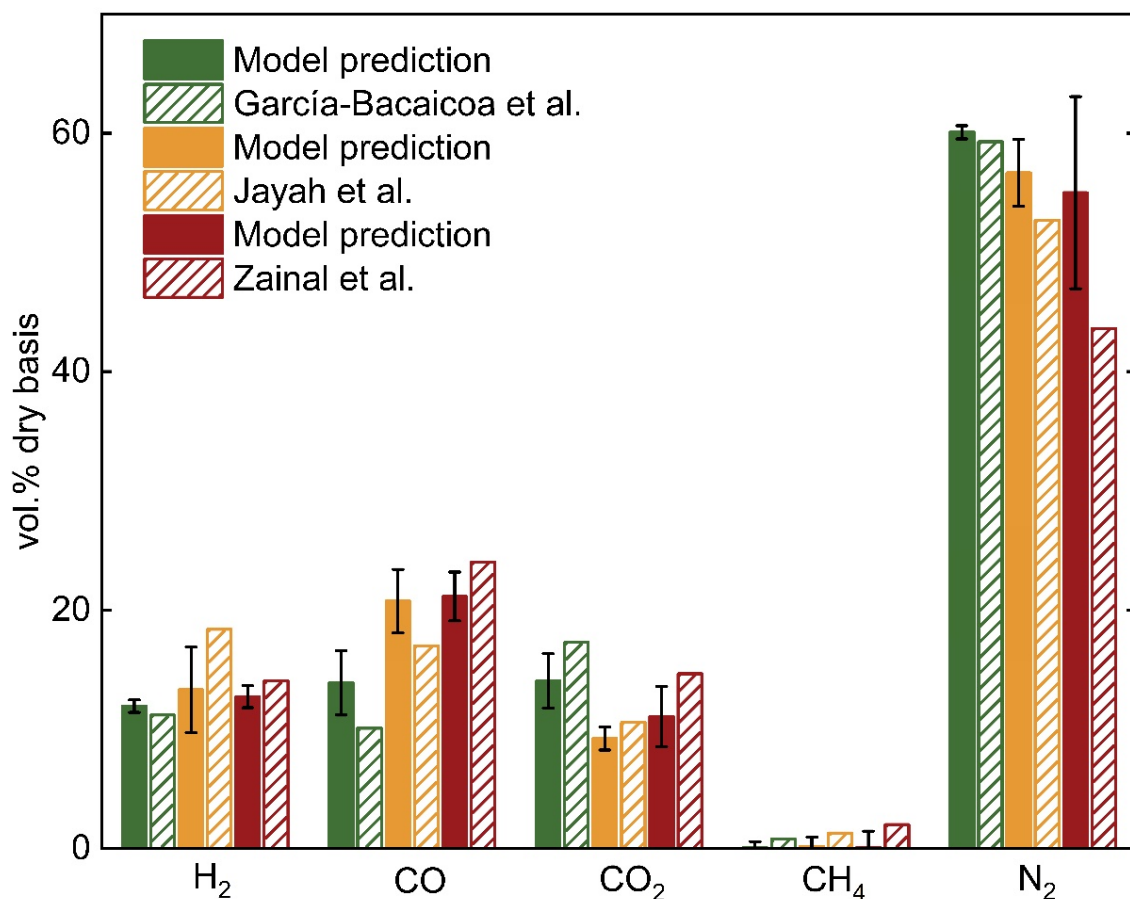


Figure 3.4 Comparisons between the kinetic model predictions and experimental results.

3.2.2 Random forest model

The stochastic kinetic model was used to generate 2,000 datasets based on the uniform and normal distributions, respectively. The RF algorithm was used to determine the importance of process parameters on the producer gas yields and to find the optimal process parameters leading to the maximum producer gas yield.

3.2.2.1 Decision tree

The results of the quality evaluation of the RF algorithm for the uniform and normal distribution cases are shown in Table 3.6. For the uniform distribution case, the value of RMSE, R^2 , and MAE is 2.516×10^{-8} , 0.996, and 2.556×10^{-5} for CH₄; 2.468×10^{-8} , 0.994, and 2.009×10^{-5} for H₂; 9.114×10^{-6} , 0.998, and 4.686×10^{-4} for CO. RMSE decreased sharply and remained stable as the number of trees increases. R^2 increased gradually and remained stable. The best numbers of the decision tree ($N_{\text{tree-best}}$) for CH₄, H₂, and CO are 292, 283, and 239 as shown in Figure 3.5(a). For the normal distribution, the values of RMSE, R^2 , and MAE are 3.526×10^{-19} , 0.994, and 1.511×10^{-10} for CH₄; 3.555×10^{-19} , 0.994, and 1.265×10^{-10} for H₂; 1.177×10^{-16} , 0.997, and 2.827×10^{-9} for CO. For CH₄, H₂, and CO, the best numbers of the decision tree ($N_{\text{tree-best}}$) are 143, 233, and 247 as shown in Figure 3.5(b).

Table 3.6 Quality indicators of RF algorithm based on the training data (uniform and normal distributions).

	Uniform distribution			Normal distribution		
	RMSE	R^2	MAE	RMSE	R^2	MAE
CH ₄	2.516×10^{-8}	0.996	2.556×10^{-5}	3.526×10^{-19}	0.994	1.511×10^{-10}
H ₂	2.468×10^{-8}	0.994	2.009×10^{-5}	3.555×10^{-19}	0.994	1.265×10^{-10}
CO	9.114×10^{-6}	0.998	4.686×10^{-4}	1.177×10^{-16}	0.997	2.827×10^{-9}

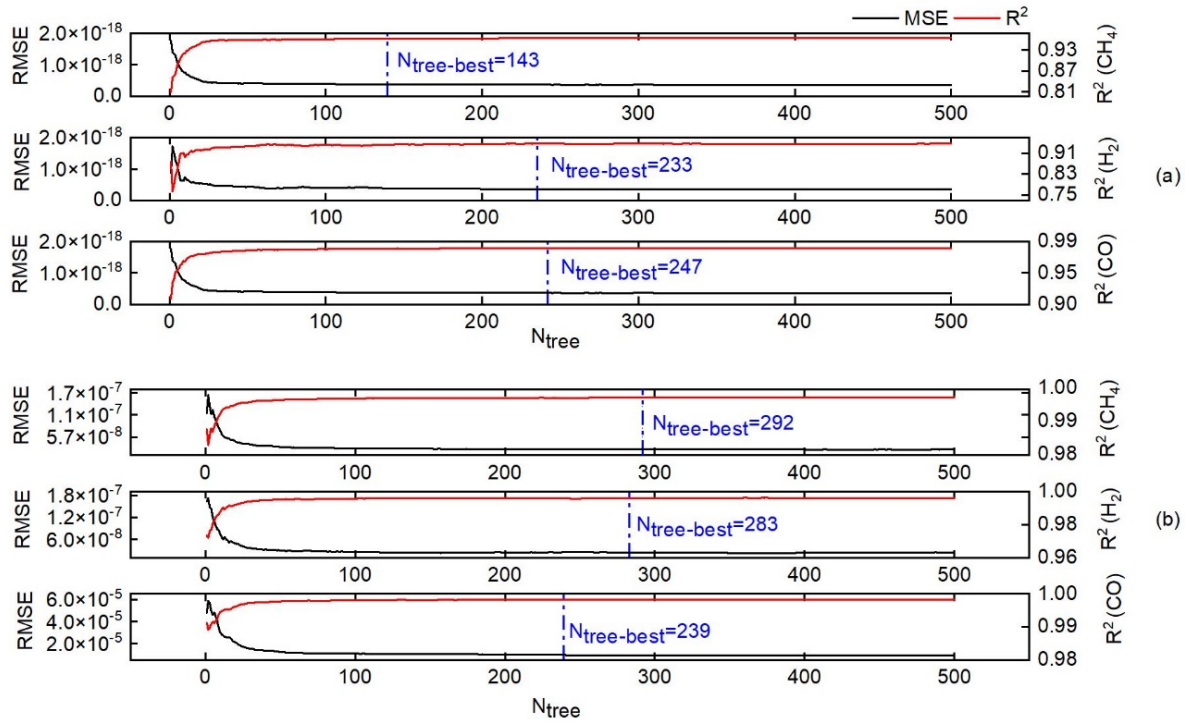


Figure 3.5 Test results for determining the optimal tree numbers in RF algorithm for H₂, CO, and CH₄ ((a) uniform and (b) normal distributions).

3.2.2.2 Variable importance

Figure 3.6(a) and (b) show the importance of process parameters on the producer gas yield based on the values of %IncMSE and IncNodePurity (as mentioned in Section 3.1.3.2). High values of these two metrics indicate high importance of a parameter on producer gas yields. The values of %IncMSE (17.04–20.30% for uniform distribution and 14.97–17.76% for normal distribution) and IncNodePurity (0.008–0.009 for uniform distribution and 0.024–0.038 for normal distribution) for temperature are higher than the other process parameters in both the uniform and normal distribution cases, so temperature has the greatest impact on producer gas yields. Furthermore, it is also shown that the yields of H₂ and CO are strongly influenced by temperature.

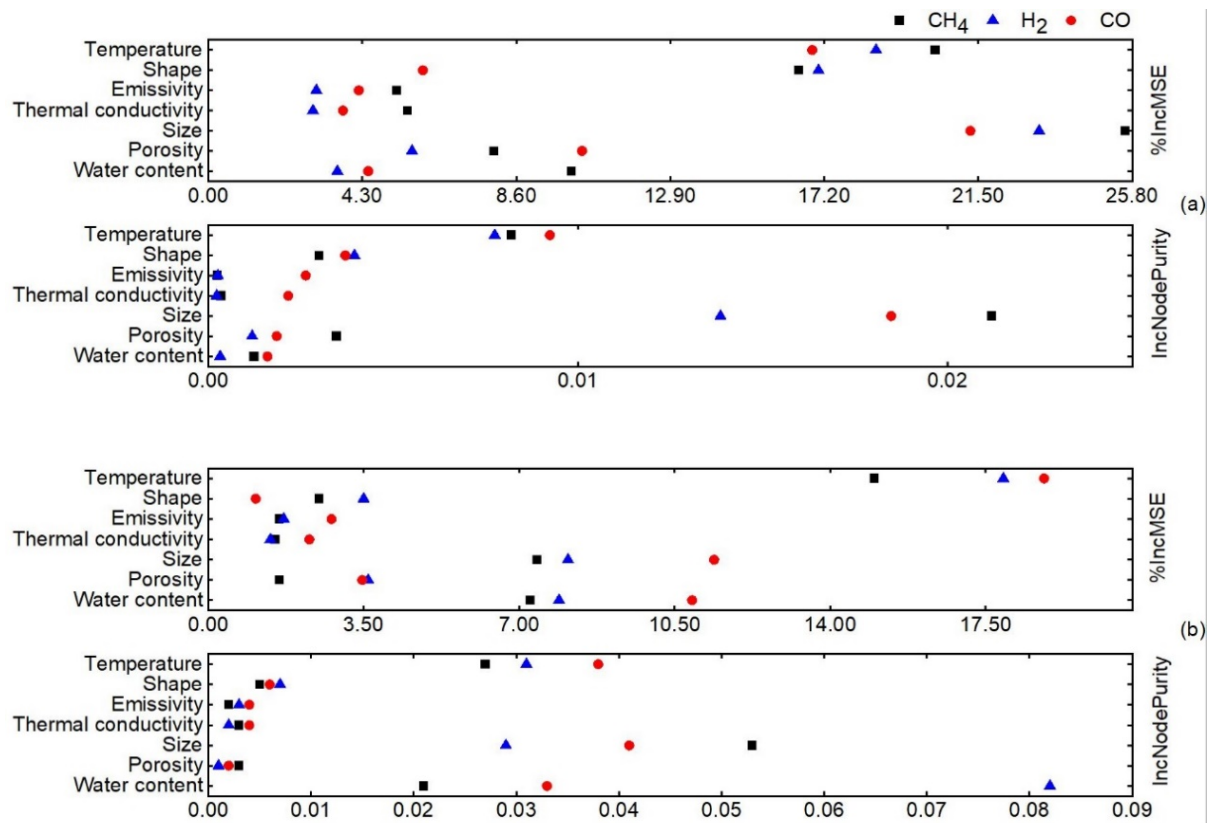


Figure 3.6 Measured relative importance of each input parameter for producer gas yield ((a) uniform and (b) normal distributions).

The values of %IncMSE and IncNodePurity for the particle size for the uniform distribution case are 21.51–25.61% and 0.014–0.021, and 7.30–8.91% and 0.028–0.053 for the normal distribution case. These indicate that, following temperature, particle size has a relatively high impact on the producer gas yields compared to the other process parameters (particle shape (%IncMSE is 8.13–17.04%, IncNodePurity is 0.003–0.004 for uniform distribution, and %IncMSE is 1.48–3.25%, IncNodePurity is 0.006–0.008 for normal distribution)).

The values of %IncMSE and IncNodePurity indicated that the water content has a minor impact on producer gas yield (the value of %IncMSE and IncNodePurity for the uniform distribution case is 3.60–10.15% and 0.001–0.003, and 7.30–9.91% and 0.021–0.081 for the normal distribution case). Both the values of %IncMSE and IncNodePurity in the uniform distribution and the normal distribution cases indicated that the emissivity, thermal conductivity, and particle porosity on producer gas yields can be neglected.

3.2.2.3 Evaluation of the RF model

The validation of the quality of the RF algorithm was achieved by comparing the predicted results with the testing data as shown in Table 3.7 and Figure 3.7. For the uniform distribution case, the values of RMSE, R^2 , and MAE are 1.779×10^{-4} , 0.996, and 6.950×10^{-5} for CH₄; 1.491×10^{-4} , 0.994, and 5.258×10^{-5} for H₂; 2.805×10^{-3} , 0.996, and 1.206×10^{-3} for CO. For the normal distribution case, the values of RMSE, R^2 , and MAE are 7.242×10^{-10} , 0.962, and 4.230×10^{-10} for CH₄; 4.700×10^{-10} , 0.967, and 3.041×10^{-10} for H₂; 1.102×10^{-8} , 0.982, and 7.397×10^{-9} for CO. Figure 3.7 shows the predictions of the RF model for both the uniform and normal distribution cases agree with the testing data.

Table 3.7 Quality indicators of the RF algorithm based on the testing data (uniform and normal distributions).

	Uniform distribution			Normal distribution		
	RMSE	R^2	MAE	RMSE	R^2	MAE
CH ₄	1.779×10^{-4}	0.996	6.950×10^{-5}	7.242×10^{-10}	0.962	4.230×10^{-10}
H ₂	1.491×10^{-4}	0.994	5.258×10^{-5}	4.700×10^{-10}	0.967	3.041×10^{-10}
CO	2.805×10^{-3}	0.996	1.206×10^{-3}	1.102×10^{-8}	0.982	7.397×10^{-9}

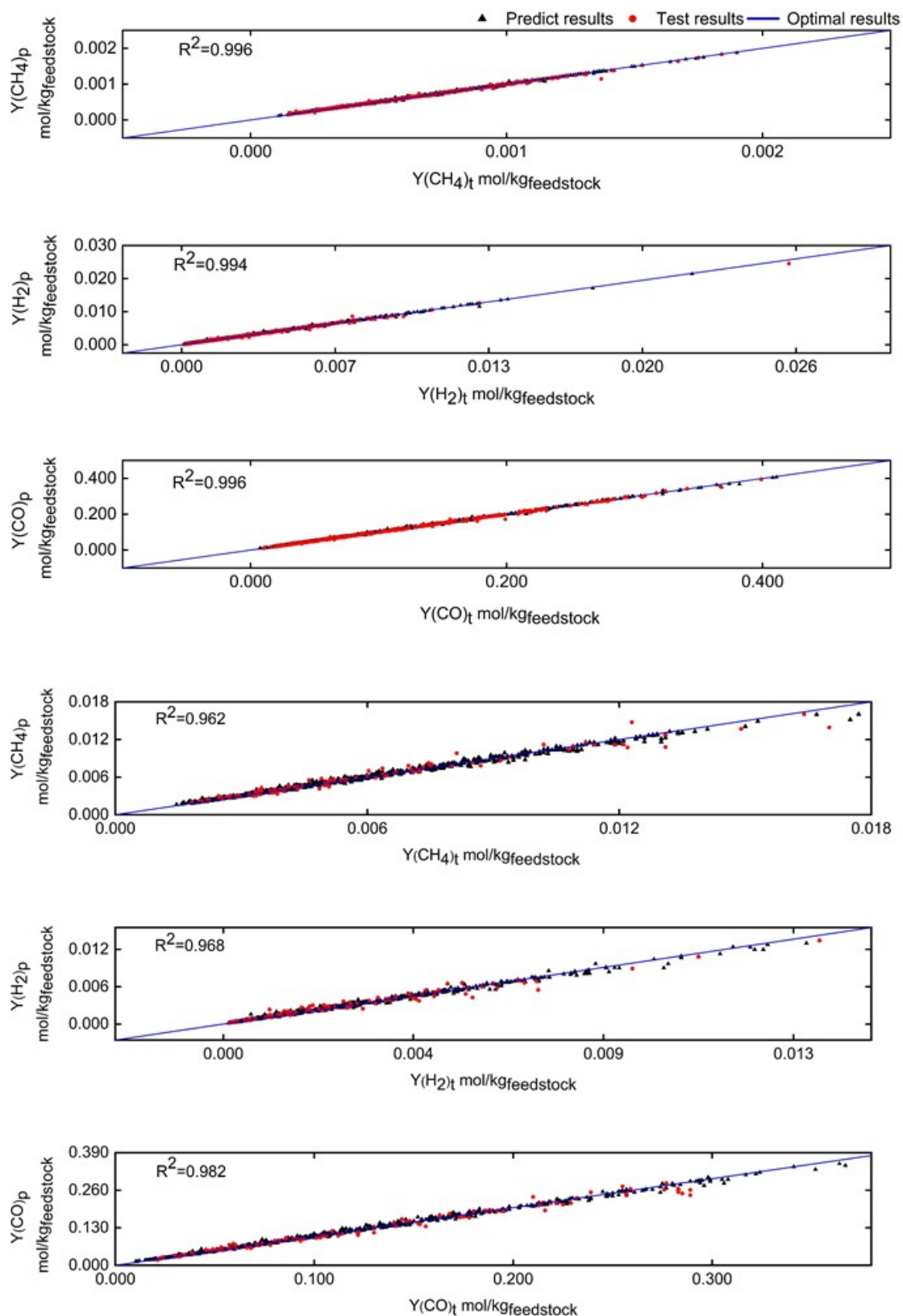


Figure 3.7 Validation results of RF algorithm for producer gas yields ((a) uniform and (b) normal distributions).

3.2.2.4 Model results

The water content, particle size, and reaction temperature were considered to have a higher impact on the producer gas yields as compared to other process parameters as shown above. The RF algorithm predicts the maximum yields of H₂, CO, and CH₄ as 2.43×10^{-2} , 40.78×10^{-2} , and 0.19×10^{-2} mol/kg_{feedstock} for the uniform distribution case and 2.31×10^{-2} , 37.89×10^{-2} , and 0.17×10^{-2} mol/kg_{feedstock} for the normal distribution case are shown in Table 15. It is also shown that the predicted optimal parameters for the normal distribution case are closer to the experimental data than the uniform distribution case. The results indicated that the normal distribution is a more reasonable representation of the actual process parameters.

3.3 Summary

In this chapter, a stochastic biomass gasification model based on the combination of the MC simulation approach and an RF algorithm is developed. The model was used to optimize the fixed bed air gasification with wood as feedstock for a broad range of process parameters. The parameters importance analysis of the RF model showed that particle size, reaction temperature, and water content have a high influence on the producer gas yield. However, the effects of particle shape, emissivity, thermal conductivity, and porosity on producer gas yield can be negligible during the gasification process. The predictions of producer gas yield in the normal distribution case are more informative and reliable, which fits the experimental better than the uniform one. The predictions for the normal distribution case were closer to the experimental data obtained from existing literature than for the uniform distribution case. The model was used to predict the optimal producer gas yield and process parameters of wood gasification and it was shown that the predictions were generally in good agreement (<12% difference for the case of normal distribution) with existing experimental results as shown in Table 3.8. The model developed in this work could be used for determining the optimal process parameters for the techno-economic analysis (TEA) and life cycle assessment (LCA) towards better system and process designs.

It is worth noting that some factors have not been included in this study partially due to lack of relevant data. For example, air to feedstock ratio is not directly considered by the model. However, this factor is closely related to the reaction temperature and particle size both of which are modelled, and thus is implicitly considered by the developed model. Therefore, a fixed air to feedstock ratio=0.29 (obtained from the literature) was applied in this study. In addition, tar formation is considered as an intermediate factor of the kinetic model affecting

the producer gas yield. As this study focuses on producer gas yield, tar production and CO₂ are not analyzed as the outputs of the model. The developed the framework could be further adapted to include the additional parameters when associated data is available in the future.

Table 3.8 Comparison of producer gas yields and optimal process parameters from the RF algorithm to the experimental data.

	CH ₄				H ₂				CO			
	Prediction		Experiment		Prediction		Experiment		Prediction		Experiment	
	Uniform	Normal	(332)	(345)	Uniform	Normal	(346)	(347)	Uniform	Normal	(168)	(348)
Maximum yield (mol/kg _{feedstock})	0.19×10^{-2}	0.17×10^{-2}	0.17×10^{-2}	0.17×10^{-2}	2.43×10^{-2}	2.31×10^{-2}	2.23×10^{-2}	2.30×10^{-2}	40.78×10^{-2}	37.89×10^{-2}	38.23×10^{-2}	33.83×10^{-2}
Process conditions												
Water content (wt.%)	11.20	10.86	8.35	7.40	10.80	10.80	8.22	8.00	11.10	11.10	9.71	12.00
Size (mm)	2.00	1.90	2.50	2.00	1.96	1.96	1.20	-	2.00	1.99	1.00	7.00
Temperature (°C)	732.56	722.79	740.00	800.00	900.10	900.10	900.00	900.00	875.27	875.27	867.00	850.00

Chapter 4 Life cycle assessment and techno-economic analysis of concentrated solar thermal gasification of biomass for continuous electricity generation

In the previous chapter, reaction temperature was defined as the most influential parameter affecting gas production in a gasifier. Specifically, optimizing the reaction temperature to $\sim 800^{\circ}\text{C}$ maximizes producer gas yield. Building upon this insight, the concentrated solar thermal gasification of biomass (CSTGB) system was meticulously designed, designing the configuration of the CST subsystem and gasifier to operate optimally at 800°C . Furthermore, the gas produced was directly integrated into a combined cycle gas turbine (CCGT) subsystem for electricity generation. The CCGT configuration was tailored to match producer gas yield volume and included a carbon capture and storage (CCS) unit to capture CO_2 emissions effectively. The content of this chapter has been published as a journal article⁽⁴⁸⁾ in the journal Energy. In this chapter, the environmental impacts and economic feasibility of the CSTGB system development in a specific location (*i.e.*, Spain) known for its abundant solar energy and biomass resources. This location selection also ensures that the system can fully leverage the synergies of three different heat supply strategies (thermal energy derived from the combustion of a partial of feedstock, solar thermal energy from the concentrated solar tower (CST) subsystem, and thermal energy stored within the thermal energy storage (TES) subsystem) in a real-world environmental. The proposal of an all-weather and 24/7 operational CSTGB system consisting of 4 main subsystems, namely CST, TES, downdraft fixed bed gasifier, and CCGT with CCS. Waste wood serves as the primary feedstock, sourced from three cities (*i.e.*, Seville, Cordoba, and Malaga). This comprehensive analysis provides a holistic understanding of the system's environmental performance and economic feasibility, contributing valuable insights to the field of the CSTGB system development and sustainable energy solutions in the future. In this chapter, the significant potential of the CSTGB system in mitigating the carbon footprint associated with electricity generation has been highlighted. According to the life cycle assessment (LCA) results, the proposed CSTGB system could potentially save over 0.5 million tons of carbon emissions, equivalent to global warming potential (GWP) reduction of -787.7 $\text{kgCO}_2\text{-eq/ton}$ of waste wood, while simultaneously generation more than 0.8 million MWh of electricity annually. The sensitivity analysis conducted for the LCA revealed that the efficiency of the CCS subsystem played a pivotal role in determining the GWP of the CSTGB system. The TEA results for the 30th year revealed a NPW of approximately $\text{€}-0.7$ billion, signifying

that the system was unprofitable and had a payback period exceeding 30 years. However, the sensitivity analysis for economic viability demonstrated that the possibility of making the system economically feasible within a considerably shorter payback period, ideally under 10 years. This could be accomplished by either reducing the operational and maintenance (O&M) costs by 19% (equivalent to 43.9 €/MWh) or enhancing the overall system efficiency by 20%.

4.1 Methodology

A schematic illustration of the methodology including system design, LCA, and techno-economic analysis (TEA) is shown in Figure 4.1. For the system design, thermodynamic analysis was carried out to decide the gasifier specification (includes reaction temperature, thermal energy demand, and air to feedstock ratio) and SolarPILOT software was used to determine the heliostat specification (*i.e.*, area and layout), and the CST receiver specification (*i.e.*, the surface area of receiver and tower height), followed by the use of our recent model (199) to decide the optimal process conditions to achieve maximum synthesis gas production. The information of process conditions and system configurations were then used in the LCA and TEA to evaluate the GWP and net present worth (NPW) of the development of the CSTGB system.

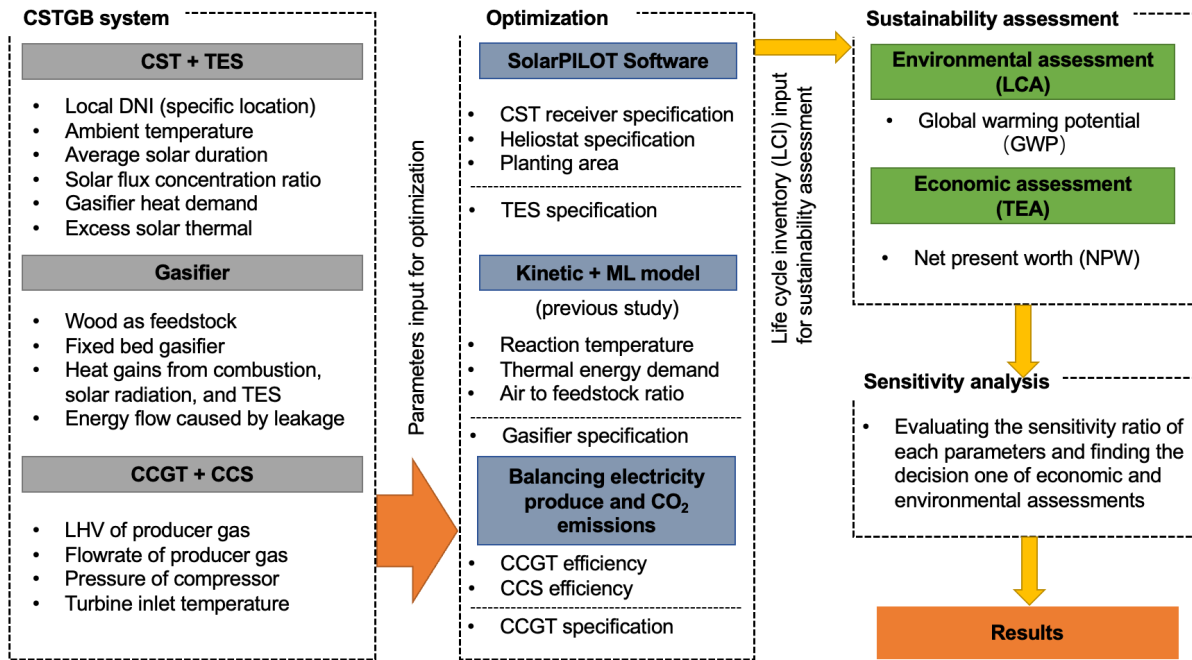


Figure 4.1 The schematic illustration of the methodology. CSTGB: concentrated solar thermal gasification of biomass; CST: concentrated solar tower; TES: thermal energy storage; CCGT: combined cycle gas turbine; CCS: carbon captured system; ML: machine learning; LHV: low heating value.

4.1.1 Thermodynamic analysis of the CSTGB system

4.1.1.1 Description of the CSTGB system

The proposed CSTGB system is powered by a synergistic thermal energy supply method that combines thermal energy from the partial feedstock combustion and the solar thermal energy from a CST subsystem and stored thermal energy from a TES subsystem. Figure 4.2 presents a schematic illustration of the proposed CSTGB system. The combination minimizes the impact of extreme weather conditions (*e.g.*, insufficient solar radiation in winter and absence of solar radiation at night) on the system. The heliostat field area, the size of the CST receiver, and the scale of the TES subsystem are determined by the local direct nominal irradiation (DNI) and the thermal energy demand of the gasifier. The excess solar thermal energy is stored into the TES subsystem and supplied to the gasifier as a backup. The performance of the TES subsystem is dependent on its thermal storage and insulation materials (349). Stone wool has been considered as the insulation material of the TES subsystem to minimize thermal energy loss. Quartz sand is used as both a heat transfer medium and heat storage material with a specific heat capacity of 0.83 kJ/(kg K); it has a high melting point of 1,577°C that avoids phase change and reduces the system complexity (350). A screw transfer

machine (STM) is used to transport the quartz sand carrying thermal energy to the TES subsystem and to the heat exchanger inside of the gasifier. Here, the gasifier has been considered as 5% gas leakage (63) and it is an indirect reactor of gasification in which the quartz sand and biomass particles are not mixed to avoid the separation process of sand and biomass/biochar particles. The high-quality producer gas with a higher low heating value (LHV) is the main product of the CSTGB system, and it is fed into the CCGT subsystem to generate electricity (the overall efficiency of the system $\eta_{\text{system_overall}}$ is used to assess the energy conversion performance of the system, *i.e.*, from biomass feedstock and solar energy to electricity) after tar and fine particle removal by a gas cleaning unit. In addition, CO₂ as the by-product of the CSTGB system is captured by a CCS subsystem, which minimizes the onsite CO₂ emission.

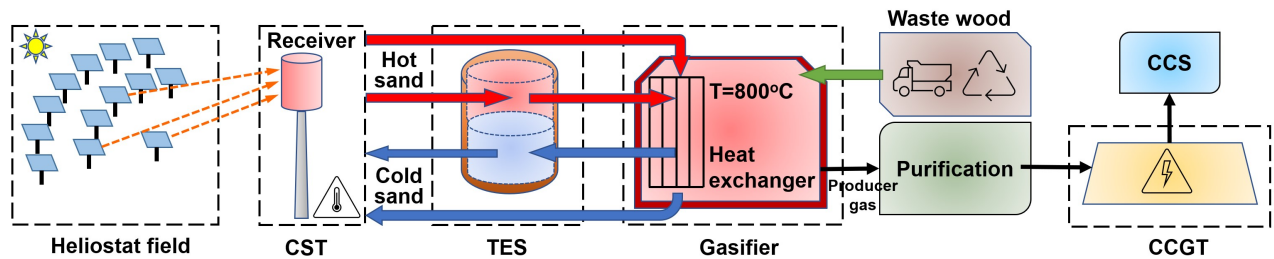


Figure 4.2 The schematic diagram of the proposed CSTGB system.

The autothermal reaction in the gasifier was taken into consideration as a backup to prevent a circumstance where the solar thermal energy and stored thermal energy are insufficient to properly drive the gasification process. In a previous study (199), a single particle shrinkage core-based kinetic gasification model was proposed and combined with the Monte Carlo (MC) approach and a random forest (RF) algorithm to predict optimal gasification process conditions with the aim of the maximum producer gas production. The model has also been applied to study the influences of various parameters (*e.g.*, water content, particle size, porosity, thermal conductivity, emissivity, shape, and reaction temperature) on producer gas production. It was found that reaction temperature had the most significant impact on gas production and quality. The model was applied in this work to determine the maximum producer gas yield and associated process conditions (199). Wood – chemical compositions are presented in Section 4.1.2.2 – and considered as feedstock, associated with an optimum reaction temperature of 800°C and a 10% heat loss rate for the air fixed-bed gasifier. The effects of air to feedstock ratio on the flow rate, LHV, cold gas efficiency (CGE), and

composition of the producer gas are shown in Figure 4.3, in which the optimum reaction temperature was maintained by controlling the air supply. It was shown that the CO_2 concentration in the producer gas increased as the air to feedstock ratio value increased up to 0.3, whereas the CGE and LHV decreased.

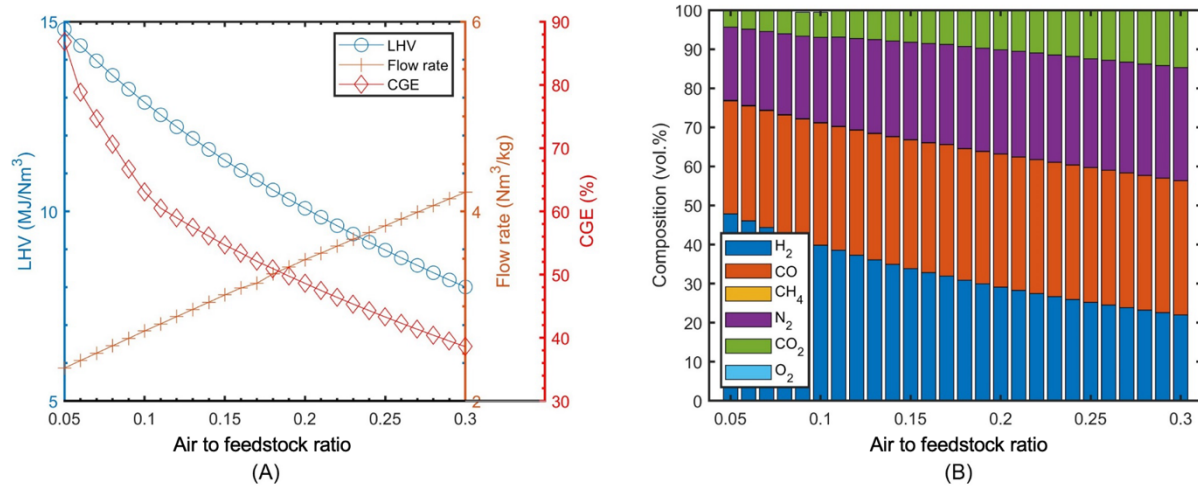


Figure 4.3 (A) Effects of air to feedstock ratio on producer gas flow rate, producer gas LHV, and system CGE; (B) Effects of air to feedstock ratio on producer gas composition.

4.1.1.2 Location

The proposed CSTGB system was assumed to be built in Seville, Spain (Lat: 37.5°, Lon: -5.3°). Seville was selected due to its significant wood waste accumulation, accounting for 73% of the country's annual wood waste generation (351). This amounts to around 8 million tons, representing 1.3% of the global annual wood waste volume (352). Spain is one of the European countries which are most suitable for the development and implementation of solar power technologies with solar radiation levels of 1,600–1,950 kW/m² (353). The considered typical meteorological year (TMY) data of this location includes the hourly DNI, global horizontal irradiance (GHI), ambient temperature, and relative humidity. The average DNI value is 641.4 W/m² and the annual sunshine hours are 3,966 h. The Photovoltaic Geographical Information System (PVGIS) from European Commission (354) was used to obtain the data of wind direction, wind speed, and precipitation in this location (reference data from 2005 to 2020). It was found that this location was dominated by northeasterly winds of 4–5 km/h from March to August and southeasterly winds of 3–4 km/h from February to September. The precipitation was sparse with an average of 53.4 mm/month. The lower wind speeds and rare precipitation allowed the designed CSTGB system to be constructed without extensive

insulation materials. Steam as a gasifying agent is less practicable than other agents (*i.e.*, air, O₂, and CO₂) due to the scarcity of water resource. The use of O₂ and CO₂ would require capture and compression with specialized equipment, which would increase the cost and GWP of transportation (355). As a result, air was deemed the most suitable gasifying agent for the proposed CSTGB system.

Wood is one of the most popular construction materials in Spain, resulting in a high proportion of waste wood being produced each year from construction and civil works (356). Waste wood was considered as the biomass feedstock for the CSTGB system. Waste wood production increased from 1 to 1.6 million tons per year from 2001 to 2010 and continues to increase. Millions of tons of CO₂ are annually emitted into the environment as a result of it being burnt and landfilled (356). The European Environment Agency (EEA) reported that Spanish government paid 50 €/ton (approximately €8 million per year) as gate fees to collect, store, and landfill waste wood (357). The average distance from the location of the proposed CSTGB system to the waste wood collection point in the surrounding cities was found to be 100 km (to Seville is 70.1 km, to Cordoba is 82.5 km, and to Malaga is 155 km). The captured CO₂ and ash will be transported back to the wood waste recycling center (358) in the surrounding cities, ensuring a direct integration into the subsequent processing and utilization stages. This allows an efficient and coordinated flow of materials, enabling optimal utilization of waste wood resources and minimizing environmental impacts.

4.1.2 Life cycle assessment

LCA is a standardized approach for assessing the environmental impacts of a given process, technology, system, or service throughout its whole life cycle. LCA is defined by the ISO 14000 series of international standards, which consists of principles and framework (ISO 14040), goal and scope definition and inventory analysis (ISO 14041), life cycle impact assessment (ISO 14042), life cycle interpretation (ISO 14043), and requirements and guidelines (ISO 14044) (257).

4.1.2.1 Goal and definition

The goal of the LCA is to evaluate the GWP of the CSTGB system to be deployed in Sevilla, Spain and apply the information for planning waste wood treatment and renewable generation. Figure 4.4 illustrates the boundary of the LCA, which encompasses all pertinent processes within the system. The LCA system boundary includes sub-process such as CO₂ emission from diesel refinery, onsite CO₂ emission, CO₂ captured by CCS subsystem,

transportation of waste wood, and electricity generated from the proposed CSTGB system. The functional unit defined in this study is the treatment of 1 ton_{waste-wood}. The entire LCA is conducted in accordance with ISO 14040 with a commercial LCA software GaBi and Ecoinvent 3.0 database (359). Two cases were compared: case 1 uses with both the CST and TES subsystems and case 2 uses without the CST and TES subsystems, which will create knowledge about the relative effectiveness of CST and TES on the development. In the proposed CSTGB system, the captured CO₂ is not used on-site, it undergoes compression and transportation by truck to the recycling center for further processes (*i.e.*, injection into deep geological formations). The treatment (*i.e.*, recovery and utilization) of the ash, generation and collection processes of wood waste is excluded from the system boundary.

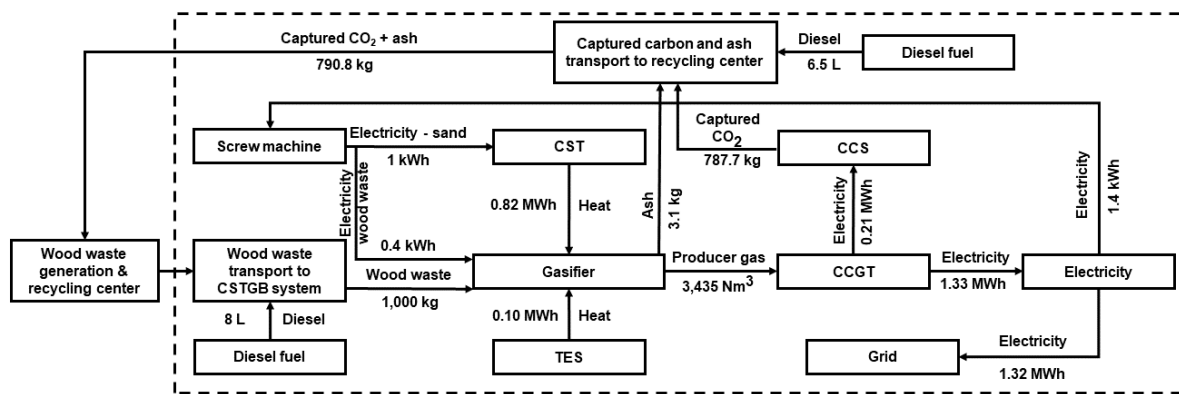


Figure 4.4 LCA boundary of the CSTGB system.

4.1.1.2 Life cycle inventory analysis

Waste wood from construction and civil works (as mentioned in Section 4.1.1.2) was dried pretreated and transported by truck to the location of the proposed CSTGB system. The chemical composition of the waste wood (50.3wt.% carbon, 7.8wt.% hydrogen, 41.8wt.% oxygen, 0.1wt.% nitrogen, the high and low heating value are 20.6 and 18.7 MJ/kg) was assumed to be the same as the wood pellet reported by an existing study (360). The processing capacity of the proposed CSTGB system was assumed to be 1,700 tons per day according to the system scale.

The specifications of the CST subsystem were determined based on a gasification reaction temperature of 800°C and a local average DNI value of 641.4 W/m² (as mentioned in Section 4.1.1.1 & 4.1.1.2). The default environmental parameters (*i.e.*, incidence angle, ambient humidity, and cloud thickness) was optimized using the software SolarPILOT (361). The optimized values were 151,488 m² for heliostat field area, 30 m² for receiver area, 80 m

for receiver tower height, 71.7% for solar thermal efficiency of the CST subsystem. The heliostat field layout and the position of each heliostat are depicted in Figure 4.5. The area of a single heliostat in the CST subsystem was decided based on a life cycle cost analysis by Bhargav *et al.* (362). The area of 120 m² was found to be more suitable for the CSTGB system in terms of economic applicability than that of 64, 96, and 148 m².

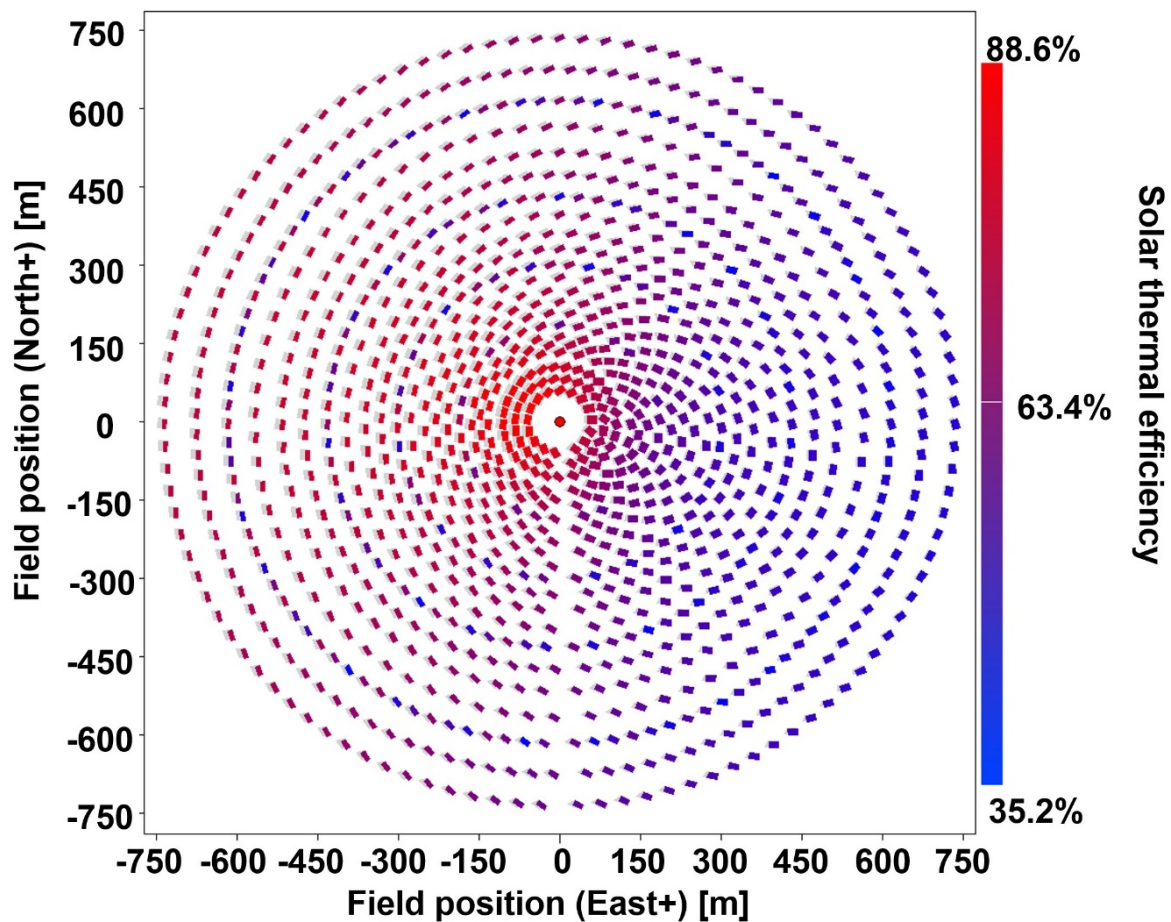


Figure 4.5 The optimal heliostat field layout of the CST subsystem.

The 300-MW_{th} capacity of the TES subsystem was determined by the required peak thermal energy storage of 296.1 MW_{th} calculated based on the day (22 June) featured by the longest solar time and the highest DNI value as shown in the TMY dataset.

The heat transfer efficiency from quartz sand to the feedstock within the gasifier was supposed to be 100% since the reactions inside the gasifier were considered in thermal equilibrium, indicating maximum energy conversion. An input temperature of 1,010°C and an output temperature of 750°C were calculated for the quartz sand for a gasification reaction temperature of 800°C. The CCGT subsystem was employed to convert producer gas to electricity. The efficiency of the producer gas-fueled CCGT with an CCS subsystem was within

a range of 10.8–19% and the CCS subsystem consumed 30% of gross power output (363).

Two distinct STMs were used in the CSTGB system. The gasifier received the waste wood through Machine I (designed for a transportation distance of 10 m). the quartz sand was moved between the CST, TES, and gasifier subsystems using Machine II (designed for a transportation distance of 284.7 m). Heat losses of all subsystems and screw pipeline were assumed to be 10% (62). Table 4.1 summarizes the specific design parameters of the proposed CSTGB system.

Table 4.1 Design parameters of the proposed CSTGB system.

Item	Value (unit)	Adapted based on data from existing studies or calculated
Location	Lat: 37.5°, Lon: -5.3°	
Altitude	169.0 m	(354)
DNI	641.4 W/m ²	(354)
Ambient temperature	19.1°C	(354)
Designed solar receiver temperature	1,111.0°C	(354)
Average solar duration	7.9 h	(354)
Solar flux concentration ratio (C)	3621.6	calculated
<i>CST receiver specification</i>		
Receiver type	External cylindrical	(364)
Receiver height	4.8 m	(364)
Receiver diameter	4.7 m	(364)
Receiver area	30 m ²	(364)
Tower height	80 m	calculated
Optical efficiency (at receiver)	71.7%	calculated
<i>Heliostat specification</i>		
Single heliostat width	12 m	(362)
Single heliostat height	10 m	(362)
Single heliostat area	120 m ²	(362)
Heliostat field	151,488 m ²	calculated
Number of single heliostats	1,263	calculated
<i>TES specification</i>		
Number of tanks	1 integrated tank	(365, 366)
Tank type	External cylindrical	(365, 366)
Tank height	20 m	calculated
Tank diameter (with 0.1 m insulation layer)	10.5 m	calculated

Numbers of hours of TES	16.1 h	calculated
Capacity of the TES	300 MW _{th}	calculated
TES heat loss	10%	(62)
Temperature of TES	448.1°C	calculated
HSM of TES	Quartz sand	(350)
Total sand weight	1,245.5 t	calculated
Total sand volume	1,660.3 m ³	calculated
<i>Gasifier specification</i>		
Gasifier type	Fixed bed	(261, 365)
Gasifier agent	Air (O ₂ :21%, N ₂ :79%)	
Gasifier heat loss	10%	(62)
Air to feedstock ratio	0.05–0.3	calculated
Inlet temperature of quartz sand entrancing the gasifier	1,010°C	calculated
Gasification temperature	800°C	calculated
Output temperature of quartz sand exiting the gasifier	750°C	calculated
Pressure	Atmospheric	
Required thermal energy to increase feedstock from the ambient temperature to 800°C	1.1 MJ/kg _{feedstock}	(360)
Required thermal energy to increase air from the ambient temperature to 800°C	1.0×10 ⁻⁶ MJ/kg _{air}	(360)
Total thermal energy needed by the gasifier	4.7 MJ/kg _{feedstock}	(360)
<i>CCGT specification</i>		
Electricity conversion efficiency ^a	40%	(367)
CO ₂ capture efficiency	90%	(365, 367, 368)
Pressure ratio of GT compressor	19	(365, 367, 368)
Turbine inlet temperature	1,288°C	(365, 367, 368)
Turbine exhaust temperature	544.2°C	(365, 367, 368)
Parameters of the high-pressure steam	521.2°C /55 bar	(365, 367, 368)
Parameters of the low-pressure steam	260.2°C / 6.9 bar	(365, 367, 368)
<i>Screw machine specification</i>		
Machine-1 for feedstock input		
Screw diameter	1 m	(48)
Screw pitch	0.6 m	(48)
Rotational speed	50 rpm	(48)
Conveying capacity	608 m ³ /h	calculated
Power	96 kW	calculated
Machine-2 for sand transfer		
Screw diameter	0.6 m	(48)
Screw pitch	0.5 m	(48)

Rotational speed	50 rpm	(48)
Conveying capacity	160 m ³ /h	calculated
Power	159.7 kW	calculated
<hr/>		
<i>Screw pipe specification</i>		
Screw pipe heat loss	10%	(62)
Pipe-1 for feedstock input		
Screw diameter	1 m	(48)
Length	30 m	calculated
Pipe-2 for sand transfer		
Screw diameter (with 0.025-m thickness insulation)	0.7 m	(48)
Length	284.7 m	calculated
<hr/>		

The material consumption of each subsystem of the CSTGB system are listed in Table 4.2. Chromium steel (melting point of 1,860°C) was used as the construction material because of its capability to withstand the CST receiver and CCGT subsystems' operation temperature of 1,111–1,288°C. The TES subsystem, gasifier, and screw pipe were built using reinforcing steel that has a melting point of 1370°C. Material losses during construction of the CSTGB system, power consumption during assembly, and emissions and energy consumption associated with demolition of the system were not included, as studies have shown that their contribution towards emissions and energy were negligible compared to operation (172).

Table 4.2 Life cycle inventory (LCI) for the construction stage of the CSTGB system. The data are normalised based on the functional unit (*i.e.*, 1 ton_{waste-wood}).

Construction materials					
Material type	Component	Value	Unit	Normalised value	Unit
Installation of CST (366)					
Heliostat					
Flat glass coated, RER	Mirror	1,514,887	kg	8.1×10^{-2}	kg/ton _{waste-wood}
Reinforcing steel, RER	Steel structure	5,335,433	kg	0.3	kg/ton _{waste-wood}
Concrete, sole plate and foundation, CH	Concrete foundation	3,939	m ³	2.1×10^{-4}	m ³ /ton _{waste-wood}
Receiver					
Chromium steel 18/8, RER	Receiver surface	5,990	kg	3.2×10^{-4}	kg/ton _{waste-wood}
CST tower (80 m)					
Concrete, sole plate and foundation, CH	Tower concrete	6,200	m ³	3.3×10^{-6}	m ³ /ton _{waste-wood}
Excavation, hydraulic digger, RER	Tower excavation	4,200	m ³	2.3×10^{-4}	m ³ /ton _{waste-wood}
Reinforcing steel, RER	Tower steel	1,200	kg	6.5×10^{-5}	kg/ton _{waste-wood}
Installation of TES (366)					
Steel, chromium steel 18/8, hot rolled	TES structure	582,232	kg	3.1×10^{-2}	kg/ton _{waste-wood}
Stone wool	TES insulation material	261,116	kg	1.4×10^{-2}	kg/ton _{waste-wood}
Installation of gasifier (369)					
Reinforcing steel, RER	Steel structure	10,000,000	kg	0.5	kg/ton _{waste-wood}
Steel, low-alloyed, RER	Steel structure	6,040,000	kg	0.3	kg/ton _{waste-wood}
Chromium steel 18/8, RER	Steel structure	16,400,000	kg	1.3×10^{-2}	kg/ton _{waste-wood}
Steel, electric, n-and low-alloyed, RER	Steel structure	242,000	kg	0.9	kg/ton _{waste-wood}
Concrete, normal, CH	Concrete foundation	94,900	m ³	5.1×10^{-3}	m ³ /ton _{waste-wood}
Aluminum, primary, RER	Aluminum structure	889,000	kg	0.5	kg/ton _{waste-wood}
Aluminum, secondary, from new scrap, RER	Aluminum structure	105,000	kg	5.6×10^{-3}	kg/ton _{waste-wood}
Aluminum, secondary, from old scrap, RER	Aluminum structure	52,400	kg	2.8×10^{-3}	kg/ton _{waste-wood}
Brass, CH	Plant material	108,000	kg	5.8×10^{-3}	kg/ton _{waste-wood}

Stone wool, CH	Insulation material	1,730,000	kg	9.3×10^{-2}	kg/ton _{waste-wood}
Glass fiber, RER	Plant material	242,000	kg	1.3×10^{-2}	kg/ton _{waste-wood}
Polyvinyl, HDPE, granulate, RER	Plant material	69,300	kg	3.7×10^{-3}	kg/ton _{waste-wood}
Polypropylene, granulate, RER	Plant material	34,700	kg	1.9×10^{-3}	kg/ton _{waste-wood}
Styrene-acrylonitrile copolymer, RER	Plant material	11,600	kg	6.2×10^{-4}	kg/ton _{waste-wood}
Flat glass, uncoated, RER	Plant material	11,700	kg	6.3×10^{-4}	kg/ton _{waste-wood}
Cast iron, RER	Plant material	435,000	kg	2.3×10^{-2}	kg/ton _{waste-wood}
Epoxy resin, liquid, RER	Plant material	91,700	kg	4.9×10^{-3}	kg/ton _{waste-wood}
Lubricating oil, RER	Plant material	384,000	kg	2.1×10^{-2}	kg/ton _{waste-wood}
Synthetic rubber, RER	Producer gas pipe	52,600	kg	2.1×10^{-3}	kg/ton _{waste-wood}
<hr/>					
Installation of CCGT (365)					
Reinforcing steel, RER	Steel structure	12,367,317	kg	6.8	kg/ton _{waste-wood}
Chromium steel 18/8, RER	Steel structure	162,613	kg	8.7×10^{-3}	kg/ton _{waste-wood}
Aluminum, RER	Aluminum structure	81,306	kg	4.4×10^{-3}	kg/ton _{waste-wood}
Concrete, sole plate and foundation, CH	Concrete foundation building	38,958,841	kg	2.9	kg/ton _{waste-wood}
<hr/>					
Installation of pipes (314.7 m) (365)					
Reinforcing steel, RER	Steel pipe	189,185	kg	1.0×10^{-2}	kg/ton _{waste-wood}
Stone wool, RER	Insulation material	173	kg	9.3×10^{-6}	kg/ton _{waste-wood}

RER: European level; CH: Switzerland level.

4.1.2.3 Life cycle impact assessment

To comprehensively evaluate the environmental impact of the CSTGB system, a life cycle impact assessment (LCIA) was conducted using the GaBi software (as mentioned in Section 4.1.2.1). The LCIA process entails categorizing the LCI data into specific impact categories and corresponding indicators that elucidate the causal relationship between the system's activities and its environmental impacts. The ReCiPe Midpoint V1.08 methodology was adopted to calculate the GWP of the CSTGB system which quantifies the total greenhouse gas emission associated with the system over a 100-year time (*i.e.*, GWP 100) horizon.

4.1.2.4 Data interpretation

Based on the LCIA adopted in Section 4.1.2.3, the environmental impact (*i.e.*, GWP) for the proposed CSTGB system was discussed, which included identification of carbon emission (370). A sensitivity analysis was performed to assess the influence of parameter (*i.e.*, CCS subsystem's efficiency, onsite emission, gasifier leakage, transportation, and diesel at refinery) variations (range of $\pm 10\%$). The sensitive ratio (SR), defined as Eq. (4.1), was used to quantify the influences. According to the study by Zahra *et al.* (371), when $SR > 0.2$, this indicates a high degree of influence of the factor on the results; when $SR < 0.2$, it is considered that the factor limited influence on the results (*i.e.*, GWP).

$$SR = \left| \frac{\frac{\varphi_i^b - \varphi_i^m}{\varphi_i^b}}{\frac{\Phi_i^b - \Phi_i^m}{\Phi_i^b}} \right| \quad (4.1)$$

where φ indicates the GWP value, and Φ indicates the value of each factor, b indicates baseline value, and m indicates modified value.

4.1.3 Techno-economic analysis

The NPW approach was used to assess the economic viability of the proposed CSTGB system. All cash flows of the proposed CSTGB system are examined over 30 years and resolved to their equivalent present worth (PW) cash flow. Revenues were considered to be positive cash flows while costs were negative (372). The NPW of the CSTGB system was calculated by Eq. (4.2)

$$NPW = CAPEX + PW(O\&M) + PW(T) - PW(ES) - PW(CT) \quad (4.2)$$

where CAPEX is the capital cost that included the initial investment cost of constructing of the CSTGB system, O&M is the operation and maintenance cost, T is the cost of transporting the waste wood from the cities to the location of the CSTGB system, ES is the incomes from selling the renewable electricity, and CT is the incomes from carbon tax. The PW is the present value, which is calculated by Eq. (4.3) with annual value (AW).

$$PW = AW \frac{(1+i)^N - 1}{i(1+i)^N} \quad (4.3)$$

where i denotes the interest rate (an interest rate of 6% was used based on the literature (372)), and N denotes the assumed operation years of 30 years in this study. The exchange rate of euro to US dollar was 1.13 and GBP to US dollar was 0.85 based on year 2019.

4.1.3.1 CAPEX and O&M cost

There was no existing CSTBG related plant that could be referred to about e.g., construction material costs and O&M costs. A process costing approach was used to calculate the CAPEX for each subsystem (*i.e.*, CST, gasifier, and CCGT) of the proposed CSTGB system which was summed to calculate the total CAPEX. Due to the inconsistency in the year of the referenced system, we used the Chemical Engineering Plant Cost Index (CEPCI) values to update the CAPEX of each subsystem to the year 2019 (calculated by Eq. (4.4)).

$$\text{Cost}_m = \text{Cost}_n \left(\frac{\text{CEPCI}_m}{\text{CEPCI}_n} \right) \quad (4.4)$$

where m and n represent the reference and base year, respectively.

The CAPEX of the heliostat field, receiver tower, and TES were considered. The CEPCI index of the reference year (2019) as 607.5 (373) was used to calculate the CAPEX of a single heliostat as €103 based on the study by Bhargav *et al.* (362) which considered €112.4 for the year 2015 (the CEPCI index is 556.8 (373)) and included mirrors, support structure, drivers, mirror modules, driver control system, field electronics, and wirings.

The CAPEX of the 100 MWth CST subsystem was calculated to be €228,693,794.8, which covered the receiver, tower, TES, indirect costs (*i.e.*, owner cost and contingency), and site preparation as €52,963,596.7, €26,854,082.3, €74,598,612.4, €111,897,919.2, €22,379,583.6 for the year 2019, respectively (data provided by the International Renewable Energy Agency (IRENA) in the year 2018 (374) and the CEPCI index is 603.1 (373)). The annual O&M cost of the CST subsystem was 17.8 €/MWh, which included replacing receivers and single heliostats, heliostat washing (*i.e.*, water consumption), and factory insurance costs (267).

The integrated concept of gasifier and CCGT technologies has been proposed by several researchers (375-377). The CAPEX of the 150 MW scale of the integral gasifier and CCGT system was calculated to be €171,992,945.6 based on the National Renewable Energy Laboratory (NREL) report at the year 2008 (376) and the CEPCI index is 575 (373). The data included gas cleanup facility, engineering fees, project contingency, and carbon capture costs (376). The O&M cost of gasifier with a CCGT

subsystem was based on a study by Cormos *et al.* (378), which concluded that the O&M cost of the gasifier with a CCGT subsystem was 36.37 €/MW in the year 2019. Thus, the total O&M costs of the proposed CSTGB system was calculated as 54.17 €/MWh.

4.1.3.2 Transportation cost

Transportation costs cover the purchasing of trucks, diesel cost, and the wages of the staff operating the truck. The CAPEX of each truck was €233,335 and the life cycle of 10 years, and the estimated annual O&M cost of 3,335 €/truck (372). According to the fuel price report from Experian Catalist (<http://www.catalist.com>), the average diesel price was 1.26 €/L in Spain for the year 2019. The transportation cost can be converted to PW using Eq. (19). It was assumed that three staff are required to operate a truck with the wage as 15.0 €/h per person for the year 2019 (working 8 hours per day) (379).

4.1.3.3 Electricity selling revenue

The electricity selling (ES) price was established based on market supply relationships, which include supplier and end-users (*i.e.*, residential, commercial, and industry) (380). Gracia *et al.* (381) assessed the Spanish market's willingness to pay for a portfolio of renewable electricity in 2010. Based on a consumer survey considering different genders, ages, education of respondent, average household monthly income, and household size, the local consumers (*i.e.*, household, company, and industry) were willing to pay Feed-in Tariff (FiT) as 50 €/MWh and included tax for electricity from renewable resources (382).

4.1.3.4 Carbon tax revenue

The carbon tax (CT) is an effective policy and economic instrument to encourage the development of more environmentally friendly technologies for carbon abatement (383). According to the literature (384), the CT price in Spain was established at 49.0 €/tCO₂ and used in the TEA of the designed CSTGB system.

4.1.3.5 Sensitivity analysis

Based on the TEA adopted in Section 4.1.3.1 to 4.1.3.4, the economic viability (*i.e.*, NPW) for the proposed CSTGB system (370). A sensitivity analysis was conducted to evaluate the relative influences of different key factors (*i.e.*, CAPEX and O&M costs of the system, transportation costs, ES price, and CT) with variations (range of $\pm 10\%$). The sensitive ratio was also calculated using Eq. (17) with φ being the NPW value.

4.2 Results and discussion

4.2.1 Thermodynamic analysis

To better illustrate the daily operation of the proposed CSTGB system, the profiles of the thermodynamic performance for the system were obtained for March 19th, June 22nd, September 22nd, and December 21st, with the meteorological conditions, *i.e.*, local TMY data collected. The results are shown in Figure 4.6.

It is shown in Figure 16B that the most solar radiation was on June 22nd, and the gasifier could be completely powered by solar thermal energy from 07:00 to 17:00. 248.6 MWh of solar thermal energy was stored in the TES subsystem and the overall system efficiency ($\eta_{\text{system_overall}}$) was 28.3%. During the period of insufficient solar radiation (18:00 to 6:00), the TES subsystem supplied 21.2 MWh of thermal energy to the gasifier, and an additional 71 MWh thermal energy was from the combustion of waste wood as required by the gasification process. The net electricity generation and the onsite CO₂ emission were 2,529.2 MWh and 63,175.7 kg on June 22nd (2,408.3 MWh and 67,688.6 kg on March 19th (Figure 4.6A); 2,358.3 MWh and 70,700.0 kg on September 22nd (Figure 4.6C). The least solar radiation was on December 21st (Figure 16D): the total electricity generated was 2,241.2 MWh and the onsite CO₂ emission generated was 74,729.2 kg

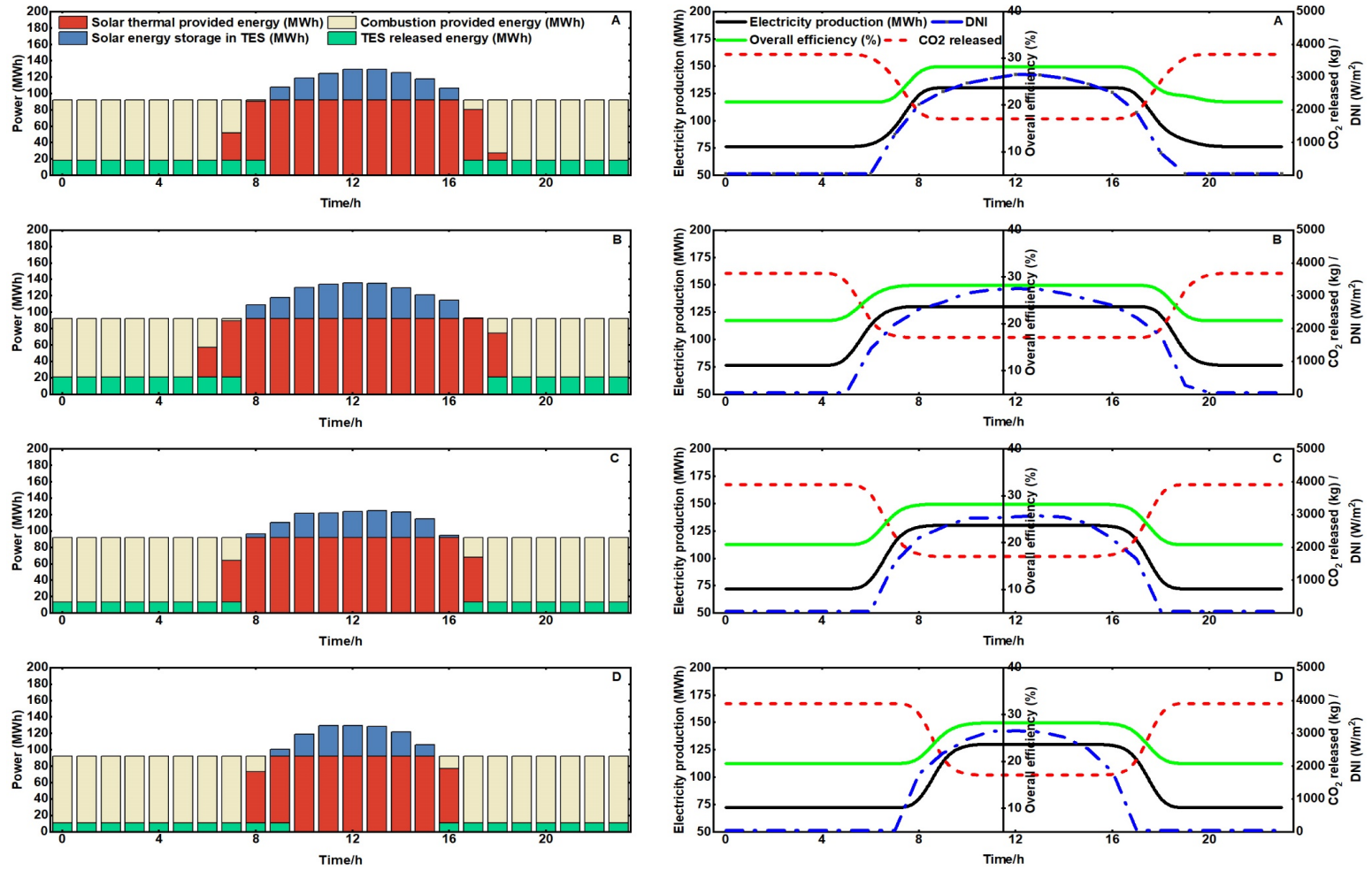


Figure 4.6. Hourly net power and efficiency of the system in the representative days, (A) the day of March 19th, (B) June 22nd, (C) September 22nd, and (D) December 21st.

The monthly and cumulative electricity generation, CO₂ captured and stored, and onsite CO₂ emissions of case 1 and case 2 are shown in Figure 4.7. It is shown that compared to case 2, the electricity output of case 1 increased by 203,485 MWh and the onsite CO₂ emission decreased by 155,552.3 tons. This means that using solar energy and TES subsystem significantly increased electricity production and reduced onsite CO₂ emission. In addition, the proposed CSTGB system (case 1) generate over 0.8 million MWh of electricity per year; it covered 0.31% of the total electricity consumption (about 260 TWh) in Spain during the year 2019 (385).

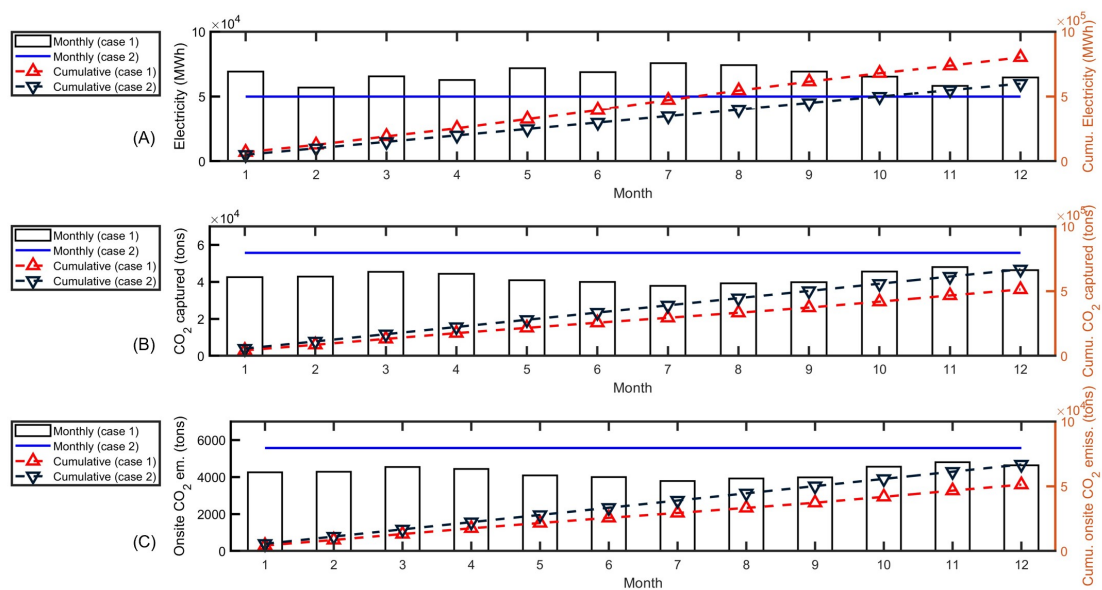


Figure 4.7. Monthly and cumulative data: (A) electricity production, (B) CO₂ captured and stored, and (C) onsite CO₂ released to environment.

4.2.2 Environmental impacts

4.2.2.1 LCA results

The GWP results of case 1 and case 2 are shown in Figure 4.8. In case 1 (Figure 4.8A), the contributions of different components to the GWP of the CSTGB system are as follows: the CCS subsystem exhibited a significant carbon abatement potential, accounting for a carbon reduction of 116% with respect to the total GWP that is equivalent to $-787.7 \text{ kgCO}_2\text{-eq/ton}_{\text{waste-wood}}$. Conversely, the gasification subsystem had a small positive carbon footprint, corresponding to a carbon emission of 1.9% that is equivalent to $13.2 \text{ kgCO}_2\text{-eq/ton}_{\text{waste-wood}}$. Onsite emissions including leakage and uncaptured CO₂ accounted for 12.8% of the total GWP that is equivalent to $87.5 \text{ kgCO}_2\text{-}$

eq/ton_{waste-wood}. Similarly, transportation accounted for 1.8% of the total GWP that is equivalent to 12.3 kgCO₂-eq/ton_{waste-wood}. The total GWP is -678.6 kgCO₂-eq/ton_{waste-wood}. The GWP of case 1 was 212.7 kgCO₂-eq/ton_{waste-wood} lower than that of case 2 (Figure 4.8B) where the GWP of the CCS subsystem was accounted for a carbon reduction of 116% with respect to the total GWP that is equivalent to -618.7 kgCO₂-eq/ton_{waste-wood}. The gasification subsystem was responsible for a carbon emission of 6.4% that is equivalent to 29.8 kgCO₂-eq/ton_{waste-wood}. Onsite emissions constituted 23.3% (108.7 kgCO₂-eq/ton_{waste-wood}) of the total GWP, while transportation contributed 3.1% (14.2 kgCO₂-eq/ton_{waste-wood}) of the total GWP. The total GWP is -465.9 kgCO₂-eq/ton_{waste-wood}. The GWP of case 2 is similar to the study by Margaret *et al.* (386) which reported a GWP of -476.63 kgCO₂-eq/ton_{feedstock} (that system assumed to have 90% carbon captured). This suggests that the proposed CSTGB system with CST and TES subsystems is more environmentally friendly from a carbon saving perspective.

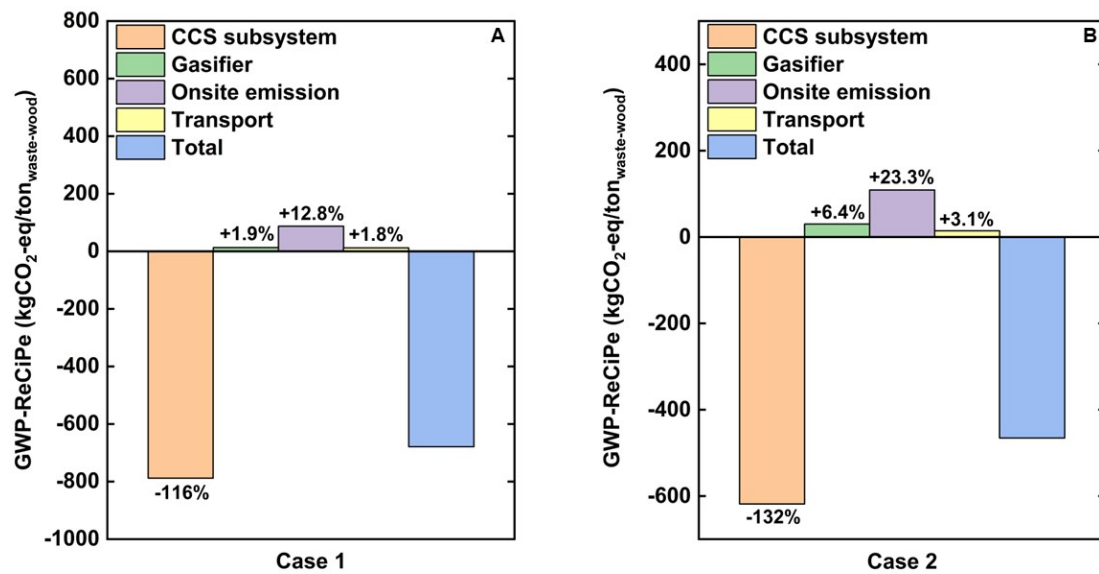


Figure 4.8. Comparison of the GWP of case 1 (CSTGB system with CST and TES subsystems) and case 2 (without CST and TES subsystems), ‘+’ represents positive impact on GWP value while ‘-’ indicates carbon reduction.

4.2.2.2 Data interpretation

Figure 4.9 illustrates the relevant impact factors on the GWP of the proposed CSTGB system and shows that the SR of the CCS subsystem-related emission to be 0.37 and the SR of the onsite CO₂ emission to be 0.34, which were larger than 0.2 and the two most influential factors (as mentioned in Section 4.1.2.4). It is promising to

reduce the carbon footprint of the proposed CSTGB system by improving the efficiency of the CCS subsystem. The GWP of the CSTGB development was less sensitive to the emissions related to transport (SR=0.15), and gasifier (SR=0.08).

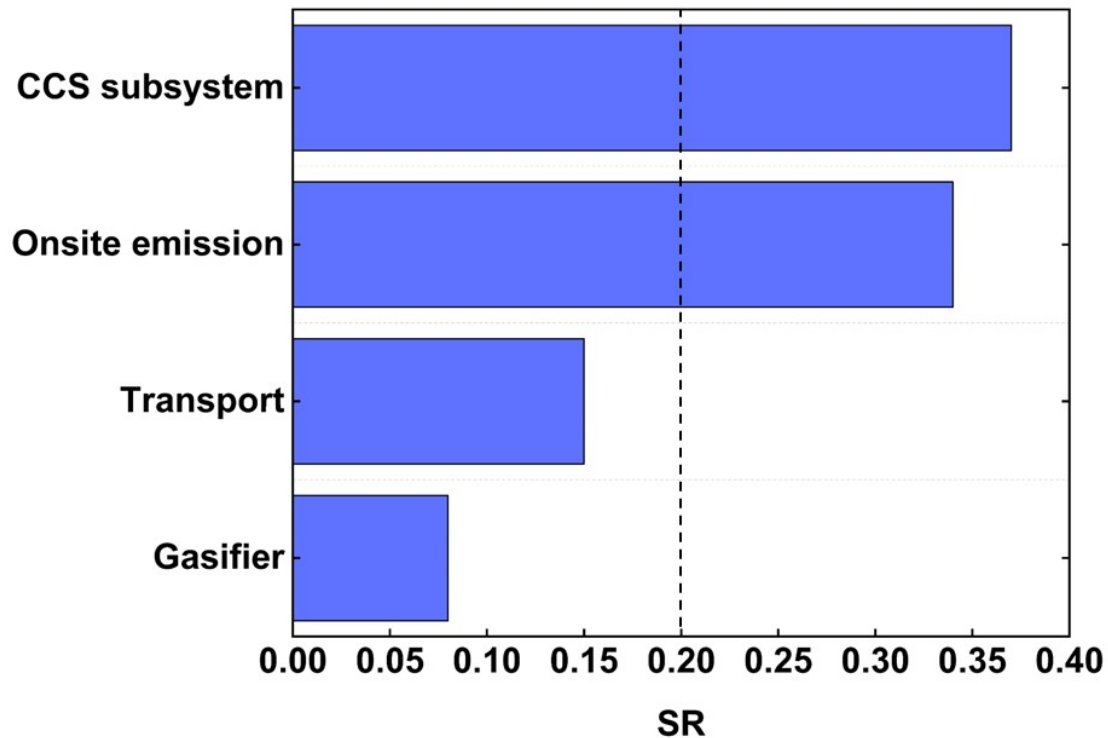


Figure 4.9. Sensitivity analysis results (influences of major factors on the GWP of CSTGB).

4.2.3 Economic analysis

4.2.3.1 TEA results

The TEA results for the CSTGB system operating for 30 years are shown in Figure 4.10. The total NPW was €-0.7 billion in the year 30th. The cumulative PW of the O&M cost of the CSTGB system was €6.4 billion in year 30. The PW of the transportation cost was €150 million, including €30 million for the wage of staff, €12 million for the CAPEX of the truck, and €780 thousand for the O&M cost, and €155 million for the diesel cost. The CAPEX of the CSTGB system was €461 million over the system's life cycle. The sources of revenue for the CSTGB system were CT and ES with the cumulative PW values being €0.3 billion and €6 billion, respectively. Here, the ES price was assumed to be 50 €/MWh in Spain as mentioned in Section 4.1.3.3. The following two conditions need to be met for the proposed CSTGB system to be

economically viable (based on a 10-year payback period): 1) the O&M cost of the system needs to be reduced 19% or 43.9 €/MWh or, 2) the overall efficiency need to be increased by 20%.

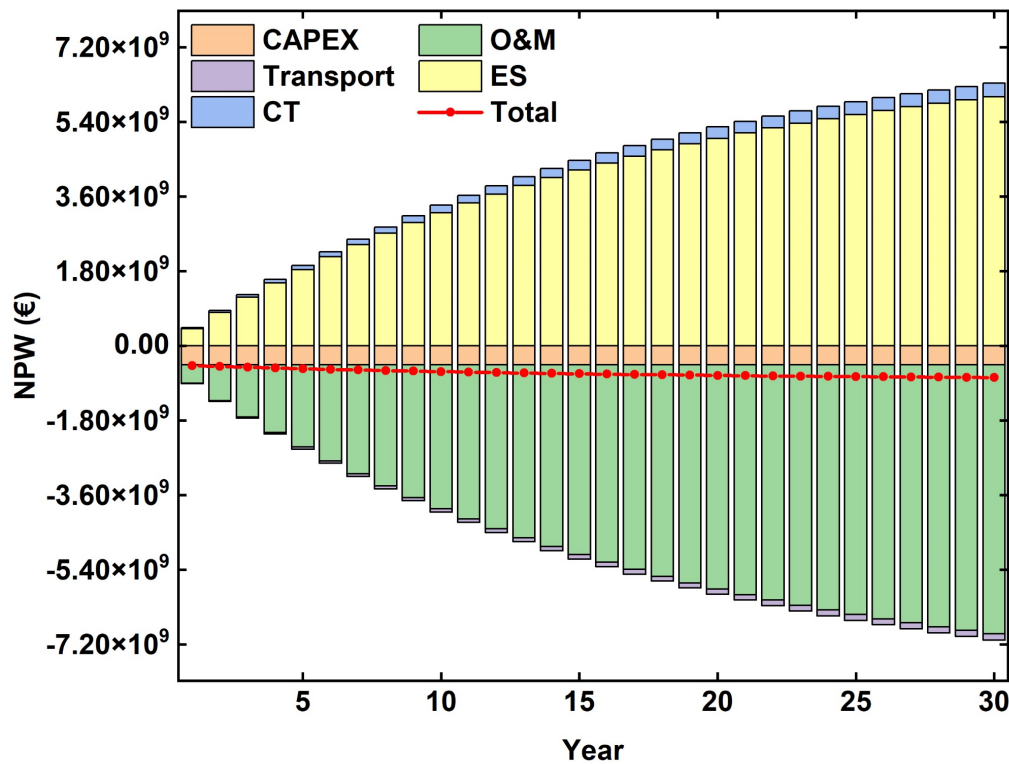


Figure 4.10. PW and NPW results of the CSTGB system in the economic analysis.

4.2.3.2 Sensitivity analysis

The impacts of five factors (*i.e.*, CAPEX, O&M, transportation cost, ES, and CT) towards NPW were studied via sensitivity analysis, and the results are shown in Figure 4.11. The O&M and ES emerged as the most influential factors, with the SR values of 0.37 and 0.34, respectively. Additionally, the CT (SR=0.16), CAPEX (SR=0.12), and transportation (SR=0.08) had a relatively limited impact on the economic viability of the CSTGB system with all SR values below 0.2. It is expected that the O&M of CSTGB development would be further reduced (387). Gracia *et al.* (381) found that the acceptable price of electricity from renewable resources is up to 440 €/MWh in Spain. Hence, there is great potential that the profitability of the CSTGB system will be significantly improved for a lowering O&M cost and a higher ES revenue.

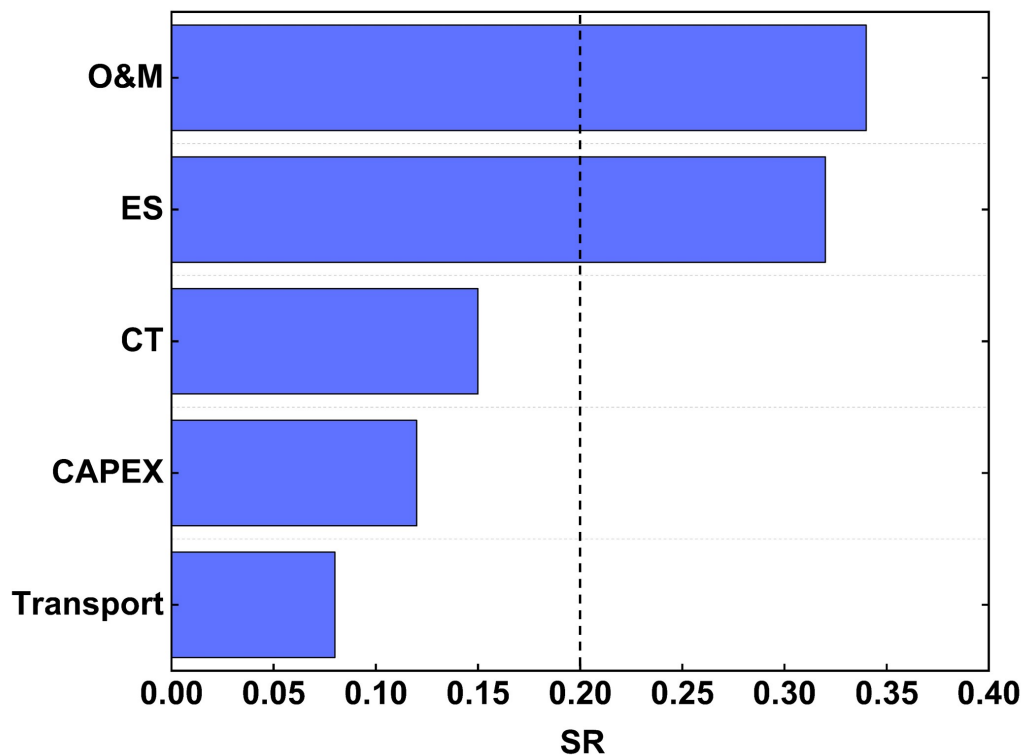


Figure 4.11. Sensitivity analysis results (influences of major factors on the NPW of CSTGB).

4.3 Summary

The CSTGB system has a great potential to reduce the carbon footprint of electricity generation. The LCA results showed that the proposed CSTGB system could save over 0.5 million tons carbon emission ($GWP = -787.7 \text{ kgCO}_2\text{-eq/ton}_{\text{waste-wood}}$) and generate over 0.8 million MWh of electricity per year, which would cover 0.31% of the total electricity consumption (about 260 TWh) in Spain in the year 2019. The results of the sensitivity analysis regarding LCA showed that the GWP of the proposed CSTGB system was primarily affected by the efficiency of the CCS subsystem. The TEA results showed that the total NPW in the 30th year was about €-0.7 billion, which is not profitable (the payback period was over 30 years). The results of the sensitivity analysis showed that the economic viability was mainly affected by the local ES price and the O&M cost. However, there was a great potential to make the system economically viable for a payback period shorter than 10 years when the O&M cost of the system could be reduced by 19% which equals 43.9 €/MWh or the overall efficiency of the system could be increased by 20%.

Chapter 5 Machine learning-based multi-objective optimization of concentrated solar thermal gasification of biomass incorporating life cycle assessment and techno-economic analysis

In the previous chapter, the potential of the concentrated solar thermal gasification of biomass (CSTGB) system in reducing carbon emission from electricity generation has been highlighted. The proposed system has the capability to annually save a substantial amount of carbon emissions while simultaneously generating a significant quantity of electricity. The efficiency of the carbon capture and storage (CCS) subsystem is crucial for the system's environmental impact. The techno-economic analysis (TEA) indicates long payback periods and a need to reduce operational and maintenance (O&M) costs or enhance system efficiency for economic viability within a shorter timeframe. The content of this chapter is prepared for publication as a journal article⁽⁴⁸⁾ in the Journal of Cleaner Production. This chapter introduced an approach to address the challenge surrounding the optimization of CSTGB system incorporating life cycle assessment (LCA) and TEA: a data-driven multi-objective optimization (MOO) approach that encompassed both environmental and economic considerations was proposed and tested to optimize the design and operation of CSTGB. The long short-term memory (LSTM) - recurrent neural network (RNN) model was utilized to capture the intricate temporal dependencies and dynamics associated with the development of a CSTGB system while Monte Carlo (MC) simulation was applied to expand the dataset for model training. The optimal compromise solutions that strike a balance between conflicting objectives, namely, minimizing environmental impacts and maximizing economic benefits were revealed. Overall, a comprehensive framework was proposed to holistically optimize the CSTGB system, offering insights into its feasibility, sustainability, and potential for the best implementation. In this Chapter, an in-depth analysis was considered to optimize the economics and carbon reduction potential of the CSTGB system, providing valuable insights for more efficient and environmentally sustainable energy production. The study began with the training of an LSTM-RNN model using data from 125 scenarios, which proved to be highly accurate in predicting electricity generation and carbon capture with a minimal 5.1% margin of error. Subsequently, this model was utilized to generate a vast dataset of 280,000 scenarios

through the MC approach for MOO. Within this MOO framework, a comprehensive assessment was undertaken to understand the impact of various CSTGB system parameters, such as feedstock composition, operating temperature, and system location, on both global warming potential (GWP) and net present worth (NPW). This analysis not only underscored the system's potential for increased efficiency and reduced emissions but also emphasized its economic viability. An important discovery was the influence of carbon tax (CT) on the MOO results. When considering CT revenue, the optimal system configuration showcased remarkable cumulative reductions in GWP, totaling 415,960 tons of CO₂-eq, and an impressive NPW of €4,298 million over a 30-year lifespan. However, without factoring in CT revenue, a trade-off scenario emerged, but even in this case, the system demonstrated valuable environmental benefits with a cumulative GWP reduction of 132,615 tons of CO₂-eq and an NPW of €3,042 million. These findings underscored the importance of a comprehensive decision-making approach, considering various factors, including technological innovation, economic benefits, and environmental feasibility, to achieve the best outcomes in energy production.

5.1 Methodology

The schematic diagram of the illustration of the methodology is depicted in Figure 5.1, including CSTGB system performance evaluation, LCA, TEA, the integration of the LSTM-RNN model with MC approach, and MOO with pareto optimal solution and technique for order of preference by similarity to ideal solution (TOPSIS) methods. This optimization framework comprehensively addressed various facets, including electricity generation, carbon capture efficiency, environmental feasibility, and economic viability.

Initiating the system design phase, a preliminary thermodynamic analysis was conducted to ascertain crucial gasifier specifications, encompassing parameters such as reaction temperature, thermal energy demand, and air-to-feedstock ratio (it refers to the ratio between the mass of air and that of the feedstock (*i.e.*, biomass waste) supplied to the gasifier). Concurrently, the SolarPILOT software (361) was applied in defining parameters for solar heliostats, including the layout and area, specifications of the concentrated solar tower (CST) receiver, and encompassing factors (*e.g.*, receiver surface area and tower height). Building upon these foundational design parameters in our previous study (388), the optimal process conditions for achieving maximum

electricity generation in a single scenario and life cycle inventory (LCI) data were determined through single-objective optimization (SOO).

The LSTM-RNN model was seamlessly integrated into the methodology, infusing a heightened level of effective decision-making capability (389). The LSTM-RNN model was trained on operational data and patterns from 125 scenarios. Each scenario encompassed variations in biomass feedstocks, geographical locations, and reaction temperatures. Subsequently, we established a dynamic data augmentation by synergizing the predictive ability of the LSTM-RNN model with the stochastic nature of the MC approach. This was achieved by stochastically selecting feature parameters within pre-defined ranges (as mentioned in Section 5.1.3). The introduction of this stochastic element led to the generation of new instances rooted in the inherent system dynamics while considering a broader spectrum of potential scenarios. It was noteworthy that this integrated approach swiftly broadens the dataset, transforming it from the initial set of 125 scenarios into an extensive collection comprising 280,000 scenarios.

The operational parameters and system configurations (*i.e.*, LCI) obtained from the extensive collection of generated scenarios were merged and utilized as inputs for both LCA and TEA. These evaluations not only encompassed the assessment of the GWP but also rigorously evaluated the economic feasibility (*i.e.*, NPW) of CSTGB system. The pareto optimal solution and TOPSIS approaches ensure that the outcomes of the MOO satisfy both environmental and economic objectives, thus fostering a well-informed decision-making framework at the confluence of green technology and economic viability.

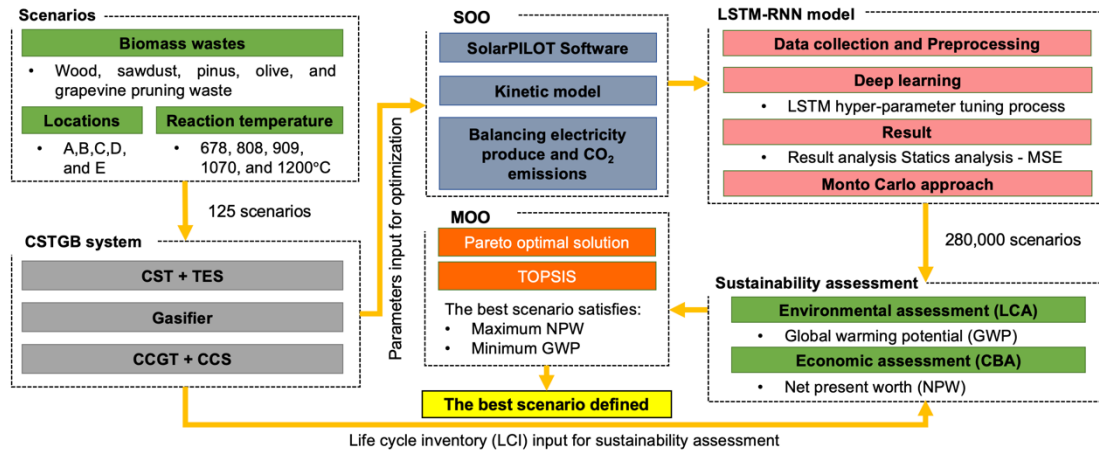


Figure 5.1 Schematic illustration of the proposed methodology. CSTGB: concentrated solar thermal gasification of biomass; CST: concentrated solar tower; TES: thermal energy storage; CCGT: combined cycle gas turbine; CCS: carbon captured system; SOO: single-objective optimization; MOO: multi-objective optimization: TOPSIS: technique for order of preference by similarity to ideal solution; LSTM-RNN: long short-term memory recurrent neural network; MSE: mean squared error.

5.1.1 Overview of the CSTGB system

For specific parameter design of the CSTGB system was provided in the previous study (388). The CSTGB system employs a synergistic thermal energy approach, in which thermal energy derived from the combustion of a partial of feedstock, the solar thermal energy from the CST subsystem, and thermal energy stored within the TES subsystem are complementing each other. The deliberate integration is designed to mitigate the adverse impact of severe weather conditions or intermittent solar thermal conditions (*i.e.*, limited solar radiation during nighttime and winter and the insufficiency of nocturnal solar irradiance) on the system's performance. Implementing this strategy enhances the system's ability to adapt and maintain consistent performance.

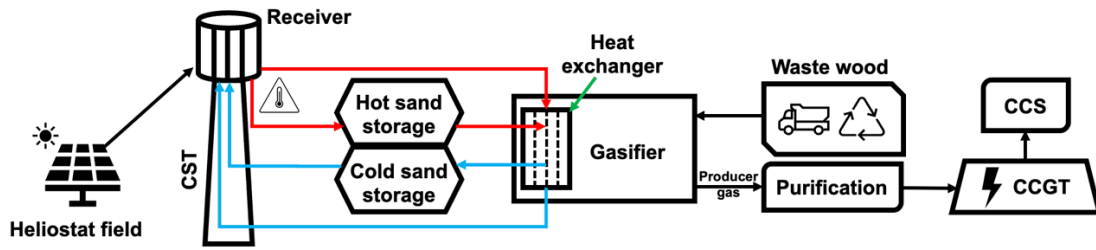


Figure 5.2 The schematic diagram of the proposed CSTGB system

Figure 5.2 presents a schematic illustration of the CSTGB system. The size of the heliostat field, the dimensions of the CST receiver, and the capacity of the TES subsystem in the CSTGB system (as shown in Table 5.3) were decided according to the regional DNI and the specific temperature (*i.e.* thermal energy) demands of the gasifier. These demands involve consideration such as the temperature and heat necessary to maintain the gasification process, which converts feedstock into producer gas. A screw transfer machine (STM) was employed for conveying thermally charged quartz sand to both the TES subsystem and the internal heat exchanger of the fixed bed gasifier (details regarding the electricity consumption of the STM is shown in Table 5.3). This gasifier employs air as its gasifying agent, based on its lower cost. The design of CSTGB follows an indirect reactor approach, where the quartz sand and feedstock particles are kept separate and a 5% gas leakage between the gasifier and the STM equipment is considered (63). The high-quality producer gas, characterized by a notably elevated low heating value (LHV) by the solar thermal heating, is the principal output of the CSTGB system. This producer gas comprises a specific mix of combustible gases including carbon monoxide (CO), hydrogen (H₂), and methane (CH₄). The LHV of the producer gas is calculated as $(CO \times LHV_{CO} + H_2 \times LHV_{H_2} + CH_4 \times LHV_{CH_4})$, where CO, H₂, and CH₄ are the volume fractions of the producer gas (390). The presence of these components in significant amounts results in a gas mixture with a suitably high energy content, making it an fuel suitable for various energy generation applications (391). Following the removal of tar and fine particles via a gas cleaning unit, the producer gas is subsequently fed into a combined cycle gas turbine (CCGT) subsystem for electricity generation. Furthermore, the by-product (*i.e.*, CO₂) produced from the CSTGB system is captured and stored by a CCS subsystem, effectively minimizing on-site CO₂ emissions.

The performance evaluation of the CSTGB system incorporates hourly TMY data to estimate annual electricity generation and CO₂ capture. By utilizing TMY data, the analysis captures the dynamic nature of system performance under a wide range of operational and environmental conditions typical of the geographical area considered. The overall system efficiency is used to assess the energy conversion performance of the system (*i.e.*, from biomass and solar energy to electricity). The annual electricity generation and CO₂ capture are quantified through the summation of hourly data over a year.

5.1.2 Dataset and features description

The study initially considered 125 scenarios which were derived based on our previous research (388) which focused on the environmental and economic evaluation of the CSTGB system. Specifically, a stochastic kinetic model for the gasification process that combines a single particle shrinkage core model and Monte Carlo simulation was applied to predict the maximum producer gas yield (199). The modelling encompassed a wide range of variables, including 5 types of biomass waste (namely wood, sawdust, pinus pruning, olive pruning, and grapevine pruning), 5 locations (labeled as A, B, C, D, and E), and 5 different gasification reaction temperatures (678°C, 808°C, 909°C, 1,070°C, and 1,200°C). Table 5.1 illustrates the ultimate compositions of biomass waste that are widely available in the areas considered (392). To ensure efficient CSTGB system operation, critical steps such as biomass waste pretreatment to maintain a moisture content below 10% and proper sorting before transportation were considered. Table 5.1 also summarized the geographical characteristics (*i.e.*, latitudes, longitudes, elevations, and average DNI) of the selected locations for the development. Figure 5.3 lists the TMY with hourly temporal DNI data for each location from the PVGIS database (354). Furthermore, the distances from these locations to Seville, Spain were measured in kilometers based on the actual transportation routes marked on Google Maps. This measurement approach was incorporated into the analysis to assess the impact of the transportation distance variations on the results of LCA and TEA.

Table 5.1 Feedstock compositions (dry ash free basis) and locations.

Feedstocks selection					
Component	Wood	Sawdust	Pinus pruning	Olive pruning	Grapevine pruning
C (wt.%)	50.31	50.26	50.55	47.50	46.97
H (wt.%)	7.82	6.14	6.12	6.00	5.80
O (wt.%)	41.77	42.20	40.2	43.66	44.49
N (wt.%)	0.10	0.07	0.45	1.06	0.67
FC (wt.%)	16.30	16.27	15.13	13.98	19.78
LHV (kJ/kg)	18.70	20.47	19.99	19.99	17.91
Location selection					
	A	B	C	D	E
Latitude	37.5	36.6	39.9	39.2	38.7
Longitude	-5.3	-5.8	-5.7	-3.3	-0.9
Elevation (m)	137.0	107.0	272.0	648.0	544.0
Distance to Seville (km)	85	130	365	450	620
Average DNI (W/m^2)	641.4	562.7	535.7	542.3	553.7

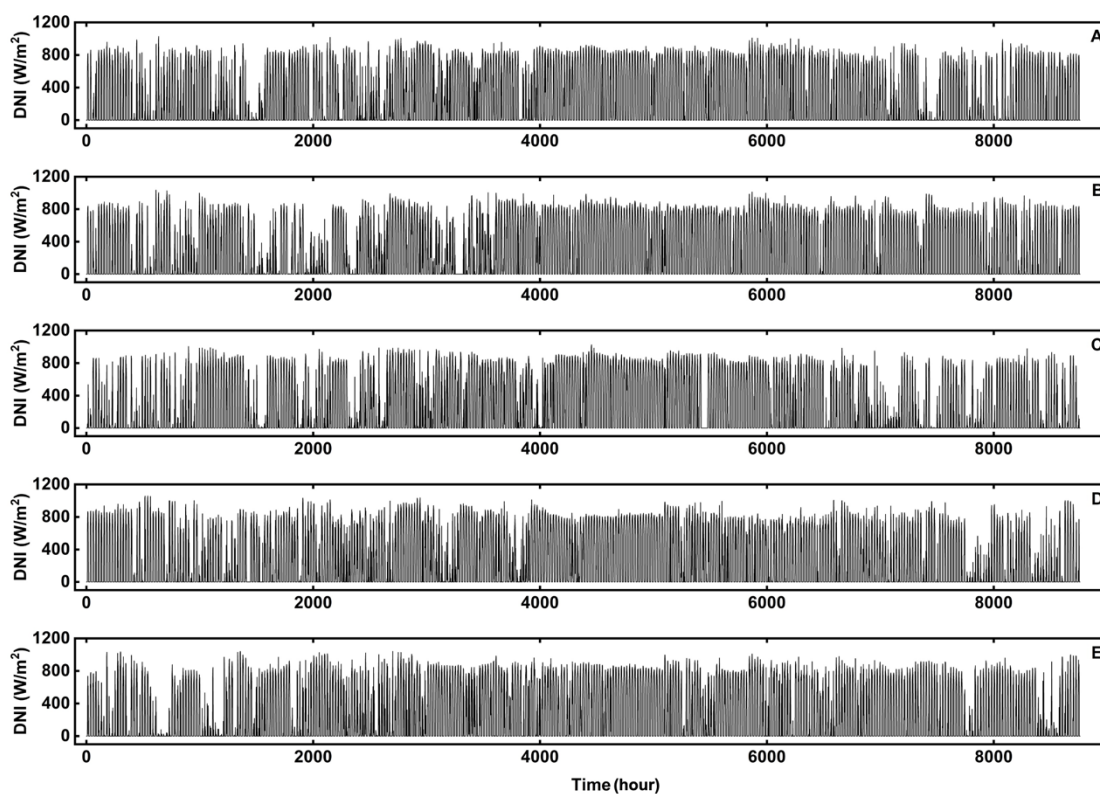


Figure 5.3. Hourly DNI data profiles for locations A, B, C, D, and E.

5.1.3 LSTM-RNN model

5.1.3.1 LSTM-RNN model architecture

The LSTM-RNN model is a type of deep learning architecture specifically designed to capture temporal dependencies in time series data (*e.g.*, DNI) and other selected linear features (*i.e.*, feedstock compositions and reaction temperature) and non-linear features (*i.e.*, locations) using the LSTM unit. In this study, we allocated 80% of the datasets from 125 scenarios for training and 20% for testing. The model was trained using an appropriate evaluation metric (*i.e.*, mean squared error (MSE)) to minimize the prediction errors and enhance the performance. Figure 5.4 displayed the main steps of the proposed LSTM-RNN model. The tuning essential hyperparameters were set as a learning rate of 2, a batch size of 100, a number of training iterations of 75, and 8 hidden layers, to control the convergence rate, balance memory usage, and training efficiency, and ensure that the model adequately learned the underlying data patterns. The optimization algorithms (*e.g.*, stochastic gradient descent) were used to effectively adjust the model's parameters to improve its fit to the training data. The accuracy of the LSTM-RNN model was evaluated using the MSE metric, which provided a quantitative assessment of its performance and prediction reliability. Python 3.11.4 was used as the programming environment. A virtual environment was created to run the LSTM-RNN model for this study. In this virtual environment, the packages (Tensorflow, Keras, Pandas, Sklearn, Numpy, and Matplotlib) were installed.

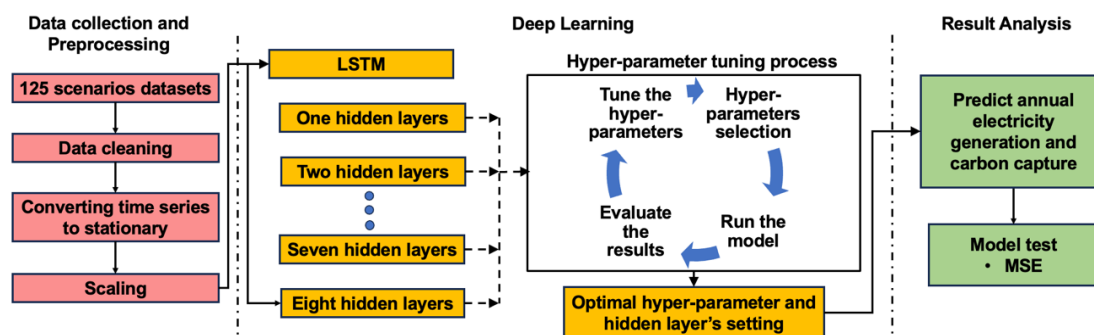


Figure 5.4 Main steps of the proposed LSTM-RNN model

5.1.3.2 Evaluation of LSTM-RNN model performance

To assess the performance of the LSTM-RNN model, two pivotal metrics were utilized: MSE for model training (training-MSE) and MSE for model validation (validation-MSE). The training-MSE gauges the degree of model fit to the training

dataset, and quantified through the computation of the average squared difference between the model prediction and the actual value (393). In contrast, the validation-MSE serves as a measure of the model's generalization prowess, addressing its performance on previously unseen data instances (394). The validation-MSE is meticulously calculated at the culmination of each training epoch, thereby facilitating the timely detection of potential overfitting or underfitting tendencies within the model (395). These two MSE metrics (396) were computed:

$$\text{MSE} = \frac{1}{N} \sum_{y_i} (y_{\text{predict}} - y_{\text{actual}})^2 \quad (5.1)$$

5.1.4 Monte Carlo simulation

The minimum and maximum percentage values for each composition component (*i.e.*, carbon (C), hydrogen (H), and oxygen (O)) were chosen as the lower and upper bounds of uniform distributions used for Monte Carlo simulation. The percentage value of N is calculated by subtracting the sum of C, H, and O from 100% (represents as $N = 100\% - (C + H + O)$, where C, H, and O are mass fractions of carbon, hydrogen, and oxygen, respectively). Within the specific ranges (as shown in Table 5.2) and 5 locations, a uniform distribution was selected for random allocation. This choice guarantees an equal likelihood across the defined value range of the selected decision variables under consideration (397). The utilization of this augmented dataset facilitates a more profound exploration of the optimization process, fostering an enhanced comprehension of the intricate relationship between the selected decision variables (input) and objective (outputs).

Table 5.2 The lower and upper bounds of selected decision variables for the CSTGB system.

Variable	Lower bound	Upper bound
C (wt.%)	46.97	50.55
H (wt.%)	5.80	7.82
O (wt.%)	40.20	44.49
N (wt.%)	0.07	1.06
FC (wt.%)	13.98	19.78
LHV (kJ/kg)	17.91	20.47
Reaction temperature (°C)	678	1,200

5.1.5 Life cycle assessment

The international standards series ISO 14000 offers a comprehensive structure for conducting LCA, covering essential elements including principles and framework (ISO 14040), goal and scope definition and inventory analysis (ISO 14043), and requirements and guidelines (ISO 14044) (257). The primary aim of this LCA is to evaluate the GWP associated with the CSTGB system intended for establish in Spain.

Figure 5.5 delineates the boundary of the LCA, which encompasses all relevant processes within the CSTGB system. Within this LCA system boundary, several critical sub-processes are included (*i.e.*, CO₂ emission stemming from diesel refinery, onsite CO₂ emission, the carbon capture performance by the CCS subsystem, the transportation of biomass wastes, and the electricity generation realized by the proposed CSTGB system. This delineation provides a robust foundation for the systematic evaluation of the environmental impacts and sustainability consideration across the entirety of the system.

The findings of this assessment will be instrumental in planning biomass feedstocks treatment and facilitating renewable energy generation. The functional unit established for treating 1 ton_{biomass-waste}. Point 1 represents the diesel consumption required for transporting the biomass waste (ranging from 8 to 62 L), contingent on transportation distance. Point 2 corresponds to the TES subsystem (storing 0.08–0.10 MWh of thermal energy) with variations based on the local DNI. Point 3 signifies electricity usage in the screw machine (a consumption of 1.0–1.1 kWh) dependent on the pipeline distance in the CSTGB system in different location. Points 4 and 5

represents the gasifier yielding 2,388–5,101 Nm³ of producer gas, while also producing 2.2–4.6 kg of ash. The quantities of the producer gas and ash were considered to depend on multiple factors, such as the chemical composition of the feedstock and gasification process condition (*i.e.*, temperature), technical characteristics of the gasifier, and DNI. Points 6, 7, 8, and 9 encompass various aspects of the system, including captured CO₂ (547.5–1,169.8 kg) and electricity usage in the CCS subsystem (0.18–0.25 MWh), electricity generation from CCGT subsystem (0.92–1.97 MWh), and the subsequent transfer of generated electricity to the grid (0.91–1.96 MWh), with all values subject to LHV and yield of producer gas, the efficiency of the CCGT and CCS subsystem. Lastly, point 10 represents the diesel consumption (4.6–73.6 L) required for transporting captured carbon and ash back to the recycling center. This interconnected system considers various factors to ensure an efficient approach to biomass waste treatment. The entire LCA procedure strictly adheres to the guidelines outlined in ISO 14040 and is executed using the GaBi commercial LCA software (359).

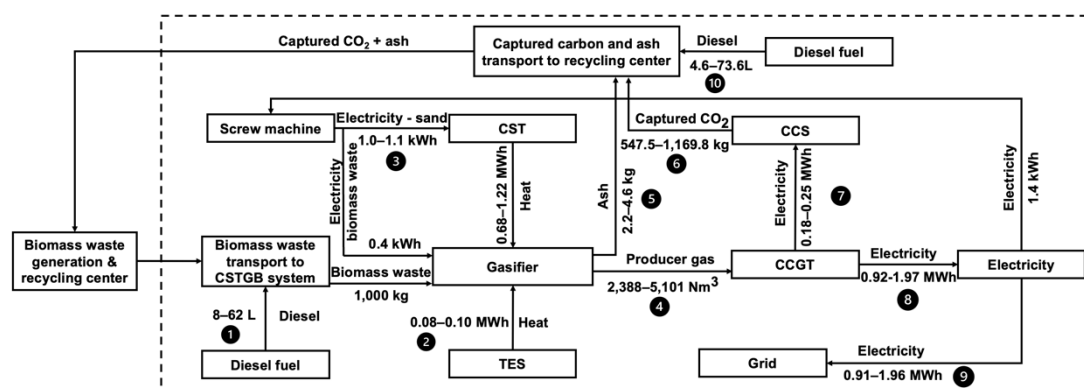


Figure 5.5 LCA boundary of the CSTGB system.

5.1.5.1 Life cycle inventory

Biomass wastes underwent a drying-pretreatment process and was subsequently transported to the CSTGB system location via trucks. The chemical composition of the biomass waste is detailed in Section 5.1.3, and it was assumed that the CSTGB system had a processing capacity of 1,700 tons per day. Table 5.3 shows the specifications of the CSTGB system determined based on factors such as gasification reaction temperature and the local average DNI (as mentioned in Section 5.1.3). The CST subsystem parameters, including the heliostat field area, receiver area, receiver tower height, and solar thermal efficiency, was optimized using the SolarPILOT software with

default environmental parameters (*i.e.*, incidence angle, ambient humidity, and cloud thickness). The individual heliostat area in the CST subsystem was set at 120 m², and the capacity of the TES subsystem was established based on the required peak thermal energy storage for each specific location (as outlined in Section 5.1.3).

The assumed heat transfer efficiency from quartz sand to the feedstock within the gasifier was set at 100%. This assumption was made to ensure that the reactions taking place inside the gasifier were in thermal equilibrium, thereby maximizing energy conversion efficiency. The heat transfer efficiency from quartz sand to the feedstock inside the gasifier was assumed to be 100%. The reactions within the gasifier were in thermal equilibrium, ensuring maximum energy conversion. This resulted in an input temperature range of 856–1,515°C and an output temperature of 637–1,125°C for the quartz sand when the gasification reaction temperature was between 678–1,200°C. To convert the producer gas into electricity, a CCGT subsystem with a 40% electricity conversion efficiency was employed (as mentioned in Table 5.3) (367). The CCS equipment consumed 30% of the gross power output (363).

The CSTGB system incorporated two distinct STMs. Machine I (designed for a transportation distance of 10 m) was responsible for delivering biomass waste to the gasifier. Machine II (designed for a transportation distance of 285, 295, 295, 295, and 295 m for the CSTGB system in location A, B, C, D, and E, respectively) facilitated the movement of quartz sand between the CST, TES, and gasifier subsystems. All subsystems and screw pipelines were assumed that heat losses amounted to 10% (388).

Table 5.3 Design parameters of the CSTGB system in each location.

Location	Location A	Location B	Location C	Location D	Location E	Unit	Adapted based on data from existing studies or calculated
	Lat: 37.5, Lon: -5.3	Lat: 36.6, Lon: -5.8	Lat: 39.9, Lon: -5.7	Lat: 39.2, Lon: -3.3	Lat: 38.7, Lon: -0.9		
Elevation	137	107	272	648	544	m	(354)
Average DNI	641.4	562.7	535.7	542.3	553.7	W/m ²	(354)
Average solar duration	11.2	10.7	10.6	10.8	10.6	hr	(354)
Average ambient temperature	19.1	18.2	15.8	15.6	15.4	°C	(354)
CST receiver specification							
Receiver type	External cylindrical		(364)				
Receiver height	4.8	4.8	4.8	4.8	4.8	m	(364)
Receiver diameter	4.7	4.7	4.7	4.7	4.7	m	(364)
Receiver area	30	30	30	30	30	m ²	(364)
Tower height	80	85	85	85	85	m	calculated
Optical efficiency (at receiver)	71.7	70.2	69.8	65.7	73.8	%	calculated
Designed solar receiver needed temperature	941.6–1,666.5	941.6–1,666.5	941.6–1,666.5	941.6–1,666.5	941.6–1,666.5	°C	calculated
Solar flux concentration ratio	687.7–13,516.6	783.8–15,407.1	823.4–16,183.6	813.3–15,986.7	796.6–15,657.5		calculated
Heliostat specification							
Single heliostat width	12	12	12	12	12	m	(362)
Single heliostat height	10	10	10	10	10	m	(362)
Single heliostat area	120	120	120	120	120	m ²	(362)
Number of single heliostats	240–4,712	274–5,371	288–5,642	284–5,573	278–5,458	unit	calculated
TES specification							
Number of tanks	1	1	1	1	1	Integrated tank	(365, 366)
Tank type	External cylindrical		(365, 366)				
Tank height	20	19	18.5	18.5	19	m	calculated
Tank diameter (with 0.1 m insulation layer)	10.5	9.5	9.5	10.0	10.0	m	calculated
TES duration	12.8	13.3	13.4	13.2	13.4	hr	calculated

Capacity of the TES	300	265	250	255	260	MW _{th}	calculated
TES heat loss	10	10	10	10	10	%	(62)
Designed Temperature of TES	450	395	375	380	390	°C	calculated
HSM of TES	Quartz sand		(350)				
Total sand weight	1,250	1,100	1,040	1,060	1,080	ton	calculated
Total sand volume	1,660	1,470	1,385	1,415	1,440	m ³	calculated
Gasifier specification							
Gasifier type	Fixed bed		(261, 365)				
Gasifier agent	Air (O2:21%, N2:79%)						
Pressure	Atmospheric	Atmospheric	Atmospheric	Atmospheric	Atmospheric		
Gasifier heat lose	10	10	10	10	10	%	(62)
Air to feedstock ratio	0.05–0.30	0.05–0.30	0.05–0.30	0.05–0.30	0.05–0.30		calculated
Inlet temperature of quartz sand	856–1,515	856–1,515	856–1,515	856–1,515	856–1,515	°C	calculated
Gasification temperature	678–1,200	678–1,200	678–1,200	678–1,200	678–1,200	°C	calculated
Output temperature of quartz sand	637–1,125	637–1,125	637–1,125	637–1,125	637–1,125	°C	calculated
CCGT specification							
Electricity conversion efficiency ^a	40	40	40	40	40	%	(367)
Efficiency of the CO ₂ capture unit	90	90	90	90	90	%	(365, 367, 368)
Pressure ratio of GT compressor	19	19	19	19	19		(365, 367, 368)
Turbine inlet temperature	1,288	1,288	1,288	1,288	1,288	°C	(365, 367, 368)
Turbine exhaust temperature	544.2	544.2	544.2	544.2	544.2	°C	(365, 367, 368)
High-pressure steam	521.2	521.2	521.2	521.2	521.2	°C /55 bar	(365, 367, 368)
Low-pressure steam	260.2	260.2	260.2	260.2	260.2	°C /6.9 bar	(365, 367, 368)
Screw machine specification							
Machine-1 for feedstock input							
Screw diameter	1	1	1	1	1	m	(48)

Screw pitch	0.6	0.6	0.6	0.6	0.6	0.6	m	(48)
Rotational speed	50	50	50	50	50	50	rpm	(48)
Conveying capacity	608	608	608	608	608	608	m ³ /h	calculated
Power	96	96	96	96	96	96	kW	calculated
Machine-2 for sand transfer								
Screw diameter	0.6	0.6	0.6	0.6	0.6	0.6	m	(48)
Screw pitch	0.5	0.5	0.5	0.5	0.5	0.5	m	(48)
Rotational speed	50	50	50	50	50	50	rpm	(48)
Conveying capacity	160	160	160	160	160	160	m ³ /h	calculated
Power	159.7	159.7	159.7	159.7	159.7	159.7	kW	calculated
Screw pipe specification								
Screw pipe heat loss	10	10	10	10	10	10	%	(62)
Pipe-1 for feedstock input								
Screw diameter	1	1	1	1	1	1	m	(48)
Length	30	30	30	30	30	30	m	calculated
Pipe-2 for sand transfer								
Screw diameter (0.025m insulation)	0.7	0.7	0.7	0.7	0.7	0.7	m	(48)
Length	285	295	295	295	295	295	m	calculated

^a Electricity conversion efficiency refers to the CCGT subsystem's capacity to convert producer gas into electricity

Table 5.4 provided a comprehensive breakdown of the material usage for each subsystem of the CSTGB system. To withstand the operational temperature range of 637–1,515°C in the CST receiver and CCGT subsystem were applied chromium steel (with melting point of 1,860°C) as the construction material. The TES subsystem, gasifier, and screw pipe were meticulously fabricated by using reinforcing steel (it has high melting point of 1,370 °C). Material losses during construction, power consumption during assembling, and emissions and energy consumption associated with demolition of the CSTGB system were omitted from consideration. Research has shown that their influence on emissions and energy is minimal compared to the operation phase (172).

Table 5.4 LCI for the construction stage of the CSTGB system is normalized based on the functional unit (*i.e.*, 1 ton_{biomass-waste}) in each location.

Construction materials							
Material type	Component	Location A	Location B	Location C	Location D	Location E	Unit
Installation of CST - 120 m² heliostat							
Flat glass coated, RER	Flat glass coated, RER	8.1×10^{-2}	9.3×10^{-2}	9.7×10^{-2}	9.6×10^{-2}	9.4×10^{-2}	kg/ton _{biomass-waste}
Reinforcing steel, RER	Reinforcing steel, RER	2.9×10^{-1}	3.3×10^{-1}	3.4×10^{-1}	3.4×10^{-1}	3.3×10^{-1}	kg/ton _{biomass-waste}
Concrete, sole plate and foundation, CH	Concrete foundation	2.1×10^{-4}	2.4×10^{-4}	2.5×10^{-4}	2.5×10^{-4}	2.5×10^{-4}	m ³ / ton _{biomass-waste}
Receiver							
Chromium steel 18/8, RER	Receiver surface	3.2×10^{-4}	kg/ton _{biomass-waste}				
CST tower							
Tower height		80	85	85	85	85	m
Concrete, sole plate and foundation, CH	Tower concrete	3.3×10^{-4}	3.5×10^{-4}	3.5×10^{-4}	3.5×10^{-4}	3.5×10^{-4}	m ³ / ton _{biomass-waste}
Excavation, hydraulic digger, RER	Tower excavation	2.3×10^{-4}	2.4×10^{-4}	2.4×10^{-4}	2.4×10^{-4}	2.4×10^{-4}	m ³ / ton _{biomass-waste}
Reinforcing steel, RER	Tower steel	6.5×10^{-5}	6.9×10^{-5}	6.9×10^{-5}	6.9×10^{-5}	6.9×10^{-5}	kg/ton _{biomass-waste}
Installation of TES							
Steel, chromium steel 18/8, hot rolled	TES structure	3.1×10^{-2}	kg/ton _{biomass-waste}				
Stone wool	TES insulation material	1.4×10^{-2}	kg/ton _{biomass-waste}				
Installation of gasifier							
Reinforcing steel, RER	Steel structure	5.4×10^{-1}	kg/ton _{biomass-waste}				
Steel, low-alloyed, RER	Steel structure	3.2×10^{-1}	kg/ton _{biomass-waste}				
Steel, electric, n-and low-alloyed, RER	Steel structure	1.3×10^{-2}	kg/ton _{biomass-waste}				
Chromium steel 18/8, RER	Steel structure	8.8×10^{-1}	kg/ton _{biomass-waste}				
Concrete, normal, CH	Concrete foundation	5.1×10^{-3}	m ³ /ton _{biomass-waste}				
Aluminum, secondary, from new scrap, RER	Aluminum structure	5.6×10^{-3}	kg/ton _{biomass-waste}				
Aluminum, secondary, from old scrap, RER	Aluminum structure	2.8×10^{-3}	kg/ton _{biomass-waste}				
Aluminum, primary, RER	Aluminum structure	4.8×10^{-2}	kg/ton _{biomass-waste}				

Brass, CH	Plant material	5.8×10^{-3}	kg/ton _{biomass-waste}				
Stone wool, CH	Insulation material	9.3×10^{-2}	kg/ton _{biomass-waste}				
Glass fiber, RER	Plant material	1.3×10^{-2}	kg/ton _{biomass-waste}				
Polyvinyl, HDPE, granulate, RER	Plant material	3.7×10^{-3}	kg/ton _{biomass-waste}				
Polypropylene, granulate, RER	Plant material	1.9×10^{-3}	kg/ton _{biomass-waste}				
Styrene-acrylonitrile copolymer, RER	Plant material	6.2×10^{-4}	kg/ton _{biomass-waste}				
Flat glass, uncoated, RER	Plant material	6.3×10^{-4}	kg/ton _{biomass-waste}				
Cast iron, RER	Plant material	2.3×10^{-2}	kg/ton _{biomass-waste}				
Epoxy resin, liquid, RER	Plant material	4.9×10^{-3}	kg/ton _{biomass-waste}				
Lubricating oil, RER	Plant material	2.1×10^{-2}	kg/ton _{biomass-waste}				
Synthetic rubber, RER	Producer gas pipe	2.8×10^{-3}	kg/ton _{biomass-waste}				
Installation of CCGT							
Reinforcing steel, RER	Steel structure	6.8	6.8	6.8	6.8	6.8	kg/ton _{biomass-waste}
Chromium steel 18/8, RER	Steel structure	8.7×10^{-3}	kg/ton _{biomass-waste}				
Aluminum, RER	Aluminum structure	4.4×10^{-3}	kg/ton _{biomass-waste}				
Concrete, sole plate and foundation, CH	Concrete foundation building	2.1	2.1	2.1	2.1	2.1	kg/ton _{biomass-waste}
Installation of pipes							
Pipe length		315	325	325	325	325	m
Reinforcing steel, RER	Steel pipe	1.0×10^{-2}	1.1×10^{-2}	1.1×10^{-2}	1.1×10^{-2}	1.1×10^{-2}	kg/ton _{biomass-waste}
Stone wool, RER	Insulation material	9.3×10^{-6}	9.6×10^{-6}	9.6×10^{-6}	9.6×10^{-6}	9.6×10^{-6}	kg/ton _{biomass-waste}

RER: European level; CH: Switzerland level.

5.1.5.2 Life cycle impact assessment

A life cycle impact assessment (LCIA) was carried out to calculate the selected environmental impact indicators. The LCIA process involved the organization of life cycle inventory (LCI) data into specific impact categories and corresponding indicators, which provide insight into the cause-and-effect relationship between the system's activities and environmental consequences. To calculate the overall GWP of the CSTGB system, *i.e.*, GHG emissions associated with the system over a 100-year period (referred to as GWP 100 horizon), the ReCiPe Midpoint V1.08 methodology was employed (388).

5.1.6 Techno-economic analysis

The economic feasibility of the proposed CSTGB system was evaluated using the NPW approach. This process entailed a detailed examination of all financial transactions linked to the CSTGB system proposal over a 30-year duration, where each cash flow was converted into its equivalent PW. Positive cash flows were attributed to revenues, while negative cash flows were associated with costs (372). The NPW of the system was calculated by

$$\text{NPW} = \text{CAPEX} + \text{PW}(\text{O\&M}) + \text{PW}(\text{T}) - \text{PW}(\text{ES}) - \text{PW}(\text{CT}) \quad (5.2)$$

where capital expenditure (CAPEX) represents the capital cost, which covers the initial investment required for establishing the CSTGB system. O&M represents the operational and maintenance costs, while T accounts for the expenses associated with transporting feedstock from Sevilla to the CSTGB system site. Electricity selling (ES) is the notation for the revenue obtained through the sale of renewable electricity, and CT denotes the income generated from carbon tax. The calculation of the present worth (PW) is determined by AW:

$$\text{PW} = \text{AW} \frac{(1+i)^N - 1}{i(1+i)^N} \quad (5.3)$$

where i represents the interest rate with a rate of 6% utilized in accordance with literature (372). N signifies the assumed operation years, which was set at 30 years for this study. Furthermore, the currency exchange rate was 1.13 euros to US dollar and

0.85 British pounds to US dollars as the year 2019.

The process costing method was employed to compute the CAPEX for each subsystem within the proposed CSTGB system, specifically the CST, gasifier, and CCGT. These individual CAPEX values were then aggregated to determine the total CAPEX (388). To standardize the CAPEX of each subsystem to the reference year 2019 (with a CEPCI index of 556.8 (373)), the chemical engineering plant cost index (CEPCI) data were used and implemented Eq. (5.4).

$$\text{Cost}_{\text{ref}} = \text{Cost}_{\text{base}} \left(\frac{\text{CEPCI}_{\text{ref}}}{\text{CEPCI}_{\text{base}}} \right) \quad (5.4)$$

Table 5.5 presents a comprehensive consolidation of the CAPEX, which includes costs related to truck acquisitions (determined by the transportation distances), along with the O&M cost and revenues generation for the CSTGB system at different locations. The CAPEX for a single heliostat was calculated as €103 it was referred by a cost of €112.4 (362) at the year 2015 (with a CEPCI of 556.8 (373)). The calculation of the O&M cost for the CST subsystem is based on the data from 100 MW-scale system published by International Renewable Energy Agency (IRENA) in 2018 (with a CEPCI index of 603.1 (373)). It encompasses costs related to the receiver, tower, TES, and indirect expense (*i.e.*, owner costs, contingency, and site preparation). These costs are summed and then divided by the total electricity generation capacity of the system to determine the annual O&M cost of the CST subsystem as 17.8 €/MWh. The CAPEX for the gasifier and CCGT subsystem was calculated based on the 2008 (with a CEPCI index of 575 (373)) report from the National Renewable Energy Laboratory (NREL) (376). The CAPEX includes the costs for gas clean-up facilities, engineering expenses, contingencies, and carbon capture cost. The O&M cost for the integrated gasifier and CCGT as 36.4 €/MWh was referred from (378) for the year 2019. The total O&M cost for the entire CSTGB system accounted for the CST, gasifier, and CCGT subsystem and was equal to 54.2 €/MWh. Transportation costs encompass the acquisition of trucks (233,335 €/truck with a 10-year lifespan with an annual O&M cost is 3,335 €/truck (372)), diesel cost as 1.26 €/L (388), and the wages of truck operator (15.0 €/h/person working 8 h/day (379)) in the 2019. The ES price in Spain was determined at 50 €/MWh, following the feed in tariff (FiT). It incorporated taxes for electricity generated from renewable sources (382). Additionally, the CT in Spain is established at 49 €/tCO₂

(384) and used in the TEA of the proposed CSTGB system.

Table 5.5 CAPEX, O&M, and transportation costs for the CSTGB system at each location.

	Location A	Location B	Location C	Location D	Location E	Unit	Ref(s)
CAPEX							
CST subsystem							
Heliostat field	0.02–0.5	0.03–0.55	0.03–0.58	0.03–0.57	0.03–0.56	million €	(362)
Receiver	52.9	52.9	52.9	52.9	52.9	million €	(374)
Receiver tower	26.9	28.5	28.5	28.5	28.5	million €	(267)
TES	74.6	65.9	62.2	63.4	64.7	million €	(267)
Gasifier+CCGT subsystems							
Gasifier	60.2	60.2	60.2	60.2	60.2	million €	(376)
CCGT	111.8	111.8	111.8	111.8	111.8	million €	(376)
Site preparation	4.3–83.5	4.9–95.2	5.1–100.0	5.0–98.7	4.9–96.7	million €	(376)
Indirect costs	21.3–417.5	24.3–475.9	25.5–499.8	25.2–493.8	24.6–483.6	million €	(376)
O&M costs							
CST subsystem	17.8	17.8	17.8	17.8	17.8	€/MWh	(375-377)
Gasifier+CCGT subsystem	12.7	12.7	12.7	12.7	12.7	€/MWh	(375-377)
CCS device	23.7	23.7	23.7	23.7	23.7	€/MWh	(375-377)
Transportation costs							
Number of trucks	17	34	136	136	136	unit	Calculated
Number of staffs	51	102	408	408	408	unit	Calculated
CAPEX of trucks (10 years)	3.9	7.9	31.7	31.7	31.7	million €	(372, 379)
O&M cost of trucks	7	13	52	52	52	€/hour	(372, 379)
Diesel cost	1,785	3,570	14,280	14,280	14,280	€/hour	Calculated
Staff cost	6,120	12,240	48,960	48,960	48,960	€/hour	Calculated

5.1.7 Multi-objective optimization

One of the most crucial and prevalent challenges lies in addressing multiple conflicting objectives in designing the CSTGB system, which requires simultaneous resolution. The pursuit of a more efficient energy system invariably results in augmented costs for both system components and the entirety of the system. Within the

domain of MOO techniques, this study leveraged the LSTM-RNN model in conjunction with the LCA and TEA methodologies to derive and compile a comprehensive set of 280,000 scenarios in this study. These scenarios collectively embody values related to system performance, GWP, and NPW. The identification of the best scenario possessing such attributes substantially facilitates the design of the CSTGB system, enabling its operation in a state that optimizes efficiency, environmental viability, and economic feasibility to the utmost degree.

Two antagonistic objectives are postulated for optimization: to minimize GWP as a representative of the carbon footprint metric, and to simultaneously maximize NPW as an economic indicator that also encompasses the performance metric of electricity generation. In pursuit of these goals, this study additionally deployed the pareto optimality and the TOPSIS method. The pareto optimality method identified scenarios where NPW can be elevated sans detriment to GWP. Meanwhile, the TOPSIS method comprehensively assesses the divergence between pareto optimal solutions and the ideal best solution. It could provide a ranked selection avenue for multi-objective decision-making. This amalgamation of techniques holistically probes trade-offs across manifold objectives within the CSTGB system design, thereby furnishing optimal scenario design parameters, GWP, and NPW values.

5.2 Results and discussion

5.2.1 Forecasting of electricity generation and carbon saving by CSTGB system

The kinetic model of CSTGB exhibited a simulation error rate below 12% and reasonably characterize the thermochemical process of gasification as highlighted in the previous paper (199, 388). As this work focuses on system optimization based on the comparison of different scenarios predicted based on the same model, it is believed the absolute accuracy of the model should have a limited impact on the selection of optimal solutions. These input variables can be subject to external influences (*i.e.*, location), which not only adds complexity and uncertainty to the resulting outcomes but also hinders the training of the LSTM-RNN model. Therefore, we have chosen to use intermediate variables (*i.e.*, electricity generation and CO₂ captured) as the output results for the LSTM-RNN model. This decision aims to better capture critical aspects of system performance and mitigate the impact of external factors on the analysis. Moreover, sensitivity analysis demonstrated that the electricity generation and CO₂ captured have a substantial impact on the outcomes of LCA and TEA (388). Higher

levels of electricity generation are inherently linked to greater energy output and revenue generation, while increased carbon capture contributes to reducing CO₂ emissions and potential carbon saving.

Figure 5.6 serves as an illustrative representation of mean values pertaining to annual electricity generation and carbon capture across various biomass waste types, temperature gradations, and geographical locales. The length of each bar correlates directly to mean values within specific parameter combinations. Analysis of mean values underscores a consistent trend, revealing sawdust waste as yielding the highest annual electricity generation, closely trailed by grapevine pruning waste, pinus pruning waste, wood waste, and olive pruning waste. This observation unequivocally suggests that sawdust and grapevine pruning waste promise as potent options for electricity generation within the spectrum of considered waste types (as detailed in Section 5.1.3 outlining feedstock composition) in the CSTGB system.

Further scrutiny extends to the impact of varying operating temperatures on energy generation and CO₂ capture efficacy. The dataset encompasses an array of temperature thresholds, unveiling a conspicuous pattern across the spectrum. With increasing temperatures, annual electricity generation demonstrates an ascending trajectory, whereas carbon capture exhibits a converse descent, irrespective of the biomass waste type. This intricate interplay can be attributed to the intricate thermal reactions and degradation mechanisms (*e.g.*, gasifying the biomass waste in high temperature) invoked at elevated temperatures. Importantly, this correlation maintains consistency across all evaluated biomass waste types.

Expanding the analysis to encompass geographical location, discernible fluctuations in annual electricity generation come to the fore. Location A consistently emerges as the pacesetter in mean electricity generation, trailed by Location B, Location C, Location D, and Location E. The fundamental reason or factor of this divergence can be traced to the superior local climate conditions prevalent at Location A. These conditions, typified by the highest average DNI of 641.4 W/m², minimal average wind speed of 3 km/h, lowest average precipitation of 53.4 mm/month, and elevated environmental temperatures 19°C, collectively contribute to its preeminence. In summary, the zenith of the system performance is attained through the utilization of sawdust waste as feedstock, operational optimization at 1,200°C, and strategic positioning at location A within the scope of 125 scenarios. Within these scenarios, the overall system efficiency (a metric for assessing the energy conversion efficiency from

biomass and solar energy to electricity) exhibits a range from 9.10% to 51.59%. This variation underscores the system's adaptability and the impact of operational conditions on the overall energy conversion efficiency. This meticulous analysis thus elucidates an optimal configuration for harnessing biomass waste, providing a robust framework for efficient and sustainable energy production strategies.

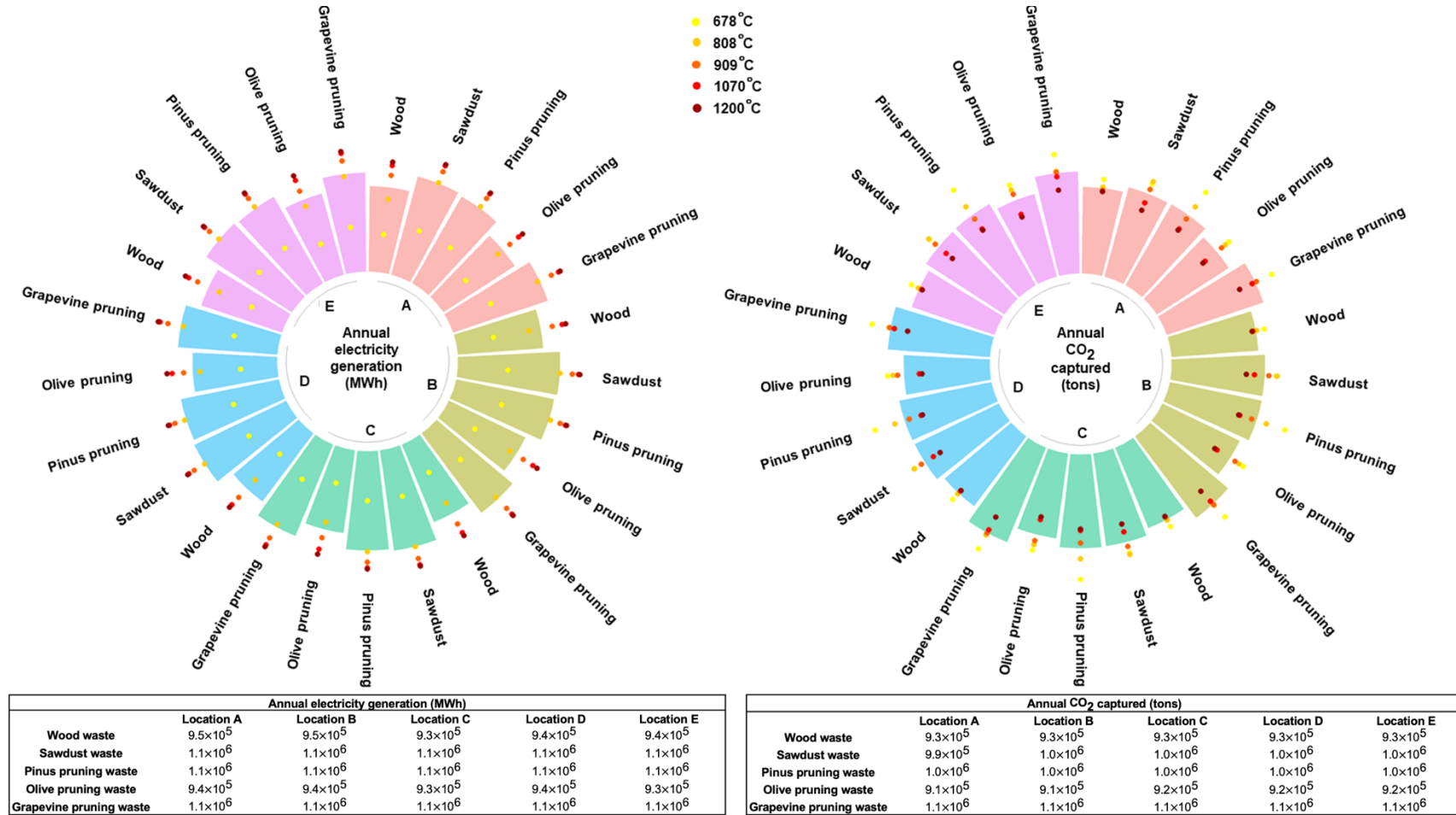


Figure 5.6 125 scenarios set descriptive statistics.

5.2.2 Performance evaluation of LSTM-RNN model

Figure 5.7A represented the evaluation of the LSTM-RNN model, a distinct trend was observed whereby the MSE exhibited rapid reduction within the 1st to 5th epochs. This characteristic signifies the model's prompt assimilation of underlying data patterns and features during its nascent learning phase. A discernible transition is observed after the 10th epoch, where the MSE stabilizes at values of 29.4 and 9.2 for the training and validation processes, respectively.

In assessing the performance of the model, the well-trained LSTM-RNN model was employed to predict electricity generation (Figure 5.7B) and carbon savings, (Figure 5.7C) and the resultant predictions were juxtaposed against the corresponding test data. The predictive outcomes closely approximated the testing data, and this congruence was quantified by an impressive average error of 5.16%.

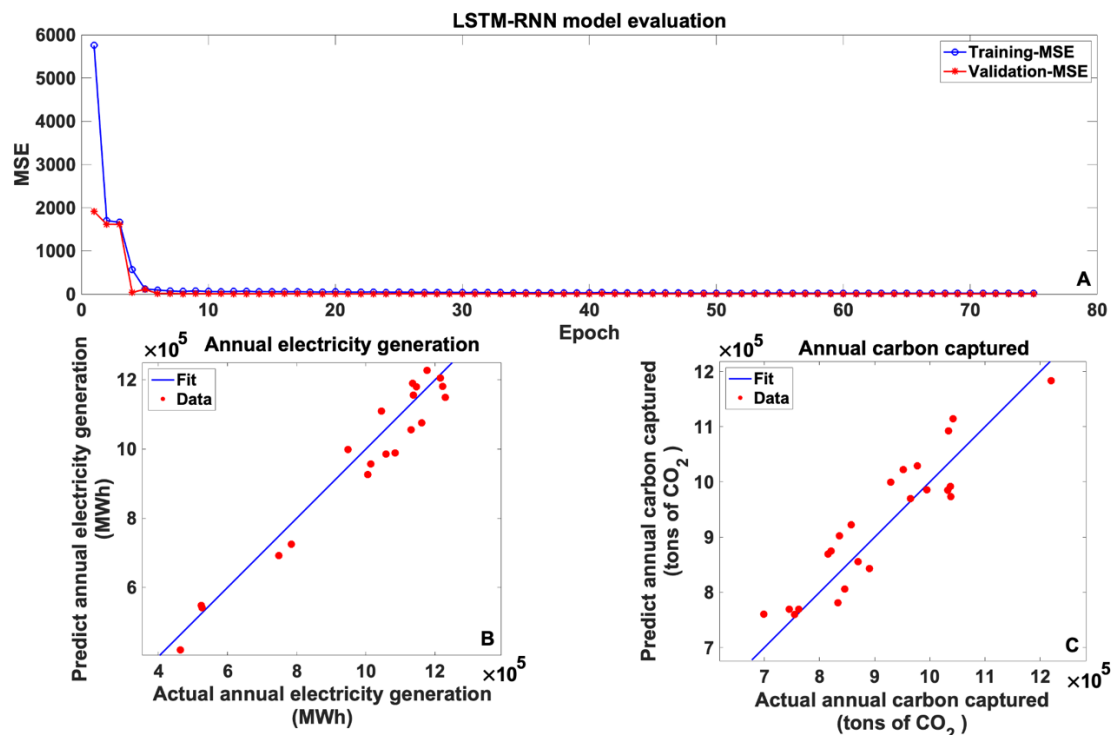


Figure 5.7 (A). the proposed LSTM-RNN model evaluation, (B). comparison of predict and actual annual electricity generation, (C). comparison of predict and actual annual carbon captured.

5.2.3 Evaluation of MOO results

A comprehensive exploration of 280,000 scenarios was undertaken using the MOO method. It is essential to emphasize that negative values were employed for the GWP metric in Figure 5.8. A lower GWP signified a higher level of CO₂ capture in the CSTGB system, indicative of a decreased efficiency of the CSTB system and a greater emission of CO₂. Notably, the inclusion of the CT in the analysis had a profound impact on the MOO results. Due to the CSTGB system was maintained under an assumption that does not account for market supply and demand interactions (refers to the availability of electricity in response to market demand) on calculating the NPW. This circumstance might have led to a heightened influence of the CT on the system revenue. This phenomenon aligns with the findings of research regarding the CT by Burnette *et al.* (398), where they asserted that the CT tend to amplify the revenue of relevant systems.

Figure 5.8A illustrated the influence of incorporating the CT in the TEA on the MOO outcomes of the CSTGB system. This incorporation led to the absence of a trade-off phenomenon in the MOO results. Consequently, this discovery enabled the swift determination of the best scenario, even in the absence of using the pareto optimality and TOPSIS methods. In the parameter configuration of the best scenario, the delicate balance of feedstock composition played a crucial role in the system efficiency: C (49.3wt.%), H (7.3wt.%), O (42.4wt.%), N (0.9wt.%), FC (18.1wt.%), and the feedstock LHV (18.5 kJ/kg). The optimal conditions converged at Location C, and the CSTGB system with 2091 heliostats operated at a gasification temperature of 825.8°C. Over the span of 30 years, the cumulative GWP reduction amounted to 415,960 tons CO₂-eq. TEA presented promising cost-effective results with NPW of €4,298 million. A key correlation emerged between CT revenue and the extent of CO₂ captured creating a symbiotic relationship, which increasing CO₂ captured capacity led to increased CT revenue. Therefore, the intentionally chosen optimal solution included processes with a higher carbon emission. This strategic choice was reflected in selecting processes that operate at lower reaction temperatures and established at Location C (characterized by the lowest average DNI of 535.7 W/m² and a longer transportation distance of 365 km).

Figure 5.8B illustrated the impact of incorporating CT in the TEA on the MOO results of the CSTGB system. Optimal scenarios were determined by using the pareto optimality and the TOPSIS method was used to make a decision of the most preferred system scenario. The best system scenario was determined as: C (48.4wt.%), H

(7.3wt.%), O (43.8wt.%), FC (19.7wt.%), the feedstock LHV (20.1 kJ/kg), and location A, which is attributed to that location A has the shortest transportation distance (85km) and the highest average DNI (641.4 W/m²). This location choice integrates transport efficiency and the availability of solar energy resources, while also underscoring its alignment with system objectives (*e.g.*, specifically the maximization of NPW and the minimization of GWP). The optimal number of heliostats was 1,789, associated with a gasification temperature of 947.2 °C. Through a comprehensive evaluation encompassing LCA and TEA of the CSTGB system, the profound positive implications of the best scenario became evident. Over a 30-year lifecycle, the cumulative reduction in GWP amounted to remarkable 132,615 tons CO₂-eq. This quantifiable achievement aligned closely with the pressing global environmental imperatives, underscoring the system's pivotal role in carbon emission mitigation and serving as a critical stride towards a sustainable future. The TEA demonstrated pronounced prospects, as reflected by the substantial NPW of €3,042 million.

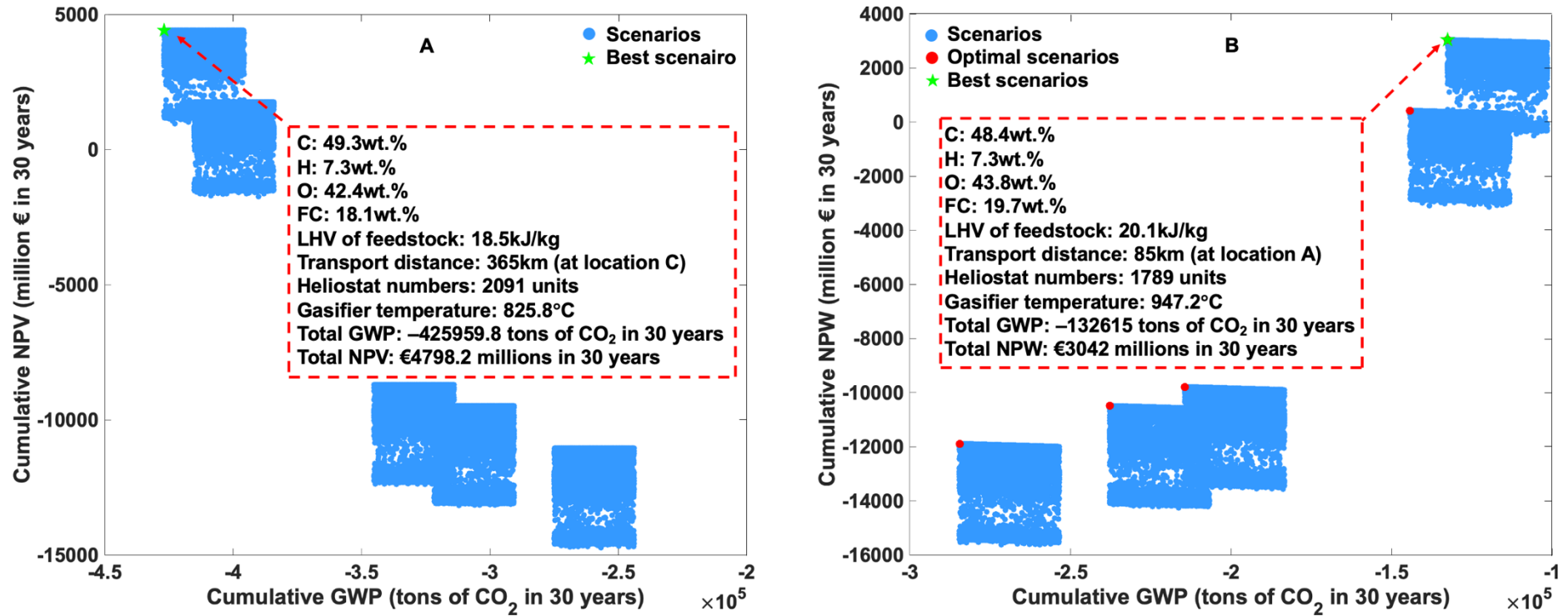


Figure 5.8 The decision making of the optimal scenario: A). the CSTGB system with considered CT as revenue, B). the CSTGB system without considered CT as revenue.

5.3 Summary

In the pursuit of optimizing the economics and carbon saving potential of CSTGB system, an exhaustive analysis of diverse influencing factors has been diligently undertaken in this chapter. This has revealed insights that pave the way for efficient and sustainable energy production strategies. The data associated with 125 scenarios were gathered for training the LSTM-RNN model that predicts electricity generation and carbon captured with an error of 5.1%. Subsequently, the LSTM-RNN model was utilized to extend these 125 scenarios to create 280,000 datasets using the Monte Carlo simulation approach for MOO. Within the MOO framework, a thorough examination of the influences of various parameters of the CSTGB system, such as the feedstock composition, operating temperature, and location of the CSTGB system towards GWP and NPW was carried out. This study not only underscored the system's potential for enhanced efficiency and emissions reduction but also emphasized its economic feasibility. Particularly significant was the revelation of the impact of the CT on MOO results. The optimal configuration of the system could avoid the trade-off phenomenon when treating the CT as revenue. Various scenarios for the CSTGB have been analyzed, focusing on environmental and economic impacts. The most favorable scenario demonstrated a significant reduction in GWP, achieving a cumulative saving of 415,960 tons of CO₂-eq and NPW of €4,298 million over a 30-year lifespan when CT was accounted for as a revenue. A scenario excluding CT corresponded to a reduction of 132,615 tons of CO₂-eq and an NPW of €3,042 million. This finding underscored the imperative of comprehensive consideration of multifaceted factors in decision-making, synergizing technological innovation, economic benefits, and environmental feasibility.

Chapter 6. Conclusions and recommendations for future work

6.1 General conclusions

This study focuses on the concentrated solar thermal gasification of biomass (CSTGB) system, an advanced integrated system combining concentrated solar tower (CST) and biomass gasifier technologies, aimed at enhancing the efficiency and economic viability of renewable energy. By comprehensively considering multiple aspects of the system, the research delves deeply into its potential in biomass gasification, carbon footprint reduction, and economic feasibility.

In Chapter 3 presents the development of a stochastic biomass gasification model based on Monte Carlo (MC) simulation methods and random forest (RF) algorithm. This model focuses on optimizing the fixed-bed air gasification process. Findings highlight particle size, reaction temperature, and water content as key factors affecting producer gas production, while the impact of particle shape, emissivity, thermal conductivity, and porosity is relatively minor. Notably, model predictions under normal distribution closely match experimental data with an error range within 12%, providing a reliable parameter base for techno-economic analysis (TEA) and life cycle assessment (LCA).

Chapter 4 further explores the significant potential of the CSTGB system in reducing the carbon footprint of electricity generation. The LCA indicates that the system can reduce over 0.5 million tons of carbon emissions annually and generate over 0.8 million MWh of electricity, accounting for 0.31% of Spain's total electricity consumption in 2019. The efficiency of the CCS subsystem significantly influences the global warming potential (GWP). However, the TEA reveals economic challenges faced by the system: a net present worth (NPW) of approximately -700 million euros over 30 years, with a payback period exceeding 30 years. Sensitivity analysis for economic viability suggests that reducing operation and maintenance (O&M) costs or increasing overall system efficiency could significantly shorten the payback period, potentially achieving long term economic feasibility.

Chapter 5 conducts a more exhaustive analysis using long short-term memory (LSTM) – recurrent neural network (RNN) models and multi-objective optimization (MOO) methods to assess the impact of various CSTGB system parameters on GWP

and NPW. This comprehensive analysis emphasizes the system's potential for enhanced efficiency and emissions reduction and highlights its economic viability. Particularly notable is that when carbon tax (CT) is considered as revenue, the system's optimization can balance environmental and economic benefits. Accounting for CT revenue, the most favorable scenario indicates that the system could cumulatively reduce 415,960 tons of CO₂-eq in GWP and achieve a NPW of 4.3 billion euros over 30 years. A scenario excluding CT revenue, though reducing 132,615 tons of CO₂-eq, would only yield a NPW of 3.0 billion euros. This further confirms the importance of integrating technological innovation, economic benefits, and environmental feasibility in formulating sustainable energy strategies.

Through the analysis in these chapters, the importance of the CSTGB system in the field of renewable energy is demonstrated, particularly in enhancing energy efficiency, reducing environmental impacts, and improving economic sustainability. These research outcomes provide a scientific basis for further development of the CSTGB system and offer valuable references for other studies in the field of renewable energy.

6.2 Recommendations for future work

The development of sustainable energy solutions, particularly through technologies like the CSTGB system, is crucial for mitigating the impacts of climate change and promoting a cleaner, safer energy future. Despite comprehensive research conducted on the CSTGB system, several challenges have been identified that need further investigation to enhance the system's understanding and efficiency. These challenges include the need for more effective catalysts, broader LCA evaluation, refined TEA, integration of advanced energy storage, and the application of machine learning for evaluating the system's O&M costs. Acknowledging these challenges, the following important areas have been identified for future research:

- **In-depth Catalyst Research:** The findings in Chapter 2 highlight the potential of catalysts in improving gasification efficiency. However, there is a gap in understanding their long-term stability and effectiveness under specific operating conditions of the CSTGB system. Future research should focus on developing catalysts specifically designed for the CSTGB system and conducting long-term tests of their durability and performance.

- **Expanded Life Cycle Assessment:** The research in Chapter 4 has indicated that LCA requires a broader approach. Future studies should consider a wider range of environmental factors, such as water usage and impacts on local ecosystems. Additionally, incorporating social and economic factors, such as job creation and community impacts, will provide a more comprehensive evaluation of the CSTGB system sustainability.
- **Refined Techno-economic Analysis:** The research presented in Chapters 4 and 5 has revealed economic barriers in the CSTGB system. To enhance the economic appeal of the CSTGB system, future research should explore innovative financing models, public-private partnerships, and policy incentives. This research could identify strategies that extend beyond simple cost reductions, potentially shortening the system's payback period. A deeper exploration of these economic barriers will provide stronger support and solutions for the economic viability of the CSTGB system.
- **Advanced Energy Storage Integration:** To comprehensive research conducted throughout the study has underscored the importance of enhancing the CSTGB system's operational efficiency and sustainability. A critical finding is the potential role of advanced energy storage technologies in achieving these goals. Future research should focus on exploring the integration of advanced energy storage technologies, such as advanced thermal storage in the CSTGB system. This focus is driven by the need to enhance the system's reliability and economic feasibility, as identified through the study's extensive analysis.
- **Machine learning for predictive maintenance:** Another significant insight gained from the research is the opportunity to optimize operational efficiency and reduce costs in the CSTGB system. Implementing machine learning algorithms for predictive maintenance of CST and gasifier components emerged as a promising strategy to achieve these objectives. Consequently, future studies should focus on developing these algorithms specifically for these components. This direction is informed by the study's findings that highlight the potential of machine learning in minimizing operational costs and downtime, thus enhancing the overall efficiency and viability of the CSTGB system.

Furthermore, the economic viability of the CSTGB system is also a key research direction. The system faces major economic barriers, including high initial investment costs, O&M costs, and insufficient market competitiveness. Future research should be dedicated to identifying and evaluating strategies to reduce these economic barriers, such as more effective cost management methods, finding more economical construction and operational approaches, and exploring government subsidies and tax incentives. Additionally, a deep understanding of market demand and energy policies is essential to explore the adaptability of the CSTGB system in different market and policy environments and to find its unique position in a competitive energy market. Summary, future research should not only focus on the technological advancements and environmental benefits of the CSTGB system but also pay attention to overcoming its economic barriers and enhancing market adaptability. This multi-faceted research approach will help to comprehensively improve the feasibility of the CSTGB system and make a significant contribution to achieving a sustainable energy future.

References

1. Alauddin ZABZ, Lahijani P, Mohammadi M, Mohamed AR. Gasification of lignocellulosic biomass in fluidized beds for renewable energy development: A review. *Renewable and Sustainable Energy Reviews*. 2010;14(9):2852-62.
2. Chylenski P, Forsberg Z, Ståhlberg J, Várnai A, Lersch M, Bengtsson O, et al. Development of minimal enzyme cocktails for hydrolysis of sulfite-pulped lignocellulosic biomass. *Journal of biotechnology*. 2017;246:16-23.
3. Balat M. Production of bioethanol from lignocellulosic materials via the biochemical pathway: a review. *Energy conversion and management*. 2011;52(2):858-75.
4. IEA. World energy balances overview 2019 [Available from: <http://biblioteca.olade.org/opac-tmpl/Documentos/cg00444.pdf>].
5. REN21. Renewables 2019 Global Status Report 2019 [Available from: https://www.ren21.net/wp-content/uploads/2019/05/gsr_2019_full_report_en.pdf].
6. Fivga A, Speranza LG, Branco CM, Ouadi M, Hornung A. A review on the current state of the art for the production of advanced liquid biofuels. *Aims Energy*. 2019;7(1):46.
7. Caputo AC, Palumbo M, Pelagagge PM, Scacchia F. Economics of biomass energy utilization in combustion and gasification plants: effects of logistic variables. *Biomass and Bioenergy*. 2005;28(1):35-51.
8. You S, Tong H, Armin-Hoiland J, Tong YW, Wang C-H. Techno-economic and greenhouse gas savings assessment of decentralized biomass gasification for electrifying the rural areas of Indonesia. *Applied Energy*. 2017;208:495-510.
9. Chen J, Xu W, Zuo H, Wu X, E J, Wang T, et al. System development and environmental performance analysis of a solar-driven supercritical water gasification pilot plant for hydrogen production using life cycle assessment approach. *Energy Conversion and Management*. 2019;184:60-73.
10. Brendelberger S, Rosenstiel A, Lopez-Roman A, Prieto C, Sattler C. Performance analysis of operational strategies for monolithic receiver-reactor arrays in solar thermochemical hydrogen production plants. *International Journal of Hydrogen*

Energy. 2020;45(49):26104-16.

11. Wu J, Wang J. Distributed biomass gasification power generation system based on concentrated solar radiation. *Energy Procedia*. 2019;158:204-9.
12. Loutzenhiser PG, Muroyama AP. A review of the state-of-the-art in solar-driven gasification processes with carbonaceous materials. *Solar Energy*. 2017;156:93-100.
13. Pramanik S, Ravikrishna R. A review of concentrated solar power hybrid technologies. *Applied Thermal Engineering*. 2017;127:602-37.
14. Puig-Arnabat M, Tora E, Bruno J, Coronas A. State of the art on reactor designs for solar gasification of carbonaceous feedstock. *Solar Energy*. 2013;97:67-84.
15. Chuayboon S, Abanades S, Rodat S. Comprehensive performance assessment of a continuous solar-driven biomass gasifier. *Fuel Processing Technology*. 2018;182:1-14.
16. Reyes L, Abdelouahed L, Campusano B, Buvat J-C, Taouk B. Exergetic study of beech wood gasification in fluidized bed reactor using CO₂ or steam as gasification agents. *Fuel Processing Technology*. 2021;213:106664.
17. Arribas L, Arconada N, González-Fernández C, Löhrl C, González-Aguilar J, Kaltschmitt M, et al. Solar-driven pyrolysis and gasification of low-grade carbonaceous materials. *International journal of hydrogen energy*. 2017;42(19):13598-606.
18. Im-orb K, Simasatitkul L, Arpornwichanop A. Analysis of synthesis gas production with a flexible H₂/CO ratio from rice straw gasification. *Fuel*. 2016;164:361-73.
19. Kruesi M, Jovanovic ZR, dos Santos EC, Yoon HC, Steinfeld A. Solar-driven steam-based gasification of sugarcane bagasse in a combined drop-tube and fixed-bed reactor—Thermodynamic, kinetic, and experimental analyses. *biomass and bioenergy*. 2013;52:173-83.
20. Ahmed I, Gupta A. Sugarcane bagasse gasification: Global reaction mechanism of syngas evolution. *Applied Energy*. 2012;91(1):75-81.
21. Bellouard Q, Abanades S, Rodat S, Dupassieux N. Solar thermochemical gasification of wood biomass for syngas production in a high-temperature continuously-fed tubular reactor. *International Journal of Hydrogen Energy*. 2017;42(19):13486-97.
22. Bellouard Q, Rodat S, Abanades S, Ravel S, Frayssines P-É. Design, simulation and experimental study of a directly-irradiated solar chemical reactor for hydrogen and syngas production from continuous solar-driven wood biomass gasification.

- International Journal of Hydrogen Energy. 2019;44(35):19193-205.
23. van der Meijden CM, Veringa HJ, Rabou LP. The production of synthetic natural gas (SNG): A comparison of three wood gasification systems for energy balance and overall efficiency. *Biomass and bioenergy*. 2010;34(3):302-11.
 24. Prins MJ, Ptasiński KJ, Janssen FJ. More efficient biomass gasification via torrefaction. *Energy*. 2006;31(15):3458-70.
 25. Cerone N, Zimbardi F, Villone A, Strjugas N, Kiyikci E. Gasification of wood and torrefied wood with air, oxygen, and steam in a fixed-bed pilot plant. *Energy & Fuels*. 2016;30(5):4034-43.
 26. François J, Abdelouahed L, Mauviel G, Feidt M, Rogaume C, Mirgaux O, et al. Estimation of the energy efficiency of a wood gasification CHP plant using Aspen Plus. *Chemical engineering transactions*. 2012;29:769-74.
 27. Ptasiński KJ. Thermodynamic efficiency of biomass gasification and biofuels conversion. *Biofuels, Bioproducts and Biorefining*. 2008;2(3):239-53.
 28. Wu H, Liu Q, Bai Z, Xie G, Zheng J, Su B. Thermodynamics analysis of a novel steam/air biomass gasification combined cooling, heating and power system with solar energy. *Applied Thermal Engineering*. 2020;164:114494.
 29. Cao C, Xu L, He Y, Guo L, Jin H, Huo Z. High-efficiency gasification of wheat straw black liquor in supercritical water at high temperatures for hydrogen production. *Energy & Fuels*. 2017;31(4):3970-8.
 30. Wang C, Li L, Chen Y, Ge Z, Jin H. Supercritical water gasification of wheat straw: Composition of reaction products and kinetic study. *Energy*. 2021;227:120449.
 31. Fang Y, Paul MC, Varjani S, Li X, Park Y-K, You S. Concentrated solar thermochemical gasification of biomass: Principles, applications, and development. *Renewable and Sustainable Energy Reviews*. 2021;150:111484.
 32. Fang Y, Li X, Ascher S, Li Y, Dai L, Ruan R, et al. Life cycle assessment and cost benefit analysis of concentrated solar thermal gasification of biomass for continuous electricity generation. *Energy*. 2023;284:128709.
 33. Gupta VK, Pandey A, Koffas M, Mussatto SI, Khare S. Biobased biorefineries: sustainable bioprocesses and bioproducts from biomass/bioresources special issue. Elsevier; 2022. p. 112683.
 34. Nguyen TLT, Hermansen JE, Nielsen RG. Environmental assessment of gasification technology for biomass conversion to energy in comparison with other alternatives: the case of wheat straw. *Journal of cleaner production*. 2013;53:138-48.

35. Colantoni A, Villarini M, Monarca D, Carlini M, Mosconi EM, Bocci E, et al. Economic analysis and risk assessment of biomass gasification CHP systems of different sizes through Monte Carlo simulation. *Energy Reports*. 2021;7:1954-61.
36. Salkuyeh YK, Saville BA, MacLean HL. Techno-economic analysis and life cycle assessment of hydrogen production from different biomass gasification processes. *International Journal of Hydrogen Energy*. 2018;43(20):9514-28.
37. Macedo SF, Peyerl D. Prospects and economic feasibility analysis of wind and solar photovoltaic hybrid systems for hydrogen production and storage: A case study of the Brazilian electric power sector. *International Journal of Hydrogen Energy*. 2022;47(19):10460-73.
38. Fereidooni M, Mostafaeipour A, Kalantar V, Goudarzi H. A comprehensive evaluation of hydrogen production from photovoltaic power station. *Renewable and Sustainable Energy Reviews*. 2018;82:415-23.
39. Gallardo FI, Ferrario AM, Lamagna M, Bocci E, Garcia DA, Baeza-Jeria TE. A Techno-Economic Analysis of solar hydrogen production by electrolysis in the north of Chile and the case of exportation from Atacama Desert to Japan. *international journal of hydrogen energy*. 2021;46(26):13709-28.
40. Shen W, Chen X, Qiu J, Hayward JA, Sayeef S, Osman P, et al. A comprehensive review of variable renewable energy levelized cost of electricity. *Renewable and Sustainable Energy Reviews*. 2020;133:110301.
41. Wiser R, Rand J, Seel J, Beiter P, Baker E, Lantz E, et al. Expert elicitation survey predicts 37% to 49% declines in wind energy costs by 2050. *Nature Energy*. 2021;6(5):555-65.
42. Stehly T, Beiter P, Duffy P. 2019 cost of wind energy review. National Renewable Energy Lab.(NREL), Golden, CO (United States); 2020.
43. Mahmood N, Wang Z, Zhang B. The role of nuclear energy in the correction of environmental pollution: Evidence from Pakistan. *Nuclear Engineering and Technology*. 2020;52(6):1327-33.
44. Nathaniel SP, Alam MS, Murshed M, Mahmood H, Ahmad P. The roles of nuclear energy, renewable energy, and economic growth in the abatement of carbon dioxide emissions in the G7 countries. *Environmental Science and Pollution Research*. 2021;28(35):47957-72.
45. Saługa PW, Szczepańska-Woszczyzna K, Miśkiewicz R, Chład M. Cost of equity of coal-fired power generation projects in Poland: Its importance for the management

- of decision-making process. *Energies*. 2020;13(18):4833.
46. Center BP. Annual energy outlook 2020. Energy Information Administration, Washington, DC. 2020;12:1672-9.
47. Morris J, Farrell J, Kheshgi H, Thomann H, Chen H, Paltsev S, et al. Representing the costs of low-carbon power generation in multi-region multi-sector energy-economic models. *International Journal of Greenhouse Gas Control*. 2019;87:170-87.
48. Screw driver website:https://www.alibaba.com/product-detail/Hot-sale-auger-screw-conveyor-for_62166933656.html?spm=a2700.7724857.0.0.128279bbpq1HUB.
49. Widjaya ER, Chen G, Bowtell L, Hills C. Gasification of non-woody biomass: A literature review. *Renewable and Sustainable Energy Reviews*. 2018;89:184-93.
50. Saidur R, Abdelaziz E, Demirbas A, Hossain M, Mekhilef S. A review on biomass as a fuel for boilers. *Renewable and sustainable energy reviews*. 2011;15(5):2262-89.
51. Balat M, Ayar G. Biomass energy in the world, use of biomass and potential trends. *Energy sources*. 2005;27(10):931-40.
52. Zhang W, Huang S, Wu S, Wu Y, Gao J. Study on the structure characteristics and gasification activity of residual carbon in biomass ashes obtained from different gasification technologies. *Fuel*. 2019;254:115699.
53. Huang S, Wu S, Wu Y, Gao J. Structure characteristics and gasification activity of residual carbon from updraft fixed-bed biomass gasification ash. *Energy Conversion and Management*. 2017;136:108-18.
54. Hoang AT, Huang Z, Nižetić S, Pandey A, Nguyen XP, Luque R, et al. Characteristics of hydrogen production from steam gasification of plant-originated lignocellulosic biomass and its prospects in Vietnam. *International Journal of Hydrogen Energy*. 2022;47(7):4394-425.
55. Sivabalan K, Hassan S, Ya H, Pasupuleti J, editors. A review on the characteristic of biomass and classification of bioenergy through direct combustion and gasification as an alternative power supply. *Journal of Physics: Conference Series*; 2021: IOP Publishing.
56. Li X, Yan P, Ma C, Wang J. Structural design and optimization of a solar spouted bed reactor of biomass gasification. *Applied Thermal Engineering*. 2021;194:117058.
57. Li J, Li L, Tong YW, Wang X. Understanding and optimizing the gasification of biomass waste with machine learning. *Green Chemical Engineering*. 2023;4(1):123-33.

58. Wang J, Dong F, Ma Z, Chen H, Yan R. Multi-objective optimization with thermodynamic analysis of an integrated energy system based on biomass and solar energies. *Journal of Cleaner Production*. 2021;324:129257.
59. Bai Z, Liu Q, Gong L, Lei J. Investigation of a solar-biomass gasification system with the production of methanol and electricity: Thermodynamic, economic and off-design operation. *Applied Energy*. 2019;243:91-101.
60. Kambo HS, Dutta A. A comparative review of biochar and hydrochar in terms of production, physico-chemical properties and applications. *Renewable and Sustainable Energy Reviews*. 2015;45:359-78.
61. Fang Y, Li Y, Ahmed A, You S. Development, economics and global warming potential of lignocellulose biorefinery. *Biomass, Biofuels, Biochemicals*. 2021:1-13.
62. Piatkowski N, Wieckert C, Weimer AW, Steinfeld A. Solar-driven gasification of carbonaceous feedstock—a review. *Energy & Environmental Science*. 2011;4(1):73-82.
63. Yang L, Zhang X, Liu S, Yu L, Zhang W. Field test of large-scale hydrogen manufacturing from underground coal gasification (UCG). *International Journal of Hydrogen Energy*. 2008;33(4):1275-85.
64. You S, Ok YS, Tsang DC, Kwon EE, Wang C-H. Towards practical application of gasification: a critical review from syngas and biochar perspectives. *Critical Reviews in Environmental Science and Technology*. 2018;48(22-24):1165-213.
65. Thomson R, Kwong P, Ahmad E, Nigam K. Clean syngas from small commercial biomass gasifiers; a review of gasifier development, recent advances and performance evaluation. *international journal of hydrogen energy*. 2020;45(41):21087-111.
66. Hathaway BJ, Davidson JH. Autothermal hybridization and controlled production of hydrogen-rich syngas in a molten salt solar gasifier. *International Journal of Hydrogen Energy*. 2021;46(29):15257-67.
67. Abanades S, Rodat S, Boujjat H. Solar thermochemical green fuels production: A review of biomass pyro-gasification, solar reactor concepts and modelling methods. *Energies*. 2021;14(5):1494.
68. Kan T, Strezov V, Evans TJ. Lignocellulosic biomass pyrolysis: A review of product properties and effects of pyrolysis parameters. *Renewable and sustainable energy reviews*. 2016;57:1126-40.
69. Yogalakshmi K, Sivashanmugam P, Kavitha S, Kannah Y, Varjani S,

- AdishKumar S, et al. Lignocellulosic biomass-based pyrolysis: A comprehensive review. *Chemosphere*. 2022;286:131824.
70. Li L, Rowbotham JS, Greenwell CH, Dyer PW. *An introduction to pyrolysis and catalytic pyrolysis: versatile techniques for biomass conversion*. Elsevier; 2013.
71. Hu B, Zhang Z-x, Xie W-l, Liu J, Li Y, Zhang W-m, et al. Advances on the fast pyrolysis of biomass for the selective preparation of phenolic compounds. *Fuel Processing Technology*. 2022;237:107465.
72. Meier D, Faix O. State of the art of applied fast pyrolysis of lignocellulosic materials—a review. *Bioresource technology*. 1999;68(1):71-7.
73. Bridgwater AV. Review of fast pyrolysis of biomass and product upgrading. *Biomass and bioenergy*. 2012;38:68-94.
74. Badger PC, Fransham P. Use of mobile fast pyrolysis plants to densify biomass and reduce biomass handling costs—A preliminary assessment. *Biomass and bioenergy*. 2006;30(4):321-5.
75. Antal M, Hofmann L, Moriera J, editors. *Bench scale radiant flash pyrolysis of biomass*. Proceedings of specialist's workshop on fast pyrolysis of biomass Copper Mountain, CO, USA; 1980.
76. Chan WCR, Kelbon M, Krieger-Brockett B. Single-particle biomass pyrolysis: correlations of reaction products with process conditions. *Industrial & engineering chemistry research*. 1988;27(12):2261-75.
77. Grønli MG, Melaaen MC. Mathematical model for wood pyrolysis comparison of experimental measurements with model predictions. *Energy & Fuels*. 2000;14(4):791-800.
78. Antal M, Hofmann L, Moreira J, Brown C, Steenblik R. Design and operation of a solar fired biomass flash pyrolysis reactor. *Solar Energy*. 1983;30(4):299-312.
79. Beattie WH, Berjoan R, Coutures J-P. High-temperature solar pyrolysis of coal. *Solar Energy*. 1983;31(2):137-43.
80. Rahman MM, Liu R, Cai J. Catalytic fast pyrolysis of biomass over zeolites for high quality bio-oil—a review. *Fuel Processing Technology*. 2018;180:32-46.
81. Mariyam S, Shahbaz M, Al-Ansari T, Mackey HR, McKay G. A critical review on co-gasification and co-pyrolysis for gas production. *Renewable and Sustainable Energy Reviews*. 2022;161:112349.
82. Hejazi B, Grace JR, Bi X, Mahecha-Botero As. Kinetic model of steam gasification of biomass in a bubbling fluidized bed reactor. *Energy & Fuels*.

2017;31(2):1702-11.

83. Yank A, Ngadi M, Kok R. Physical properties of rice husk and bran briquettes under low pressure densification for rural applications. *Biomass and Bioenergy*. 2016;84:22-30.
84. Parvez AM, Wu T, Afzal MT, Mareta S, He T, Zhai M. Conventional and microwave-assisted pyrolysis of gumwood: A comparison study using thermodynamic evaluation and hydrogen production. *Fuel Processing Technology*. 2019;184:1-11.
85. Cao Y, Wang Q, Du J, Chen J. Oxygen-enriched air gasification of biomass materials for high-quality syngas production. *Energy Conversion and Management*. 2019;199:111628.
86. Freda C, Nanna F, Villone A, Barisano D, Brandani S, Cornacchia G. Air gasification of digestate and its co-gasification with residual biomass in a pilot scale rotary kiln. *International Journal of Energy and Environmental Engineering*. 2019;10(3):335-46.
87. Valin S, Ravel S, de Vincent PP, Thiery S, Miller H. Fluidized bed air gasification of solid recovered fuel and woody biomass: Influence of experimental conditions on product gas and pollutant release. *Fuel*. 2019;242:664-72.
88. Kumar MS, Kesavan M. Development of an empirical relationship and influence of process parameters on biomass gasification system. *development*. 2019;7(03).
89. Yang H, Liu J, Zhang H, Han X, Jiang X. Experimental research for biomass steam gasification in a fluidized bed. *Energy Sources, Part A: Recovery, Utilization, and Environmental Effects*. 2019;41(16):1993-2006.
90. Baruah D, Baruah D. Modeling of biomass gasification: A review. *Renewable and Sustainable Energy Reviews*. 2014;39:806-15.
91. Cerone N, Zimbardi F, Contuzzi L, Baleta J, Cerinski D, Skvorčinskienė R. Experimental investigation of syngas composition variation along updraft fixed bed gasifier. *Energy Conversion and Management*. 2020;221:113116.
92. Boujjat H, Junior GMY, Rodat S, Abanades S. Dynamic simulation and control of solar biomass gasification for hydrogen-rich syngas production during allothermal and hybrid solar/autothermal operation. *International Journal of Hydrogen Energy*. 2020.
93. Boujjat H, Rodat S, Chuayboon S, Abanades S. Numerical simulation of reactive gas-particle flow in a solar jet spouted bed reactor for continuous biomass

- gasification. *International Journal of Heat and Mass Transfer*. 2019;144:118572.
94. Jin H, Wang C, Fan C. Simulation Study on Hydrogen-Heating-Power Poly-Generation System based on Solar Driven Supercritical Water Biomass Gasification with Compressed Gas Products as an Energy Storage System. *Journal of Thermal Science*. 2020;29(2):365-77.
95. Boujjat H, Junior GMY, Rodat S, Abanades S. Dynamic simulation and control of solar biomass gasification for hydrogen-rich syngas production during allothermal and hybrid solar/autothermal operation. *International Journal of Hydrogen Energy*. 2020;45(48):25827-37.
96. Chopra S, Jain A. A review of fixed bed gasification systems for biomass. 2007.
97. Beohar H, Gupta B, Sethi V, Pandey M. Parametric study of fixed bed biomass gasifier: a review. *International Journal of Thermal Technologies*. 2012;2(1):134-40.
98. Yoon SJ, Son Y-I, Kim Y-K, Lee J-G. Gasification and power generation characteristics of rice husk and rice husk pellet using a downdraft fixed-bed gasifier. *Renewable Energy*. 2012;42:163-7.
99. Xiang X, Gong G, Wang C, Cai N, Zhou X, Li Y. Exergy analysis of updraft and downdraft fixed bed gasification of village-level solid waste. *International Journal of Hydrogen Energy*. 2021;46(1):221-33.
100. Li X, Shen Y, Wei L, He C, Lapkin AA, Lipiński W, et al. Hydrogen production of solar-driven steam gasification of sewage sludge in an indirectly irradiated fluidized-bed reactor. *Applied Energy*. 2020;261:114229.
101. Wan Z, Yang S, Wei Y, Hu J, Wang H. CFD modeling of the flow dynamics and gasification in the combustor and gasifier of a dual fluidized bed pilot plant. *Energy*. 2020:117366.
102. Ram M, Mondal MK. Investigation on fuel gas production from pulp and paper waste water impregnated coconut husk in fluidized bed gasifier via humidified air and CO₂ gasification. *Energy*. 2019;178:522-9.
103. Safarian S, Unnþórsson R, Richter C. A review of biomass gasification modelling. *Renewable and Sustainable Energy Reviews*. 2019;110:378-91.
104. Zang G, Jia J, Shi Y, Sharma T, Ratner A. Modeling and economic analysis of waste tire gasification in fluidized and fixed bed gasifiers. *Waste Management*. 2019;89:201-11.
105. Suárez-Almeida M, Gómez-Barea A, Ghoniem A, Pfeifer C. Solar gasification of biomass in a dual fluidized bed. *Chemical Engineering Journal*. 2020:126665.

106. Ku X, Wang J, Jin H, Lin J. Effects of operating conditions and reactor structure on biomass entrained-flow gasification. *Renewable Energy*. 2019;139:781-95.
107. Feng P, Lin W, Jensen PA, Song W, Hao L, Li S, et al. Characterization of solid residues from entrained flow gasification of coal bio-oil slurry. *Energy & Fuels*. 2020;34(5):5900-6.
108. Kibria M, Sripada P, Bhattacharya S. Steady state kinetic model for entrained flow CO₂ gasification of biomass at high temperature. *Energy*. 2020;196:117073.
109. Van Eyk PJ, Ashman PJ, Nathan GJ. Effect of high-flux solar irradiation on the gasification of coal in a hybrid entrained-flow reactor. *Energy & Fuels*. 2016;30(6):5138-47.
110. Chuayboon S, Abanades S, Rodat S. Insights into the influence of biomass feedstock type, particle size and feeding rate on thermochemical performances of a continuous solar gasification reactor. *Renewable Energy*. 2019;130:360-70.
111. Krishnamoorthy V, Pisupati SV. Effect of Temperature, Pressure, Feed Particle Size, and Feed Particle Density on Structural Characteristics and Reactivity of Chars Generated during Gasification of Pittsburgh No. 8 Coal in a High-Pressure, High-Temperature Flow Reactor. *Energies*. 2019;12(24):4773.
112. Safin R, Prosvirnikov D, Stepanova T, editors. *Processing of Renewable Wood Biomass into Thermally Modified Pellets with Increased Combustion Value*. International Conference on Industrial Engineering; 2019: Springer.
113. Hernández JJ, Aranda-Almansa G, Bula A. Gasification of biomass wastes in an entrained flow gasifier: Effect of the particle size and the residence time. *Fuel Processing Technology*. 2010;91(6):681-92.
114. Kodama T, Bellan S, Gokon N, Cho HS. Particle reactors for solar thermochemical processes. *Solar Energy*. 2017;156:113-32.
115. Yu J, Sun L, Berrueco C, Fidalgo B, Paterson N, Millan M. Influence of temperature and particle size on structural characteristics of chars from Beechwood pyrolysis. *Journal of Analytical and Applied Pyrolysis*. 2018;130:127-34.
116. Weldekidan H, Strezov V, Li R, Kan T, Town G, Kumar R, et al. Distribution of solar pyrolysis products and product gas composition produced from agricultural residues and animal wastes at different operating parameters. *Renewable Energy*. 2020;151:1102-9.
117. Chuayboon S, Abanades S, Rodat S. Experimental analysis of continuous steam gasification of wood biomass for syngas production in a high-temperature particle-fed

solar reactor. *Chemical Engineering and Processing-Process Intensification*. 2018;125:253-65.

118. Bisht AS, Thakur N. Pine needle biomass gasification based electricity and cold storage systems for rural Himalayan region: optimal size and site. *International Journal of Renewable Energy Technology*. 2017;8(3-4):211-21.

119. Pinna-Hernández MG, Martínez-Soler I, Villanueva MJD, Fernández FGA, López JLC. Selection of biomass supply for a gasification process in a solar thermal hybrid plant for the production of electricity. *Industrial Crops and Products*. 2019;137:339-46.

120. Perkins CM, Woodruff B, Andrews L, Lichty P, Lancaster B, Weimer A, et al. Synthesis gas production by rapid solar thermal gasification of corn stover. National Renewable Energy Lab.(NREL), Golden, CO (United States); 2008.

121. Ansari SH, Ahmed A, Razzaq A, Hildebrandt D, Liu X, Park Y-K. Incorporation of solar-thermal energy into a gasification process to co-produce bio-fertilizer and power. *Environmental Pollution*. 2020;266:115103.

122. Siddiqui O, Dincer I. Design and assessment of a new solar-based biomass gasification system for hydrogen, cooling, power and fresh water production utilizing rice husk biomass. *Energy Conversion and Management*. 2021;236:114001.

123. Ravenni G, Elhami O, Ahrenfeldt J, Henriksen U, Neubauer Y. Adsorption and decomposition of tar model compounds over the surface of gasification char and active carbon within the temperature range 250–800° C. *Applied Energy*. 2019;241:139-51.

124. Salem AM, Dhimi HS, Paul MC. Syngas production and combined heat and power from scottish agricultural waste gasification—a computational study. *Sustainability*. 2022;14(7):3745.

125. Ren J, Liu Y-L, Zhao X-Y, Cao J-P. Biomass thermochemical conversion: A review on tar elimination from biomass catalytic gasification. *Journal of the Energy Institute*. 2020;93(3):1083-98.

126. Lind F, Seemann M, Thunman H. Continuous catalytic tar reforming of biomass derived raw gas with simultaneous catalyst regeneration. *Industrial & engineering chemistry research*. 2011;50(20):11553-62.

127. Quitete CP, Souza MM. Application of Brazilian dolomites and mixed oxides as catalysts in tar removal system. *Applied Catalysis A: General*. 2017;536:1-8.

128. Richardson Y, Blin J, Julbe A. A short overview on purification and conditioning of syngas produced by biomass gasification: catalytic strategies, process intensification

- and new concepts. *Progress in Energy and Combustion Science*. 2012;38(6):765-81.
129. Simell P, Kurkela E, Ståhlberg P, Hepola J. Catalytic hot gas cleaning of gasification gas. *Catalysis Today*. 1996;27(1-2):55-62.
130. Qin Y, He Y, Ren W, Gao M, Wiltowski T. Catalytic effect of alkali metal in biomass ash on the gasification of coal char in CO₂. *Journal of Thermal Analysis and Calorimetry*. 2020;139(5):3079-89.
131. Gall D, Pushp M, Larsson A, Davidsson K, Pettersson JB. Online measurements of alkali metals during start-up and operation of an industrial-scale biomass gasification plant. *Energy & Fuels*. 2018;32(1):532-41.
132. Moud PH, Andersson KJ, Lanza R, Engvall K. Equilibrium potassium coverage and its effect on a Ni tar reforming catalyst in alkali-and sulfur-laden biomass gasification gases. *Applied Catalysis B: Environmental*. 2016;190:137-46.
133. Feng D, Zhao Y, Zhang Y, Xu H, Zhang L, Sun S. Catalytic mechanism of ion-exchanging alkali and alkaline earth metallic species on biochar reactivity during CO₂/H₂O gasification. *Fuel*. 2018;212:523-32.
134. Sutton D, Parle S, Ross J. The CO₂ reforming of the hydrocarbons present in a model gas stream over selected catalysts. *Fuel Processing Technology*. 2002;75(1):45-53.
135. Haldar KK, Tanwar S, Biswas R, Sen T, Lahtinen J. Noble copper-silver-gold trimetallic nanobowls: An efficient catalyst. *Journal of colloid and interface science*. 2019;556:140-6.
136. Tomishige K, Asadullah M, Kunimori K. Syngas production by biomass gasification using Rh/CeO₂/SiO₂ catalysts and fluidized bed reactor. *Catalysis Today*. 2004;89(4):389-403.
137. Sikarwar VS, Zhao M, Fennell PS, Shah N, Anthony EJ. Progress in biofuel production from gasification. *Progress in Energy and Combustion Science*. 2017;61:189-248.
138. Siwal SS, Zhang Q, Sun C, Thakur S, Gupta VK, Thakur VK. Energy Production from Steam Gasification Processes and Parameters that Contemplate in Biomass Gasifier-A review. *Bioresource Technology*. 2019:122481.
139. Cao Y, Wang Y, Riley JT, Pan W-P. A novel biomass air gasification process for producing tar-free higher heating value fuel gas. *Fuel Processing Technology*. 2006;87(4):343-53.
140. Callaghan CA. Kinetics and catalysis of the water-gas-shift reaction: A

microkinetic and graph theoretic approach: Worcester Polytechnic Institute; 2006.

141. Tang Q, Bian H, Ran J, Zhu Y, Yu J, Zhu W. Hydrogen-rich gas production from steam gasification of biomass using CaO and a Fe-Cr water-gas shift catalyst. *BioResources*. 2015;10(2):2560-9.
142. Sepe AM, Li J, Paul MC. Assessing biomass steam gasification technologies using a multi-purpose model. *Energy Conversion and Management*. 2016;129:216-26.
143. Puig-Arnavat M, Bruno JC, Coronas A. Modified thermodynamic equilibrium model for biomass gasification: a study of the influence of operating conditions. *Energy & Fuels*. 2012;26(2):1385-94.
144. Srinivas T, Gupta A, Reddy B. Thermodynamic equilibrium model and exergy analysis of a biomass gasifier. *Journal of Energy Resources Technology*. 2009;131(3).
145. Formica M, Frigo S, Gabbriellini R. Development of a new steady state zero-dimensional simulation model for woody biomass gasification in a full scale plant. *Energy conversion and management*. 2016;120:358-69.
146. Jarunghammachote S, Dutta A. Equilibrium modeling of gasification: Gibbs free energy minimization approach and its application to spouted bed and spout-fluid bed gasifiers. *Energy Conversion and Management*. 2008;49(6):1345-56.
147. Li X, Grace J, Watkinson A, Lim C, Ergüdenler A. Equilibrium modeling of gasification: a free energy minimization approach and its application to a circulating fluidized bed coal gasifier. *Fuel*. 2001;80(2):195-207.
148. Wang J, Ma C, Wu J. Thermodynamic analysis of a combined cooling, heating and power system based on solar thermal biomass gasification☆. *Applied Energy*. 2019;247:102-15.
149. Gomaa MR, Mustafa RJ, Al-Dmour N. Solar thermochemical conversion of carbonaceous materials into syngas by Co-Gasification. *Journal of Cleaner Production*. 2020;248:119185.
150. Wei Z, Khor C, Rahim W, Razak N, Ishak M, Rosli M, et al., editors. Mechanical aspects analysis of the cyclone gasifier design via finite element method. *AIP Conference Proceedings*; 2018: AIP Publishing LLC.
151. Baggio P, Baratieri M, Fiori L, Grigiante M, Avi D, Tosi P. Experimental and modeling analysis of a batch gasification/pyrolysis reactor. *Energy Conversion and Management*. 2009;50(6):1426-35.
152. Karmakar M, Datta A. Generation of hydrogen rich gas through fluidized bed

- gasification of biomass. *Bioresource Technology*. 2011;102(2):1907-13.
153. Yao Z, He X, Hu Q, Cheng W, Yang H, Wang C-H. A hybrid peripheral fragmentation and shrinking-core model for fixed-bed biomass gasification. *Chemical Engineering Journal*. 2020;400:124940.
154. Probststein RF, Hicks RE. *Synthetic fuels*: Courier Corporation; 2006.
155. Salem AM, Paul MC. An integrated kinetic model for downdraft gasifier based on a novel approach that optimises the reduction zone of gasifier. *Biomass and Bioenergy*. 2018;109:172-81.
156. Panjwani MK, Narejo GB. Effect of altitude on the efficiency of solar panel. *International Journal of Engineering Research and General Science*. 2014;2(4).
157. Dejtrakulwong C, Patumsawad S. Four zones modeling of the downdraft biomass gasification process: effects of moisture content and air to fuel ratio. *Energy Procedia*. 2014;52:142-9.
158. Sharma AK. Modeling and simulation of a downdraft biomass gasifier 1. Model development and validation. *Energy Conversion and Management*. 2011;52(2):1386-96.
159. Hameed S, Ramzan N, Rahman Z-u, Zafar M, Riaz S. Kinetic modeling of reduction zone in biomass gasification. *Energy conversion and management*. 2014;78:367-73.
160. Kumar U, Paul MC. CFD modelling of biomass gasification with a volatile break-up approach. *Chemical Engineering Science*. 2019;195:413-22.
161. Carrillo AJ, González-Aguilar J, Romero M, Coronado JM. Solar energy on demand: A review on high temperature thermochemical heat storage systems and materials. *Chemical Reviews*. 2019;119(7):4777-816.
162. Oevermann M, Gerber S, Behrendt F. Euler–Lagrange/DEM simulation of wood gasification in a bubbling fluidized bed reactor. *Particuology*. 2009;7(4):307-16.
163. Boujjat H, Rodat S, Chuayboon S, Abanades S. Experimental and CFD investigation of inert bed materials effects in a high-temperature conical cavity-type reactor for continuous solar-driven steam gasification of biomass. *Chemical Engineering Science*. 2020;228:115970.
164. González WA, Pérez JF. CFD analysis and characterization of biochar produced via fixed-bed gasification of fallen leaf pellets. *Energy*. 2019;186:115904.
165. Ismail TM, Abd El-Salam M, Monteiro E, Rouboa A. Eulerian – Eulerian CFD model on fluidized bed gasifier using coffee husks as fuel. *Applied Thermal*

Engineering. 2016;106:1391-402.

166. Yao Z, You S, Ge T, Wang C-H. Biomass gasification for syngas and biochar co-production: Energy application and economic evaluation. *Applied Energy*. 2018;209:43-55.

167. Wang S, Luo K, Fan J. CFD-DEM coupled with thermochemical sub-models for biomass gasification: Validation and sensitivity analysis. *Chemical Engineering Science*. 2020;217:115550.

168. Janajreh I, Al Shrah M. Numerical and experimental investigation of downdraft gasification of wood chips. *Energy Conversion and Management*. 2013;65:783-92.

169. You S, Wang W, Dai Y, Tong YW, Wang C-H. Comparison of the co-gasification of sewage sludge and food wastes and cost-benefit analysis of gasification-and incineration-based waste treatment schemes. *Bioresource technology*. 2016;218:595-605.

170. Chang S, Zhang Z, Cao L, Ma L, You S, Li W. Co-gasification of digestate and lignite in a downdraft fixed bed gasifier: Effect of temperature. *Energy Conversion and Management*. 2020;213:112798.

171. Yao Z, You S, Dai Y, Wang C-H. Particulate emission from the gasification and pyrolysis of biomass: Concentration, size distributions, respiratory deposition-based control measure evaluation. *Environmental Pollution*. 2018;242:1108-18.

172. Ramachandran S, Yao Z, You S, Massier T, Stimming U, Wang C-H. Life cycle assessment of a sewage sludge and woody biomass co-gasification system. *Energy*. 2017;137:369-76.

173. Zang G, Zhang J, Jia J, Lora ES, Ratner A. Life cycle assessment of power-generation systems based on biomass integrated gasification combined cycles. *Renewable Energy*. 2020;149:336-46.

174. You S, Li W, Zhang W, Lim H, Kua HW, Park Y-K, et al. Energy, economic, and environmental impacts of sustainable biochar systems in rural China. *Critical Reviews in Environmental Science and Technology*. 2020:1-29.

175. Alnouss A, Parthasarathy P, Shahbaz M, Al-Ansari T, Mackey H, McKay G. Techno-economic and sensitivity analysis of coconut coir pith-biomass gasification using ASPEN PLUS. *Applied Energy*. 2020;261:114350.

176. Wasinarom K, Charoensuk J. Experiment and Numerical Modeling of Stratified Downdraft Gasification Using Rice Husk and Wood Pellet. *BioResources*. 2019;14(3):5235-53.

177. Sittisun P, Tippayawong N, Pang S. Biomass gasification in a fixed bed downdraft reactor with oxygen enriched air: a modified equilibrium modeling study. *Energy Procedia*. 2019;160:317-23.
178. Ferreira S, Monteiro E, Calado L, Silva V, Brito P, Vilarinho C. Experimental and Modeling Analysis of Brewers' Spent Grains Gasification in a Downdraft Reactor. *Energies*. 2019;12(23):4413.
179. Askaripour H. CFD modeling of gasification process in tapered fluidized bed gasifier. *Energy*. 2020;191:116515.
180. Zhang J-L, Wang G-W, Shao J-G, Zuo H-B. A modified random pore model for the kinetics of char gasification. *BioResources*. 2014;9(2):3497-507.
181. Bhatia S, Perlmutter D. A random pore model for fluid-solid reactions: II. Diffusion and transport effects. *AIChE Journal*. 1981;27(2):247-54.
182. Guo B, Li D, Cheng C, Lü Z-a, Shen Y. Simulation of biomass gasification with a hybrid neural network model. *Bioresource Technology*. 2001;76(2):77-83.
183. Weber K, Li T, Løvås T, Perlman C, Seidel L, Mauß F. Stochastic reactor modeling of biomass pyrolysis and gasification. *Journal of Analytical and Applied Pyrolysis*. 2017;124:592-601.
184. Xing J, Wang H, Luo K, Wang S, Bai Y, Fan J. Predictive single-step kinetic model of biomass devolatilization for CFD applications: A comparison study of empirical correlations (EC), artificial neural networks (ANN) and random forest (RF). *Renewable Energy*. 2019;136:104-14.
185. Iwaszenko S, Howaniec N, Smoliński A. Determination of random pore model parameters for underground coal gasification simulation. *Energy*. 2019;166:972-8.
186. Mazaheri N, Akbarzadeh A, Madadian E, Lefsrud M. Systematic review of research guidelines for numerical simulation of biomass gasification for bioenergy production. *Energy conversion and management*. 2019;183:671-88.
187. Ahmed I, Gupta A. Experiments and stochastic simulations of lignite coal during pyrolysis and gasification. *Applied energy*. 2013;102:355-63.
188. İskenderoğlu FC, Baltacıoğlu MK, Demir MH, Baldinelli A, Barelli L, Bidini G. Comparison of support vector regression and random forest algorithms for estimating the SOFC output voltage by considering hydrogen flow rates. *International Journal of Hydrogen Energy*. 2020;45(60):35023-38.
189. Ceylan Z, Ceylan S. Application of machine learning algorithms to predict the performance of coal gasification process. *Applications of Artificial Intelligence in*

Process Systems Engineering: Elsevier; 2021. p. 165-86.

190. Gopirajan PV, Gopinath KP, Sivaranjani G, Arun J. Optimization of hydrothermal gasification process through machine learning approach: Experimental conditions, product yield and pollution. *Journal of Cleaner Production*. 2021;306:127302.
191. Wang MW, Goodman JM, Allen TE. Machine learning in predictive toxicology: recent applications and future directions for classification models. *Chemical research in toxicology*. 2020;34(2):217-39.
192. Guan Y, Chaffart D, Liu G, Tan Z, Zhang D, Wang Y, et al. Machine learning in solid heterogeneous catalysis: Recent developments, challenges and perspectives. *Chemical Engineering Science*. 2022;248:117224.
193. Umenweke GC, Afolabi IC, Epelle EI, Okolie JA. Machine learning methods for modeling conventional and hydrothermal gasification of waste biomass: A review. *Bioresource Technology Reports*. 2022;17:100976.
194. Sahoo P, Roy I, Wang Z, Mi F, Yu L, Balasubramani P, et al. MultiCon: a semi-supervised approach for predicting drug function from chemical structure analysis. *Journal of Chemical Information and Modeling*. 2020;60(12):5995-6006.
195. Bahadar A, Kanthasamy R, Sait HH, Zwawi M, Algarni M, Ayodele BV, et al. Elucidating the effect of process parameters on the production of hydrogen-rich syngas by biomass and coal Co-gasification techniques: A multi-criteria modeling approach. *Chemosphere*. 2022;287:132052.
196. Shahbaz M, Taqvi SA, Loy ACM, Inayat A, Uddin F, Bokhari A, et al. Artificial neural network approach for the steam gasification of palm oil waste using bottom ash and CaO. *Renewable Energy*. 2019;132:243-54.
197. Bishnu SK, Alnouri SY, Al Mohannadi DM. Computational applications using Data Driven Modeling in Process Systems: A Review. *Digital Chemical Engineering*. 2023:100111.
198. Bien JD, Bien B. Forecasting the municipal sewage sludge amount generated at wastewater treatment plants using some machine learning methods. *DESALINATION AND WATER TREATMENT*. 2023;288:265-72.
199. Fang Y, Ma L, Yao Z, Li W, You S. Process optimization of biomass gasification with a Monte Carlo approach and random forest algorithm. *Energy Conversion and Management*. 2022;264:115734.
200. Fózér D, Tóth AJ, Varbanov PS, Klemeš JJ, Mizsey P. Sustainability assessment

of biomethanol production via hydrothermal gasification supported by artificial neural network. *Journal of Cleaner Production*. 2021;318:128606.

201. Brown PT, Caldeira K. Greater future global warming inferred from Earth's recent energy budget. *Nature*. 2017;552(7683):45-50.

202. Energiewende A. Sandbag (2019) The European power sector in 2018: up-to-date analysis on the electricity transition, London, Sandbag 2019 [Available from: <https://www.agora-energiewende.de/en/publications/the-european-power-sector-in-2019/>].

203. Li W, Paul M, Baig H, Siviter J, Montecucco A, Mallick T, et al. A three-point-based electrical model and its application in a photovoltaic thermal hybrid roof-top system with crossed compound parabolic concentrator. *Renewable Energy*. 2019;130:400-15.

204. Liu M, Tay NS, Bell S, Belusko M, Jacob R, Will G, et al. Review on concentrating solar power plants and new developments in high temperature thermal energy storage technologies. *Renewable and Sustainable Energy Reviews*. 2016;53:1411-32.

205. Islam MT, Huda N, Abdullah A, Saidur R. A comprehensive review of state-of-the-art concentrating solar power (CSP) technologies: Current status and research trends. *Renewable and Sustainable Energy Reviews*. 2018;91:987-1018.

206. Gang P, Huide F, Huijuan Z, Jie J. Performance study and parametric analysis of a novel heat pipe PV/T system. *Energy*. 2012;37(1):384-95.

207. Avila-Marin AL. Volumetric receivers in solar thermal power plants with central receiver system technology: a review. *Solar Energy*. 2011;85(5):891-910.

208. Gil A, Medrano M, Martorell I, Lázaro A, Dolado P, Zalba B, et al. State of the art on high temperature thermal energy storage for power generation. Part 1—Concepts, materials and modellization. *Renewable and Sustainable Energy Reviews*. 2010;14(1):31-55.

209. He Y-L, Wang K, Qiu Y, Du B-C, Liang Q, Du S. Review of the solar flux distribution in concentrated solar power: non-uniform features, challenges, and solutions. *Applied Thermal Engineering*. 2019;149:448-74.

210. Sun J, Zhang Z, Wang L, Zhang Z, Wei J. Comprehensive Review of Line-Focus Concentrating Solar Thermal Technologies: Parabolic Trough Collector (PTC) vs Linear Fresnel Reflector (LFR). *Journal of Thermal Science*. 2020:1-28.

211. Cheng Z, He Y, Cui F. Numerical investigations on coupled heat transfer and

synthetical performance of a pressurized volumetric receiver with MCRT–FVM method. *Applied thermal engineering*. 2013;50(1):1044-54.

212. Qiu Y, He Y-L, Li P, Du B-C. A comprehensive model for analysis of real-time optical performance of a solar power tower with a multi-tube cavity receiver. *Applied Energy*. 2017;185:589-603.

213. Zhu H-H, Wang K, He Y-L. Thermodynamic analysis and comparison for different direct-heated supercritical CO₂ Brayton cycles integrated into a solar thermal power tower system. *Energy*. 2017;140:144-57.

214. Lubkoll M, von Backström TW, Kröger DG, editors. Survey on pressurized air receiver development. 2nd Southern African Solar Energy Conference 2014; 2014.

215. Avila-Marin A, Fernandez-Reche J, Martinez-Tarifa A. Modelling strategies for porous structures as solar receivers in central receiver systems: A review. *Renewable and Sustainable Energy Reviews*. 2019;111:15-33.

216. Minardi JE, Chuang HN. Performance of a “black” liquid flat-plate solar collector. *Solar Energy*. 1975;17(3):179-83.

217. Simonetti M, Restagno F, Sani E, Noussan M. Numerical investigation of direct absorption solar collectors (DASC), based on carbon-nanohorn nanofluids, for low temperature applications. *Solar Energy*. 2020;195:166-75.

218. Islam MW. A review of dolomite catalyst for biomass gasification tar removal. *Fuel*. 2020;267:117095.

219. Tavakolpour AR, Zomorodian A, Golneshan AA. Simulation, construction and testing of a two-cylinder solar Stirling engine powered by a flat-plate solar collector without regenerator. *Renewable Energy*. 2008;33(1):77-87.

220. Schmitz M, Schwarzbözl P, Buck R, Pitz-Paal R. Assessment of the potential improvement due to multiple apertures in central receiver systems with secondary concentrators. *Solar Energy*. 2006;80(1):111-20.

221. Sinha R, Gulhane NP. Numerical study of radiation heat loss from solar cavity receiver of parabolic dish collector. *Numerical Heat Transfer, Part A: Applications*. 2020;77(7):743-59.

222. Barlev D, Vidu R, Stroeve P. Innovation in concentrated solar power. *Solar Energy Materials and Solar Cells*. 2011;95(10):2703-25.

223. Pozzobon V, Salvador S, Bézian JJ. Biomass gasification under high solar heat flux: Advanced modelling. *Fuel*. 2018;214:300-13.

224. Matuszko D. Influence of the extent and genera of cloud cover on solar radiation

- intensity. *International Journal of climatology*. 2012;32(15):2403-14.
225. Cheng Z, He Y, Cui F, Xu R, Tao Y. Numerical simulation of a parabolic trough solar collector with nonuniform solar flux conditions by coupling FVM and MCRT method. *Solar Energy*. 2012;86(6):1770-84.
226. He Y-L, Xiao J, Cheng Z-D, Tao Y-B. A MCRT and FVM coupled simulation method for energy conversion process in parabolic trough solar collector. *Renewable Energy*. 2011;36(3):976-85.
227. Yu Q, Wang Z, Xu E, editors. *Simulation and experimental research of 1MWe solar tower power plant in China*. AIP Conference Proceedings; 2016: AIP Publishing LLC.
228. Aldali Y, Muneer T, Henderson D. Solar absorber tube analysis: thermal simulation using CFD. *International Journal of Low-Carbon Technologies*. 2013;8(1):14-9.
229. Kearney D, Kelly B, Herrmann U, Cable R, Pacheco J, Mahoney R, et al. Engineering aspects of a molten salt heat transfer fluid in a trough solar field. *Energy*. 2004;29(5-6):861-70.
230. Gómez-Villarejo R, Martín EI, Navas J, Sánchez-Coronilla A, Aguilar T, Gallardo JJ, et al. Ag-based nanofluidic system to enhance heat transfer fluids for concentrating solar power: nano-level insights. *Applied Energy*. 2017;194:19-29.
231. Karim M, Islam M, Arthur O, Yarlagadda PK. Performance of Graphite-Dispersed Li₂CO₃-K₂CO₃ Molten Salt Nanofluid for a Direct Absorption Solar Collector System. *Molecules*. 2020;25(2):375.
232. Saha G, Paul MC. Numerical analysis of the heat transfer behaviour of water based Al₂O₃ and TiO₂ nanofluids in a circular pipe under the turbulent flow condition. *International Communications in Heat and Mass Transfer*. 2014;56:96-108.
233. Agrafiotis C, von Storch H, Roeb M, Sattler C. Solar thermal reforming of methane feedstocks for hydrogen and syngas production—a review. *Renewable and Sustainable Energy Reviews*. 2014;29:656-82.
234. Zeng K, Gauthier D, Soria J, Mazza G, Flamant G. Solar pyrolysis of carbonaceous feedstocks: A review. *Solar Energy*. 2017;156:73-92.
235. Zhao H, Liu T, Bai Z, Wang L, Gao W, Zhang L. Corrosion behavior of 14Cr ODS steel in supercritical water: The influence of substituting Y₂O₃ with Y₂Ti₂O₇ nanoparticles. *Corrosion Science*. 2020;163:108272.
236. Evangelisti L, Vollaro RDL, Asdrubali F. Latest advances on solar thermal

collectors: A comprehensive review. *Renewable and Sustainable Energy Reviews*. 2019;114:109318.

237. Yadav D, Banerjee R. A review of solar thermochemical processes. *Renewable and Sustainable Energy Reviews*. 2016;54:497-532.

238. Rodat S, Abanades S, Boujjat H, Chuayboon S. On the path toward day and night continuous solar high temperature thermochemical processes: A review. *Renewable and Sustainable Energy Reviews*. 2020;132:110061.

239. Kribus A, Zaibel R, Carey D, Segal A, Karni J. A solar-driven combined cycle power plant. *Solar energy*. 1998;62(2):121-9.

240. Malato S, Maldonado MI, Fernandez-Ibanez P, Oller I, Polo I, Sánchez-Moreno R. Decontamination and disinfection of water by solar photocatalysis: The pilot plants of the Plataforma Solar de Almeria. *Materials Science in Semiconductor Processing*. 2016;42:15-23.

241. Matsumura Y, Minowa T, Potic B, Kersten SR, Prins W, van Swaaij WP, et al. Biomass gasification in near-and super-critical water: status and prospects. *Biomass and Bioenergy*. 2005;29(4):269-92.

242. Nakamura A, Kiyonaga E, Yamamura Y, Shimizu Y, Minowa T, Noda Y, et al. Detailed analysis of heat and mass balance for supercritical water gasification. *Journal of chemical engineering of Japan*. 2008;41(8):817-28.

243. Boukis N, Galla U, Müller H, Dinjus E, editors. Biomass gasification in supercritical water. Experimental progress achieved with the VERENA pilot plant. 15th European biomass conference & exhibition; 2007.

244. Yakaboylu O, Albrecht I, Harinck J, Smit K, Tsalidis G-A, Di Marcello M, et al. Supercritical water gasification of biomass in fluidized bed: First results and experiences obtained from TU Delft/Gensos semi-pilot scale setup. *Biomass and Bioenergy*. 2018;111:330-42.

245. Chen J, Xu W, Zuo H, Wu X, Jiaqiang E, Wang T, et al. System development and environmental performance analysis of a solar-driven supercritical water gasification pilot plant for hydrogen production using life cycle assessment approach. *Energy Conversion and Management*. 2019;184:60-73.

246. Piatkowski N, Steinfeld A. Solar gasification of carbonaceous waste feedstocks in a packed-bed reactor—Dynamic modeling and experimental validation. *AIChE Journal*. 2011;57(12):3522-33.

247. Piatkowski N, Wieckert C, Steinfeld A. Experimental investigation of a packed-

bed solar reactor for the steam-gasification of carbonaceous feedstocks. *Fuel Processing Technology*. 2009;90(3):360-6.

248. Pantoleonos G, Koutsonikolas D, Lorentzou S, Karagiannakis G, Lekkos C, Konstandopoulos A. Dynamic simulation and optimal heat management policy of a coupled solar reforming–heat storage process. *Chemical Engineering Research and Design*. 2018;131:600-16.

249. Gokon N, Ono R, Hatamachi T, Liuyun L, Kim H-J, Kodama T. CO₂ gasification of coal cokes using internally circulating fluidized bed reactor by concentrated Xe-light irradiation for solar gasification. *International Journal of Hydrogen Energy*. 2012;37(17):12128-37.

250. Nathan GJ, Jafarian M, Dally BB, Saw WL, Ashman PJ, Hu E, et al. Solar thermal hybrids for combustion power plant: A growing opportunity. *Progress in Energy and Combustion Science*. 2018;64:4-28.

251. Bai Z, Liu Q, Lei J, Hong H, Jin H. New solar-biomass power generation system integrated a two-stage gasifier. *Applied Energy*. 2017;194:310-9.

252. Servert J, San Miguel G, Lopez D. Hybrid solar-biomass plants for power generation; Technical and economic assessment. *Global NEST Journal*. 2011;13(3):266-76.

253. Elfeky K, Li X, Ahmed N, Lu L, Wang Q. Optimization of thermal performance in thermocline tank thermal energy storage system with the multilayered PCM (s) for CSP tower plants. *Applied Energy*. 2019;243:175-90.

254. Kim DH, Yoon SH, Kim Y, Lee KH, Choi JS. Experimental studies on the charging performance of single-tank single-medium thermal energy storage. *Applied Thermal Engineering*. 2019;149:1098-104.

255. Elouali A, Kousksou T, El Rhafiki T, Hamdaoui S, Mahdaoui M, Allouhi A, et al. Physical models for packed bed: Sensible heat storage systems. *Journal of Energy Storage*. 2019;23:69-78.

256. Gokon N, Jie CS, Nakano Y, Kodama T, Bellan S, Cho H. Thermal charge/discharge performance of iron–germanium alloys as phase change materials for solar latent heat storage at high temperatures. *Journal of Energy Storage*. 2020;30:101420.

257. Arvanitoyannis IS. ISO 14040: life cycle assessment (LCA)—principles and guidelines. *Waste management for the food industries*. 2008:97-132.

258. Kalinci Y, Hepbasli A, Dincer I. Life cycle assessment of hydrogen production

from biomass gasification systems. *International journal of hydrogen energy*. 2012;37(19):14026-39.

259. Powell KM, Rashid K, Ellingwood K, Tuttle J, Iverson BD. Hybrid concentrated solar thermal power systems: A review. *Renewable and Sustainable Energy Reviews*. 2017;80:215-37.

260. Volkart K, Bauer C, Boulet C. Life cycle assessment of carbon capture and storage in power generation and industry in Europe. *International Journal of Greenhouse Gas Control*. 2013;16:91-106.

261. Milani R, Szklo A, Hoffmann BS. Hybridization of concentrated solar power with biomass gasification in Brazil's semiarid region. *Energy Conversion and Management*. 2017;143:522-37.

262. Fthenakis V, Frischknecht R, Raugei M, Kim HC, Alsema E, Held M, et al. Methodology guidelines on life cycle assessment of photovoltaic electricity. IEA PVPS Task. 2011;12.

263. Zhu X, Labianca C, He M, Luo Z, Wu C, You S, et al. Life-cycle assessment of pyrolysis processes for sustainable production of biochar from agro-residues. *Bioresource Technology*. 2022:127601.

264. Banacloche S, Herrera I, Lechón Y. Towards energy transition in Tunisia: Sustainability assessment of a hybrid concentrated solar power and biomass plant. *Science of The Total Environment*. 2020;744:140729.

265. Verghese KL, Horne R, Carre A. PIQET: the design and development of an online 'streamlined' LCA tool for sustainable packaging design decision support. *The International Journal of Life Cycle Assessment*. 2010;15:608-20.

266. Zhang Y, Baral A, Bakshi BR. Accounting for ecosystem services in life cycle assessment, part II: toward an ecologically based LCA. *Environmental science & technology*. 2010;44(7):2624-31.

267. Zhuang X, Xu X, Liu W, Xu W. LCOE analysis of tower concentrating solar power plants using different molten-salts for thermal energy storage in China. *Energies*. 2019;12(7):1394.

268. Aarum I, Devle H, Ekeberg D, Horn SJ, Stenstrøm Y. The effect of flash pyrolysis temperature on compositional variability of pyrolyzates from birch lignin. *Journal of Analytical and Applied Pyrolysis*. 2017;127:211-22.

269. Gilani IH, Amjad M, Khan SS, Khan I, Larkin S, Raw B, et al. PEMFC application through coal gasification along with cost-benefit analysis: A case study for

- South Africa. *Energy Exploration & Exploitation*. 2021;39(5):1551-87.
270. Koupaie EH, Leiva MB, Eskicioglu C, Dutil C. Mesophilic batch anaerobic co-digestion of fruit-juice industrial waste and municipal waste sludge: Process and cost-benefit analysis. *Bioresource Technology*. 2014;152:66-73.
271. Denholm P, Jorgenson J, Miller M, Zhou E, Wang C. *Methods for Analyzing the Economic Value of Concentrating Solar Power with Thermal Energy Storage*. National Renewable Energy Lab.(NREL), Golden, CO (United States); 2015.
272. Golberg A, Polikovskiy M, Epstein M, Slegers PM, Drabik D, Kribus A. Hybrid solar-seaweed biorefinery for co-production of biochemicals, biofuels, electricity, and water: Thermodynamics, life cycle assessment, and cost-benefit analysis. *Energy Conversion and Management*. 2021;246:114679.
273. Rahbari A, Shirazi A, Venkataraman MB, Pye J. A solar fuel plant via supercritical water gasification integrated with Fischer–Tropsch synthesis: Steady-state modelling and techno-economic assessment. *Energy Conversion and Management*. 2019;184:636-48.
274. Wang X, Li C, Lam CH, Subramanian K, Qin Z-H, Mou J-H, et al. Emerging waste valorisation techniques to moderate the hazardous impacts, and their path towards sustainability. *Journal of hazardous materials*. 2022;423:127023.
275. Brown TR. A techno-economic review of thermochemical cellulosic biofuel pathways. *Bioresource technology*. 2015;178:166-76.
276. Sorunmu Y, Billen P, Spatari S. A review of thermochemical upgrading of pyrolysis bio-oil: Techno-economic analysis, life cycle assessment, and technology readiness. *Gcb Bioenergy*. 2020;12(1):4-18.
277. Barahmand Z, Eikeland MS. Techno-Economic and Life Cycle Cost Analysis through the Lens of Uncertainty: A Scoping Review. *Sustainability*. 2022;14(19):12191.
278. Halliday C, Hatton TA. Net-negative emissions through molten sorbents and bioenergy with carbon capture and storage. *Industrial & Engineering Chemistry Research*. 2020;59(52):22582-96.
279. Wei X, Manovic V, Hanak DP. Techno-economic assessment of coal-or biomass-fired oxy-combustion power plants with supercritical carbon dioxide cycle. *Energy Conversion and Management*. 2020;221:113143.
280. Adnan M, Zaman M, Ullah A, Gungor A, Rizwan M, Naqvi SR. Thermo-economic analysis of integrated gasification combined cycle co-generation system hybridized with concentrated solar power tower. *Renewable Energy*. 2022;198:654-66.

281. Sahoo U, Kumar R, Singh S, Tripathi A. Energy, exergy, economic analysis and optimization of polygeneration hybrid solar-biomass system. *Applied Thermal Engineering*. 2018;145:685-92.
282. Pantaleo A, Simpson M, Rotolo G, Distaso E, Oyewunmi O, Sapin P, et al. Thermo-economic optimisation of small-scale organic Rankine cycle systems based on screw vs. piston expander maps in waste heat recovery applications. *Energy Conversion and Management*. 2019;200:112053.
283. Oyekale J, Heberle F, Petrollese M, Brüggemann D, Cau G. Biomass retrofit for existing solar organic Rankine cycle power plants: Conceptual hybridization strategy and techno-economic assessment. *Energy Conversion and Management*. 2019;196:831-45.
284. Mohamed U, Zhao Y, Huang Y, Cui Y, Shi L, Li C, et al. Sustainability evaluation of biomass direct gasification using chemical looping technology for power generation with and w/o CO₂ capture. *Energy*. 2020;205:117904.
285. Yan L, Cao Y, Wang Z, He B. On a novel carbon-negative IGCC system with cascade CO₂ combined cycle. *Energy Conversion And Management*. 2020;221:113202.
286. Mouaky A, Rachek A. Thermodynamic and thermo-economic assessment of a hybrid solar/biomass polygeneration system under the semi-arid climate conditions. *Renewable Energy*. 2020;156:14-30.
287. Hussain CI, Norton B, Duffy A. Comparison of hybridizing options for solar heat, biomass and heat storage for electricity generation in Spain. *Energy Conversion and Management*. 2020;222:113231.
288. Tola V, Pettinau A. Power generation plants with carbon capture and storage: A techno-economic comparison between coal combustion and gasification technologies. *Applied Energy*. 2014;113:1461-74.
289. Erlach B, Wirth B, Tsatsaronis G, editors. Co-production of electricity, heat and biocoal pellets from biomass: a techno-economic comparison with wood pelletizing. *World Renewable Energy Congress-Sweden*; 2011.
290. Wu C, Huang H, Zheng S, Yin X. An economic analysis of biomass gasification and power generation in China. *Bioresource technology*. 2002;83(1):65-70.
291. Regis F, Monteverde AHA, Fino D. A techno-economic assessment of bioethanol production from switchgrass through biomass gasification and syngas fermentation. *Energy*. 2023;274:127318.

292. Indrawan N, Kumar A, Moliere M, Sallam KA, Huhnke RL. Distributed power generation via gasification of biomass and municipal solid waste: A review. *Journal of the Energy Institute*. 2020;93(6):2293-313.
293. Medina Jimenez AC, Bereche RP-, Nebra S. Three municipal solid waste gasification technologies analysis for electrical energy generation in Brazil. *Waste Management & Research*. 2019;37(6):631-42.
294. Kalinci Y, Hepbasli A, Dincer I. Exergoeconomic analysis and performance assessment of hydrogen and power production using different gasification systems. *Fuel*. 2012;102:187-98.
295. McGowin CR, Wiltsee GA. Strategic analysis of biomass and waste fuels for electric power generation. *Biomass and Bioenergy*. 1996;10(2-3):167-75.
296. Screw driver website: [Available from: https://www.alibaba.com/product-detail/Hot-sale-auger-screw-conveyor_for_62166933656.html?spm=a2700.7724857.0.0.128279bbpq1HUB].
297. Adusei KK, Ng KTW, Karimi N, Mahmud TS, Doolittle E. Modeling of municipal waste disposal behaviors related to meteorological seasons using recurrent neural network LSTM models. *Ecological Informatics*. 2022;72:101925.
298. Abbas MN. Modeling of porosity equation for water flow through packed bed of monosize spherical packing. *Journal of engineering and development*. 2011;15(4):205-26.
299. Inuiguchi M, Kato K, Katagiri H. Fuzzy multi-criteria optimization: possibilistic and fuzzy/stochastic approaches. *Multiple criteria decision analysis: State of the art surveys*. 2016:851-902.
300. Slowinski R, Teghem Jr J. Fuzzy versus stochastic approaches to multicriteria linear programming under uncertainty. *Naval Research Logistics (NRL)*. 1988;35(6):673-95.
301. Philip A, Sebastian K. Environmental analysis of pallets using life cycle analysis and multi-objective dynamic programming. 2010.
302. Georgakellos DA. Climate change external cost appraisal of electricity generation systems from a life cycle perspective: the case of Greece. *Journal of Cleaner production*. 2012;32:124-40.
303. Zhang Q, Hu J, Lee D-J. Biogas from anaerobic digestion processes: Research updates. *Renewable Energy*. 2016;98:108-19.
304. Hussain M, Ali O, Raza N, Zabiri H, Ahmed A, Ali I. Recent advances in

dynamic modeling and control studies of biomass gasification for production of hydrogen rich syngas. *RSC advances*. 2023;13(34):23796-811.

305. Wieckert C, Obrist A, Zedtwitz Pv, Maag G, Steinfeld A. Syngas production by thermochemical gasification of carbonaceous waste materials in a 150 kWth packed-bed solar reactor. *Energy & fuels*. 2013;27(8):4770-6.

306. Diyoke C, Aneke M, Wang M, Wu C. Techno-economic analysis of wind power integrated with both compressed air energy storage (CAES) and biomass gasification energy storage (BGES) for power generation. *RSC advances*. 2018;8(39):22004-22.

307. Pantaleo AM, Camporeale SM, Sorrentino A, Miliozzi A, Shah N, Markides CN. Hybrid solar-biomass combined Brayton/organic Rankine-cycle plants integrated with thermal storage: Techno-economic feasibility in selected Mediterranean areas. *Renewable Energy*. 2020;147:2913-31.

308. Asadullah M. Biomass gasification gas cleaning for downstream applications: A comparative critical review. *Renewable and sustainable energy reviews*. 2014;40:118-32.

309. Rakesh N, Dasappa S. A critical assessment of tar generated during biomass gasification-Formation, evaluation, issues and mitigation strategies. *Renewable and Sustainable Energy Reviews*. 2018;91:1045-64.

310. Nicodemus JH, McGuinness M, Easton P, editors. Carbon-Neutral Solar Syngas: Cost and Policy Considerations. Proceedings of the American Solar Energy Society Solar 2014 Conference, San Francisco, CA, July; 2014.

311. Seo SB, Go ES, Ling JJJ, Lee SH. Techno-economic assessment of a solar-assisted biomass gasification process. *Renewable Energy*. 2022;193:23-31.

312. Asadullah M. Barriers of commercial power generation using biomass gasification gas: A review. *Renewable and Sustainable Energy Reviews*. 2014;29:201-15.

313. Sansaniwal S, Rosen M, Tyagi S. Global challenges in the sustainable development of biomass gasification: An overview. *Renewable and Sustainable Energy Reviews*. 2017;80:23-43.

314. Saw WL, Guo P, van Eyk PJ, Nathan GJ. Approaches to accommodate resource variability in the modelling of solar driven gasification processes for liquid fuels synthesis. *Solar Energy*. 2017;156:101-12.

315. Wang Y, Kinoshita C. Kinetic model of biomass gasification. *Solar energy*. 1993;51(1):19-25.

316. Yu J, Smith JD. Validation and application of a kinetic model for biomass gasification simulation and optimization in updraft gasifiers. *Chemical Engineering and Processing-Process Intensification*. 2018;125:214-26.
317. Smith JD, Alembath A, Al-Rubaye H, Yu J, Gao X, Golpour H. Validation and application of a kinetic model for downdraft biomass gasification simulation. *Chemical Engineering & Technology*. 2019;42(12):2505-19.
318. Sommariva S, Grana R, Maffei T, Pierucci S, Ranzi E. A kinetic approach to the mathematical model of fixed bed gasifiers. *Computers & chemical engineering*. 2011;35(5):928-35.
319. Babu B, Chaurasia A. Heat transfer and kinetics in the pyrolysis of shrinking biomass particle. *Chemical Engineering Science*. 2004;59(10):1999-2012.
320. Wei L, Lu Y, Wei J. Hydrogen production by supercritical water gasification of biomass: Particle and residence time distribution in fluidized bed reactor. *International journal of hydrogen energy*. 2013;38(29):13117-24.
321. Gerber S, Behrendt F, Oevermann M. An Eulerian modeling approach of wood gasification in a bubbling fluidized bed reactor using char as bed material. *Fuel*. 2010;89(10):2903-17.
322. Hobbs M, Radulovic P, Smoot dL. Combustion and gasification of coals in fixed-beds. *Progress in Energy and Combustion Science*. 1993;19(6):505-86.
323. Arthur J. Reactions between carbon and oxygen. *Transactions of the Faraday Society*. 1951;47:164-78.
324. Jones W, Lindstedt R. Global reaction schemes for hydrocarbon combustion. *Combustion and flame*. 1988;73(3):233-49.
325. Varma AK, Chatwani AU, Bracco FV. Studies of premixed laminar hydrogen-air flames using elementary and global kinetics models. *Combustion and flame*. 1986;64(2):233-6.
326. Ascher S, Watson I, You S. Machine learning methods for modelling the gasification and pyrolysis of biomass and waste. *Renewable and Sustainable Energy Reviews*. 2021:111902.
327. Couhert C, Salvador S, Commandre J-M. Impact of torrefaction on syngas production from wood. *Fuel*. 2009;88(11):2286-90.
328. Huang F, Jin S. Investigation of biomass (pine wood) gasification: Experiments and Aspen Plus simulation. *Energy Science & Engineering*. 2019;7(4):1178-87.
329. Fercher E, Hofbauer H, Fleck T, Rauch R, Veronik G. Two years experience

with the FICFB-gasification process: na; 1998.

330. Sheth PN, Babu B. Production of hydrogen energy through biomass (waste wood) gasification. *International journal of hydrogen energy*. 2010;35(19):10803-10.
331. Qin K, Lin W, Fæster S, Jensen PA, Wu H, Jensen AD. Characterization of residual particulates from biomass entrained flow gasification. *Energy & fuels*. 2013;27(1):262-70.
332. Plis P, Wilk R. Theoretical and experimental investigation of biomass gasification process in a fixed bed gasifier. *Energy*. 2011;36(6):3838-45.
333. Sheth PN, Babu B. Experimental studies on producer gas generation from wood waste in a downdraft biomass gasifier. *Bioresource technology*. 2009;100(12):3127-33.
334. González WA, Pérez JF, Chapela S, Porteiro J. Numerical analysis of wood biomass packing factor in a fixed-bed gasification process. *Renewable Energy*. 2018;121:579-89.
335. Breiman L. Random forests. *Machine learning*. 2001;45(1):5-32.
336. Wang Y, Liao Z, Mathieu S, Bin F, Tu X. Prediction and evaluation of plasma arc reforming of naphthalene using a hybrid machine learning model. *Journal of hazardous materials*. 2021;404:123965.
337. Yuan Y, Wu L, Zhang X. Gini-Impurity Index Analysis. *IEEE Transactions on Information Forensics and Security*. 2021;16:3154-69.
338. Xing J, Luo K, Wang H, Gao Z, Fan J. A comprehensive study on estimating higher heating value of biomass from proximate and ultimate analysis with machine learning approaches. *Energy*. 2019;188:116077.
339. Dewi C, Chen R-C. Random forest and support vector machine on features selection for regression analysis. *Int J Innov Comput Inf Control*. 2019;15(6):2027-37.
340. Cutler DR, Edwards Jr TC, Beard KH, Cutler A, Hess KT, Gibson J, et al. Random forests for classification in ecology. *Ecology*. 2007;88(11):2783-92.
341. Ullah Z, Naqvi SR, Farooq W, Yang H, Wang S, Vo D-VN. A comparative study of machine learning methods for bio-oil yield prediction—A genetic algorithm-based features selection. *Bioresource Technology*. 2021;335:125292.
342. García-Bacaicoa P, Mastral J, Ceamanos J, Berrueco C, Serrano S. Gasification of biomass/high density polyethylene mixtures in a downdraft gasifier. *Bioresource technology*. 2008;99(13):5485-91.
343. Jayah T, Aye L, Fuller RJ, Stewart D. Computer simulation of a downdraft wood gasifier for tea drying. *Biomass and bioenergy*. 2003;25(4):459-69.

344. Zainal Z, Rifau A, Quadir G, Seetharamu K. Experimental investigation of a downdraft biomass gasifier. *Biomass and bioenergy*. 2002;23(4):283-9.
345. Simone M, Nicoletta C, Tognotti L. Numerical and experimental investigation of downdraft gasification of woody residues. *Bioresource technology*. 2013;133:92-101.
346. Lucas C, Szewczyk D, Blasiak W, Mochida S. High-temperature air and steam gasification of densified biofuels. *Biomass and bioenergy*. 2004;27(6):563-75.
347. Saw W, McKinnon H, Gilmour I, Pang S. Production of hydrogen-rich syngas from steam gasification of blend of biosolids and wood using a dual fluidised bed gasifier. *Fuel*. 2012;93:473-8.
348. Aydin ES, Yucel O, Sadikoglu H. Experimental study on hydrogen-rich syngas production via gasification of pine cone particles and wood pellets in a fixed bed downdraft gasifier. *International Journal of Hydrogen Energy*. 2019;44(32):17389-96.
349. Hasnain S. Review on sustainable thermal energy storage technologies, Part I: heat storage materials and techniques. *Energy conversion and management*. 1998;39(11):1127-38.
350. Abe T, Gokon N, Izawa T, Kodama T. Internally-circulating fluidized bed reactor using thermal storage material for solar coal coke gasification. *Energy Procedia*. 2015;69:1722-30.
351. Aliaño-González MJ, Gabaston J, Ortiz-Somovilla V, Cantos-Villar E. Wood waste from fruit trees: Biomolecules and their applications in agri-food industry. *Biomolecules*. 2022;12(2):238.
352. Cardoza D, Romero I, Martínez T, Ruiz E, Gallego FJ, López-Linares JC, et al. Location of biorefineries based on olive-derived biomass in Andalusia, Spain. *Energies*. 2021;14(11):3052.
353. Energy GR. Energy Yield and Performance Ratio of Photovoltaic Systems. *Green Rhino Energy*. 2022.
354. Commission E. Photovoltaic Geographical Information System (PVGIS) [Available from: https://re.jrc.ec.europa.eu/pvg_tools/en/#TMY].
355. Fernandez-Lopez M, López-González D, Puig-Gamero M, Valverde JL, Sanchez-Silva L. CO₂ gasification of dairy and swine manure: A life cycle assessment approach. *Renewable Energy*. 2016;95:552-60.
356. Llatas C. A model for quantifying construction waste in projects according to the European waste list. *Waste management*. 2011;31(6):1261-76.

357. Villoria Sáez P, del Río Merino M, Porrás-Amores C. Estimation of construction and demolition waste volume generation in new residential buildings in Spain. *Waste management & research*. 2012;30(2):137-46.
358. Zamorano M, Molero E, Grindlay A, Rodríguez M, Hurtado A, Calvo F. A planning scenario for the application of geographical information systems in municipal waste collection: A case of Churriana de la Vega (Granada, Spain). *Resources, Conservation and Recycling*. 2009;54(2):123-33.
359. Gupta R, Miller R, Sloan W, You S. Economic and environmental assessment of organic waste to biomethane conversion. *Bioresource Technology*. 2022;345:126500.
360. Zhou N, Zhou J, Dai L, Guo F, Wang Y, Li H, et al. Syngas production from biomass pyrolysis in a continuous microwave assisted pyrolysis system. *Bioresource Technology*. 2020;314:123756.
361. Wagner MJ, Wendelin T. SolarPILOT: A power tower solar field layout and characterization tool. *Solar Energy*. 2018;171:185-96.
362. Bhargav K, Gross F, Schramek P. Life Cycle cost optimized heliostat size for power towers. *Energy Procedia*. 2014;49:40-9.
363. PIHL E. Reducing Carbon Emissions From Natural Gas-fired Power Plants. 2012.
364. Kuenlin A, Augsburg G, Gerber L, Maréchal F, editors. Life cycle assessment and environmental optimization of concentrating solar thermal power plants. 26th international conference on efficiency, cost, optimization, simulation and environmental impact of energy systems (ECOS2013); 2013.
365. Singh B, Strømman AH, Hertwich E. Life cycle assessment of natural gas combined cycle power plant with post-combustion carbon capture, transport and storage. *International Journal of Greenhouse Gas Control*. 2011;5(3):457-66.
366. Gasa G, Lopez-Roman A, Prieto C, Cabeza LF. Life cycle assessment (LCA) of a concentrating solar power (CSP) plant in tower configuration with and without thermal energy storage (TES). *Sustainability*. 2021;13(7):3672.
367. Baratieri M, Baggio P, Bosio B, Grigante M, Longo G. The use of biomass syngas in IC engines and CCGT plants: a comparative analysis. *Applied Thermal Engineering*. 2009;29(16):3309-18.
368. Rubin ES, Chen C, Rao AB. Cost and performance of fossil fuel power plants with CO₂ capture and storage. *Energy policy*. 2007;35(9):4444-54.

369. Bauer C. Life cycle assessment of fossil and biomass power generation chains. An analysis carried out for ALSTOM Power Services. 2008.
370. Verma A, Kumar A. Life cycle assessment of hydrogen production from underground coal gasification. *Applied Energy*. 2015;147:556-68.
371. Ouderji ZH, Gupta R, Mckeown A, Yu Z, Smith C, Sloan W, et al. Integration of anaerobic digestion with heat Pump: Machine learning-based technical and environmental assessment. *Bioresource Technology*. 2023;369:128485.
372. Ascher S, Li W, You S. Life cycle assessment and net present worth analysis of a community-based food waste treatment system. *Bioresource technology*. 2020;305:123076.
373. Jenkins S. The Chemical Engineering Plant Cost Index. Available from: <https://www.chemengonline.com/pci-home>.
374. Turchi CS, Boyd M, Kesseli D, Kurup P, Mehos MS, Neises TW, et al. CSP systems analysis-final project report. National Renewable Energy Lab.(NREL), Golden, CO (United States); 2019.
375. Kanniche M, Bouallou C. CO₂ capture study in advanced integrated gasification combined cycle. *Applied Thermal Engineering*. 2007;27(16):2693-702.
376. Craig KR, Mann MK. Cost and performance analysis of biomass-based integrated gasification combined-cycle (BIGCC) power systems. National Renewable Energy Lab.(NREL), Golden, CO (United States); 1996.
377. Descamps C, Bouallou C, Kanniche M. Efficiency of an Integrated Gasification Combined Cycle (IGCC) power plant including CO₂ removal. *Energy*. 2008;33(6):874-81.
378. Cormos A-M, Cormos C-C. Techno-economic assessment of combined hydrogen & power co-generation with carbon capture: The case of coal gasification. *Applied Thermal Engineering*. 2019;147:29-39.
379. Mahajan K, Velaga NR, Kumar A, Choudhary A, Choudhary P. Effects of driver work-rest patterns, lifestyle and payment incentives on long-haul truck driver sleepiness. *Transportation research part F: traffic psychology and behaviour*. 2019;60:366-82.
380. Fuller JC, Schneider KP, Chassin D, editors. Analysis of residential demand response and double-auction markets. 2011 IEEE power and energy society general meeting; 2011: IEEE.
381. Gracia A, Barreiro-Hurlé J, y Pérez LP. Can renewable energy be financed with

- higher electricity prices? Evidence from a Spanish region. *Energy Policy*. 2012;50:784-94.
382. Solar T. *Solar Panels in Spain: facts, tariffs, development, financing*. 2023.
383. Zhang K, Wang Q, Liang Q-M, Chen H. A bibliometric analysis of research on carbon tax from 1989 to 2014. *Renewable and sustainable energy reviews*. 2016;58:297-310.
384. Ortega-Izquierdo M, del Río P. Benefits and costs of renewable electricity in Europe. *Renewable and Sustainable Energy Reviews*. 2016;61:372-83.
385. IEA. *Key energy statistics 2020*. Available from: <https://www.iea.org/countries/spain>.
386. Mann MK, Spath PL. *Life cycle assessment of a biomass gasification combined-cycle power system*. National Renewable Energy Lab.(NREL), Golden, CO (United States); 1997.
387. Cohen GE, Kearney DW, Kolb GJ. *Final report on the operation and maintenance improvement program for concentrating solar power plants*. Sandia National Laboratories (SNL), Albuquerque, NM, and Livermore, CA ...; 1999.
388. Fang Y, Li X, Ascher S, Li Y, Dai L, Ruan R, et al. Life cycle assessment and cost benefit analysis of concentrated solar thermal gasification of biomass for continuous electricity generation. *Energy*. 2023:128709.
389. Liu J, Huang X, Li Q, Chen Z, Liu G, Tai Y. Hourly stepwise forecasting for solar irradiance using integrated hybrid models CNN-LSTM-MLP combined with error correction and VMD. *Energy Conversion and Management*. 2023;280:116804.
390. Yin R, Liu R, Wu J, Wu X, Sun C, Wu C. Influence of particle size on performance of a pilot-scale fixed-bed gasification system. *Bioresource technology*. 2012;119:15-21.
391. Lü X, Wu Y, Lian J, Zhang Y, Chen C, Wang P, et al. Energy management of hybrid electric vehicles: A review of energy optimization of fuel cell hybrid power system based on genetic algorithm. *Energy Conversion and Management*. 2020;205:112474.
392. Lapuerta M, Hernández JJ, Pazo A, López J. Gasification and co-gasification of biomass wastes: Effect of the biomass origin and the gasifier operating conditions. *Fuel processing technology*. 2008;89(9):828-37.
393. Bottou L. Stochastic gradient learning in neural networks. *Proceedings of Neuro-Nimes*. 1991;91(8):12.

394. Qiu B, Huang Z, Liu X, Meng X, You Y, Liu G, et al. Noise reduction in optical coherence tomography images using a deep neural network with perceptually-sensitive loss function. *Biomedical optics express*. 2020;11(2):817-30.
395. Zahra MM, Essai MH, Abd Ellah AR. Performance functions alternatives of MSE for neural networks learning. *International Journal of Engineering Research & Technology (IJERT)*. 2014;3(1):967-70.
396. Amidi A, Amidi S. *Vip cheatsheet: Recurrent neural networks*. Stanford University Stanford, CA, USA; 2018.
397. Wang M, Yu H, Jing R, Liu H, Chen P, Li C. Combined multi-objective optimization and robustness analysis framework for building integrated energy system under uncertainty. *Energy Conversion and Management*. 2020;208:112589.
398. Burnette SD. *A Cost-benefit Analysis of the Australian Carbon Tax and the Economics of Climate Change*. 2015.